Advances in Polymer Science 257

Walter Kaminsky *Editor*

Polyolefins: 50 years after Ziegler and Natta I

Polyethylene and Polypropylene

Springer

257
Advances in Polymer Science

For further volumes:
http://www.springer.com/series/12

Aims and Scope

The series Advances in Polymer Science presents critical reviews of the present and future trends in polymer and biopolymer science. It covers all areas of research in polymer and biopolymer science including chemistry, physical chemistry, physics, material science.

The thematic volumes are addressed to scientists, whether at universities or in industry, who wish to keep abreast of the important advances in the covered topics.

Advances in Polymer Science enjoys a longstanding tradition and good reputation in its community. Each volume is dedicated to a current topic, and each review critically surveys one aspect of that topic, to place it within the context of the volume. The volumes typically summarize the significant developments of the last 5 to 10 years and discuss them critically, presenting selected examples, explaining and illustrating the important principles, and bringing together many important references of primary literature. On that basis, future research directions in the area can be discussed. Advances in Polymer Science volumes thus are important references for every polymer scientist, as well as for other scientists interested in polymer science - as an introduction to a neighboring field, or as a compilation of detailed information for the specialist.

Review articles for the individual volumes are invited by the volume editors. Single contributions can be specially commissioned.

Readership: Polymer scientists, or scientists in related fields interested in polymer and biopolymer science, at universities or in industry, graduate students.

Special offer:
For all clients with a standing order we offer the electronic form of Advances in Polymer Science free of charge.

Walter Kaminsky
Editor

Polyolefins: 50 years after Ziegler and Natta I

Polyethylene and Polypropylene

With contributions by

L.L. Böhm · V. Busico · R. Cheng · M.S. Eisen · G. Fink · X. He · B. Liu · Z. Liu · B. Monrabal · L.A. Novokshonova · P. Qiu · S.L. Scott · T. Taniike · M. Terano · V.A. Zakharov · L. Zhong

Springer

Editor
Walter Kaminsky
Dept. of Chemistry
Inst. for Techn. and Macromol. Chemistry
University of Hamburg
Hamburg
Germany

ISSN 0065-3195 ISSN 1436-5030 (electronic)
ISBN 978-3-642-40807-6 ISBN 978-3-642-40808-3 (eBook)
DOI 10.1007/978-3-642-40808-3
Springer Heidelberg New York Dordrecht London

Library of Congress Control Number: 2013957181

Printed on acid-free paper

Springer is part of Springer Science+Business Media (www.springer.com)

Preface

Fifty years after the Nobel Prize was awarded to Karl Ziegler and Giulio Natta in 1963, the polymerization of olefins by metallorganic catalysts has grown to one of the most fascinating areas in academic and industrial polymer science and now has the largest use in polymer production. Ziegler had discovered 10 years earlier that a mixture of transition metal compounds, especially titanium chlorides and aluminum alkyls, was able to polymerize ethene by an insertion reaction. This spectacular milestone was expanded a year later when Natta prepared and characterized isotactic polypropylene and introduced stereospecific polymerization. In contrast to the high-pressure ethene polymerization invented in 1935 by ICI (Imperial Chemical Industries, Great Britain), the catalyzed olefin polymerization requires only low pressure and low temperature.

Today, more than 130 million tons of polyolefins are produced worldwide per year, the major part with the help of Ziegler–Natta catalysts. Polyolefins have changed the world! They are not only the polymers with the highest production volume, but they also show an unbroken production increase. Containing only carbon and hydrogen atoms, polyolefins are sustainable materials, light in weight, and offer a wide variety of properties. The production requires only easily available and nontoxic monomers and proceeds with almost no losses or side reactions. After their end of use, polyolefins can easily be recycled through mechanical procedures to simple articles, by pyrolysis to gas and oil, or by incineration to energy.

In recent decades, new generations of catalysts with higher activities and stereospecificities and modern production processes have been invented to produce a great variety of polyolefins ranging from high density polyethylene (HDPE) to linear low density polyethylene (LLDPE), high melting polypropylene, high modulus polyolefin fibers, ethene–propene rubber (EPR), ethene–propene–diene monomer rubber (EPDM). The chromium-based Phillips catalysts opened the field of gas phase polymerization for HDPE. New supported Ziegler–Natta catalysts make it possible to increase the activity, to control the morphology, and for polypropylene to increase the isotacticity by adding different kinds of donors.

A great development in this research field was the discovery of metallocene and other transition metal complexes activated by methylaluminoxane. These catalysts

are up to 10 times more active than Ziegler–Natta catalysts, are soluble in hydrocarbons, show only one type of active site (single site catalysts), and can easily be modified in their chemical structure. These properties make it possible to predict the properties of the resulting polyolefins very accurately from the knowledge of the structure of the catalyst, and thus to control molecular weight and distribution, comonomer content, and tacticity by careful selection of the appropriate reactor conditions. The single site character of metallocene-based catalysts leads to a better understanding of the mechanism of olefin polymerization and to the introduction of other bulky cocatalysts.

The different chapters in this book deal with the development of olefin polymerization 50 years after the pioneering work of Ziegler and Natta. Academic and industrial developments of ethene and propene polymerizations are presented, including short biographies of Ziegler and Natta, research on Phillips catalysts, kinetic and active site measurements, and polyolefin characterization. Review chapters also describe the latest results of olefin homo-, living-, and copolymerizations by metallocene and other single site catalysts, such as the synthesis of ansa metallocenes, supported iron catalysts, syndiotactic polypropylene, long chain branched polyolefins, and cyclic and functional copolymers. Remarkable progress has been achieved in the synthesis of polyolefin nanocomposites by an in-situ polymerization process using clay, layered silicates, carbon fibers, and carbon nanotubes as fillers.

I thank all the authors very much for giving their time to write these exciting chapters.

Hamburg, Germany Walter Kaminsky

Contents

Adv Polym Sci (2013) 257: 1–36
DOI: 10.1007/12_2013_225

Published online: 14 June 2013

Contributions to the Ziegler–Natta Catalysis: An Anthology

Gerhard Fink

Abstract This anthology summarizes contributions to Ziegler–Natta catalysis that have led through novel experimental methods to well-founded results, to continuing conclusions, and to increasing knowledge about the course of this catalysis. The complex and manifold mechanism has been elucidated in extensive kinetic studies in a half continuous tank reactor, in a plug flow reactor with oligomer distribution analysis as an additional "measuring instrument," by dynamic NMR spectroscopy with line shape analysis, through use of ^{13}C-enriched reacting ethylene as a molecular surveyor, and by observation of the individual behavior of a large number of particles with supported catalysts by transmission electron microscopy and video microscopy. The synopsis of the results of the different experimental methods gives assurance that we are safely on the right path.

Keywords Catalysis · Kinetic analysis · Mechanistic detail · Stereospecific polymerization · Silica-supported Metallocene/MAO catalysts · Videomicroscopy

Contents

Studies with W. Zoller, R. Rottler, D. Schnell, W. Fenzl, R. Mynott, N. Herfert, J. van der Leek, M. Reffke, R. Kleinschmidt, R. Goretzki, K Angermund, V. Jensen, W. Thiel, B. Tesche, B. Steinmetz, C. Przybyla, J. Zechlin, B. Weimann, K. Hauschild, F. Korber, S. Knoke, A. Alexiades, and D. Ferrari.

G. Fink (✉)
Max-Planck-Institut für Kohlenforschung, Kaiser-Wilhelm-Platz 1, Mülheim an der Ruhr, Germany
e-mail: fink@mpi-muelheim.mpg.de

1 Introduction

Within the programme "Historical Landmarks of Chemistry"[1] [1], on the 8th May 2008 the Gesellschaft Deutscher Chemiker (GDCh, Society of German Chemists) and the Max-Planck-Institut für Kohlenforschung (Max Planck Institute for Coal Research) in Mülheim an der Ruhr honoured the achievements of Karl Ziegler, whose pioneering research in the field of organic chemistry led to a revolution in organometallic catalysis and organometallic chemistry (Fig. 1). In 1953, he submitted a patent application describing the preparation of high molecular weight polyethylene at normal pressure and room temperature with the help of so-called *metallorganische Mischkatalysatoren* (organometallic mixed-catalysts) formed by treating transition metal compounds with alkyl-aluminium species and this led to an unprecedented growth in the industrial production of polyolefins. Polyolefins, such as polypropylene and polyethylene, are inexpensive, ecologically acceptable synthetic polymers that find use in a whole range of products and make up over half of the 250 million tons of synthetic polymers produced annually. The discovery also accelerated the development of homogeneous catalysis using soluble organometallic complexes. This has become one of the most innovative fields in modern chemistry and is of considerable importance in the production of organic compounds by the pharmaceutical and chemical industries. Karl Ziegler and the chemistry associated with his name found world-wide acclaim, and in 1963 he was awarded the Nobel Prize for Chemistry along with the Italian Giulio Natta who had determined the stereochemistry of the polypropylene formed using Ziegler catalysts.

[1] The programme "Historical Landmarks of Chemistry" (*Historische Stätten der Chemie*) was instigated by the GDCh in order to draw the attention of the general public to research of particular significance to the development of chemistry in Germany. The objective is ultimately to further an interest in the cultural inheritance of chemistry while emphasizing its historical basis. The locations where important scientists made their most significant discoveries are recalled in an inaugural act with the unveiling of a plaque and with the publication of a booklet [1] describing their work and its present day relevance.

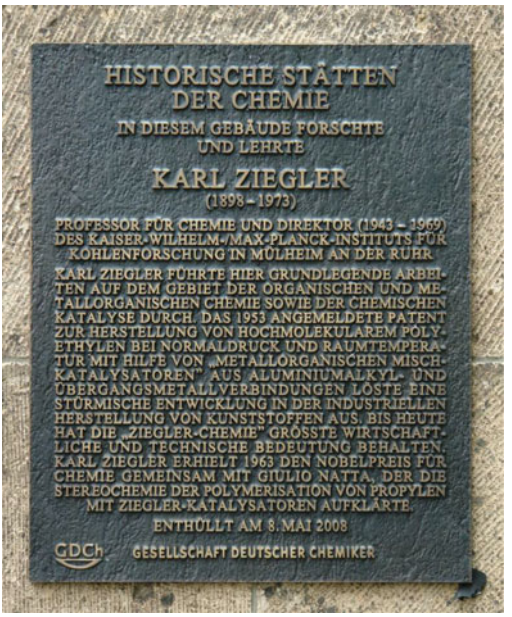

.
Translation: Karl Ziegler (1898–1973) worked in this building as Professor of Chemistry and Director of the Kaiser-Wilhelm-/Max-Planck-Institut für Kohlenforschung in Mülheim an der Ruhr from 1943 until 1969.

Karl Ziegler carried out fundamental investigations in the areas of organic and organometallic chemistry as well as in chemical catalysis. The patent submitted in 1953 for the preparation of high molecular weight polyethylene at normal pressure and room temperature with the help of "organometallic mixed-catalysts" from aluminium alkyl and transition metal compounds led to a rapid development of the industrial production of synthetic polymers. Ziegler-chemistry is still of considerable economic and technical importance. In 1963, Karl Ziegler received the Nobel Prize for Chemistry together with Giulio Natta who had established the stereochemistry of the product of the polymerization of propylene using Ziegler catalysts. Unveiled on the 8th May 2008.

Fig. 1 Bronze plaque next to the entrance to the original laboratory building of the Kaiser-Wilhelm-/Max-Planck-Institut für Kohlenforschung, Kaiser-Wilhelm-Platz 1, Mülheim an der Ruhr (Photo: M. Teske, 2008)

1.1 Biographical Data

26.11.1898	Karl Ziegler is born in Helsa near Kassel as the second son of the pastor Carl August Ziegler and his wife Luise, neé Rall. He spent his early years in Helsa and, after 1910, in Marburg
Summer 1915	*Abitur* from the Realgymnasium of Marburg
1916–1920	Chemistry student at the University of Marburg
03.08.1920	Doctoral degree from the University of Marburg with a thesis entitled *Untersuchungen über Semibenzole und verwandte Verbindungen* (Investigations on semibenzenes and related compounds). Supervisor: Karl von Auwers
11.03.1922	Marriage to Maria Kurtz from Marburg. The couple were to have two children – Marianne and Erhard
1923	*Habilitation* at the University of Marburg with a thesis entitled *Zur Kenntnis des dreiwertigen Kohlenstoffs*: *Über Tetra-Aryl-Allyl-Radikale und ihre Derivate* (Three valent carbon: tetra-aryl-allyl-radicals and their derivatives)
1925/1926	Temporary lectureship with Julius von Braun at the University of Frankfurt am Main
1926	*Privatdozent* (lecturer) with Karl Freudenberg at the University of Heidelberg
18.01.1928	Promotion to *außerordentlicher* (associate) Professor at the University of Heidelberg

(continued)

1936	Visiting Professor at the University of Chicago, USA
1936–1945	Full Professor and Director of the Chemical Institute of the University of Halle an der Saale
01.10.1943	Director of the Kaiser-Wilhelm-Institut für Kohlenforschung in Mülheim an der Ruhr as successor to Franz Fischer
20.09.1946	Cofounder of the Gesellschaft Deutscher Chemiker (GDCh, Society of German Chemists) in the British zone of the divided Germany and Chairman until 1949
15.08.1949	Honorary Professor at the Rheinisch-Westfälischen Technischen Hochschule Aachen
1949–1951	President of the GDCh after the amalgamation of the regional branches in Frankfurt am Main on the 20.09.1949
1952	Visiting Professor at the Universities of Madison and Urbana, USA
1954–1957	Chairman of the Deutsche Gesellschaft für Mineralölwissenschaft und Kohlechemie (DGMK, German Society for Mineral Oil Science and Coal Chemistry)
1955–1957	Chairman of the Chemical-Physical-Technical-Section and Senator of the Max Planck Society
09.07.1969	Retirement and appointment of Günther Wilke as his successor
1970–1971	President of the Rheinisch-Westfälische Akademie der Wissenschaften (Academy of Science) in Düsseldorf
11.08.1973	Karl Ziegler dies in his 74th year in Mülheim an der Ruhr and is buried in the main cemetery

An overall list of the honours that Ziegler received includes honorary doctorates from the Technical University of Hannover (1951), the University of Gießen (1958), the University of Heidelberg (1958), and the Technical University of Darmstadt (1968). Ziegler was elected Honorary Senator of the Max-Planck-Gesellschaft (Max Planck Society) in 1968 and in 1964 he was awarded the *Große Verdienstkreuz* with star and shoulder band of the Federal Republic of Germany. In 1969 he was elected to the Order *Pour le Mérite* in the arts and sciences as the direct successor to Otto Hahn. In 1946 he was cofounder of the GDCh and until 1951 acted as its first President. In 1963, the town of Mülheim an der Ruhr awarded him the freedom of the city and in 1974 the local high school was renamed after him. Karl Ziegler was Director of the Kaiser-Wilhelm-Institut für Kohlenforschung and (after 1949) of the Max-Planck-Gesellschaft from 1943 to 1969. The income from his patents ensured the financial independence of the Institute for over 40 years and enabled an unprecedented expansion. The creation of the Ziegler Fund in 1968 and the Ziegler Foundation in 1970 ensured the continued financial support of the Institute and these still make a substantial contribution to the annual budget. Together with his wife Maria, he thanked the town of Mülheim an der Ruhr with the gift of their valuable collection of twentieth century art (Stiftung Sammlung Ziegler im Kunstmuseum Mülheim an der Ruhr; see Fig. 2), while the generosity of their daughter Dr. Marianne Witte (who passed away in June 2012) enables the GDCh to award a *Karl-Ziegler-Preis* and a *Karl-Ziegler-Förderpreis* [1].

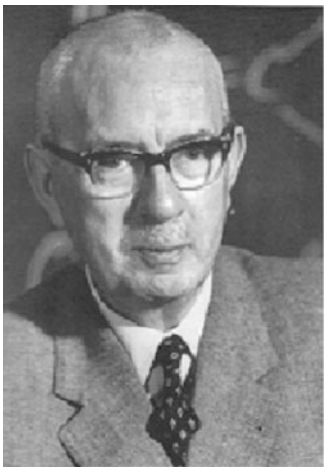

Fig. 2 Stiftung Sammlung Ziegler, im Kunstmuseum Mülheim an der Ruhr, Synagogenplatz 1, 45468 Mülheim an der Ruhr. http://sammlung-ziegler.de

Broadly, the polymerization of ethylene and α-olefins by organometallic catalysts is one of the most important catalytic processes in the chemical industry and the Ziegler–Natta catalysis an impressive example of polymerization on and with molecular catalysts per se or on a support. The detailed understanding of this fundamental catalysis on all relevant chemical and physical scales, the molecular level of the catalyst structure, the microkinetic mechanistic reaction paths, and the macrokinetic reaction engineering level of the total polymerization process, reflects a story of innovations in science and technology that is still today undergoing further development.

Another fascinating story surrounding the discovery of the Ziegler catalysts is the struggle to get international patent right protection and the early temptation by polyolefin producers to neglect the patent owner's right by infringement. Heinz Martin [2], a co-inventor of the polymerization processes had assisted Ziegler with the technological aspects as well as with patent matters and represented the Institute's interests in negotiations with potential licensees and in disputes over infringements [1]. In 2002, Martin published a book entitled *Polymere und Patente-Karl Ziegler, das Team 1953–1998* (published in English in 2007 as *Polymers, Patents, Profits – A Classic Case Study for Patent Infighting*) in which he described in detail the complicated and fascinating story of patent defence [3].

This anthology outlines some essential contributions from our group, the results of which have led to well-founded knowledge and to an increasing number of conclusions on detailed mechanisms. This is in line with a deductive development that started from individual experiments and aimed towards an overall physical and chemical description.

2 Early Soluble Unbridged Metallocene Catalysts in Connection with Alkyl Aluminum Chlorides

Due to the complexity of the solid Ziegler–Natta catalysts, homogeneous systems based on bis(cyclopentadienyl) group IV compounds, in particular on hydrocarbon-soluble titanocene complexes, gained increasing interest in the hope for more mechanistic insight. They were discovered in the 1950s [4–7], shortly after the appearance of Ziegler's and Natta's reports on solid state catalysts. Alkyl aluminum compounds such as $AlEt_2Cl$ or $AlEtCl_2$ are required to activate these soluble catalysts.

The central problem of the insertion polymerization with Ziegler catalysts is the lack of detailed knowledge concerning the nature, the lifetime, and the exact concentration of the polymerization active species. These questions can be met – in our opinion – only via a quantitative detection of all elementary reactions involved in the Ziegler–Natta catalysis.

A useful concept pointing the way for the description of these metallocene catalyst systems goes back to the kinetic studies of Reichert and Meyer [8–10]. In [8] in the summary Reichert wrote:

> The rate of polymerization of ethylene by the soluble Ziegler–Natta catalysts $Cp_2TiEtCl/AlEtCl_2$ was investigated in toluene as solvent. From the dependence of the initial rate of the polymerization follows, that the primary complex, formed by the catalyst components, is not the active species of this system. The obtained dependences rather suggest, that the active species is to be viewed as an equilibrium product and the location of this equilibrium is determined by the ratio of the catalyst compounds in that manner, that only at high Al/Ti-ratios the charged Ti(IV)-compound is equal to the initial concentration of the active species.

In the summary of [10], he continues: "The active species of this catalyst system is formed extremely rapid and seems to be a very dynamic equilibrium product. Its concentration depends on the ratio Al/Ti. The propagation reaction therefore corresponds to an intermitting process."

Hence, during the growth of a polymer chain, each metal species with a pendant chain appears to alternate between a "dormant" state and a state in which it actively grows. This "intermittent-growth" model was further elaborated by Fink and coworkers [11–19] in extensive kinetic and reactivity studies using precise experimental tools designed especially for dealing with fast reactions (rapid in situ start in the stirred back-mix reactor with highly sensitive and rapid measuring of monomer consumption, plug-flow and stop-flow reactor, dynamic ^{13}C NMR spectroscopy, use of ^{13}C-enriched ethylene as a molecular surveyor during the polymerization). For the first time, these experiments demonstrated a sequence of very fast elementary catalyst-forming reactions and also the dynamic alkyl and chloride exchange reactions inherent in these homogeneous polymerization systems.

It was Fink's conclusion that, as a consequence of these successive equilibria and their very different locations, the dependence of the initial polymerization rate on the charged Al concentration (i.e., the Al isotherm) has to show a pronounced sigmoid curve course in the initial part. Namely, in this case in the overall rate

law of the polyreaction $r_p = k_p[C^*][M]$, the quantity [C*] is a function of the two equilibrium constants (K_1 and K_2) and the concentration of the charged components (Ti and Al), i.e., $[C^*] = f(K_1, K_2, [Ti]_0, [Al]_0)$. Hence, we intensively concentrated our experimental efforts on determining the exact conditions of the two equilibrium steps, their thermodynamic data, and the detection of the kinetic sigmoid curve!

2.1 *Kinetic Analysis by Means of a Half Continuous Stirred Tank Reactor: Ethylene Polymerization with an In Situ Start [11]*

Figure 3 shows a flow chart of the polymerization plant with the injection system, on-line registration of the polymerization rate, temperature course and pressure, and the stirrer tachometer. The injection system allows the immediate in situ start of the reaction, and the flow meters enable measurement of the true initial rates (monomer consumption in dependence on time). With this very rapid technique it is also possible to pursue strong unsteady polymerizations versus time courses.

Figure 4 shows the dependence of polymerization rates (v_p) on time; the third parameter is the ratio Al/Ti, which is marked on the maxima of the curves. Note the strong unsteady polymerization courses and the strong changes with increasing Al concentration. The arrows in Fig. 4 identify that time (or rather interval) from which the clear reaction solution becomes cloudy through precipitating polyethylene. This precipitation divides the reaction into two phases: a homogeneous phase and a heterogeneous phase. The homogeneous initial part of Fig. 4 shows a significant behavior dependence on the ratio Al/Ti: the polyreaction starts immediately and, the higher the ratio Al/Ti, the faster the initial rate (intersection point with the ordinate).

Figure 5 demonstrates the kinetic evaluation of these results. On the left-hand side, the initial velocity v_p (intersection points with the ordinate) is plotted versus the concentration of the Al component while the Ti concentration was kept constant. The result is the Al isothermal curve of the second equilibrium reaction generating the active species. It demonstrates in the initial part the demanded sigmoid curve course according to the location of the two successive equilibria. This induction period is enlarged in Fig. 6. It can be clearly seen how sensitively the initial polymerization rate responds to the ratio Al/Ti. With a ratio >1 (i.e., here $[AlEtCl_2] > 3\times10^{-3}$ mol L^{-1}), the formation of the active species increases drastically.

Figure 5 additionally demonstrates on the right-hand side the kinetic counter-experiment. Again the initial polymerization rate is plotted, but now versus the concentration of the titanium component while the Al concentration is kept constant. The result is the Ti isothermal curve with the expected inverse characteristic. The important message here is that if the active species is formed in only one single equilibrium reaction, the course of the Ti isotherm has to show the same

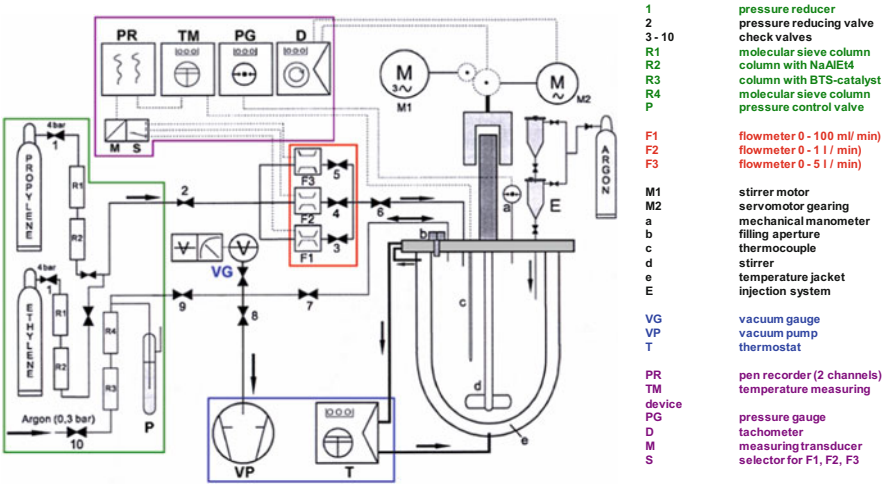

Fig. 3 Flow chart of the polymerization plant

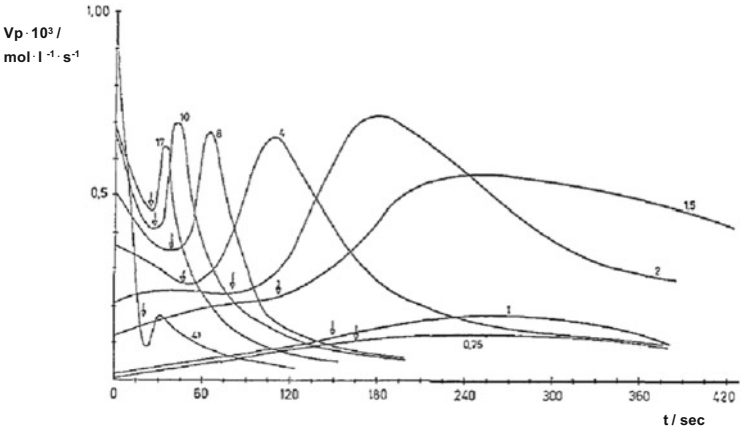

Fig. 4 Polymerization rate v_p in dependence on time for different ratios Al/Ti in the system. $Cp_2TiPropylCl/AlEtCl_2/Ethylene$. $[Cp_2TiPropylCl] = 3\times10^{-3}\,mol\,L^{-1}$, $[C_2H_4] = 0.089\,mol\,L^{-1}$, toluene, 283 K

course as the Al isotherm. The passage through a maximum in the Ti isotherm proves that, towards a surplus of the Ti component, the succession of the equilibria stops at the polymerization inactive primary complex. The curve shape towards higher Ti concentrations is for comparison with the initial part of the Al isotherm.

Hence, the existence and the divergent location of the two successive equilibria is unambiguously proven with the Al and Ti isothermal curves: the primary complex equilibrium is located on the extreme right-hand side and the secondary active species equilibrium is located on the left-hand side and is shifted into the saturation region only with a very high Al surplus.

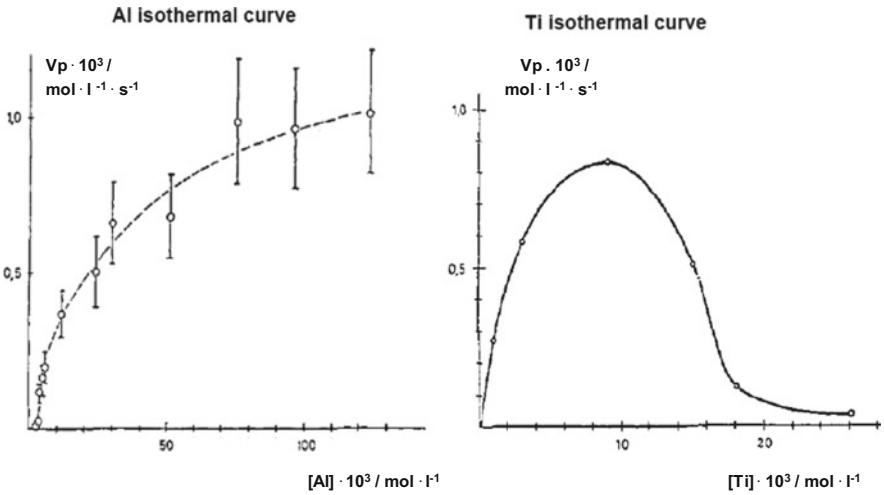

Fig. 5 Initial polymerization rates v_p in dependence on the catalyst components: *left*, Al; *right*, Ti. $[Cp_2TiPropylCl] = 3\times10^{-3}$ mol L^{-1}, $[C_2H_4] = 0.089$ mol L^{-1}, toluene, 283 K

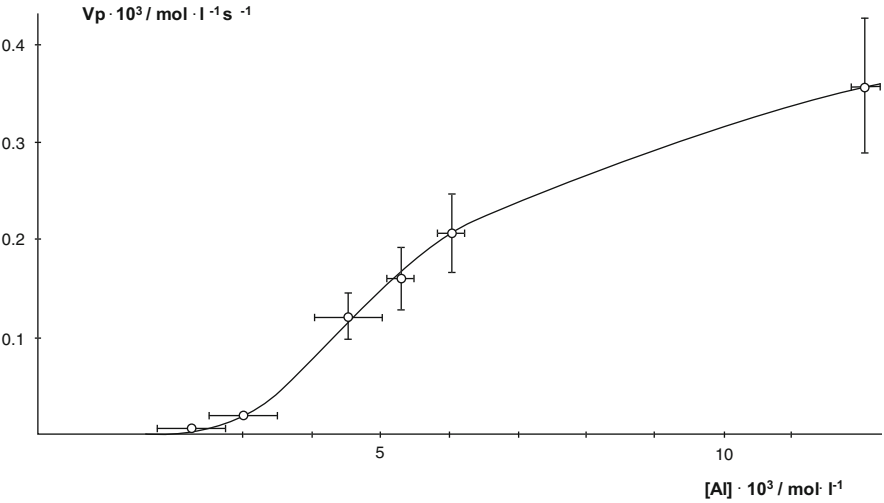

Fig. 6 Initial part of the Al isothermal curve with induction period. $[Cp_2TiPropylCl] = 3\times10^{-3}$ mol L^{-1}, $[C_2H_4] = 0.089$ mol L^{-1}, toluene, 283 K

Figure 7 summarize the kinetic results of this analysis and the conclusions concerning the mechanistic course. The primary complex formation occurs in a diffusion (i.e., physically) controlled reaction with a rate constant of about 10^{10}–10^{11} L mol^{-1} s^{-1}. The reverse reaction, the primary complex dissociation, has a rate constant of 10^6–10^7 s^{-1}. This means that K_1, the equilibrium constant of the primary complex, has a value of about 1×10^4 L mol^{-1} and proves that

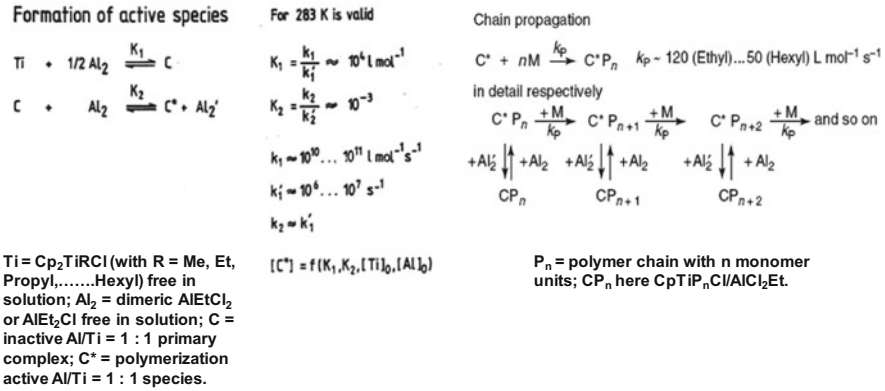

Fig. 7 *Left*: Reaction scheme of the successive equilibria for the formation of the polymerization active species C*. *Right*: "Intermittent growth model" involving equilibria between polymer-bearing, but inactive, primary complexes CP_n and active catalyst species C^*P_n

this equilibrium is located completely at the right-hand side. These constants were determined by means of ^{13}C NMR spectroscopy and quantitative line shape analysis [15].

The exact opposite is the case in the subsequent equilibrium reaction, forming the active species with the Al component still being a part of the process. Whereas the rate constants are in the same order of magnitude, the equilibrium constant K_2 has here a value of 1×10^{-3} and demonstrates the strong left-hand location of this equilibrium.

Furthermore, as a consequence of the fact that the polymerization active species is the product of reversible equilibria reactions, the propagating process of a growing species is an intermittent process (Fig 7, right), which results in a particular development of the molar mass distribution of the polymers formed. This molar mass distribution is now an important additional tool for the elucidation of complex polymerization mechanisms. It is well known that the molar mass distribution contains and reflects the complete kinetic history. We will refer to this important relation in Sect. 2.3.

2.2 *Ethylene Polymerization in the NMR Tube: Direct Insight into the Catalytic Action Using Enriched ^{13}C Ethylene [12, 17, 18]*

A suitable method for obtaining information on catalytically active systems without disturbing the reaction is ^{13}C NMR spectroscopy. In these experiments, we used ethylene enriched in ^{13}C to over 90 atom%. Besides providing a considerable gain in sensitivity over ethylene with ^{13}C at natural abundance (1.1%), this allows the carbons in the polymer chain derived from ^{13}C-enriched ethylene to be

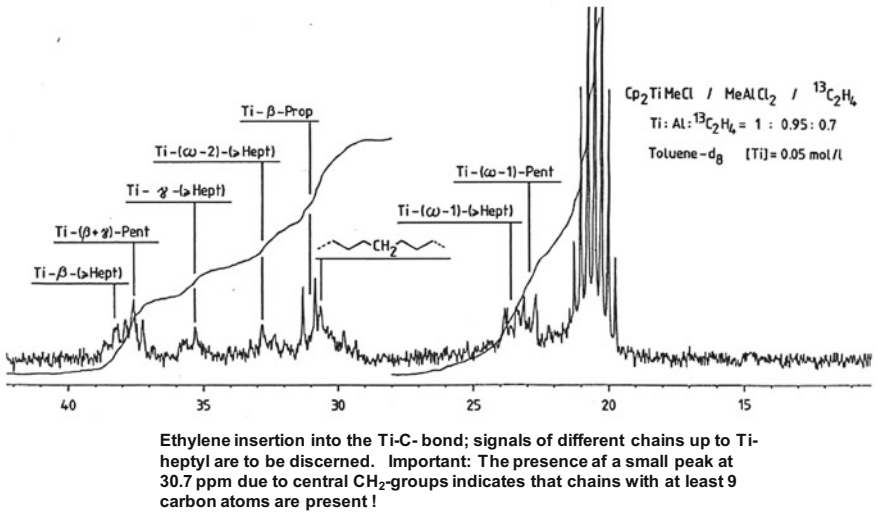

Fig. 8 75.5 MHz ^{13}C NMR spectrum of the system $Cp_2TiMeCl/AlMeCl_2$ reacting with $^{13}C_2H_4$. The ratio [Ti]:[Al]:[$^{13}C_2H_4$] = 1:0.95:0.7; the sample was reacted for 70 min at 258 K and then cooled rapidly to 213 K

distinguished from those from the Ti-Me or Al-Me carbons on the basis of their signal intensities. Whereas ^{13}C–^{13}C spin–spin couplings are observed in natural abundance ^{13}C NMR spectra only as very weak satellites, in enriched samples they can cause the signals to appear as multiplets. The proton-decoupled spectrum of enriched free ethylene in solution is a singlet because the two ^{13}C nuclei are magnetically equivalent. Once incorporated into a chain, these carbons are no longer chemically equivalent and the coupling between neighboring ^{13}C nuclei is observed.

For details of the preparation of the NMR samples in an all-glass dosing and filling apparatus constructed for these experiments and of the difficult polymerizations in the NMR tube see [12, 18].

Figure 8 illustrates the first of a series of ^{13}C NMR spectra of the system reacting with ethylene. The sample was reacted for 70 min at 258 K and then cooled rapidly to 213 K and measured. The enlargement in Fig. 8 shows that the first insertion steps occurred into the Ti–C bond, as indicated by the peaks of the β-carbons of Ti-propyl and Ti-pentyl. The ethylene signal at 123 ppm (not visible in Fig. 8) remains a sharp singlet and is unshifted, demonstrating that even at the chosen ratio $Ti/Al/C_2H_4$ = 1.0:0.95:0.7 no interaction with the catalyst is detectible. Thus, pre-coordination of the monomer to the primary complex (for instance, the π-complex of Cossee [20, 21]) is not observed and can be present only to a very minor extent.

The β, γ, ω-2 and ω-1 signals of the different chains up to Ti-heptyl can also be discerned in Fig. 8. This proves again that the insertion has occurred into the Ti–C

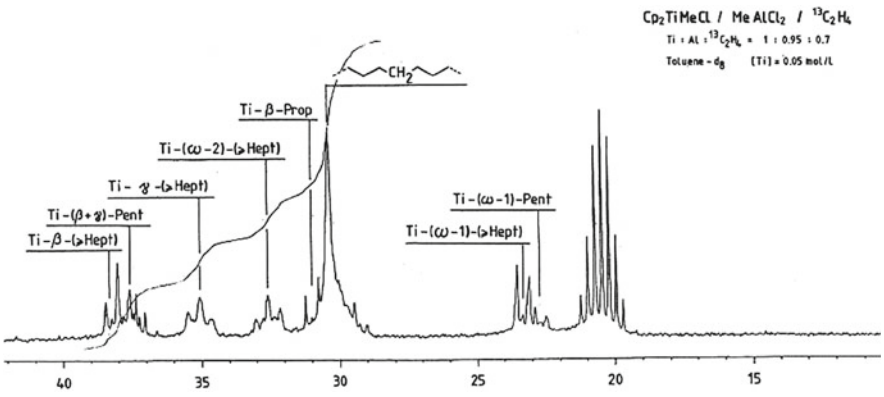

Fig. 9 Oligomer distribution after 3 h polymerization time at 258 K

bond (monometallic versus bimetallic mechanisms [22, 23]). In addition, the presence of a small peak at 30.7 ppm due to central CH_2 groups indicates that chains with at least nine carbon atoms are present. Figure 9 shows the situation after 180 min. The signals reveal the developing oligomer distribution and that the size of the peak of the central CH_2 groups has increased considerably, showing that most chains are longer than Ti-nonyl!

Let us now consider how this result could arise when the initial concentration ratio Ti/C_2H_4 was 1.0:0.7. If all the initial added Ti had been active, then at the end of the reaction on average less than one ethylene per $Ti\text{-}CH_3$ would have undergone insertion. In this case we would find mostly Ti-propyl chains and possibly a small quantity of Ti-pentyl chains. It is assumed that all the ethylene has been consumed and, as can be seen in Fig. 9, there are much longer oligomer chains present even though there is a considerable amount of unreacted ethylene left.

The observation that longer oligomer chains have been formed is very important because it proves that not all the Ti has been able to undergo insertion. A large amount of $Ti\text{-}CH_3$ must therefore still be present. This is confirmed by the corresponding signal at 64 ppm, which represents a considerable concentration of Ti-methyl groups because the methyl group has natural ^{13}C abundance. These results give further strong evidence for the formation of the active species in two successive equilibrium steps. Consequently, at low ratios of Al/Ti, there is only a very small concentration of active species C* available.

After the long reaction time of 15 h, small quantities of α-olefins are formed, as indicated by weak signals at 114 and 140 ppm (Fig. 9). This means that the transfer reaction to the monomer via β-H elimination has occurred [17].

We have carried out further investigations aimed at obtaining more details on the chain propagation itself. Figure 10 illustrates the series of spectra recorded for a sample of $Cp_2TiMeCl/AlMe_2Cl/^{13}C_2H_4$ in the ratio 1:2:2, to increase the concentration of active species.

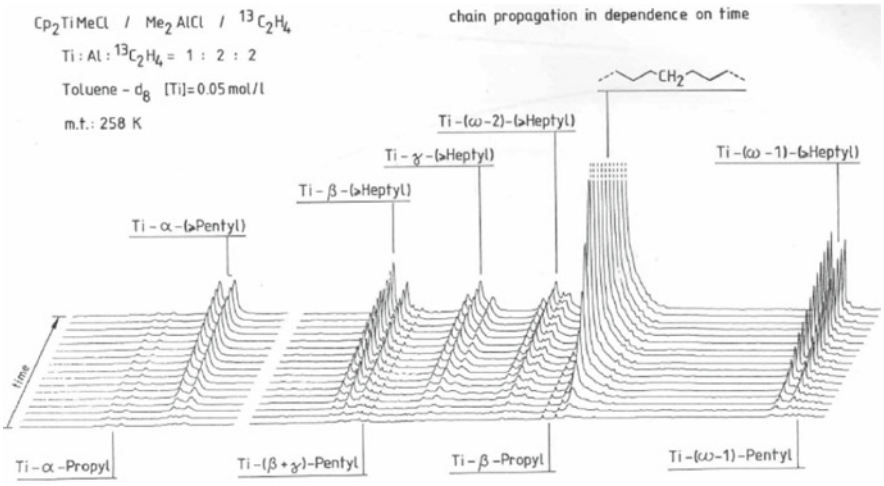

Fig. 10 Series of spectra recorded successively over periods of about 1 h in order to follow the development in chain growth

Table 1 Insertion rate constants

Insertion step	Rate constant	k (L mol^{-1} s^{-1})
$C_1 \rightarrow C_3$	k_{methyl}	1
$C_2 \rightarrow C_4$	k_{ethyl}	120
$C_3 \rightarrow C_5$	k_{propyl}	96
$C_4 \rightarrow C_6$	k_{butyl}	62
$C_5 \rightarrow C_7$	k_{pentyl}	48
$C_6 \rightarrow C_8$	k_{hexyl}	47

The potential of this approach is apparent. Detailed assignment and analysis of the signal intensities provides information on the chain length dependency of the propagation constants and the overall rate of formation of the various oligomers [18]. The insertion rate constants (see Table 1) show a maximum value in the case of Ti-ethyl and a decrease for longer chains. Why the insertion into a Ti-methyl group precedes two orders of magnitude more slowly than that into the Ti-ethyl group is an open question.

2.3 Kinetic Analysis in a Plug Flow Reactor [13, 16]

In the context of Fig. 4 (Sect. 2.1) we discussed that the rate time curves are divided, through precipitating polyethylene, into an initial homogeneous and a subsequent heterogeneous part. Hence, we decided to carry out a kinetic analysis only in the homogeneous initial part in order to approach or to elucidate the elementary processes. As a consequence, we constructed an all-glass plug flow

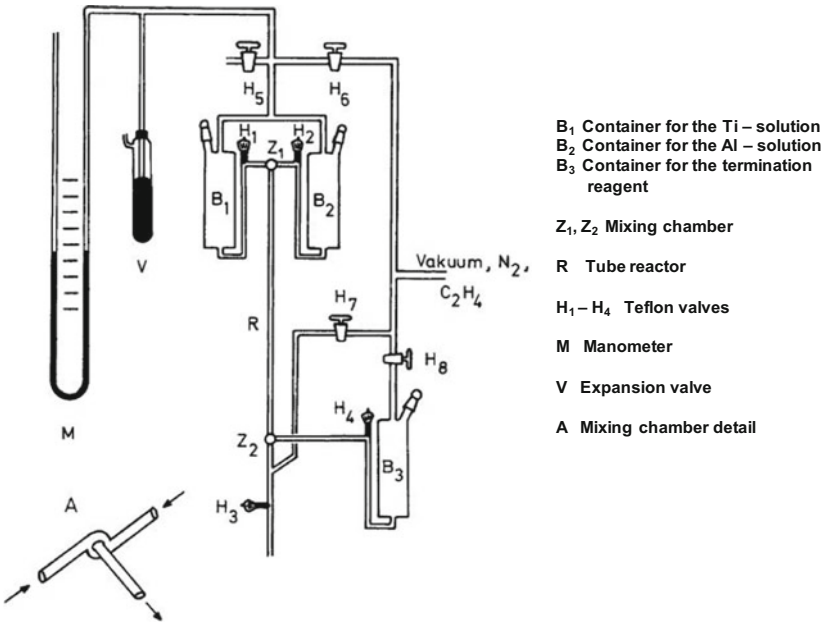

Fig. 11 Kinetic analysis in a plug flow reactor $Cp_2TiRCl/AlEtCl_2/C_2H_4$ with R = Et or higher alkyl

reactor in order to realize very short reaction times, the measurement of fast reactions, and the precise analysis and determination of the formed oligomers. The following two conditions have to be fulfilled absolutely:

1. The mixing times in Z_1 and Z_2 have to be negligibly small in comparison with the reaction time
2. The Reynold number has to be large in order to avoid hydrodynamic influence on the oligomer distribution, and there must be the possibility for a pre-run in order to avoid any impurity traces

Figure 11 shows the plug flow apparatus. Mixing times below 10 ms, flow rates from 1.19 to 2.05 m s^{-1} and residence times from 1.74 to 0.095 s have been realized.

2.3.1 Molar Mass Distribution and Reaction Scheme

As mentioned above, there is a specific relation between the mechanism of a polyreaction and the resulting molecular weight distribution of the formed polymer. In order to apply this "measuring instrument," a sequence of oligomer distributions was produced in dependence on the reaction time, ratio Al/Ti (i.e., the concentration of active species), chain length of the starting Ti-component, monomer concentration, and temperature (see Figs. 12 and 13).

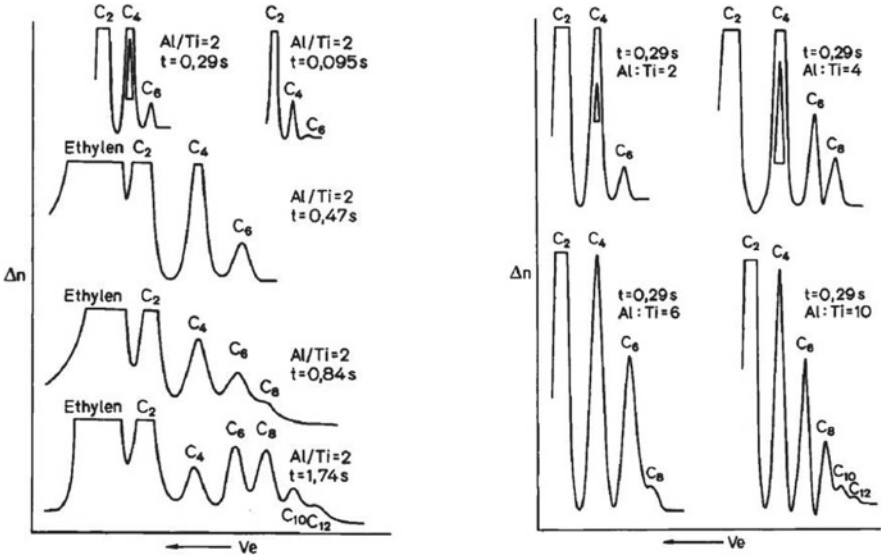

Fig. 12 *Left*: Gel permeation-chromatographical alkane oligomer distributions in dependence on the reaction time (tube lengths 206–19.5 cm). *Right*: Gel permeation-chromatographical alkane oligomer distributions in dependence on the ratio of Al/Ti component ($\tau = 0.29$ s)

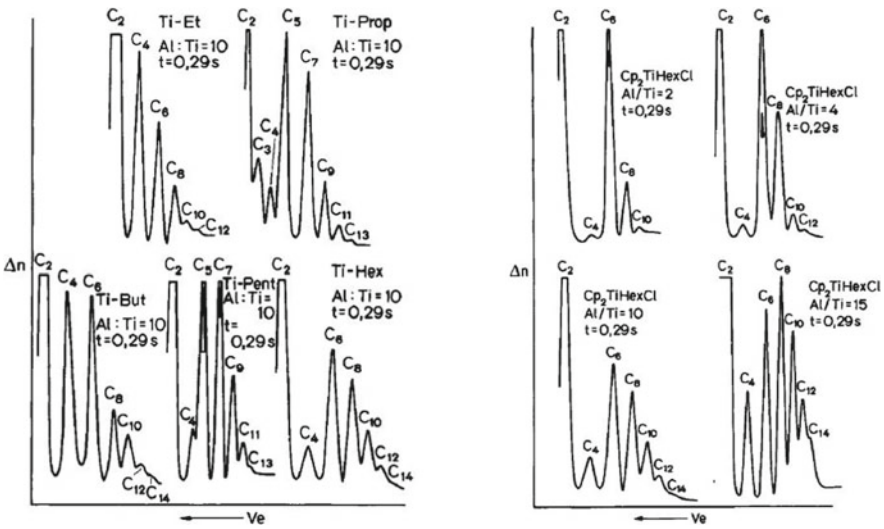

Fig. 13 *Left*: Gel permeation-chromatographical alkane oligomer distributions in dependence on the alkyl chain length of the Ti component (Al/Ti = 10; $\tau = 0.29$). *Right*: Gel permeation-chromatographical alkane oligomer distributions in dependence on the ratio Al/Ti with Ti-hexyl as starting component ($\tau = 0.29$ s)

In Fig. 12, left-hand side, the oligomer distribution shows the expected course: with increasing reaction time, higher oligomers are formed. But, the result shown in Fig 12, right, was at first surprising because the increasing concentration of C* (ratio Al/Ti) should, for a constant reaction time, produce a higher amount of oligomers and not a higher degree of oligomers. However, this result is again an important and decisive finding and gives – again according to the reaction scheme of the two successive equilibria and the propagating process as an intermittent process (see again Fig. 7) – the basis for the theoretical calculation of the developing oligomer distributions (see below).

Figure 13, left, proves the dependency of the propagation rate on the alkyl chain length of the Ti component. Here, the shorter the starting Ti chain, the more the oligomer distribution proceeds towards higher alkanes. In the distributions of Fig. 13, right, Ti-hexyl is the starting component. Here, with increasing ratio Al/Ti an increasing butane peak appears, indicating an alkyl transfer reaction between the Al and the Ti component.

2.3.2 Theoretical Calculation of the Oligomer Distributions and Comparison with Experimental Results

The theoretical model simulates the reaction scheme of the intermittent propagation of Fig. 7 on the basis of a statistical distribution of the polymerization activity onto all molecules (C_n) present in the reactor. In other words, the possibility to become an active species is again distributed newly after each insertion step, because the concentration of the different alkyl chains is changed after each insertion step. Figure 14 shows the binomial distribution formula or, more precisely, the Bernoulli scheme for two incompatible events. In this formula, α is the probability for the event, $1-\alpha$ the non-probability for the event, and ν the number of times that the event occurs.

Figure 14, right, demonstrates two characteristic examples of the properties of the distribution model. The upper graph shows (with constant α) the variation of n, the number of insertion steps, which is represented in the experiments through the reaction time. The lower graph shows (with constant n) the variation of α, represented in the experiment through the ratio Al/Ti; for larger α, the larger are the "portions" with which the distribution is developed.

For the quantitative comparison of calculated and experimental oligomer distributions, a broad spectrum of distributions was estimated with a variation of α in distances of 0.005 (i.e. 0.5%) and a variation of the insertion steps from 1 to 40. This gave a catalogue of about 1,600 frequency distributions. The results are compared comprehensively in [16] and confirm the correct agreement.

$$Z_{n,v} = \binom{n}{v} \cdot \alpha^{v} \cdot (1 - \alpha)^{n-v} \cdot Z_0$$

n = number of insertion steps, i.e. time

v = kinetic chain length

α = momentary active fraction of the charged Ti-compound, i.e. equlibrium concentration C*

Z_o = charged Ti-compound

$Z_{n,v}$ = fraction of Z_o which has the kinetic chain length v after n insertion steps

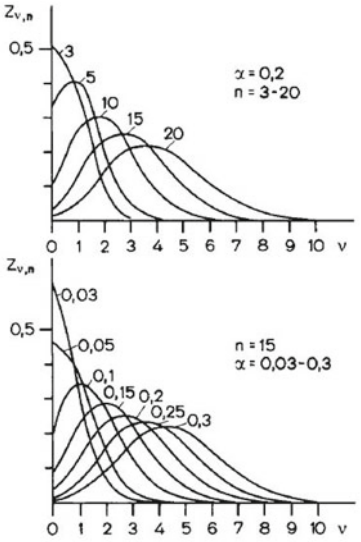

Fig. 14 Theoretical binomial distributions calculated on the basis of the reaction scheme of the two successive equilibria and the propagation process of a growing species as an intermittent insertion process. *Upper graph* shows effect of variation in *n* at constant α; *lower graph* shows the effect of variation in α at constant *n*

2.3.3 Novel Determination of the Chain Propagation Constant by Means of the Distribution Development

With the proof of congruence of experimental and theoretical calculated distributions, the evaluation possibilities of the "measuring quantity distribution" are not limited. A further consequence of the model calculation opens an access to the true values of the chain propagation rate constants. In Fig. 15, the step-by-step development of the oligomer distribution is outlined from the first insertion until the 20th insertion. As one can see, with each and every insertion step a new highest oligomer degree is formed; this longest alkane is marked in the diagrams with an arrow.

It is obvious that the higher the number of insertion steps, the further this longest alkane is from the average field and its concentration is more and more decreased. Hence, this longest alkane is soon under the analytical detection limitation and, as a consequence, the analytically visible longest alkane $\nu_{max(exp)}$ is considerably shorter. This is illustrated in the sketch in Fig. 16, top left.

However, the true longest alkane $\nu_{max(cal)}$ is accessible (according to Fig. 15) in the calculated distributions and, in the case of congruence of experimentally visible and the corresponding part of the calculated distribution, the desired true longest alkane can be estimated from the latter. The relation between k_p and the longest alkane ν_{max} follows from the rate law for the propagation reaction as formulated in Fig. 16, below left. ν_{max}/t corresponds to the number of monomers that at given monomer concentration [M] are inserted on an active species: $k_p = \nu_{max}/[M]t$.

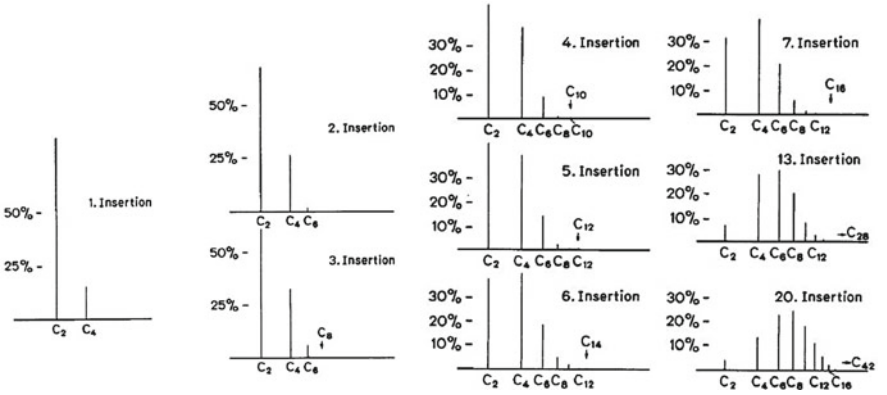

Fig. 15 Novel determination of the chain propagation constant by means of the distribution development

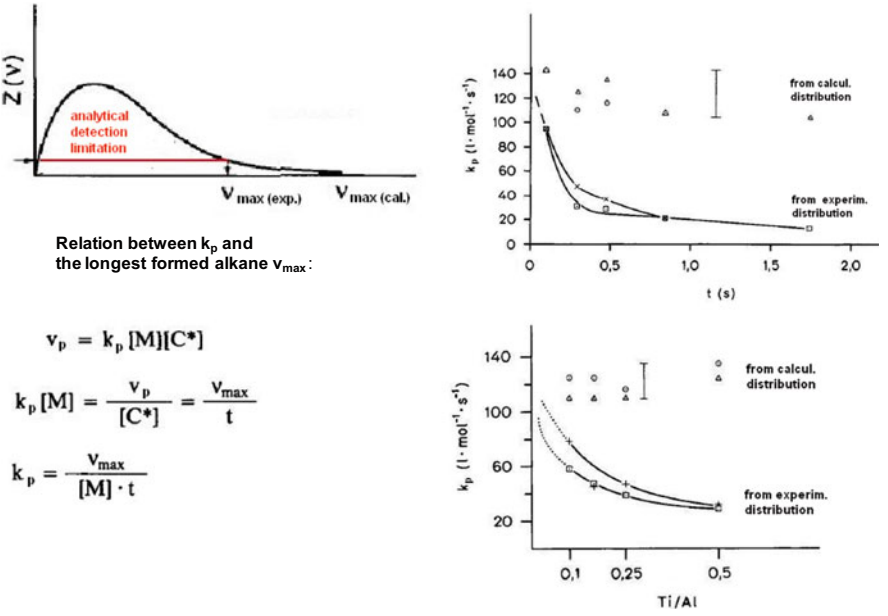

Fig. 16 Determination of the chain propagation constant k_p via the longest formed alkane. *Graphs* show determination of k_p from oligomer distribution as a function of time (*above*) and Al/Ti ratio (*below*)

The diagrams in Fig. 16 demonstrate this evaluation: the upper graph shows the determination of the propagation rate constants from the oligomer distributions in dependence on time; the lower graph shows the determination from the distributions in dependence on the ratio Ti/Al (the concentration of the active species C*).

In both diagrams, the rate constants determined via $\nu_{\max(\mathrm{cal})}$ by means of all calculated distributions result in the same values of 120 L mol^{-1} s^{-1}. The rate constants determined via $\nu_{\max(\mathrm{exp})}$ result, as expected, in lower values. However, the course of these values extrapolated in the diagrams backwards to zero point aims at this theoretical $\nu_{\max}$ value of 120 L mol^{-1} s^{-1}. Indeed, an excellent agreement!

2.3.4 Kinetic Evaluation of Oligomer Distribution in Dependence on Different Parameters

From the integrated peak areas of the oligomer distributions, even a total monomer consumption can be determined, which leads to an "average" but, because of the very short reaction times, precise polymerization rate. This kinetic evaluation was carried out according to the equation:

$$v_{\mathrm{p}} = \frac{\sum_{0}^{v} m_v \cdot v}{p \cdot t},$$

with m_v being the chromatogram-determined amount of alkane in mol, ν the kinetic chain length, p the analytical probe volume, and t the reaction time. It should be emphasized again that these rates are determined absolutely in the homogeneous phase of the polymerization course without any influence from precipitating polyethylene.

The kinetic analysis is shown in Fig. 17 and leads to detail concerning the concentration of the active species, insight into the superposition of the Al isotherm and its dependence on the chain length of the starting Ti-alkyl group, and determination of a reaction order equal to one for the monomer dependence.

Figure 17a shows the monomer dependence. The resulting slope leads to tg $\alpha = [\mathrm{C}^*]k_{\mathrm{p}}$. Using the k_{p} values from Sect. 2.3.3 (Fig. 16), we can estimate the concentration of C* at 5% of the charged Ti component at a ratio Al/Ti = 2. Figure 17b shows the polymerization rates in dependence on the reaction time. Further evaluation of this diagram follows the equations:

$$v_{\mathrm{p}} = -\mathrm{d}M/\mathrm{d}t = k_{\mathrm{p}}[\mathrm{C}^*][\mathrm{M}]_0 \text{ and hence, } \ln[\mathrm{M}]_0/[\mathrm{M}]_t = k_{\mathrm{p}}[\mathrm{C}^*]t.$$

Hence, the data plotted according to $\log[\mathrm{M}]_0/[\mathrm{M}]_t$ versus t in Fig. 17c result in a slope of tg $\alpha = k_{\mathrm{p}}[\mathrm{C}^*] \times 0.434$. Again using the k_{p} values of Fig. 16, this estimation leads to 5% of the charged Ti component at a ratio Al/Ti = 2. The analogous evaluation at a ratio of 4 gives [C*] = 9% of $[\mathrm{Ti}]_0$, which is in best agreement with the stirred tank reactor kinetics.

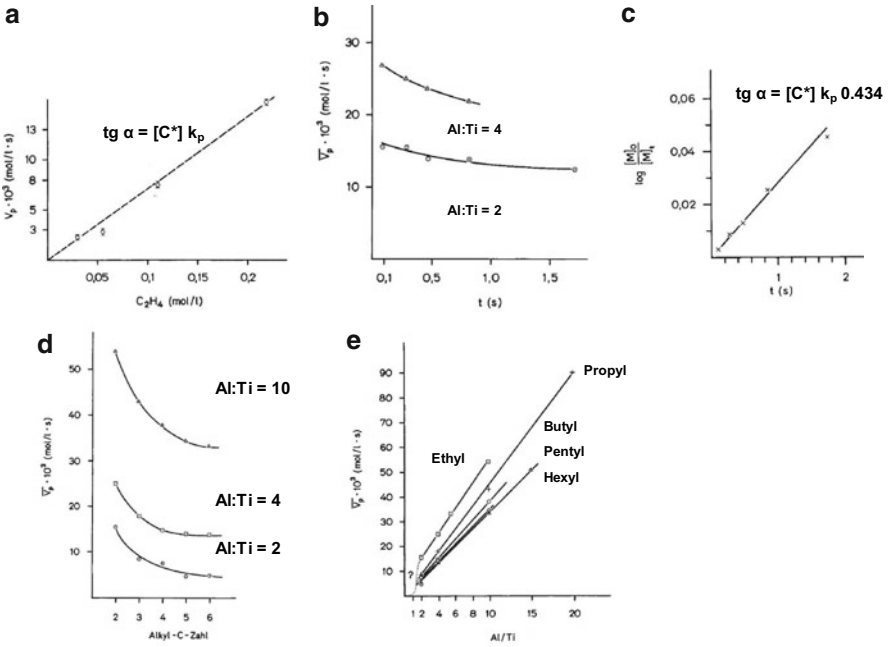

Fig. 17 (**a**–**e**) Kinetic evaluation from the plug flow reactor distributions. Integration of the peak areas led to a total monomer consumption, i.e., an "average polymerization rate," but determined at very short reaction times. See text for description of figure parts

Figure 17d demonstrates the dependence of polymerization rate on chain length. Sections parallel to the ordinate lead to the dependence of the polymerization rates on the Al alkyl concentration, with the Ti chain length superimposed as third parameter (Fig. 17e). It is very interesting to see that the sigmoid curve of the Al isotherm (remember Fig. 5) is also confirmed in this way.

In similar experiments, the activation energies of the propagation reaction and of the Al alkyl transfer reaction were determined to be 29 and 58 kJ mol^{-1}, respectively.

3 Stereorigid Bridged Metallocene Catalysts in Connection with MAO as Activator

The discovery of metallocenes for the isotactic and sydiotactic polymerization of α-alkenes [24–26] was also a highlight of the development of Ziegler–Natta polymerization catalysis. In contrast to solid Ziegler catalysts, these homogenous systems feature narrow molecular weight distributions, which has led to them being referred to as "single-site catalysts" and raised hopes with respect to the investigation of the nature and structure of the active species. See also other

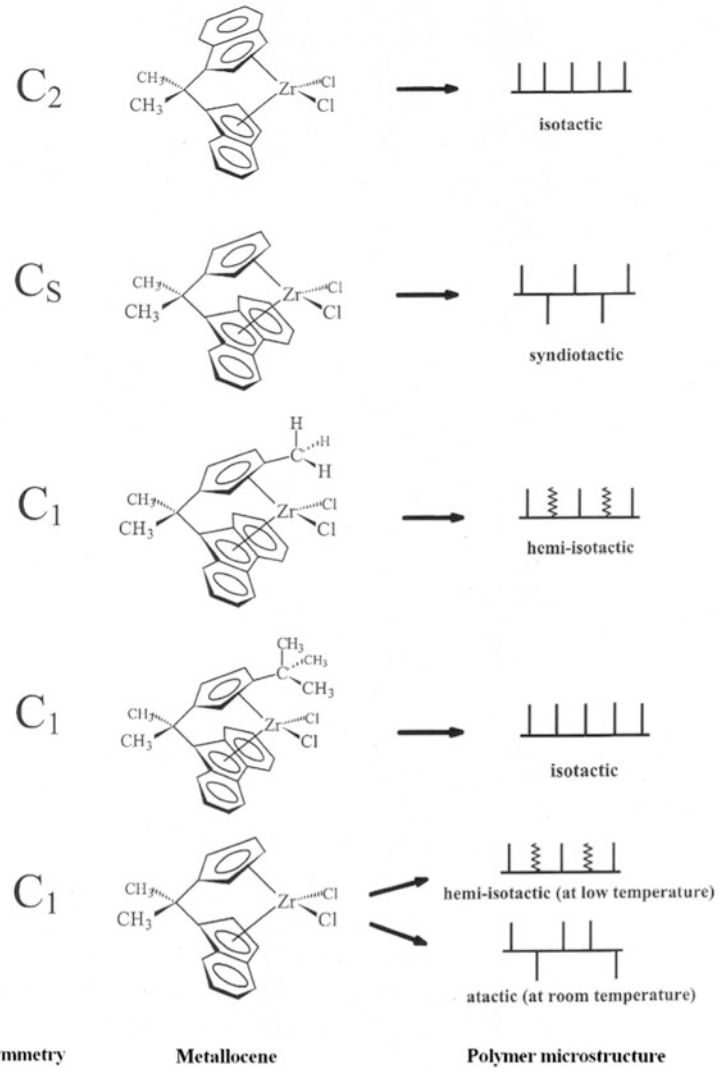

Fig. 18 Symmetry and structures of metallocene catalysts in relation to the microstructure of the polymers formed

contributions on this theme, e.g., from Busico [27], Kaminsky and Sinn [28], and Brintzinger and Fischer [29].

The chiral metallocene-based catalysts are characterized by a defined active center, forming a sound basis for establishing relationships between the molecular structure of the catalyst and the microstructure of the resulting polymer. Catalyst–polymer correlations are addressed using approaches ranging from symmetry-based rules [30, 31] (as illustrated in Fig. 18) to more elaborate computational approaches that attempt to accurately predict the polymer microstructure (see below).

3.1 Mechanism of Stereochemical Control

Breaking away from the symmetry considerations (summarized in Fig. 18), Fink, Angermund and coworkers [32] developed a uniform model that accurately describes the experimental microstructures of the polymers by means of four lowest-energy conformers of the metallocene species coordinating the prochiral propylene (R_{re}, S_{re}, S_{si}, R_{si}) and the positional changes that the polymer chain undergoes during insertion (*R* and *S* relate to the configuration of the Zr center; re and si relate to the different coordinations of the α-olefin).

The relative energy levels of the four diastereomers were determined by molecular modeling calculations [32, 33]. Figure 19 demonstrates as examples the R_{re}-π complex conformers of four zirconocene(propylene)(isobutyl) species. In Fig. 20, the relative energies of four diastereomers (I–IV) are compared for four zirconocenes – each differently substituted at the Cp ring.

It becomes clear that it is not the symmetry of the catalysts that is decisive for the stereospecificity, but the energy graduations, in particular the size of the energy gap between the individual diastereomeric states. Thus, catalyst I operates syndiotactically because $R_{re} = S_{si} < S_{re} = R_{si}$; catalyst II hemiisotactically because $R_{re} < S_{re}, S_{si}, R_{si}$; catalyst III isotactically because $R_{re}, S_{re} < S_{si}, R_{si}$; and catalyst IV atactically because $R_{re} \approx S_{re}, S_{si}, R_{si}$. The "symmetry rule" still applies, but is not the decisive factor and is only a subordinated aspect of the more uniform model.

To find out whether the stereospecificity of a catalyst should ultimately be determined at the transition state of the rate-determining reaction step, Angermund, Jensen and coworkers [34, 35] recalculated the system using density functional theory (DFT). This computational approach is based on the simplest possible combination of quantum chemistry (QM) and molecular mechanics (MM). The geometry of the central part, where bond breaking and bond forming takes place (termed aggregate), was first optimized in a separate DFT calculation and then later used "as is" in a series of force field-based calculations. As an example, Fig. 21, left, shows the structure of a transition state optimized in this way for the insertion of propylene in the zirconocene cation [*i*Pr(3-Me-Cp)(Flu)Zr(propylene)(isobutyl)]$^+$ with the four-membered ring as central part (aggregate) [36]. For an exact description of the course of stereospecificity, four different transition state conformers are also necessary here (shown in Fig. 21, right).

Furthermore, supposing that the single insertions occur independently of each other, these relative transition state energies are converted via a suitable averaged Boltzmann statistic into the corresponding pentad distributions, which are representative for the sequence of five transition states. These theoretical pentads are in very good agreement with the experimental pentads at low and intermediate temperatures, which proves that stereoregulation (i.e., the stereosequence of a polymer chain and the stereo-errors) can be calculated and predicted with this model. Stereo-errors occur as a result of insertion with the wrong enantiofacial orientation of propylene (triad errors), and this route of insertion becomes more important with rising temperature. At temperatures >50°C discrepancies occur

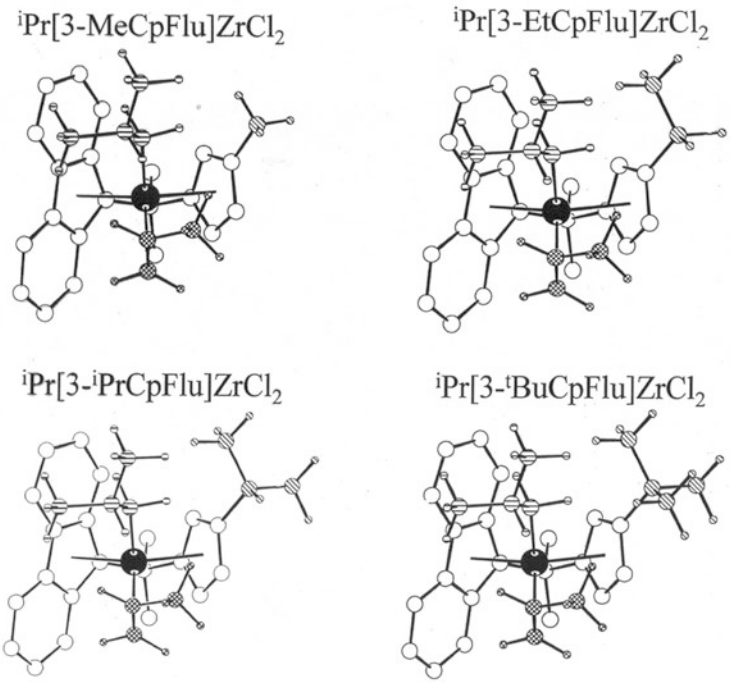

Fig. 19 R_{re}-conformers of four [*i*Pr(3-R-Cp)(Flu)Zr(propene)(isobutyl] catalyst species with different substituents at the Cp-ring (R = Me, Et, *i*Pr and *t*Bu); minimum-energy force field calculations

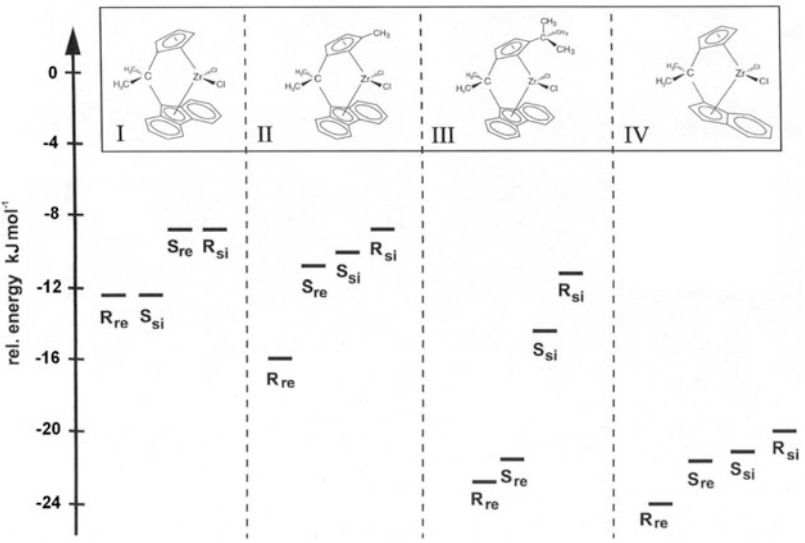

Fig. 20 Comparison of the energy differences between the diastereomers for the catalysts I–III and IV

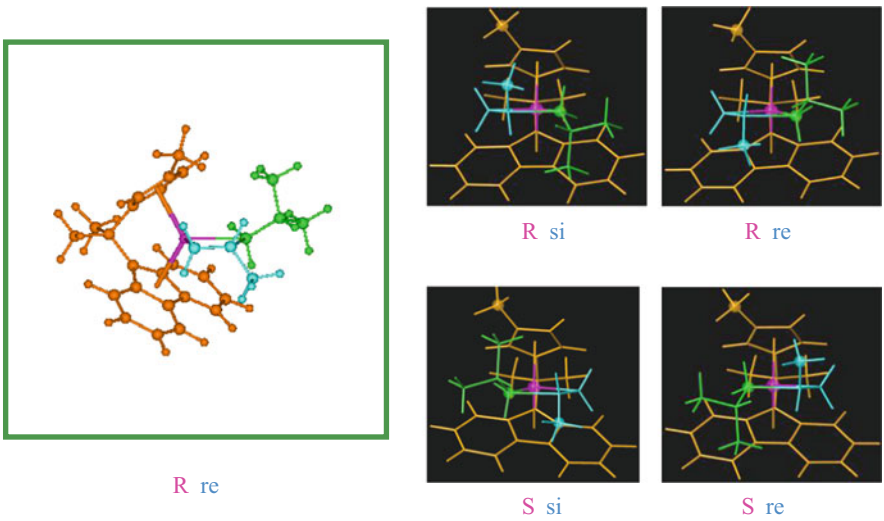

Fig. 21 Transition state of the cation [*i*Pr(3-Me-Cp)(Flu)Zr(propene)(isobutyl)]$^+$ optimized with density functional theory calculations [36]

between calculated and experimental pentad distributions. One reason could be the inversion of the growing chain at the Zr center after an insertion and before the coordination of the next monomer ("back-skip" of the polymer chain); this process generates dyad stereo-errors. Other reasons can be the epimerization reaction of the last inserted monomer [37], transfer reactions, or regio-errors such as 2,1-insertions of the olefin.

3.2 Stereospecific Propylene Polymerization: The Rotation Effect, an Insight into Mechanistic Detail

Figure 22 deals with the MAO-activated propylene polymerization of a series of metallocene catalysts (see Figs. 18 and 19) having a substituent of increasing steric demand at the cyclopentadienyl ring. To each catalyst is appointed the syndiotactic (rrrr), hemiisotactic, or isotactic (mmmm) NMR pentads (%). These pentad distributions are measured from samples polymerized at 10°C and 70°C.

The top entry in Fig. 22 shows the catalyst *i*Pr[Cp][Flu]$ZrCl_2$ with the basic ligand framework of this series. It has a highly syndiotactic behavior at 10°C with 93.1% rrrr and a statistic atactic behavior at 70°C with 58.6% rrrr. Hence, the syndiotacticity decreases with increasing temperature because of stereo-errors through the more distorted ligand framework.

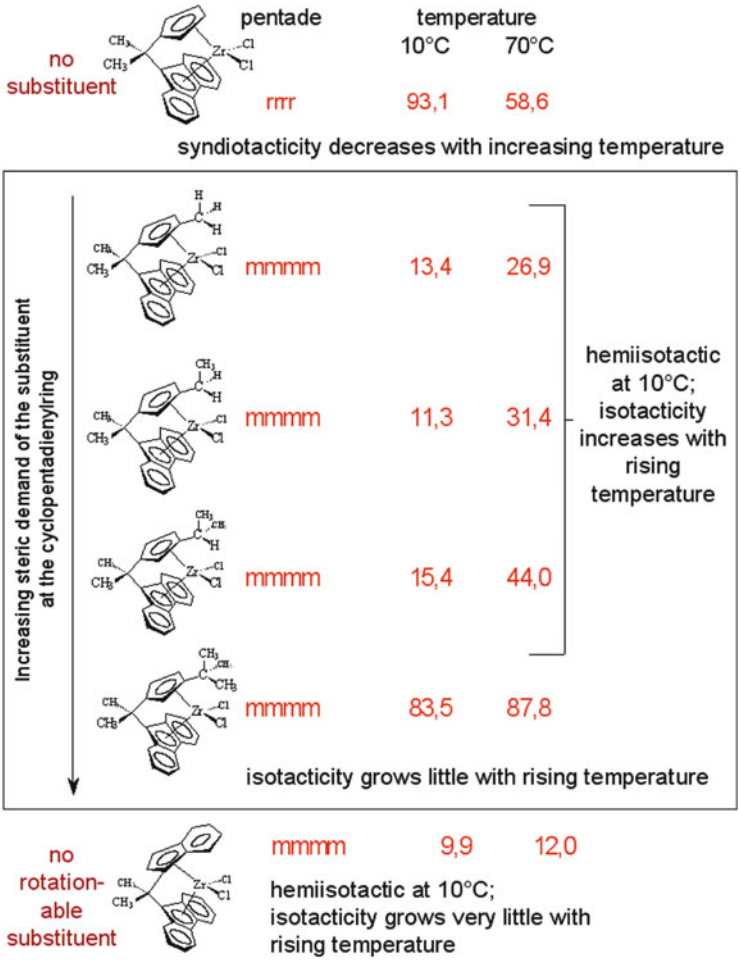

Fig. 22 Stereospecific propylene polymerization: the rotation effect

The catalyst *i*Pr[3-Me-Cp][Flu] $ZrCl_2$ (first line in the box), with a methyl group at the Cp ring, shows hemiisotactic behavior at 10°C with a mmmm pentad of 13.4%, and increases the isotactic pentad to 26.9% with rising temperature up to 70°C. The catalyst *i*Pr[3-Et-Cp][Flu] $ZrCl_2$, with the bulkier ethyl group at the Cp ring, further increases the isotacticity with rising temperature from 11.3% at 10°C to 31% at 70°C. The catalyst *i*Pr[3-*i*Pr-Cp][Flu] $ZrCl_2$, with the even more bulky isopropyl group at the Cp ring, again further increases the isotacticity from 15.4% to 44% with rising temperatures, i.e., by nearly a factor of three. The catalyst *i*Pr[3-*t*Bu-Cp][Flu] $ZrCl_2$, with the most sterically demanding tertiary butyl group at the Cp ring, shows highly isotactic behavior, with scarcely any alteration with rising temperature (only from 83.5% to 87.8%).

What is the reason for this behavior?

We think that there is a rotation influence caused by the substituent at the Cp ring. With increasing reaction temperature, the rotation volume of the substituent is enhanced and the effect is stronger for higher steric demand of the group. In other words, with rising temperature, the catalysts substituted on the Cp ring with 3-Me, 3-Et, and 3-*i*Pr resemble more and more the *i*Pr[3-*t*Bu-Cp][Flu] $ZrCl_2$ catalyst and its stereospecific behavior.

We wanted to prove this mechanistic hypothesis and synthesized a catalyst with the same basic ligand framework, but with a non-rotatable substituent at the Cp ring. This catalyst is shown in Fig 22 below the box. Its stereospecific polymerization behavior lies between hemiisotactic and atactic and, indeed, scarcely changed with rising temperature. Hence, the mechanistic hypothesis of the rotating group seems to be true. *Quod erat demonstrandum*!

4 Silica-Supported Metallocene/MAO Catalysts

Metallocenes immobilized on solid support materials have been successfully introduced in industry as polymerization catalysts for the production of new, application-oriented polymer materials (see also the contribution of Brintzinger and Fischer [29]). Industrial polymerization processes, which are carried out either as a slurry process in liquid propylene or as a gas-phase process, require that catalysts are used in the form of solid grains or pellets; soluble metallocene catalysts thus have to be supported on a solid carrier (so-called drop-in catalysts).

An additional objective of the heterogenization process was to combine the advantages of homogeneous metallocenes with those of supported catalysts. On the one hand, it was intended to preserve the advantages of homogeneous metallocenes, such as the high activity, narrow molecular weight distributions, stereospecificity, and uniform comonomer incorporation. On the other hand, it was intended to combine these features with the properties of supported catalyst technologies, such as controlled particle growth and formation of morphologically uniform polymer particles of the desired size and shape, which mirror the starting catalyst particles but are at least 20 times their size and show high bulk density and no reactor fouling.

4.1 Polymerization Kinetics and Polymer Particle Growth

An important aspect of olefin polymerization with solid catalysts concerns the characteristics of particle growth during the course of polymerization, taking into account the aspects of mass and heat transfer. Ineffective monomer transfer can limit catalyst productivity, while ineffective removal of polymerization heat from the growing particle in the early stages of polymerization can cause the formation of hot spots, which may in turn lead to catalyst decay. In the absence

of prepolymerization, exotherms of up to 20°C have been measured for individual catalyst particles in the early stages of polymerization [38]. Furthermore, the catalyst particles have to be mechanically stable to avoid disintegration and formation of polymer fines; however, they have to be sufficiently fragile to permit fragmentation into primary particles of submicrometer size by the hydraulic forces of the growing polymer. The morphology of the starting support is replicated in the final polymer so that a spherical support in the size range of 50–100 μm will give a spherical polymer morphology with particle sizes in the range of 1,000–3,000 μm, depending on the catalyst productivity. In this way, each polymerizing particle can be considered as a single microreactor with its own mass and heat balance [39].

For instance, the kinetics of a propylene polymerization promoted by SiO_2-supported metallocene catalysts depends on various factors: the applied reaction engineering (gas-phase, bulk, or slurry-polymerization), the degree of catalyst/cocatalyst distribution on the support, and the reaction conditions and parameters chosen.

High polymerization temperature and concentration of active species on the support lead to an increase in polymerization activity, as does a high monomer concentration in the reacting solution. A detailed kinetic investigation, however, is facilitated by choosing especially mild reaction conditions (low temperature, low catalyst concentration, low monomer concentration). In doing so [40, 41, 44, 45], it is possible to resolve the individual phases of polymerization and polymer growth from the start of the reaction. The polymerization rate–time plot (Fig 23a) shows a course that is characteristic for these systems. The reaction starts with a short increase in activity, the "prepolymerization period," followed by a drop in the polymerization rate to almost zero. The low level is kept for some minutes; in the case of supported metallocene catalysts, the length of this "induction period" can vary distinctively. After the induction period, the activity rises again ("polymer growth") until a plateau of maximum activity is reached ("particle expansion").

These individual kinetic stages of the propylene polymerization can be interpreted as follows. During the prepolymerization stage, the polymer forms a regular thin layer around the particle, which partially continues to grow into the marginal areas of the micro- and mesoporous silica gel (Fig. 23b). The layer of highly crystalline polypropylene (up to 75%) serves as a diffusion barrier for following propylene and induces the period of very low activity.

After this diffusion phase, successively active centers in the inner part of the particles are also provided with monomer and polymer growth from the outside to the inside continues. Because of the hydraulic forces from the growing polymer, fragmentation of the SiO_2 support from the surface to the interior occurs (to consider as "shell-by-shell" or "layer-by-layer" fragmentation). Consequently, new active centers are released and the overall polymerization rate increases until the highest possibly activity is reached and the whole support is fragmented in the polymer.

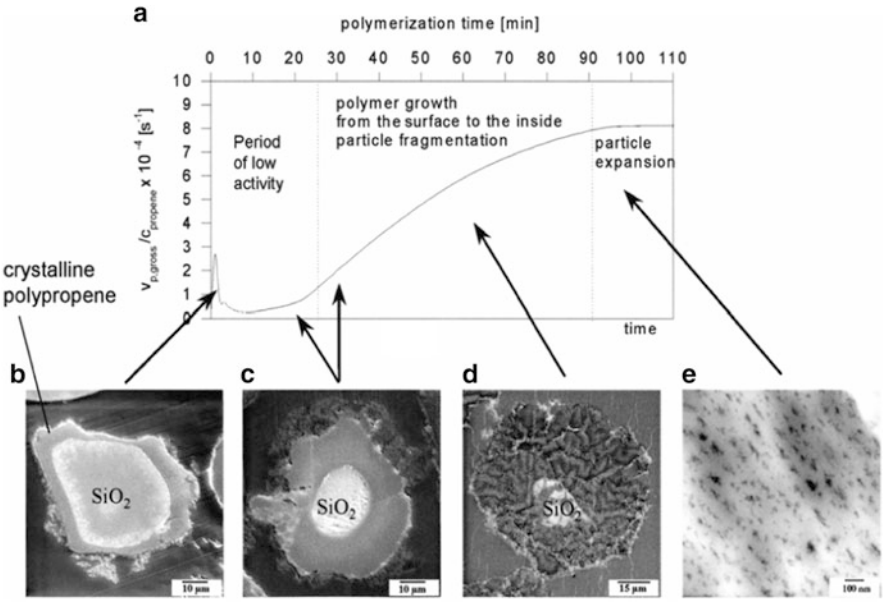

Fig. 23 Propylene polymerization with a silica-supported metallocene/MAO catalyst. (**a**) Plot of polymerization rate against time. Electron microscope images of particles at stages of (**b**) prepolymerization, (**c**, **d**) particle fragmentation, and (**e**) particle expansion. See text for details

This progression of the fragmentation has been characterized by electron microscopy analysis of cross-sections of single polymer particles (Fig 23c, d). The SiO_2 support material, which was initially composed of particles 30–60 µm in size, passes through the fragmentation phase and corresponds finally to the primary particles, here 10–20 nm in size, within the polymer matrix (Fig 23e), which expanded with progressing polymerization. Now the number of active centers no longer increases; however, the amount of polymer increases and consequently the size of the polymer grains.

It could also be demonstrated that a very rapid passing of these stages occurs when the polymerization is carried out in liquid propylene [45–47]; this means that the industrially important bulk polymerization can also be exactly described by this "polymer growth and particle expansion model" [41–43, 48].

It is also evident that, considering the diffusion processes, the diameter of the catalyst particles will have an important influence on the kinetics and total activity. The smaller the particle diameter, the shorter are the diffusion paths, the shorter is the induction period, and the faster the polymerization rate increases. Another reason could be the particle fragmentation, which starts earlier for small particles because a lower volume is connected with less diffusion limitation of the polymer layer.

Based on these kinetic and microscopic observations, the total polymerization process of SiO_2-supported metallocene catalysts can be described as a shell-by-shell

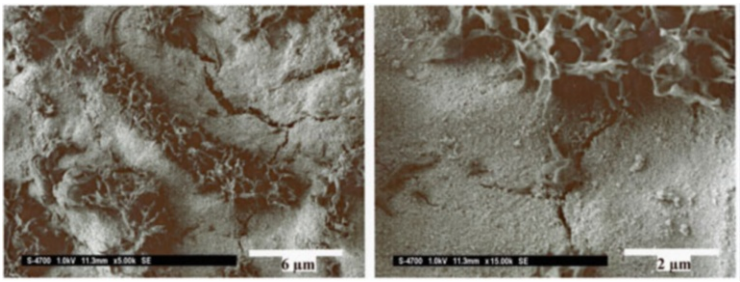

Fig. 24 Enlarged SEM micrographs of a deactivated catalyst surface after 5 min polymerization time: *left*, polypropylene growth; *right*, nascent polymer

fragmentation, which progresses concentrically from the surface to the center of the support particles. This comprehensive kinetic and mathematical polymer growth and particle expansion model [41, 48] – based on the ideas of the multigrain model [49–51] and extended for this complex polymerization process – includes the rate constants for all relevant activation, propagation, transfer, and termination steps and also for the different diffusion coefficients.

It was intended to observe the initial polymer growth directly below the forming polymer shell. Therefore, the active centers on the particle surface were specifically deactivated, and a catalyst prepared in such a way was used for propylene polymerization. The SEM micrographs presented in Fig. 24 show the surface of a particle polymerized for 5 min. A heterogeneous polymer growth takes place, producing polymer strings of defined structure. These strings clearly derive from the subsurface of the particle. They break up the porous silica gel layer and thereby enable further fragmentation of the support. As a consequence of the turbulent mixing of the catalyst particle in the reactor, the position of the polymer strings on the surface is disordered.

These SEM investigations show for the first time how the polymer, which is formed in the pores of the silica gel, is able to use hydraulic forces and mechanically break up the structure of the support, thereby setting free new active centers.

Other types of supports have other physical and mechanical properties and therefore different fragmentation behavior and kinetic characteristics. $MgCl_2$ as a support fragments much earlier and extensively even at low polymer yields because it consists of loose agglomerations of many small crystalline subparticles [52–54]. Hence, here the polymerization rate shows no initial period of low activity, but immediately rises steeply, passes through a maximum, and decelerates slowly in a diffusion-controlled manner. A similar kinetic behavior is observed when reversibly aggregated polymer latex nanoparticles are used as support. In ethylene slurry polymerization [55], the monomer at once has access to the primary latex particles so that polymerization and macroparticle growth start immediately and rise steeply.

5 Video Microscopy for the Investigation of Gas-Phase Polymerization

Detailed insight into particle growth and fragmentation processes is available using a new innovative tool: video microscopy [44, 56–64]. This technique, first applied by Reichert [65], enables the simultaneous detection of the individual behavior of a large number of single catalyst particles in gas-phase polymerization. In addition to visualizing polymer growth and the replication of catalyst grain through polymer grain morphology, it is able to provide detailed information about the polymerization kinetics of numerous catalyst particles.

The experimental set-up for video microscopy consists of a combination of a 50-mL gas-phase reactor with a microscope connected to a high-resolution digital camera that allows the observation of single catalyst grains during the whole polymerization [44].

Figure 25 shows the projection areas of growing particles after 0, 20, 40, and 60 min of polymerization (Fig. 25a) and demonstrates the particle growth evaluation (Fig. 25b). These collected images are processed to determine the projection area of each catalyst particle. Although the projection area is the primary quantity measured, it is easier to comprehend the size of the particles in terms of their diameter and volume. Hence, the projection area is used to estimate the diameter of a circle of equivalent area (equivalent circle diameter, ECD) and from that the volume of a sphere having an equivalent projection area (equivalent sphere volume, ESV).

Figure 26 shows ESV curves in dependence on time for 40 ethylene (1 MPa) polymerizing grains with a metallocene/MAO catalyst supported on SiO_2. The inset represents the "starting phase" of the microreactors and demonstrates the "induction period" of a silica-supported metallocene system. The individual behavior of the particles is more strongly pronounced in the subsequent acceleration (layer-by-layer fragmentation) phase shown in Fig. 26 and can be partly attributed to an inhomogeneous distribution of the catalyst and cocatalyst throughout the particle [46] or partly to impurities in the monomer gas, which deactivate the surface of the catalyst particles; this affects smaller particles more than larger particles.

The kinetic profile is even clearer after the differentiation of the particle volume with time. Hence, in Fig. 27, the derivative d_{ESV}/dt is plotted versus polymerization time for several particles of Fig. 26. The resulting "polymerization rate"–time curves are normalized then to the initial particle volume, ECD_0. Again, different rate maxima can be observed.

At this point, it is very useful to calculate from these dESV/dt curves the activity of a single grain in $g_{polymer}\ mol_{Zr}^{-1}\ h^{-1}$ (this is important for comparison with results from industrial processes) or the polymerization rate in mol $L^{-1}\ s^{-1}$ (this is important for comparison with other catalyst systems and their polymerization kinetics). But, for this evaluation, knowledge of the density of the expanding

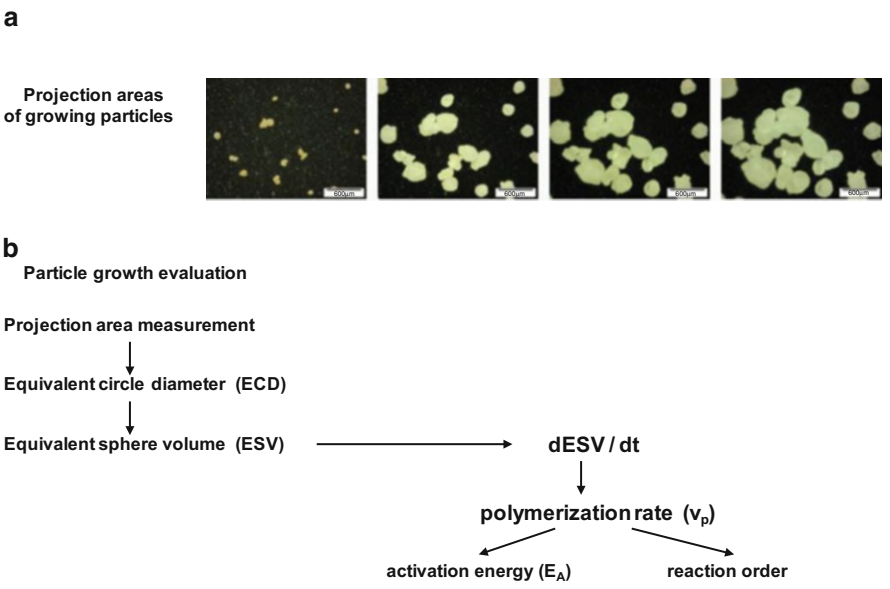

Fig. 25 Video microscopy: particle growth evaluation

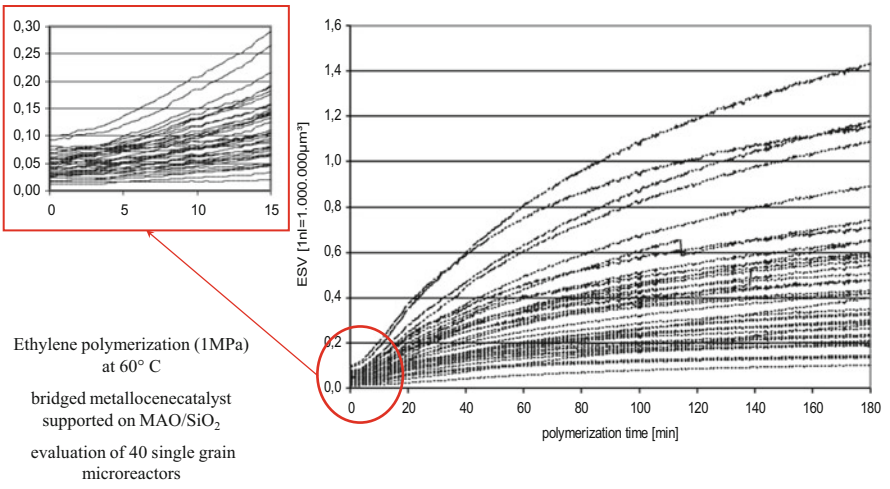

Fig. 26 Video microscopy kinetics: "time conversion curves"

catalyst–polymer grains, which changes during the polymerization, is necessary. To overcome this "density problem" [64], which is an unsolved question in the literature, the densities during the course of polymerization have to be determined with additional experimental series for each system [64] (see Figs. 28 and 29).

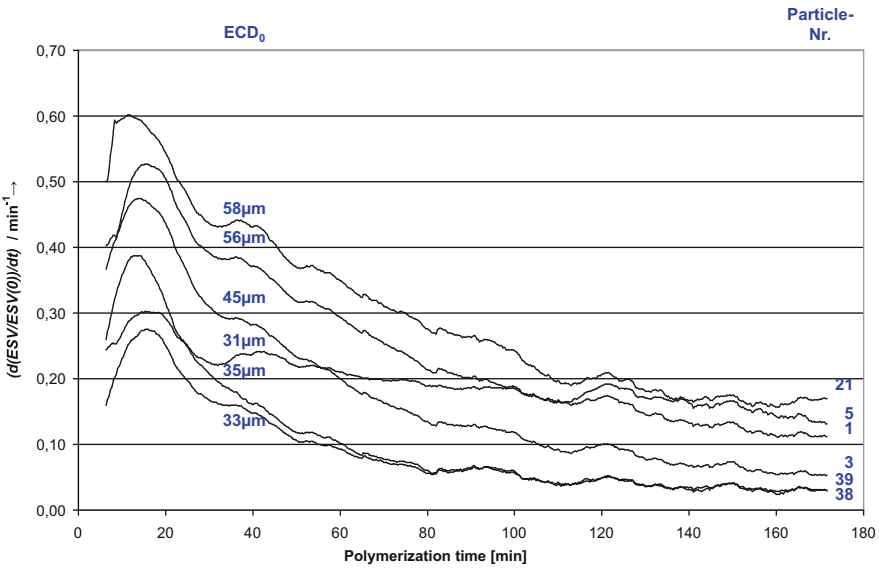

Fig. 27 Video microscopy kinetics: "polymerization rate–time profiles" for several particles

$$v_{P_{MAX}} = \frac{dESV/dt_{MAX} \cdot d_{PE}}{V_R \cdot MG_E \cdot 60}$$

v_p: polymerization rate [mol_E/l s]
$dESV/dt_{max}$: maximum of the differentiated ESV-profiles [cm^3/min]
d_{PE}: PE density [g/cm^3]
MG_E: ethylene molecular weight [g/mol]
V_R: reactor volume [l]

Fig. 28 Kinetic investigation of the density problem

As a further demonstration of the potential of the video microscopy analysis, Ferrari et al. [63, 64] applied this technique to the gas phase copolymerization. Figure 30 shows the results of an ethylene/propylene copolymerization with an industrial $MgCl_2$-supported $TiCl_4/AlEt_3$ Ziegler-catalyst system.

The particles in Fig. 30 represent an excellent replica of the catalyst particle distribution through the polymer particle distribution; the spherical form of the initial particles is retained and the equivalent circle diameters are enlarged from about 90 µm to about 360 µm after 190 min polymerization time. Their dependence on time indicates a very active catalyst system with a fast copolymerization rate and a fast particle expansion caused by the loosely agglomerated $MgCl_2$ support and the volume increase of the amorphous copolymer. It seems that this copolymerization system follows the multigrain model.

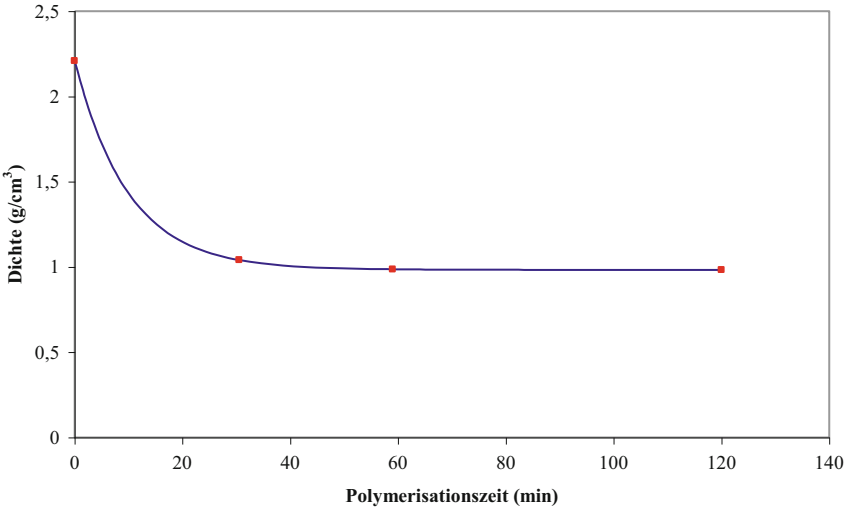

Density measured after 0, 30, 60 and 120 minutes polymerization at 50°C and 0.2 MPa ethylene; generation of a Fit-Function to convert the ESV into single particle activity in $g_{PE}/mol_{Zr}h$.

Fig. 29 Particle density change

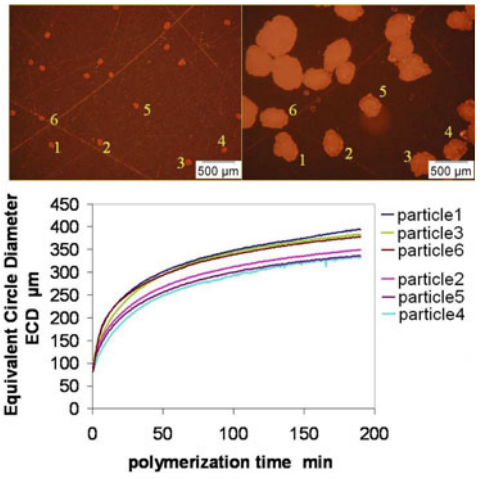

Fig. 30 Ethylene/propylene copolymerization (gas feed ratio 0.25) with the Ziegler-catalyst system $TiCl_4/AlEt_3$/external donor supported on $MgCl_2$ (0.2 MPa, 50°C): video microscopic snap-shots and kinetic evaluation of six particles

Hence, video microscopy analysis is not only a tool for screening of supported catalysts [66] but is also useful for the assignment of a given (industrial) catalyst system to the appropriate kinetic profile and the describing mathematical model. Finally, it is possible to explain certain aspects of crystalline homopolymer growth versus amorphous copolymer growth and the comonomer effect [63–66].

References

1. Haenel MW (2009) Historische Stätten der Chemie: Karl Ziegler. Max-Planck-Institut für Kohlenforschung, Mülheim An der Ruhr. English version available at www.kofo.mpg.de/media/2/D1105213/0478051227/Festschrift_e.pdf (Accessed 3 May 2013)
2. Martin H (1995) In: Fink G, Mülhaupt R, Brintzinger HH (eds) Ziegler catalysts: recent scientific innovations and technological improvements. Springer, Berlin, p 15
3. Martin H (2002) Polymere und Patente – Karl Ziegler, das Team, 1953–1998. Wiley-VCH, Weinheim
4. Breslow DS, Newburg NR (1957) J Am Chem Soc 79:5072
5. Natta G, Pino P, Mazzanti G, Gianinni U (1957) J Am Chem Soc 79:2975
6. Long WP (1959) J Am Chem Soc 81:5312
7. Chien JCW (1959) J Am Chem Soc 81:86
8. Meyer K, Reichert K-H (1970) Angew Makromol Chem 12:175
9. Reichert KH (1970) Angew Makromol Chem 13:177
10. Reichert KH, Meyer KR (1973) Makromol Chem 169:163
11. Fink G, Zoller W (1981) Makromol Chem 182:3265
12. Fink G, Rottler R (1981) Angew Makromol Chem 94:25
13. Schnell D, Fink G (1974) Angew Makromol Chem 39:131
14. Fink G, Rottler R, Schnell D, Zoller W (1976) J Appl Polym Sci 20:2779
15. Fink G, Rottler R, Kreiter CG (1981) Angew Makromol Chem 96:1
16. Fink G, Schnell D (1982) Angew Makromol Chem 105(15):31–39
17. Fink G, Fenzl W, Mynott R (1985) Z Naturforsch 40B:158
18. Mynott R, Fink G, Fenzl W (1987) Angew Makromol Chem 154:1
19. Fink G, Döllinger G (1981) J Appl Polym Symp 36:67
20. Cossee P (1964) J Catal 3:80
21. Arlman EJ (1964) J Catal 3:89–99
22. Natta G, Mazzanti G (1960) Tetrahedron 8:86
23. Patat F, Sinn H (1958) Angew Chem 70:496
24. Brintzinger HH, Fischer D, Mülhaupt R, Rieger B, Waymouth R (1995) Angew Chem Int Ed Engl 34:1143–1170
25. Kaminsky W, Külper K, Brintzinger HH, Wild FRWP (1985) Angew Chem 97:507
26. Ewen JA (1984) J Am Chem Soc 106:6355
27. Busico V (2013) Giulio Natta and the development of the stereoselective propene polymerization. Adv Polym Sci. doi:10.1007/12_2013_213
28. Kaminsky W, Sinn H (2013) Methylaluminoxane: key component for new polymerization catalysts. Adv Polym Sci. doi:10.1007/12_2013_226
29. Brintzinger HH, Fischer D (2013) Development of ansa-metallocenes for isotactic olefin polymerization. Adv Polym Sci. doi:10.1007/12_2013_215
30. Ewen JA, Mol J (1998) Catal A 128:103
31. Rappe AK, Skiff WM, Casewit CJ (2000) Chem Rev 100:1435
32. van der Leek J, Angermund K, Reffke M, Kleinschmidt R, Goretzki R, Fink G (1997) Chem Eur J 3:585
33. Kleinschmidt R, Reffke M, Fink G (1999) Macromol Rapid Commun 20:284

34. Angermund K, Fink G, Jensen VR, Kleinschmidt R (2000) Macromol Rapid Commun 21:91
35. Angermund K, Fink G, Jensen VR, Kleinschmidt R (2000) Chem Rev 100:1457
36. Thiel W, Angermund K, Jensen VR, Fink G (2002) In: MPG-Jahrbuch 2002, p 508. Max-Plank-Gesellschaft, München
37. Cipullo R, Busico V (1994) J Am Chem Soc 116:932
38. Pater TM, Weickert G, van Swaaij WPM (2003) AICHEJ 49:450
39. Böhm LL (2003) Angew Chem Int Ed Engl 42:5010
40. Steinmetz B, Tesche B, Przybyla C, Zechlin J, Fink G (1997) Acta Polym 48:3
41. Przybyla C, Zechlin J, Weimann B, Fink G (1999) In: Kaminsky W (ed) Metalorganic catalysts for synthesis and polymerization. Springer, Berlin, pp 321–333
42. Zechlin J, Steinmetz B, Zechlin J, Zechlin J, Tesche B, Fink G (2000) Macromol Chem Phys 201:515
43. Zechlin J, Hauschild K, Fink G (2000) Macromol Chem Phys 201:597
44. Knoke S, Ferrari D, Tesche B, Fink G (2003) Angew Chem 115:5244
45. Korber F, Hauschild K, Fink G (2001) Macromol Chem Phys 202:3329
46. Knoke S, Korber F, Fink G, Tesche B (2003) Macromol Chem Phys 204:607
47. Knoke S, Ferrari D, Tesche B, Fink G (2003) Angew Chem Int Ed 42:5090
48. Alexiadis A, Andes C, Ferrari D, Korber F, Hauschild K, Bochmann M, Fink G (2004) Macromol Mater Eng 289:456
49. Nagel EJ, Kirrillov VA, Ray WH (1980) Ind Eng Chem Prod Res 19:372
50. Hutchinson RA, Chen CM, Ray WH (1992) J Appl Polym Sci 44:1389
51. Debling JA, Ray WH (1995) Ind Eng Chem Res 34:3466
52. Ferrero MA, Sommer R, Spanne P, Jones KW, Conner WC (1993) J Polym Sci Polym Chem Ed 31:2507
53. Niegisch WD, Crisafulli ST, Nagel TS, Wagner BE (1989) Macromolecules 25:3910
54. Kakugo M, Sadatoshi H, Sakai J, Yokoama M (1989) Macromolecules 22:3172
55. Jang Y.-J, Bieber K, Naundorf C, Nenov N, Klapper M, Müllen K, Ferrari D, Knoke S, Fink G (2005) e-Polymers 2005:013
56. Abboud M, Denifl P, Reichert K-H (2005) Macromol Mater Eng 290:558
57. Pater JTM, Weickert G, van Swaaij WPM (2003) J Appl Polym Sci 87:1421
58. Pater TM, Weickert G, Loos J, van Swaaij WPM (2001) Chem Eng Sci 56:4107
59. Zöllner K, Reichert K-H (2001) Chem Ing Tech 73:707
60. Zöllner K, Reichert K-H (2002) Chem Ing Tech 74:585
61. Abboud M, Denifl P, Reichert K-H (2005) Macromol Mater Eng 290:1220
62. Pater JTM, Weickert G, van Swaaij WPM (2001) Chimia 55:231
63. Ferrari D, Fink G (2005) Macromol Mater Eng 290:1125
64. Ferrari D, Knoke S, Tesche B, Fink G (2006) Macromol Symp 236:78
65. Eberstein C, Garmater B, Reichert KH, Sylvester G (1996) Chem Eng Technol 68:820
66. Abboud M, Kallio K, Reichert K-H (2004) Chem Eng Technol 27:694

Adv Polym Sci (2013) 257: 37–58
DOI: 10.1007/12_2013_213

Published online: 30 May 2013

Giulio Natta and the Development of Stereoselective Propene Polymerization

Vincenzo Busico

Abstract This chapter looks back at the fascinating history of isotactic polypropylene, the first man-made stereoregular polymer, from the largely serendipitous discovery to the modern technologies for the industrial production of reactor blends with high-yield Ziegler–Natta catalysts featuring highly controlled morphology. This is also the story of a great man, Giulio Natta, winner of the 1963 Nobel Prize in Chemistry, and his team of incredibly talented young coworkers at the Milan Polytechnic, who in just a few years at the end of the 1950s elucidated the structure of the new polymer and that of the novel $TiCl_3$-based catalysts leading to its formation. The pioneering studies that followed on chain microstructure and the origin of the stereocontrol, and the first educated guesses on the nature of the active species, are critically reviewed, and re-visited with the aid of modern experimental and computational tools and methods, to highlight the current picture of what still represents a most important and lively area of polymer science and organometallic catalysis.

Keywords Isotactic · Polypropylene · Stereocontrol · Stereoselective polymerization · Titanium trichloride · Ziegler–Natta catalysis

Contents

V. Busico (✉)
Laboratory of Stereoselective Polymerizations (LSP), Department of Chemical Sciences, Federico II University of Naples, Naples 80126, Italy
e-mail: busico@unina.it

Fig. 1 Development of global installed capacity of the polyethylene and polypropylene industry (1958–2012) [1]

1 Premise

This chapter focuses on the birth and initial developments of Ziegler–Natta (ZN) catalysts for isotactic polypropylene (iPP). It's certainly not the first time that this story has been written (and won't be the last), but its charm has not faded. The dramatic sequence of lucky shots triggering Ziegler's and Natta's discoveries contributes some thrill, but the main power of the narration is that it tells about one of the most outstanding achievements of chemistry and the chemical industry, in an absolute sense, with an impact on society that can hardly be overestimated. A quantitative indicator is the global capacity of iPP production, which has been growing exponentially and is now close to an astounding 60 million tons/year, thus almost catching up to polyethylene production (Fig. 1) [1].

Albeit indirectly and ex-post, I was personally involved in the story as a coworker of Paolo Corradini and Adolfo Zambelli, the two associates of Natta who elucidated, respectively, the crystal structure and the microstructure of polypropylene. Moreover, a large part of my professional life (more than three decades, alas) has been dedicated to the stereochemistry of this fascinating polymer. I decided to let all this transpire from the pages, which may imply here and there a subjective opinion but no deliberate bias.

This chapter tries to combine a modern view with a historical perspective. This is because ZN catalysts were invented when polymer science was already robust, whereas the fundamentals of organometallic chemistry were still largely unknown and important elements for a correct interpretation of the early discoveries not yet available. A paradigmatic example is the starting idea of Ti as a cocatalyst [2],

plausible at a time when Ziegler's "Aufbau" reaction [3] was the only known process of ethene oligomerization under comparatively mild conditions, but much less so once the foundations of transition metal chemistry were in place. On the other hand, ZN catalysis is the most effective man-made reaction for making polymers, and therefore *any* ZN scientist *should* know about polymer chemistry and physics. In particular, a proper assessment of chain microstructure is key to understanding the properties of polyolefin-based materials and also in investigating the behavior of organometallic catalytic species, which remain elusive even now after 60 years of application. The subject has been treated exhaustively in several books and reviews [4–6].

One last introductory remark concerns the bibliography. Many key achievements of early ZN catalysis for iPP were only disclosed in patents, or appeared first in articles published in Italian journals and language. For the sake of simplicity, I will mainly refer to (more) easily accessible books and reviews in English, wherein interested readers can find detailed citations of the original literature.

2 ZN Catalysts for Polypropylene: Definition and Genealogy

According to Boor, who authored one of the first comprehensive books on the subject [7], a ZN catalyst is a combination of a transition metal compound and a main group metal-alkyl compound. Although the definition may look unrealistically broad (and in fact covers a huge number of combinations that are not active as olefin polymerization catalysts), it is a sensible one because active combinations have been reported for transition metals in almost all groups of the periodic table and a generous number of main group metals. In a sense it is instead too narrow, because it does not include the so-called main group metal-alkyl-free (MAF) catalysts, which are well-documented [8] albeit thus far irrelevant for application (with the very notable exception of heterogeneous Cr-based systems for polyethylene, known as Phillips catalysts [9] and starring in another fascinating story). One may also wonder if molecular (metallocene and post-metallocene) catalysts can or should be included in the definition; my personal view is that they can but they should not, because although the basic catalysis is the same, the activation chemistry and the high electrophilicity of the cationic active species introduce clear aspects of specificity compared with "classical" heterogeneous Ti-based systems [10]. Last but not least is the question of whether or not "Ziegler–Natta" is the correct designation for the latter systems, looking back at history and the patent litigations that went on for decades [11]. On this of course I have an opinion, like most others in the field, but it is a personal one and as such of very limited importance. The reason why I will refer to both catalysts and catalysis as "Ziegler–Natta" is for the *inclusive* character of this choice. This book celebrates the 50th anniversary of the Nobel Prize to two outstanding scientists named Karl Ziegler and Giulio Natta, and when I write about the marvelous chemistry that they started it seems natural to me to merge the two names into one.

Much less pregnant of implications but of some practical relevance is the classification of ZN systems for polypropylene [11]. I have always found it confusing to

identify a ZN catalyst in terms of "generations" and in the following I refrain from using a scheme that is not univocal. I prefer to set just one major divide between unsupported (or self-supported) $TiCl_3$-based catalysts [7] and ($MgCl_2$-)supported ones [11], and within the former to classify $TiCl_3$ polymorphs according to their crystal structure, i.e., as fibrillar (β) or layered (α, γ and δ) [12].

The emphasis of this chapter will be on the basic principles of ZN catalysis for iPP, rather than on iPP properties and applications. In particular, the objective is to illustrate the mechanism of asymmetric induction in the insertion of a monomer that has no functional groups other than a C=C bond, and yet reacts yielding a much larger enantiomeric excess than most highly functional substrates of enantioselective catalysis. That this occurs at the surface of simple and inexpensive inorganic solids is another amazing aspect that contributes to make ZN catalysts "unique and marvelous" [7].

3 From Ziegler's *Metallorganische Mischkatalysator* to ZN Catalysts

It is a fact that the impact of transition metals on olefin polymerization was discovered by accident. The details of how the accident occurred may vary somewhat depending on the literature source, but what is certain is that the fortuitous presence of traces of Ni in a reactor where ethene oligomerization at Al centers was being carried out changed the process into a selective dimerization [13]. I find this an example of how Fate challenges humans. Of all transition metals, Ni is one of the least suited to mediate polyolefin chain growth; the strong propensity of Ni-alkyl bonds to undergo β-H elimination make Ni-based catalysts mainly suited to oligomerization [14]. Indeed, Ni contamination in Ziegler's autoclave led to 1-butene, which is the shortest oligomer that can form from ethene polyinsertion under fast β-H elimination. Decades afterwards, elegant work by Brookhart and coworkers demonstrated that high molecular weight polyethylene can actually form in the presence of Ni-based catalysts bearing a proper ancillary ligand framework [15], but that's yet another story. For the one of interest here, Fate's verdict was: "Ni is no good for the 'Aufbau' reaction." In Ziegler's group, on the other hand, they knew about Sybilline oracles and re-phrased the verdict into a more general "[Transition] Metals can change the course of the 'Aufbau' reaction," and realized its vast implications. The systematic screening that followed was serendipitous and fortunate; nowadays, even a freshman student of organometallics would privilege early transition metals, but in 1953 Zr and Ti were just metals other than Ni. In the modern jargon of high-throughput experimentation [16], Cr was a "hit" and Zr a "lead." The real breakthrough followed, i.e., the combination of $AlEt_3$ and $TiCl_4$ [13]. What that meant for polyethylene can be read in a previous chapter of this book.

Why not polypropylene too? This embarrassing question may be given many different answers, but the simplest probably is that whoever finds a treasure tends to enjoy it for a while before searching for another. On the other hand, once it is known that somebody has found a treasure in a certain place, it is natural for others to

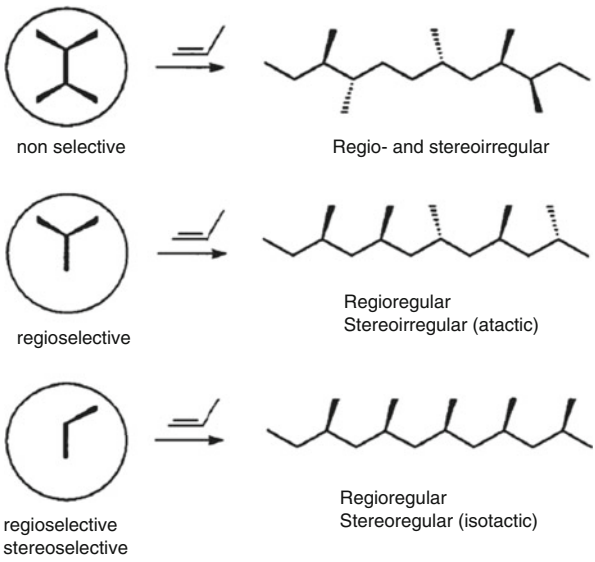

Fig. 2 The four possible insertion modes of propene in polypropylene chain propagation (adapted from [5])

search in the vicinity, just in case... Being a mushroom hunter, I have done that many times, usually with excellent results. Natta too knew about mushrooms, by the way.

Trying propene after ethene may seem obvious, but it actually isn't. The distance between the two monomers is, in a sense, larger than that between the Earth and the Moon. If we forget about the possibility of branches and differences in molecular mass, enchaining ethylene units gives just one chain structure; doing the same with propylene units can produce endless regio- and stereostructures [5, 6] (Fig. 2). It has been noted that a polypropylene chain 1,000-monomeric-units long can have 4^{1000} isomers, and to make all of them there is not enough C in the Universe! In view of this, not even the wildest dreamer would have anticipated that a trivial mixture of $AlEt_3$ and $TiCl_4$ gives rise to a partly stereoselective propene polymerization catalyst, and producing a hypothetical rubbery propene polymer probably did not look like a glorious target after high-melting linear polyethylene. Natta's precedents with butyl rubber may have originated a different opinion; in any case, believing that the process might result in something of interest and trying it out was his first merit. The famous laconic note "*Fatto il polipropilene*" ("Made polypropylene") that he wrote in his agenda on 11 March 1954 [11] to mark the synthesis of the first man-made stereoregular polymer is revealing of the man's character.

The discovery of iPP is a model case history of how a breakthrough can be transferred from a laboratory bench to industrial production. It took some 3 years from that 11 March 1954 to start the first commercial iPP plants in Italy and the USA, which is truly amazing; metallocene catalysts, to make a homogeneous comparison, have been struggling for decades, and those for iPP are not there yet [17]. The ingredients were a chemical company (Montecatini) with a long-term vision and a firm belief in research; a university professor combining uncommon scientific and managerial skills; and a consultancy agreement between the company and the professor

enabling the latter, inter alia, to call on bright young chemists and chemical engineers selected from all over Italy for academic or industrial positions (depending on need). The quality of those young scientists, incidentally, is demonstrated by the fact that by the 1960s most of them had become chair-holders and had founded schools of excellence at top Institutes in Italy and abroad, whose legacy has not entirely dispersed after half a century. All that could happen because the company trusted the professor, who fully deserved the trust, and a lean legislation and bureaucracy assisted in the endeavor. In Italy, and not only in Italy, this simple recipe was lost quite a while ago, which may be one reason for the present stagnation. Of course, that Ziegler was also a consultant for Montecatini, which was therefore aware about the "Nickel effect" and passed the information over to Natta almost in real time, was crucial for the following developments [11].

The original Ziegler's catalyst system, i.e., a mixture of $TiCl_4$ and $AlEt_3$ in heptane, was a rather poor catalyst for iPP; typically, less than 40% by weight of the produced polymer had a degree of stereoregularity resulting in high crystallinity and high melting temperature [7, 11]. Understanding that alkylated $TiCl_3$ was the real catalyst, discovering the polymorphism of $TiCl_3$, and finding new highly stereoselective catalyst systems for iPP based on the combination of the right polymorph(s) and Al-alkyl (s) were the achievements of Natta's group on the inorganic and organometallic chemistry side. Elucidating the stereostructure of the unprecedented new polymer (and many more deriving from the stereoselective polymerization of higher 1-alkenes, styrene, and conjugated dienes), on the other hand, was their monumental contribution to polymer science. By the end of the 1950s, the picture was practically complete. In retrospect, I honestly find that even a Nobel Prize is not an adequate reward for such an extraordinary enterprise.

4 The Structure of $TiCl_3$-Based ZN Catalysts for iPP

Under standard conditions, $TiCl_4$ is a readily hydrolyzable molecular liquid miscible with aliphatic and aromatic hydrocarbons, in which its tetrahedral molecules have no tendency to aggregate. When $TiCl_4$ and $AlEt_3$ are in contact in an aliphatic hydrocarbon (e.g., heptane) a reaction occurs, as is indicated by the immediate change of the liquid phase from colorless to yellow, and the progressive separation of a brown solid (rather slow below room temperature; faster above, in which case the color of the precipitate tends to darken and ultimately becomes black) [7, 11, 18, 19]. The process is believed to entail a first step of metathesis, leading to the formation of $TiCl_3Et$ and $AlEt_{3-x}Cl_x$ mixtures. $TiCl_3Et$ is metastable and decomposes homolytically into $TiCl_3$ and Et radicals; the latter mostly disproportionate to ethane and ethene, whereas the former aggregate into highly defective and partly ethylated $TiCl_3$ crystallites, precipitating from the nonpolar liquid in view of the predominantly ionic character of the bonding [7, 11, 18, 19]. Natta and coworkers discovered that this heterogeneous system was an active catalyst for the polymerization of propene, and unexpectedly found by X-ray diffraction that the polymer was partly crystalline, which evidently

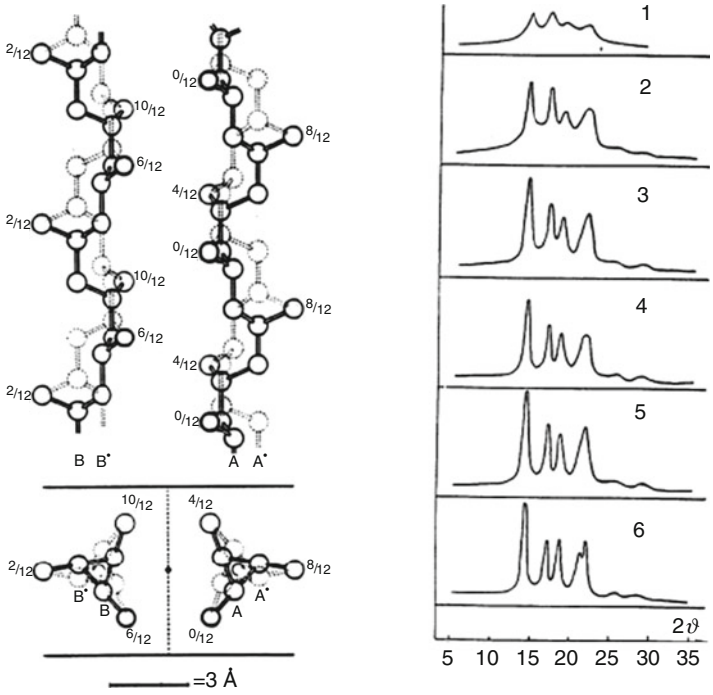

Fig. 3 *Right*: X-ray diffraction patterns of iPP fractions of increasing degree of stereoregularity (increasing from *1* to *6*), as obtained by solvent extraction from a raw sample produced with a $TiCl_4/AlEt_3$ catalyst system. *Left*: Enantiomorphous 3_1 helices in the crystal lattice of the stable iPP α-phase (adapted from [6])

called for chain stereoregularity, and therefore a stereoselective active species [7, 11]. Moreover, the ultimate melting point of the material when observed at the hot stage microscope exceeded 165°C, i.e., well above that of polyethylene!

The team in Milan had to face two major scientific problems: assign the structure of the new polymer and explain its genesis. The first part could be accomplished with a clever analysis of the X-ray diffraction patterns, recognized by Corradini [20; and references therein] as compatible with the 3_1 helical conformation anticipated by Bunn [21] for a hypothetical stereoregular hydrocarbon with the configuration that we now name "isotactic" after the suggestion by Natta's wife [11] (Fig. 3). I am not a believer in Lukacs' reflection theory [22], but I find it a fascinating coincidence that Watson and Crick published their fundamental work on the α-helix of DNA at about the same time [23].

Equally fast was the intuition that the formation of stereoselective active sites had to do with specific structural features of the solid catalyst surface, and the consequential decision to investigate its crystal lattice. This rapidly led to the discovery that $TiCl_3$ is polymorphic and that the different modifications can be grouped into two classes, with fibrillar (β) and layered (α, γ, δ) structures respectively [7, 11, 12]. Very recent quantum mechanics (QM) models of the ordered α, β, and γ phases [24], in full agreement with

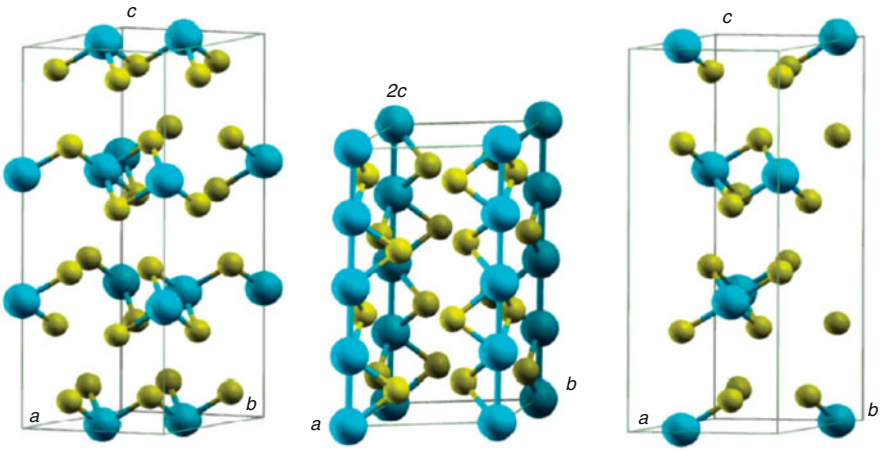

Fig. 4 QM models of unit cell in the crystal lattices of $TiCl_3$ in the α (*left*), β (*center*), and γ (*right*) phase (reproduced with permission from [24]; Ti and Cl are represented as *large dark* and *small light spheres*, respectively)

the conclusions of Natta, Allegra, and Corradini based on powder X-ray diffraction data [12], are shown in Fig. 4. All lattices look rather similar, with (quasi-)close-packed Cl atoms hosting the Ti atoms in one third of the available octahedral cavities. The main difference is the cavity occupation motif. This is mono-dimensional in the β phase, which can be viewed as an inorganic polymer with ideally infinite $(TiCl_3)_n$ chains where every Ti shares three Cl bridges with each first neighbor. In all other phases, the Ti atoms occupy alternate planes of octahedral cavities filled by two thirds, which results in identical Cl–Ti–Cl "sandwiches" (structural layers) held together by comparatively weak dispersive forces; the variable here is the stacking sequence of the Cl planes: $[AB]_n$ or $[ABC]_n$, respectively, in the α and γ phases; disordered in the δ phase.

Importantly, the said structural differences between fibrillar and layered polymorphs produce dramatic diversities with respect to electronic properties (apparent already on inspection: the β phase is brown in color, the layered ones are violet), magnetic behaviors [24], and – most relevant for catalysis – local configuration of Ti (nonchiral in the β phase, chiral in all others). Ziegler's good luck did not cover the latter feature; in fact, testing "violet" $TiCl_3$ (made, e.g., by reduction of $TiCl_4$ with H_2 or Al) in propene polymerization and finding that this was much more stereoselective than the "brown" counterpart (80% or more "highly isotactic" polymer instead of less than 40%) was entirely due to Natta's group [7, 11]. Theirs was also the discovery, a few years later, that using $AlEt_2Cl$ in the place of $AlEt_3$ can push the fraction of highly isotactic polymer up to 95% [7, 11].

Modern readers can hardly imagine the absolute novelty of those findings and the embarrassing inadequacy of vast sectors of the chemical community to assess or even understand them. As a matter of fact, until 1954 it was largely believed that stereoregular polymers can only have natural origin (as can be read in the motivation of the Nobel Prize to Natta [25]). That the world was just not ready is demonstrated

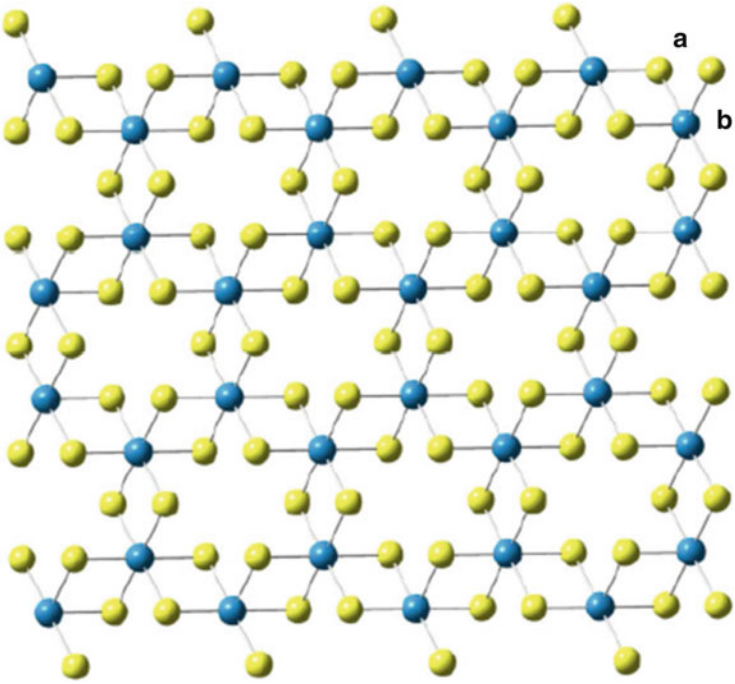

Fig. 5 QM models of 100-type (**a**) and 110-type (**b**) lateral terminations of a violet $TiCl_3$ structural layer (adapted from [27]; Ti and Cl are represented as *blue* and *yellow spheres*, respectively)

by the fact that it took one year for the first paper by Natta et al. to find a scientific journal that would dare to publish something seemingly too revolutionary to be true; on the other hand, the communication to the *J. Am. Chem. Soc.*, which appeared in March 1955 [26], was immediately saluted by unbiased polymer scientists (and in particular by Paul J. Flory) as a groundbreaking announcement.

The Δ or Λ configuration of Ti in violet $TiCl_3$ lattices, with three pairs of bent Cl bridges between first neighbors in the lattice, is shown in Fig. 5; the helical leitmotiv may call for undue but suggestive associations with the chain conformation of iPP. Relating the intrinsic chirality of Ti with the stereoselectivity of the active sites in propene polymerization was an easy logical process. Building up a detailed mechanism of asymmetric induction, on the other hand, took a long time and the contributions of many brilliant scientists [6]. The next milestone was the seminal work of Cossee and Arlman [28]. Moving from the structure of the bulk, they speculated that the basal 001 planes of violet $TiCl_3$ crystals cannot offer chemisorption sites and as such have no interest for catalysis, whereas lateral terminations of the structural layers (e.g., parallel to the 110 or 100 crystallographic directions) expose linear racemic arrays of enantiomorphic Ti centers, with two residual *cis* pairs of Cl bridges toward the crystal interior, one terminal Cl from the third broken bridge pair to ensure the electroneutrality, and one coordination vacancy (Fig. 5). Cossee proposed [29] that the catalytic species would form by metathesis of the terminal Cl with an alkyl group of the Al-alkyl cocatalyst;

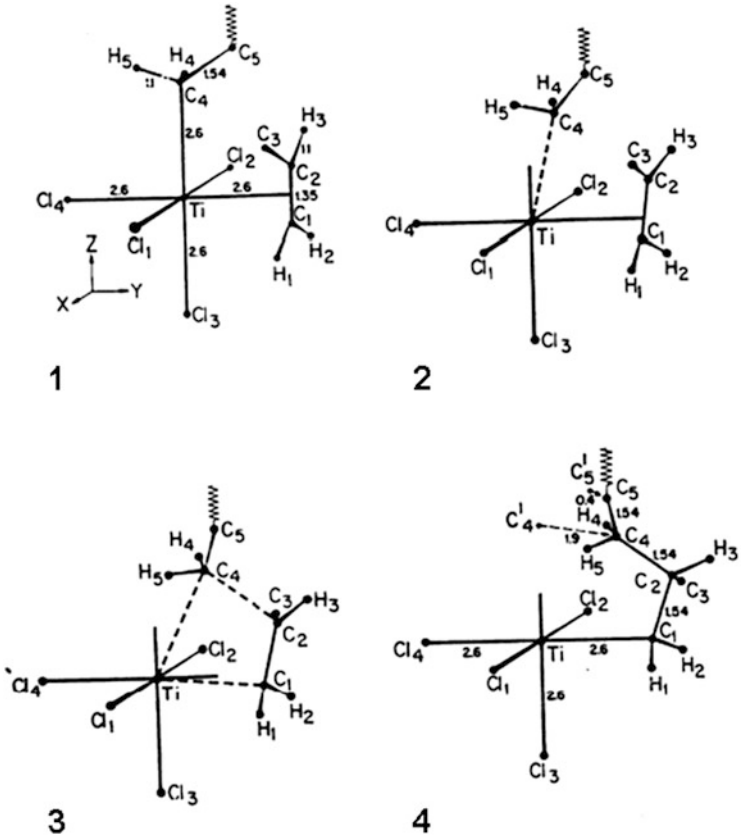

Fig. 6 The Cossee mechanism of chain-migratory propene insertion into a Ti–R bond on the edge of a violet $TiCl_3$ crystal (adapted from [29])

propene would then chemisorb at the remaining empty site of the octahedron and insert into the Ti–R bond, as schematically depicted in Fig. 6. I always found that drawing illuminating and like to make reference to it whenever I can; it elegantly anticipated the concept of "chain migratory insertion" [6], which is now part of the fundamentals of organometallic chemistry. The geometric representation of the reaction path, with the four-center insertion transition state, was incredibly accurate for the time (as a matter of fact, the various steps as depicted could well be snapshots taken from modern molecular dynamics simulations). Yet, that propene insertion would occur with 1,2 regiochemistry and be enantioselective due to site control [5, 6], opposite monomer enantiofaces being preferred at Ti centers of opposite chirality, were all and only educated guesses. Moreover, the steric contacts involved in the chiral recognition were not identified.

In the mid-1970s, with the development of ^{13}C NMR spectroscopy, the insertion regiochemistry and the site-controlled origin of the stereoselectivity could be experimentally confirmed by Zambelli and coworkers [30–32]. The unambiguous identification of predominant . . .*mmmmrrmmmm*. . .-type stereodefects in ZN iPP

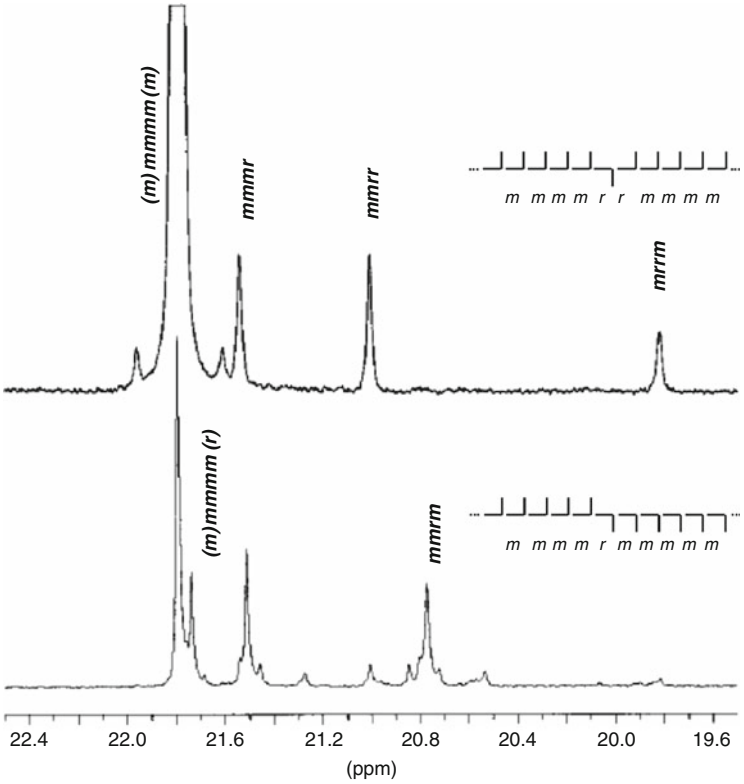

Fig. 7 ^{13}C NMR methyl fingerprints of typical iPP samples obtained under (*top*) enantiomorphic-sites control, and (*bottom*) chain-end control (adapted from [5])

chains by means of steric pentad analysis on the methyl resonance (Fig. 7; [*mmmr*]:[*mmrr*]:[*mrrm*]≈2:2:1, in agreement with the so-called enantiomorphic-sites chain propagation model [33]) was a classical early demonstration of active site "fingerprinting" from the polymer chain microstructure [6].

In the late 1970s, the resolution of the picture was further increased by the school of Corradini, with pioneering applications of molecular mechanics (MM) [34–36] providing a semi-quantitative character to Cossee's speculations. As is well-known, MM cannot evaluate transition states, and also due to the difficulties arising from the poorly defined set of geometries and potentials to be used in the calculations (which were among the first of their kind for organometallic systems) those studies can be viewed as the digital version of traditional stick-and-ball models. This does not diminish their value and rather demonstrates that limitations in tools can be overcome by means of intuition and imaginative thinking.

Figure 8 shows MM models of 100 and 110 terminations for a structural layer of α-$TiCl_3$ [34–36]. In the former case (Fig. 8a), a local C_2 axis relates the two coordination sites available for catalysis at each surface Ti atom, which implies their equivalence (homotopicity). In each of them, a growing polymer chain

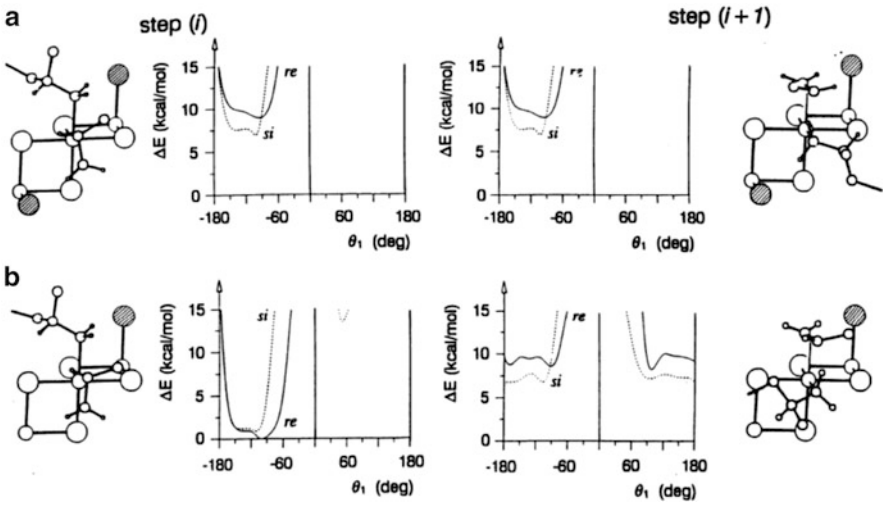

Fig. 8 MM models of catalytic species on 100 (**a**) and 110 (**b**) lateral terminations of an α-$TiCl_3$ structural layer. Consecutive insertion events under chain migratory regime are labeled step *i* and step (*i* + 1) (adapted from [36])

experiences repulsive nonbonded contacts with one of the Cl atoms of the surface (shaded in Fig. 8); as a result, the first C–C bond is conformationally constrained and chirally oriented. In turn, this was proposed to favor the 1,2 insertion of a propene molecule π-coordinated to the other site with the enantioface that directs the methyl substituent *anti* to the said C–C bond. On 110 model terminations (Fig. 8b), on the other hand, the absence of one of the two surface Cl atoms required for the orientation of the growing chain lowers the local symmetry of Ti to C_1, which makes the two active coordination sites non-equivalent (diastereotopic), and propene insertion as represented at step (*i* + 1) non-enantioselective. Therefore, chain propagation here can be isotactic only provided that monomer insertion occurs in preference as shown at step *i* (I will come back to this later).

The experimental confirmation to Corradini's model came, again, from ^{13}C NMR analysis, in this case of the polymer chain ends. In fact, Zambelli and coworkers found that for highly isotactic-selective ZN catalysts, the enantioselectivity of 1,2 propene insertion into initial Ti-[^{13}C-labeled]-alkyl bonds is different from that of the subsequent ones. They observed no enantioselectivity for insertion into a Ti–$^{13}CH_3$ bond and only partial (~80%) enantioselectivity for that into a Ti–$^{13}CH_2$–CH_3 bond, whereas the following propagation steps were almost completely enantioselective [37]. These findings highlighted the steric requirements for the asymmetric induction and proved, in particular, that for the onset of the stereocontrol the alkyl group bound to Ti needs to be a "chain," i.e., consist of at least two C atoms and preferably more [6].

As we shall see in next section, starting from the 1970s, violet $TiCl_3$-based catalysts gave way to $MgCl_2$-supported ones [11] and were practically abandoned before QM modeling had become feasible. To the best of my knowledge, the only

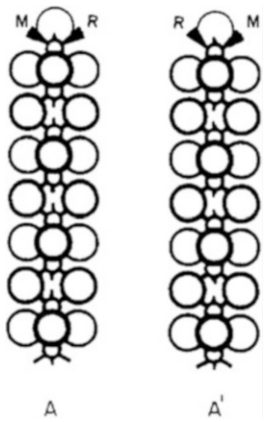

Fig. 9 Models (*A* and *A*′) of enantiomorphic active sites on the surface of a β-$TiCl_3$ crystal (adapted from [19]; *R* alkyl, *M* monomer)

available QM study is a PhD dissertation from my own research group [27] that investigated with periodic DFT-D methods – inter alia – the relative stability of possible crystal terminations for different $TiCl_3$ polymorphs. In brief, the conclusion was that, apart from trivial 001 planes, plausible surfaces indeed have the structures postulated in Figs. 5, 6, and 8. For α-$TiCl_3$, 100-type terminations (Fig. 8a) would be slightly lower in energy than 110-type (Fig. 8b); the calculated values of surface energy after full relaxation were 0.14 and 0.15 J m^{-2}, respectively. In the same work [27], it was also found that the chemisorption of $AlEt_2Cl$ on 110-type terminations at $\theta = 0.5$ (where θ is the degree of surface coverage), which is the highest allowed by steric interference between neighboring adsorbates, is exergonic and makes the residual exposed Ti centers rather similar to those on 100-type terminations, as far as the local coordination environment is concerned. A weaker chemisorption of $AlEt_3$ compared with $AlEt_2Cl$ might be the reason for the lower stereoselectivity of violet-$TiCl_3$/$AlEt_3$ catalyst systems than for violet-$TiCl_3$/$AlEt_2Cl$ ones. It should be noted, however, that no QM studies of catalytic reactivity for these surfaces have been published so far.

Also pending is an explanation for the partial stereoselectivity of catalyst systems based on β-$TiCl_3$. ^{13}C NMR analysis of the highly isotactic PP fraction demonstrates that the stereocontrol must be traced to inherently chiral active sites [19], but in this case the Ti centers in the bulk of the crystal are not stereogenic [12]. It was noted that the terminal Ti atoms of the fibrils are chiral if they bear three different ligands (e.g., one dangling Cl, the growing chain and the monomer; Fig. 9 [19]), but no quantitative studies of propene insertion were carried out. My own educated guess is that, under polymerization conditions, β-$TiCl_3$ crystallites are likely to reconstruct into more stable layered structures, at least locally. In fact, β-$TiCl_3$ is metastable and changes into the γ polymorph by thermal annealing at moderately high temperature (a few hours at 150–250°C). In the presence of $TiCl_4$, the transformation is much faster and occurs readily well below 100°C [11].

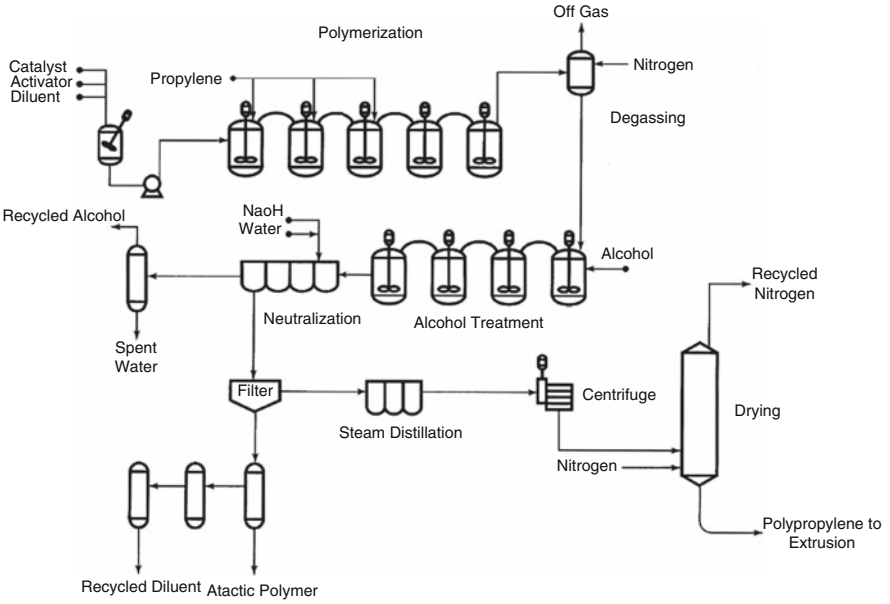

Fig. 10 Flow-chart of an early iPP production plant based on violet $TiCl_3$ catalysis (Hercules technology; reproduced with permission from [11])

5 From "Self-Supported" $TiCl_3$-Based to $MgCl_2$-Supported $TiCl_4$-Based ZN Catalysts

The schematic layout of an iPP production plant based on violet $TiCl_3$ catalysts in the 1960s is shown in Fig. 10 [11]. Notably, a large part of the plant was for operations other than polymerization, such as catalyst alcoholysis and neutralization and separation of the "highly isotactic" PP part from a "less tactic" part by filtration. The latter made it necessary to work in a low-boiling aliphatic hydrocarbon diluent, because the less tactic PP fraction is partly insoluble in liquid propene.

Polyolefins are low-value-added products and simplifying their production technology is of crucial importance. The main weak point of violet $TiCl_3$ was its comparatively low productivity. Even with catalysts characterized by high surface areas (such as those developed by Solvay, including weak Lewis bases such as ethers to stabilize crystallite terminations by means of labile chemisorption), 10–15 kg of iPP per gram of catalyst was the maximum achievable mileage [11]. Due to the acidity of Ti–Cl bonds, which readily hydrolyze liberating HCl, this value was still too low to avoid a cost-intensive polymer de-ashing procedure.

Supporting the active Ti species on an inert matrix, thus increasing the productivity referred to Ti, looked like an obvious solution to the problem. However, one should realize that in violet $TiCl_3$ the bulk of the crystal is not an innocent self-support because its structure determines that of the catalytic surfaces and in particular the stereogenic environment of the exposed Ti centers. As a matter of fact, when typical supports like

Table 1 Typical formulations and performance of $MgCl_2$-supported Ti-based ZN catalyst systems for iPP

Internal donor	External donor	Productivity[a]	Index of isotacticity[b]	M_w/M_n[c]
Aromatic monoester (e.g., ethylbenzoate)	Aromatic monoester (e.g., methyl-*p*-toluate)	0.5	>95	5–6
Aromatic diester (e.g., dibutyl-*o*-phthalate)	Alkoxysilane [e.g., $R^1R^2Si(OMe_2)$]	1–2	>97	5–6
2,2′-dialkyl-1,3-dimethoxypropane	Alkoxysilane [e.g., $R^1R^2Si(OMe_2)$]	>2	>97	3–4
Aliphatic diester (e.g., dialkylsuccinate)	Alkoxysilane [e.g., $R^1R^2Si(OMe_2)$]	1–2	>98	>7

[a] 10^3 kg(PP) g(Ti)$^{-1}$
[b] Wt% of highly isotactic PP
[c] Polydispersity index

calcined silica or alumina were impregnated with $TiCl_4$ and reacted with Al-alkyls for Ti alkylation/reduction, the results were very poor (at most, moderate activity in the polymerization of ethene; low or no activity and no stereoselecivity in that of propene) [11]. The breakthrough came, once again, serendipitously: highly active catalysts for ethene polymerization were obtained when $TiCl_4$ was supported on MgO, and it did not take too long to realize that (1) $TiCl_4$ chlorinates MgO to give $MgCl_2/TiCl_4$ adducts, and (2) $MgCl_2$ has a layered structure very similar to that of violet $TiCl_3$ (i.e., stacked Cl–Mg–Cl sandwiches with all octahedral cavities in between the two Cl planes occupied by Mg) [11].

Using authentic $MgCl_2$ as the support led to even better catalysts for polyethylene, whereas the performance for polypropylene was ambivalent: high productivity (>150 kg of polymer per gram of Ti) but poor stereoselectivity (less than 40% highly isotactic polymer) [11]. However, the addition of proper Lewis bases to the catalyst formulation (Table 1), as components of the solid precatalyst ("internal donor") or complexed with the Al-alkyl cocatalyst ("external donor"), improved both the productivity (up to 2–3 tons of polymer per gram of Ti) and the stereoselectivity (>95% highly isotactic polymer) [11, 38, 39].

Other chapters of this book cover modern "high-yield" $MgCl_2$-supported ZN catalysts [11, 38, 39]; here I will only elaborate on their structural relationships with violet $TiCl_3$. As a matter of fact, it is plausible to imagine that the chemisorption of $TiCl_4$ on lateral terminations of $MgCl_2$ structural layers, followed by alkylation and reduction of the adsorbates by an Al-alkyl, results into local environments mimicking the edges of authentic violet $TiCl_3$ structural layers. In other words, according to this hypothesis, $MgCl_2$ would act as a template for the epitaxial adsorption of $TiCl_n$ species (n=4 or 3) [6].

Giannini [40] and Corradini [41] were the first to extend to the new systems the crystallochemical approach used before by Cossee and Arlman (Sect. 4). Their starting point was the identification of plausible nontrivial $MgCl_2$ crystal surfaces, proposed to be 100 (with penta-coordinated Mg atoms) and 110 (with tetra-coordinated Mg atoms). According to a pioneering paper by Corradini et al. [41], precursors of stereoselective active species would result from the epitaxial chemisorption of $TiCl_4$

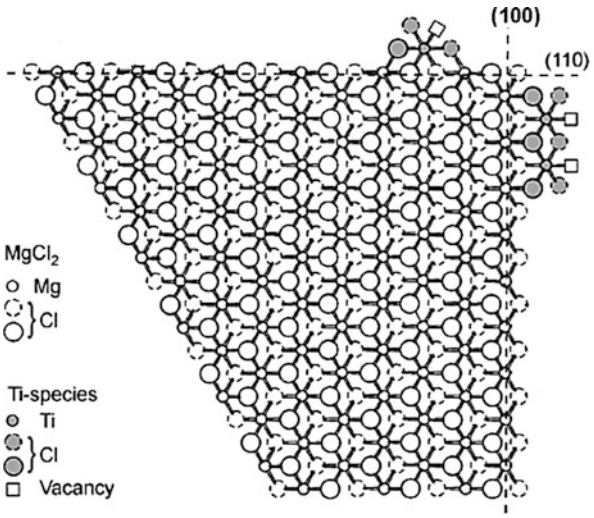

Fig. 11 Models of precursors of active $TiCl_3$ species on (100) and (110) edges of a $MgCl_2$ structural layer (re-elaborated after [41])

in the form of dinuclear Ti_2Cl_8 adducts on 100 $MgCl_2$ surfaces, whereas mononuclear chemisorption on 110 surfaces would lead to non-stereoselective (albeit chiral) active species (Fig. 11). The difference between the two would be the lack of steric hindrance necessary to enforce growing chain orientation in the latter case. In view of a postulated higher Lewis acidity, 110 surfaces were proposed [41] to bind Lewis bases in preference to $TiCl_4$, which would then prevent the formation of non-stereoselective sites; the role of Lewis bases in enhancing catalyst stereoselectivity would thus be *indirect* [6, 41].

^{13}C NMR and temperature rising elution fractionation (TREF) polymer characterization data, on the other hand, pointed to a *direct* effect of Lewis bases on site enantioselectivity; in fact, the highly isotactic polymer fraction yielded by catalysts modified with Lewis bases is not only much more abundant, but also more stereoregular compared with that of Lewis-base-free systems, while keeping the typical fingerprint of enantiomorphic-site control [42]. This suggests that Lewis base molecules are in nonbonded contact with the inherently chiral catalytic species, and shape their active pocket to make them better able to discriminate between the two enantiofaces of propene at the insertion step.

Recent periodic DFT(-D) (dispersion-corrected density functional theory) evaluations of relative stability for different $MgCl_2$ crystal surfaces concluded that well-formed α-$MgCl_2$ crystals should only feature basal planes and lateral terminations with penta-coordinated Mg (104 or equivalent) [43]. Surfaces exposing tetra-coordinated Mg (110 or equivalent) are appreciably higher in energy and should at most constitute a small minority [43]; on the other hand, they turned out to bind Lewis bases much more strongly, which should favor their formation in $MgCl_2$/Lewis base adducts [43–45]. The latest state-of-the-art QM calculations indicated that $TiCl_4$ chemisorption is also much stronger (and possibly even exclusive) on 110-type faces [46], which is in line with the results of recent vibrational spectroscopy studies [47, 48].

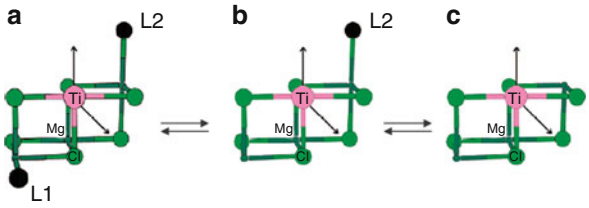

Fig. 12 The three-site model of active species for $MgCl_2/TiCl_4$/Lewis base catalyst systems; *L1* and *L2* generically denote chemisorbed Lewis base molecules. *a*, *b* and *c* are proposed to give rise to highly isotactic, poorly isotactic ("isotactoid") and (chain-end-controlled) syndiotactic polypropylene chain propagation, respectively (adapted from [50])

In view of the above, the current picture of $MgCl_2/TiCl_4$/Lewis base catalysts assigns a dominant role to 110-type $MgCl_2$ crystallite terminations [46–49]. A model of catalytic species reconciling all available experimental and computational evidence, including the observed formation of less tactic polypropylene fractions containing poorly isotactic and syndiotactic stereoblocks, is shown in Fig. 12 [6, 50]. The isotactic-selective species, in particular, is similar to the homologous model for violet $TiCl_3$ (Fig. 8) with respect to the Ti first coordination sphere, but features Lewis base molecules rather than Cl atoms to enforce the orientation of the growing polymer chain necessary for the onset of the enantioselectivity.

An important extra benefit of $MgCl_2$ as a support is the superior control over pre-catalyst morphology that it ensures [39]. Sophisticated technologies have been implemented for the production of activated $MgCl_2$ in the form of spherical secondary particles with controlled shape and porosity, even after the harsh protocols necessary for the chemisorption of $TiCl_4$ and the ID. With a proper pre-treatment (e.g., a mild pre-polymerization process "gluing" the primary particles together), once in the polymerization reactor such particles expand regularly under the hydraulic pressure of the product springing radially from the billions of constituent primary $MgCl_2$ nanoparticles, ending up with polymer granules faithfully replicating pre-catalyst morphology (Fig. 13, left). The advantages of this achievement can hardly be overestimated, ranging from improved control over reactor fluid dynamics to the possibility of production of in-situ finely dispersed polymer blends in reactor cascades (e.g., intimate mixtures of iPP and ethylene/propylene rubber known on the market as "impact-resistant" or "heterophasic" PP; Fig. 13 right) [39]. All this considered, one can conclude that $MgCl_2$ is a rare example of a nanostructured support dictating practically all aspects of catalyst behavior from the atomic to macroscopic scale, i.e., from stereoselectivity to morphology.

6 Concluding Remarks

It has been estimated that up to one half of all scientific discoveries are serendipitous in origin [51]. ZN catalysis, from $TiCl_3$-based to $MgCl_2$-supported, represents an outstanding case history in this respect, but at the same time demonstrates that

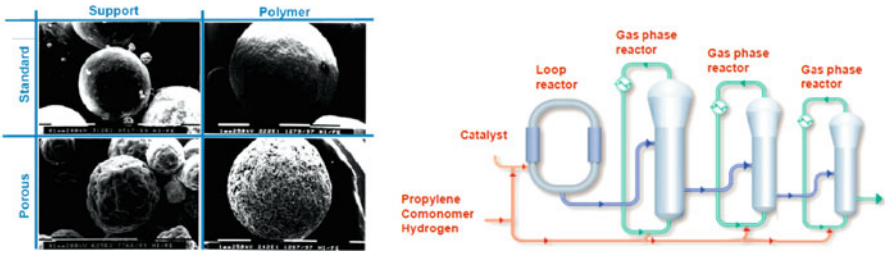

Fig. 13 *Left*: Scanning electron micrographs documenting the replication of pre-catalyst morphology in $MgCl_2$-supported ZN catalysis for PP (courtesy of J. Pater, Lyondellbasell). *Right*: A typical reactor cascade for the production of "heterophasic" PP; (adapted from http://www.borouge.com/aboutus/Pages/ProcessOverview.aspx)

serendipity is only one part in a cocktail [51] that also includes the ability to recognize the importance and the possible implications of an unexpected result, the availability of adequate human and material resources to elaborate on such implications, and a chain-of-knowledge approach spanning all elements from initial discovery to practical application.

In my opinion, the progress of technology will greatly speed up the process of discovery [16], but is not likely to change its mechanisms in the short or medium term. If I am correct, then Natta's success story is not only of purely historical concern and should rather be looked at by scientists and managers in industry and academia as a valid model and source of inspiration for a brighter future.

Acknowledgements I am grateful to Prof. Walter Kaminsky, editor of this book, for the invitation to write the present chapter. For me, it was an opportunity to take a pause and look back, enjoying many nice memories of a time vibrant with passion and expectations. I like to thank my coworkers, and in particular Roberta Cipullo and Luca Rongo, for helping me to assemble the material and compose parts of the chapter.

Appendix: Some Biographic Notes on Giulio Natta

Whoever goes through the numerous biographies (see for example [52]) of Giulio Natta (Fig. 14) cannot but realize that the discovery of iPP and stereoselective olefin polymerization was diligently prepared by Fate. Born in 1903 in a family of judges and lawyers, Natta developed a passion for chemistry that made him build, during his studies in chemical engineering at the Milan Polytechnic, a small laboratory in his apartment to carry out "private" experiments in his spare time. The Milan Poly was in the 1920s a world-leading center in X-ray diffraction, which set the stage for Natta's interest in the still-young chemical crystallography (key to interpretation of the events of March 1954). Subsequently, he worked on electron diffraction in Freiburg; that Hermann Staudinger was a professor there was certainly more than influential on Natta's formation. Back in Italy, he went through a rapid academic career that saw him Professor of General Chemistry in Pavia, of Physical Chemistry in Rome, and of

Fig. 14 Giulio Natta (1903–1979)

Industrial Chemistry, at Turin Polytechnic first and at Milan Polytechnic from 1938 until his retirement in 1973. As for many academic chemists in Europe at that time, the forthcoming war prompted Natta to move the focus of his research to the synthesis of strategic materials. In particular, he expanded his studies in catalysis, which were pre-existing and had already led him to important achievements in oxosynthesis in the early 1930s, to the production of synthetic rubber. The interest in polymers with elastomeric properties never faded, and is another key part of the puzzle. After the war, Italy entered the most vital and productive period of its recent history, and the Italian chemical industry began an impressive growth. At that point Fate played a wild card and made the young Natta meet Piero Giustiniani, on the way to becoming CEO of Montecatini, one of the largest and most advanced Italian chemical companies. The two began a collaboration that in 1947 led them to travel to the USA, where they discovered the modern organization of the American chemical companies, employing hundreds of researchers and well ahead in the transition from coal to oil chemistry. That journey imprinted both of them and resulted in a strategic alliance that made Montecatini associate Natta as a consultant and establish at the Milan Polytechnic an "Advanced School in Aliphatic Chemistry," where brilliant chemistry and chemical engineering graduates from all over Italy received hands-on research training in chemical syntheses and characterizations. They joined the academic staff on fundamental and applied projects under Natta's leadership, in most cases in preparation to a career in Montecatini. The modernity of this organization, with a strong multidisciplinary character and a simple albeit efficient structure, amazes me when I compare it with the present painful situation of Italian chemical research. When in 1952 Natta attended the Achema Conference in Frankfurt, where Karl Ziegler gave an account of his work on the "Aufbau-Reaktion," all parts of the puzzle could perfectly fit together. Natta had no difficulty in convincing Giustiniani and Montecatini to contract Ziegler as a consultant and to take a license on the developments of Al-mediated ethene oligomerization, even though the real industrial interest of that

process was not yet clearly established. What came afterwards is told in the previous sections of this chapter.

A precocious Parkinson disease forced Natta to a rather early retirement, which makes me feel sad for him, and in a way for me too, because I dare to look at him as a grandfather that I never met. When I read that he was a reserved, almost shy man I have no difficulties in believing that. In my 20 years of collaboration with Paolo Corradini and, for a much shorter but highly fascinating period, with Adolfo Zambelli, I seldom heard them mention "Il Professore" or tell anecdotes about him. They had been working under Natta for many years, and shared with him the most heart-shaking experience a scientist could dream about, and yet "Il Professore" seemed to me, through them, to be a silent presence in the background. Some of his comments, of course, surfaced to their memories, and these were all modest, humble even: "we have been lucky" was a recurrent one. On the other hand, Natta was of course well-aware of the importance of his discoveries. I have been especially impressed by a recollection of Lido Porri, another well-known Natta coworker, in a recent article for a special issue of the Italian Chemical Society journal celebrating the 50th anniversary of Natta's Nobel Prize [53]. Porri recalls that Natta used to say: "I believe that research in this field will continue until the next century." Well, "Professore," here we are indeed!

References

1. Jansz J (2012) Fifth annual India chemical industry outlook conference, Mumbai, 23–24 February 2012. http://www.chemweek.com/Assets/Session3_EBB_Jansz.pdf. Accessed 21 December 2012
2. Patat F, Sinn H (1958) Angew Chem 70:496–500
3. Ziegler K, Gellert HG, Zosel K, Lehmkuhl W, Pfohl W (1955) Angew Chem 67:424
4. Tonelli AE (1989) NMR spectroscopy and polymer microstructure: the conformational connection. VCH, Deers Field
5. Resconi L, Cavallo L, Fait A, Piemontesi F (2000) Chem Rev 100(4):1253–1346
6. Busico V, Cipullo R (2001) Prog Polym Sci 26:443–533
7. Boor J Jr (1979) Ziegler-Natta catalysts and polymerizations. Academic, New York
8. Jordan RF, Bajgur CS, Willett R, Scott B (1986) J Am Chem Soc 108:7410–7411
9. McDaniel MP (2010) Adv Catal 53:123–606
10. Chen EY-X, Marks TJ (2000) Chem Rev 100(4):1391–1434
11. Moore EP Jr (ed) (1996) Polypropylene handbook: polymerization, characterization, properties, applications. Hanser, Munich
12. Natta G, Allegra G, Corradini P (1961) J Polym Sci 156:399–410
13. Fischer K, Jonas K, Misbach P, Stabba R, Wilke G (1973) Angew Chem Int Ed 12:943–953
14. Speiser F, Braunstein P, Saussine L (2005) Acc Chem Res 38:784–793
15. Ittel SD, Johnson LK, Brookhart M (2000) Chem Rev 100(4):1169–1204
16. Hagemeyer A, Strasser P, Volpe AF Jr (eds) (2004) High throughput screening in catalysis. Wiley-VCH, Weinheim
17. Tullo AH (2010) C&EN 88(42):10–16
18. Auriemma F, Busico V, Corradini P, Trifuoggi M (1992) Eur Polym J 28:513–518
19. Busico V, Corradini P, De Martino L, Trifuoggi M (1992) Eur Polym J 28:519–523
20. Natta G, Corradini P (1959) J Polym Sci 39:29–46
21. Bunn CW (1942) Proc R Soc London A180:67–81

22. Lee T-G (2004) The politics of realism: Lukacs and reflection theory. The AnaChronisT, The Free Library On Line. http://www.thefreelibrary.com/The+politics+of+realism%3A+Lukacs+and+reflection+theory.-a0225938464. Accessed 21 December 2012
23. Watson JD, Crick FHC (1953) Nature 171:737–738
24. Sementa L, D'Amore M, Barone V, Busico V, Causà M (2009) Phys Chem Chem Phys 11: 11264–11275
25. Fredga A (1963) Presentation speech for the Nobel prize in Chemistry 1963. http://www.nobelprize.org/nobel_prizes/chemistry/laureates/1963/press.html. Accessed 21 December 2012
26. Natta G, Pino P, Corradini P, Danusso P, Mantica E, Mazzanti G, Moraglio G (1955) J Am Chem Soc 77:1708–1710
27. Sementa L (2009) PhD Dissertation, 'Federico II' University of Naples, Naples
28. Arlman EJ, Cossee P (1964) J Catal 3:99–104
29. Cossee P (1967) The mechanism of Ziegler-Natta polymerization. II. Quantum chemical and crystal-chemical aspects. In: Ketley AD (ed) The stereochemistry of macromolecules, vol. 1, Chap. 3. Marcel Dekker, New York, pp 145–175
30. Zambelli A, Locatelli P, Bajo G, Bovey FA (1975) Macromolecules 8:687–689
31. Zambelli A, Locatelli P, Zannoni G, Bovey FA (1978) Macromolecules 11:923–924
32. Zambelli A, Locatelli P, Bajo G (1979) Macromolecules 12:154–156
33. Shelden RA, Fueno T, Tsunetsugu T, Furukawa J (1965) J Polym Sci B 3:23–26
34. Corradini P, Barone V, Fusco R, Guerra G (1979) Eur Polym J 15:1133–1141
35. Corradini P, Guerra G, Fusco R, Barone V (1980) Eur Polym J 16:835–842
36. Corradini P, Busico V, Cavallo L, Guerra G, Vacatello M, Venditto V (1992) J Mol Catal 74: 433–442
37. Zambelli A, Sacchi MC, Locatelli P, Zannoni G (1982) Macromolecules 15:211–212
38. Albizzati E, Giannini U, Morini G, Galimberti M, Barino L, Scordamaglia R (1995) Macromol Symp 89:73–89
39. Cecchin G, Morini G, Piemontesi F (2006) In: Kirk-Othmer (ed) Encyclopedia of chemical technology, vol 26. Wiley, New York, pp 502–554
40. Giannini U (1981) Makromol Chem Suppl 5:216–229
41. Corradini P, Barone V, Fusco R, Guerra G (1983) Gazz Chim Ital 113:601–607
42. Morini G, Albizzati E, Balbontin G, Mingozzi I, Sacchi MC, Forlini F, Tritto I (1996) Macromolecules 29:5770–5776
43. Busico V, Causà M, Cipullo R, Credendino R, Cutillo F, Friederichs N, Lamanna R, Segre A, Van Axel Castelli V (2008) J Phys Chem C 112:1081–1089
44. Credendino R, Busico V, Causà M, Barone V, Budzelaar PHM, Zicovich-Wilson C (2009) Phys Chem Chem Phys 11:6525–6532
45. Credendino R, Pater JTM, Correa A, Morini G, Cavallo L (2010) J Phys Chem C 115: 13322–13328
46. D'Amore M, Credendino R, Budzelaar PHM, Causà M, Busico V (2012) J Catal 286:103–110
47. Brambilla L, Zerbi G, Piemontesi F, Nascetti S, Morini G (2007) J Mol Catal A Chem 263: 103–111
48. Brambilla L, Zerbi G, Piemontesi F, Nascetti S, Morini G (2010) J Phys Chem C 114: 11475–11484
49. Correa A, Credendino R, Pater JTM, Morini G, Cavallo L (2012) Macromolecules 45: 3695–3701
50. Busico V, Cipullo R, Monaco G, Talarico G, Vacatello M, Chadwick JC, Segre A, Sudmeijer O (1999) Macromolecules 32:4173–4182
51. Dunbar K, Fugelsang J (2005) Causal thinking in science: how scientists and students interpret the unexpected. In: Gorman ME, Tweney RD, Gooding D, Kincannon A (eds) Scientific and technical thinking. Lawrence Erlbaum Associates, Mahwah, pp 57–79
52. See, e.g.: http://www.nobelprize.org/nobel_prizes/chemistry/laureates/1963/natta-bio.html. Last checked on 10 Mar 2013
53. Porri L (2013) Chim Ind 2013(1):100–106

Adv Polym Sci (2013) 257: 59–80
DOI: 10.1007/12_2013_214

Published online: 4 May 2013

The Slurry Polymerization Process with Super-Active Ziegler-Type Catalyst Systems: From the 2 L Glass Autoclave to the 200 m^3 Stirred Tank Reactor

L.L. Böhm

Abstract Since the discovery of the ethene polymerization with transition metal catalysts of group IV of the periodic table in combination with aluminum alkyl compounds as cocatalysts at low pressures and moderately high temperatures by Ziegler and colleagues in 1953, this catalytic polymerization process has been developed over six decades in an outstanding way and is now a mature technology for the production of high-density polyethylene grades with excellent properties for wide fields of application. Today, super-active heterogeneous catalysts are available. The catalyst must be designed to achieve high activity over a long polymerization time, be able to control average molecular mass over a wide range using hydrogen, to copolymerize ethene with higher 1-olefins, and to produce an unimodal polymer with a relative narrow molecular mass distribution. It is of greatest importance to avoid overheating of the growing polymer particle, especially when the polymerization starts at the virgin catalyst particle. This is not easy to achieve because the polymerization process is highly exothermic. The transformation of a catalyst particle into a polymer grain can be described and is well understood by the microreactor model. The technical process can be divided into three clear distinguishable levels: the microscale, the mesoscale, and the macroscale. The microscale level comprises all processes inside and at the surface of the growing polymer particle, i.e., the microreactor behavior. The mesoscale level deals with all processes inside the three-phase reactor content comprising gas bubbles, hydrocarbon diluent and the solid growing polymer particles. It is important to achieve reproducible and stable conditions on the basis of a

In former time the author L.L. Böhm was working with Hoechst AG (Frankfurt (M), Germany), Hostalen Polyethylen GmbH (Frankfurt (M), Germany), Elenac GmbH (Kehl, Germany) and Basell Polyolefins (Wesseling, Germany).

L.L. Böhm (✉)
Leonhardstr. 36, 65795 Hattersheim, Germany
e-mail: hanni.ludwigboehm@t-online.de

detailed chemical engineering on this mesoscale level throughout the reactor. If this is the case, then this polymerization process can be well controlled on the macroscale level, comprising the polymerization vessel as a whole. By controlling a limited number of process data, the slurry polymerization process can be operated with excellent stability over a long time and can be controlled within narrow ranges. The modern slurry technology process is very flexible in controlling product properties by using the cascaded reactor technology. This technology involves two or even three reactors operated in series under different process conditions. The catalyst is only introduced into the first reactor. The polymerizing particle then passes through all reactors, producing different types of macromolecules to form a polymer blend within each polymer grain. A further enormous advantage of this cascade technology is the high flexibility in product change and product development. Just by changing process parameters of the different reactors, products with different average molecular mass, different molecular mass distributions, different copolymer compositions, and different comonomer distributions can be produced without changing the catalyst system.

Keywords High density polyethylene · Process control · Process design · Process modelling · Product portfolio · Super-active catalysts · Ziegler slurry polymerization

Contents

1 Introduction

In 1953, Ziegler and colleagues described a process for polymerization of ethene at moderately high temperatures and low pressures to generate a new type of polyethylene, known as high-density polyethylene (PE-HD) [1]. The characteristics of this process can be summarized as following: in a hydrocarbon diluent (e.g. diesel oil) under a blanket of nitrogen excluding traces of oxygen and water, a soluble transition metal compound of the 4th to 6th group of the periodic table, preferably $TiCl_4$, is contacted with an aluminumorganic compound such as an aluminumalkyl or aluminumalkylchloride to form an active, insoluble $TiCl_3$-based

catalyst. Introducing ethene, the polymerization process starts to generate a high molecular mass polyethylene. Under the given reaction conditions (temperature below 100°C), the polyethylene is insoluble in the hydrocarbon diluent and precipitates as a powder to form a slurry (slurry polymerization process). This process was performed in a 2 L glass autoclave [1, 2]. For industrial use, it was of essential importance that this process was protected by a patent [3, 4]. Within a very short time, a technical plant came on stream and in 1955 the first products were offered on the market [5–9]. This new process was regarded as so important that a small plant was presented at the Brussels World Exhibition in 1958 to demonstrate this technology and the product [10]. In his Nobel Prize lecture in 1963, Ziegler could show how fast his invention had been transferred into technical processes worldwide [2].

Today, this process is operated in principle in the same way as described by Ziegler et al. [1–4]. However, over the six decades since the discovery enormous progress has been achieved, and a detailed understanding of all relevant processes on all scales of this technology is available. The process is now run using super-active catalysts on the basis of a $MgCl_2$ particle loaded with $TiCl_4$ [11–21]. These catalysts are at least two orders of magnitude more active than the catalysts used by Ziegler and colleagues. The activity under comparable reaction conditions reaches more than 100 kg polymer per gram titanium (the amount of polymer is usually related to the active component of the catalyst, in this case to titanium) resulting in a catalyst residue of less than 10 ppm Ti, usually in the range of around 1 ppm Ti or even less. From a technical point of view, this is an outstanding advantage because all catalyst residues can remain in the polymer without any treatment to save product quality.

The whole process can be separated into three clear distinguishable levels (micro-, macro-, and mesoscale) as first proposed by Ray [22]. The most important processes are running on the microscale level, meaning inside and at the surface of the growing polymer particle. Here all relevant chemical reactions take place. The polymerization reaction is well understood on the basis of the Cossee–Arlman model [23–25]. All other relevant chemical processes are known based on a reaction model published in 1978 [26]. This reaction model was used to develop an advanced process control strategy, as described later. On the microscale level, the most important process is the transfer of a catalyst particle to a polymer grain. This process is called the particle-forming process [27]. Because all reactions take place inside this particle, it has to be regarded as a small reactor, called a microreactor. Different models have been published for this particle-forming process, but the simplest model, the polymeric flow model [27, 28], was found to describe this process quite well. The polymerization reaction is highly exothermic. Therefore, it is very important at least for the technical process to avoid overheating of these microreactors. Wicke et al. has shown that there are two stable points with respect to the temperature and concentration profiles inside and at the surface of such microreactors [29–31]. There is a stable point controlled by kinetics, with small temperature gradients inside and at the surface of the polymerizing particle, and a diffusion-controlled stable point with strong temperature gradients and a

much higher temperature of the microreactor compared to the temperature of the surrounding diluent. This upper stable point must be avoided because otherwise it can lead to a situation where the polymer grains are swollen with the hydrocarbon diluent or even melt and then stick together throughout the whole reactor, with the consequence that the reactor can no longer be controlled and must be shut down. In the worst case, the whole reactor content must be removed and the reactor cleaned. It is now known how to design the catalyst particle, how to react the catalyst with the aluminumorganic cocatalyst, and how to run the polymerization process to avoid overheating of the microreactor, even for super-active catalysts [32, 33].

The mesoscale level comprises all processes inside the slurry phase. At this level, there are no process-relevant chemical reactions. Here run the transport processes for ethene, hydrogen to control average molecular mass, and e.g., 1-butene or other 1-olefines to control density. Further, the heat transfer from the polymerizing polymer grains to the diluent and then to the cooler system is located here. It is important to establish a stable stationary state for both concentrations of the reacting components and temperature, with stable concentration and temperature gradients in the polymerization reactor from top to bottom and vice versa. It is further essential that the bulk mixing time is far below average residence time for each vessel. This is achieved using modern state-of-the-art stirrer systems with blades or impellers or turbines at different heights [34–36]. On the basis of this know-how, it is possible to construct polymerization vessels with increasing size, up to 200 m^3. The relevant criteria will be discussed in Sect. 3.2.

The macroscale level comprises the polymerization reactor as a whole. Based on a detailed understanding of all processes on the microscale and mesoscale levels, it was possible to develop a process model indicating which intensive and extensive process variables must be controlled within which ranges to hold the relevant product data in the required ranges [37–39]. It was a great surprise that only a very limited number of variables have to be controlled and it was further surprising to see a nearly perfect agreement between calculated and measured process data. It is now possible to run large plants with throughputs up to 50 tons/h safely, without uncontrolled shutdowns, with less pollution, with outstanding product qualities, and with high reproducibility.

Polyethylene products are no longer only commodity grades but are now used for technical applications like pipes for drinking water, waste water, industrial piping, and gas transport systems; containers for industrial packaging, especially for the transport of dangerous goods; automotive fuel tanks; extremely tough films; and many more applications [32, 33, 40–50]. Using the cascade technology with two or even three reactors in series (advanced cascade process), and introducing the catalyst only into the first reactor, this technology reaches an outstanding flexibility in product development because no catalyst change is necessary for the development of new grades. Only the process parameters of the different reactors must be modified. This is an outstanding advantage and opens a lot of opportunities for further product development.

Table 1 Crystallographic data of δ $MgCl_2$ and δ $TiCl_3$

Crystallographic parameters	
δ $MgCl_2$	δ $TiCl_3$
Hexagonal closest layer structure of the Cl^- ions	
$a = b = 3.63$ Å	$a = b = 3.54$ Å
$c = 5.93$ Å	$c = 5.86$ Å
Cation coordination: octahedral	
Mg–Cl: 1.23 Å	Ti–Cl: 1.25 Å
Mg^{2+}: 0.65 Å	Ti^{4+}: 0.68 Å
	Ti^{3+}: 0.76 Å

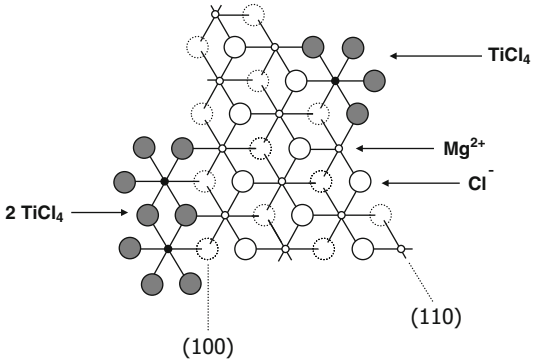

Fig. 1 Surface structure of $TiCl_4$ on δ $MgCl_2$

2 Super-Active Catalysts

The breakthrough in preparation of super-active Ti-based catalysts was achieved by using anhydrous δ $MgCl_2$ as a support being treated with $TiCl_4$ in a hydrocarbon diluent [11–18]. The reason for this outstanding role of δ $MgCl_2$ is its crystal structure in comparison to δ $TiCl_3$, as shown on Table 1.

At the δ $MgCl_2$ surface, $TiCl_4$ can be bound as described by Corradini et al. [51]. At the 1 0 0 and 1 1 0 planes, $TiCl_4$ can be chemisorbed as shown in Fig. 1.

These $TiCl_4$ complexes must react with an aluminumalkyl compound as cocatalyst to be transferred into active sites. This is a two-step process: in the first step, one chlorine is exchanged by an alkyl group. Then in a second step, a further chlorine is substituted by an alkyl group. This complex is unstable and reduction of Ti(IV) to Ti(III) takes place to form a vacant site at the titanium, as defined by Cossee and Arlman [23–25]. This reaction sequence is shown in Fig. 2.

By controlling this activation process it is possible to influence the catalyst activity in the start-up phase of the virgin catalyst particle. Before introducing the catalyst into the polymerization reactor, the catalyst is preactivated with a small amount of cocatalyst outside the polymerization vessel. Doing this, only

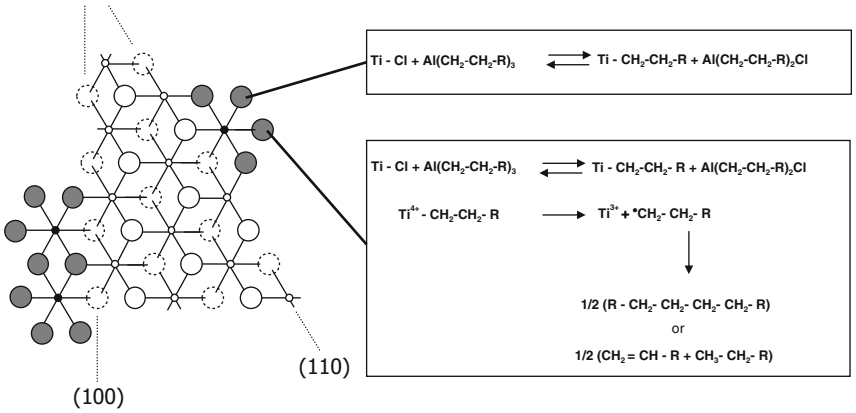

Fig. 2 Activation process with aluminum alkyl compounds as cocatalysts

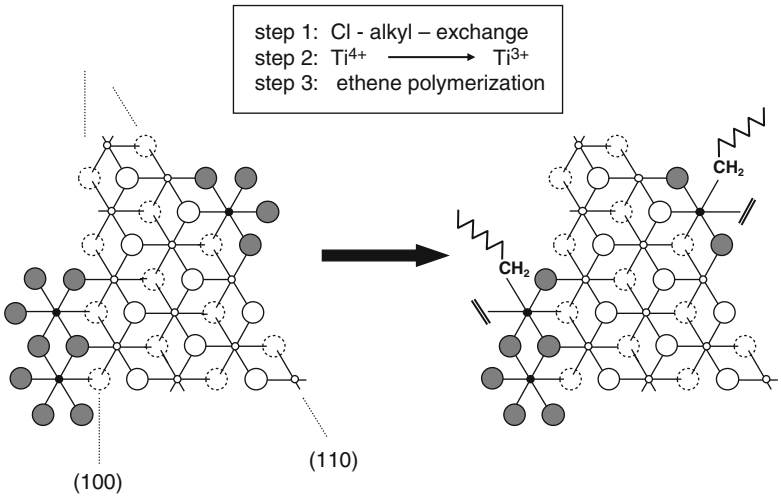

Fig. 3 Active site formation for ethene polymerization

the active sites at the outer surface of the catalyst particle start to polymerize. Further activation of the titanium complexes is achieved in the polymerization vessel by the diffusion of the dissolved aluminumalkyl compound into the polymerizing particle to create further active centers. This means that the activity increases over time to finally reach maximum activity. This activation process can be influenced via the aluminumalkyl compound used as cocatalyst, via the preactivation step of the virgin catalyst, and via the concentration of the aluminumalkyl compound in the polymerization reactor to realize the best start-up behavior without any problems due to overheating of the polymerizing particle. This demonstrates that there are many parameters for optimizing the start-up behavior as well as the overall performance of the catalyst–cocatalyst system. The activation process is summarized in Fig. 3. At these sites, polymerization of

ethene, copolymerization with 1-butene or other 1-olefins, and chain transfer reactions especially with hydrogen are running in line with the reaction model as published elsewhere [26]. The high activity is caused by the high number of active sites and the particle structure of these super-active catalysts. The catalyst particle, with a diameter in micrometer range (10–50 μm), is an agglomerate of nanosized particles, called primary particles. It has been found that close to 100% of all titanium complexes are involved in the polymerization process [52]. The catalyst particle must fulfil the following conditions: It must be stable enough to be pumped as a slurry with the hydrocarbon diluent into the polymerization vessel and, on the other hand, it must be easily disrupted down to the primary particles by the polymer, and these primary particles must then be evenly distributed over the whole polymer grain.

3 Modeling the Slurry Polymerization Process

This polymerization process can be separated into three different levels as proposed by Ray [22]. First this is the microscale level, modeling all processes at the surface and inside the growing polymer particle. The next level is the mesoscale level, describing all mass and heat transfer processes inside the three-phase slurry containing gas bubbles, hydrocarbon diluent with the dissolved aluminumalkyl compound, and the solid growing polymer particles loaded with the active sites. Finally, there is the macroscale level comprising the polymerization vessel as a whole, with sensors to control this slurry polymerization process. These three levels are shown in Fig. 4.

3.1 The Microscale Level

A key process of the slurry polymerization is the particle-forming process, which involves the transformation of a catalyst particle into a polymer grain. It has been found that each catalyst particle is transferred into one polymer grain, as shown in Fig. 5.

Figure 5 shows in a schematic way that the catalyst particle with a diameter in the range of 10–50 μm is an agglomerate of nanosized particles called primary particles. During the polymerization, these primary particles are separated by the polymer. Then, each primary particle is enveloped by a polymer layer. These small polymer grains are held together by the polymer to form a stable polymer particle. The particle-forming process is not understood in all details, and it is also not known which forces are responsible for the stability of both the catalyst particle and the polymer grain. However, from experience with industrial catalysts it can be concluded that the particle-forming process runs well without problems in a technical plant.

All chemical reactions take place inside these microreactors. These chemical reactions and the mass and heat transfer processes are regarded as the

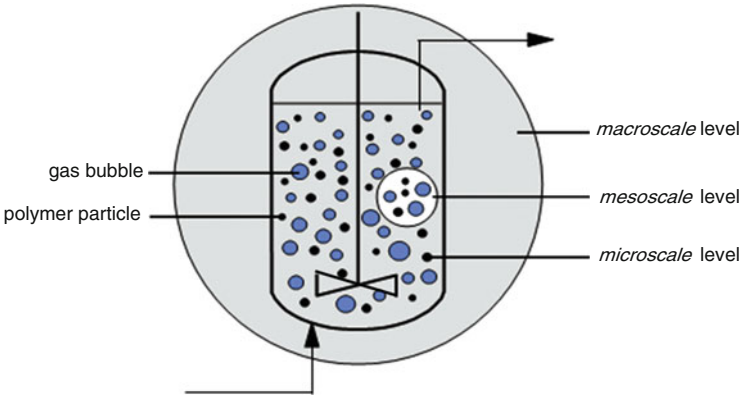

Fig. 4 Scheme for modeling the slurry polymerization process

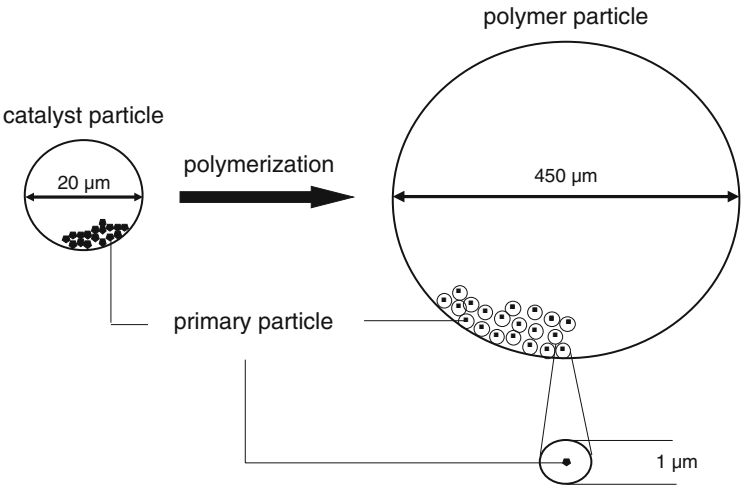

Fig. 5 Particle-forming process

microscale level of the polymerization process. The most important point is to avoid overheating of these particles by the highly exothermic polymerization reaction. As described by Wicke et al. [29–31], there are different stable points for such microreactors (Fig. 6).

To avoid any overheating of this microreactor or growing polymer particle, the temperature of the particle must remain at the lower stable reaction point (T_{min}) close to the temperature of the surrounding diluent (T_0). Then the process is kinetically controlled. At the upper stable reaction point (T_{max}), the temperature of the growing particle is much higher than the diluent temperature (T_0) and the process is diffusion controlled. For the technical process, it is of great importance that all microreactors always run at the lower stable reaction point (Fig. 7).

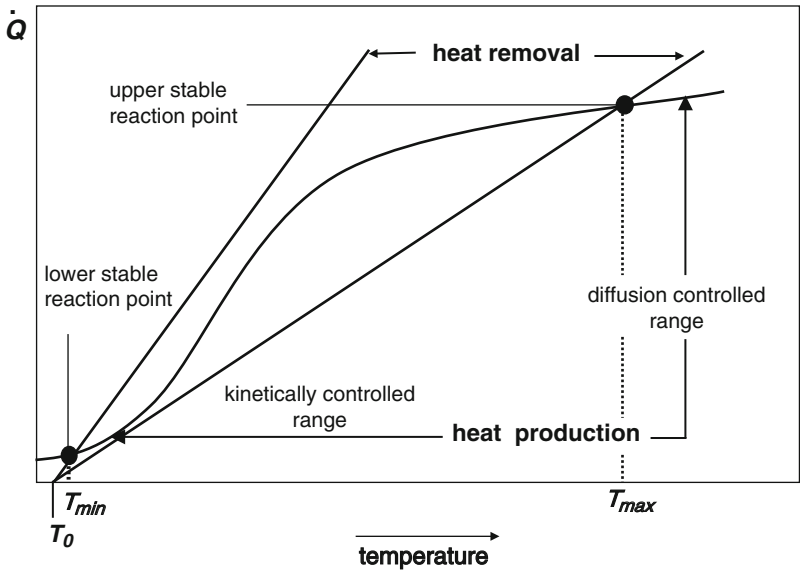

Fig. 6 Stable reaction points at the microreactor

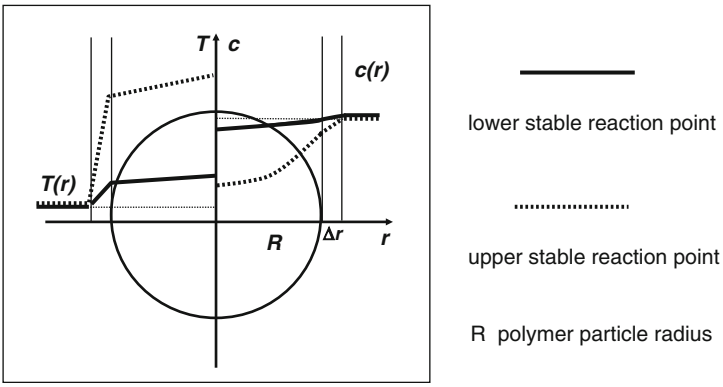

Fig. 7 Temperature (T) and concentration (c) profiles at the microreactor

The catalyst–cocatalyst system must be managed as described above in such a way that, at the beginning of the polymerization process at the virgin catalyst particle there is a balance between heat production by the polymerization process and heat removal via the particle surface to avoid overheating of the polymerizing particle. Heat removal must always be higher than heat production. This is achieved by low activity in the start-up phase of the polymerization, achieved by optimized catalyst design in combination with a controlled activation process by the aluminumalkyl compound. With increasing reaction time, the catalyst becomes more active and must hold this high activity over a long time, in the range of the

average residence time. It is a very special know-how to design the catalyst and the activation process with the cocatalyst system in this way.

Using the polymeric flow model [27, 28] and assuming constant temperature of the growing particle at the lower stable reaction point, it can be shown that the polymerization process always runs in the kinetically controlled range, with an overall rate constant for the ethene polymerization in the range of 100 $dm^3\ mol^{-1}\ s^{-1}$ and an effective diffusion constant for ethene inside the microreactor of about $1 \times 10^{-4}\ cm^2\ s^{-1}$ at the preferred temperature of about 80°C. This means that the growing particle (the microreactor) is at a temperature range near to the temperature of the diluent (T_0), with only small temperature and concentration gradients at the surface and inside these particles [32, 33].

In conclusion, super-active catalysts used in technical processes have a very high activity but do not overheat at the start-up of polymerization and remain at this high activity level over a long period of time in the range of the average residence time of around 1–2.5 h depending on process design (see Sect. 4). Only with those catalysts can the modern process be operated effectively.

3.2 The Mesoscale Level

As shown in Fig. 4, the mesoscale level deals with all processes in the three-component slurry phase. On this level, mass and heat transfer processes play key roles. To guarantee a stable stationary state throughout the whole reactor and to establish stable concentration and temperature gradients from top to bottom and vice versa, the reactor must be equipped with an optimized stirring and cooling system. This is a challenge for large volume tall-thin reactors because the height-to-diameter ratio is much higher than 1. However, such stirring systems are now available [34–36]. The design is characterized by several blades, impellers, or turbines at different levels along the stirrer axis. In that way it is possible to generate a virtual draft tube with sufficient mixing throughout the tall-thin reactor, as described elsewhere [36]. Figure 8 shows the design of such a stirring system, together with scale-up criteria applied for these tall-thin reactors.

With this stirrer design, it is possible to have good local and bulk mixing. It can be estimated that using such optimized stirring systems, a bulk mixing time can be realized within a few minutes, which is lower by at least one order of magnitude than the average residence time of 1–2.5 h. This is sufficient because each polymer particle passes through the whole reactor many times before leaving the polymerization vessel. Together with effective outercooler loops, it is possible to have only small temperature gradients inside the whole slurry phase. Further, it is essential to generate a polymer powder with a high bulk density in the range of 400 g dm^{-3} to run a high polymer content in the slurry of up to about 25% by weight. It is important that the polymer particles have a ball-like structure to reduce friction between the particles. As shown elsewhere, the viscosity of the slurry phase can be limited in a range that is not more than ten times higher than the viscosity of the diluent [32, 33]. This does not seriously influence local and bulk mixing.

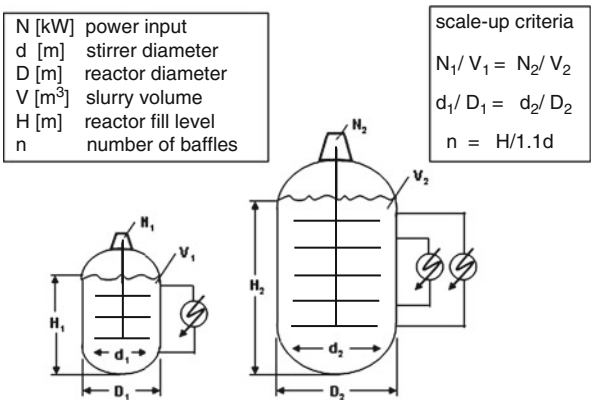

Fig. 8 Stirrer design and scale-up criteria

As shown in Fig. 8, there are some scale-up criteria. In principle, a larger volume of the reactor is realized by adding one ore more volume segments together with a further stirrer for each segment along the stirrer axis. The specific power input remains the same. The bulk mixing time increases due to the larger volume but it is still much lower than the average residence time for each polymerization reactor.

3.3 The Macroscale Level

The macroscale level comprises the whole polymerization reactor as shown in Fig. 4 and all sensors to control the relevant process data. At this level, all information must be available to run the polymerization process according to the recipes and to hold all product data in the required range. For this macroscale level, a process model was developed and an excellent agreement between calculated and measured data was found for the technical plant [37]. This is shown in Fig. 9.

Figure 9 shows the calculated data for the gasphase composition (mole fractions) and the product data as a function of the Damköhler number I (lines), and the measured data in the polymerization reactor (points). The process is running at 83°C. The Damköhler number $Da_{I.1}$ is related to ethene (component 1) as the main component and has a value of 53. The Damköhler number is given by $Da_{I.1} = k_p f\, n_k/V\, \tau$ where $k_p f$ is the overall propagation rate constant for ethene polymerization, n_k/V the catalyst content in the reactor, and τ the average residence time. Using this reaction model it is possible to calculate how the two most important product parameters, copolymer composition (n_1/n_2) related to the density (d) and the number average degree of polymerization (P_n) related to the melt flow rate (MFR 190/5) [53], are influenced by the different process parameters, as shown on Fig. 10 for the ethene stream into the reactor as an example.

From such curves as shown in Fig. 10 it is possible to evaluate which parameters, and how sensitively changes in those parameters, influence the product density and melt flow rate (MFR 190/5). The result is summarized in Fig. 11, which

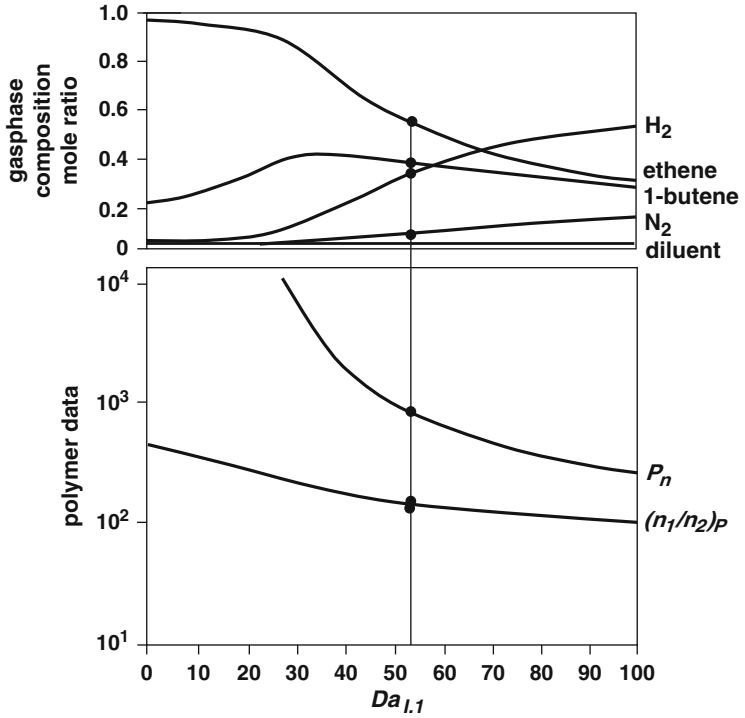

Fig. 9 Gasphase composition and polymer data as a function of the Damköhler number I (see text for details)

indicates all these process parameters together with the ranges to be controlled and held constant.

Modern plants are equipped with all these sensors of the required sensitivities. Excellent process control is a key item in running a plant safely and in reaching a high quality level for all products.

4 Process Design

To achieve highest product quality levels, especially for technical applications combined with high flexibility in grade change and product development, process design is the salient point. The advanced cascade process (ACP) design, with three polymerization reactors running in series, fulfils the above-mentioned recommendations in a perfect way. The key feature of this process design is no catalyst change. All products can be produced with the same catalyst. This is an outstanding advantage because catalyst development is a time-consuming process with an uncertain issue. Running three polymerization reactors in series, and introducing the catalyst only into the first polymerization reactor, the molecular

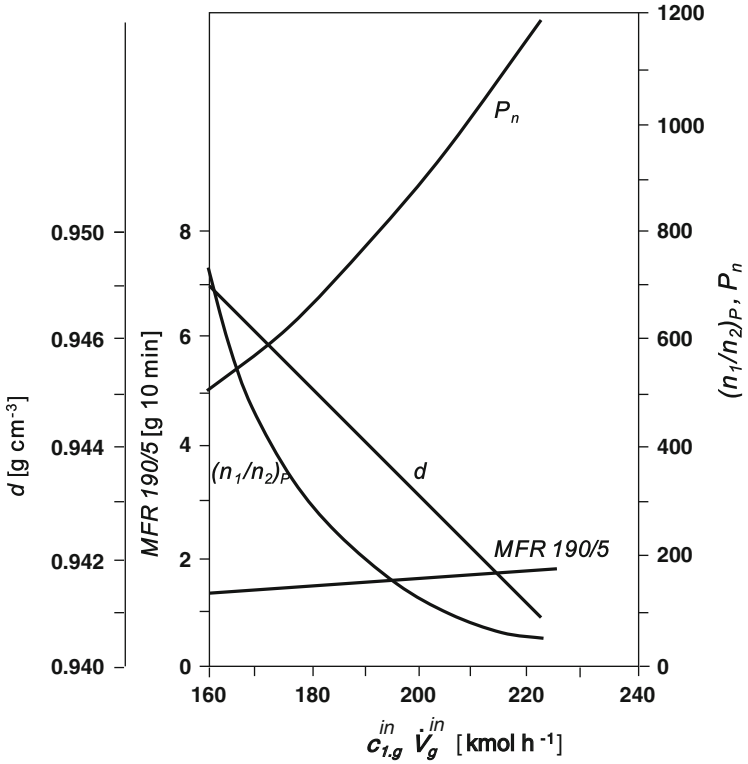

Fig. 10 Density (*d*) and melt flow rate (MFR 190/5) as functions of the ethene stream into the polymerization reactor

mass distribution and the comonomer distribution in the final product can be varied in an easy way. The process design of this cascaded process is shown in Fig. 12.

In this cascade process, the first polymerization reactor is operated under a high hydrogen content to generate the low molecular mass fraction. This fraction contains no or only a minor amount of comonomer. The high hydrogen content offers a further advantage because hydrogen reduces the activity of the catalyst [26]. This helps to avoid overheating of the polymer particles with the fresh catalyst introduced into this polymerization reactor. From this polymerization reactor, the growing polymer particles pass into the second polymerization reactor to generate a medium molecular mass fraction with a small amount of comonomer. Then, the growing polymer particles enter the third reactor to form the very high molecular mass fraction with a high amount of comonomer. This process allows the molecular mass distribution to be shaped from narrow to broad, and the comonomer distribution from homogeneous to heterogeneous. Operating one reactor, only the average molecular mass and comonomer content can be varied. The molecular mass distribution is given by the catalyst. For the cascaded process, the molecular mass distribution as given by the catalyst should not be too broad.

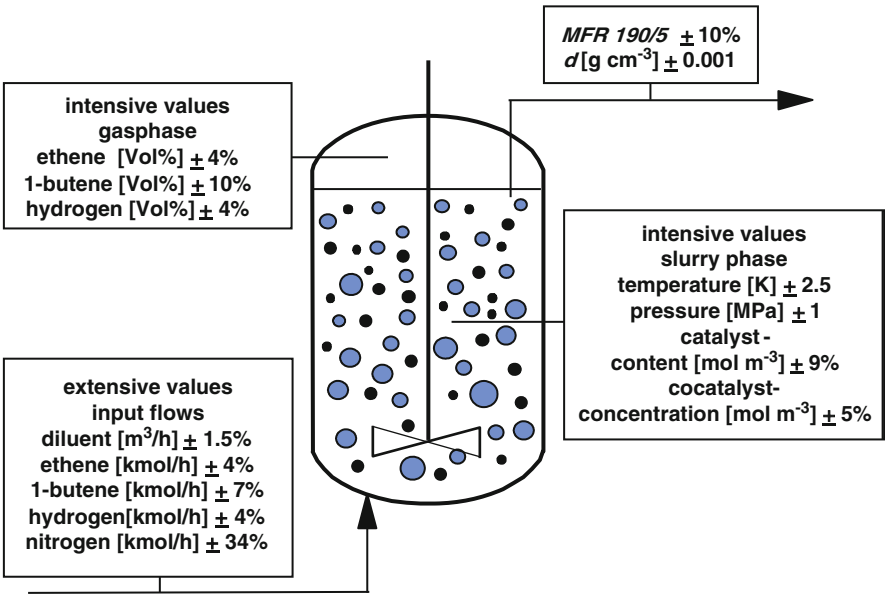

Fig. 11 Process control parameters

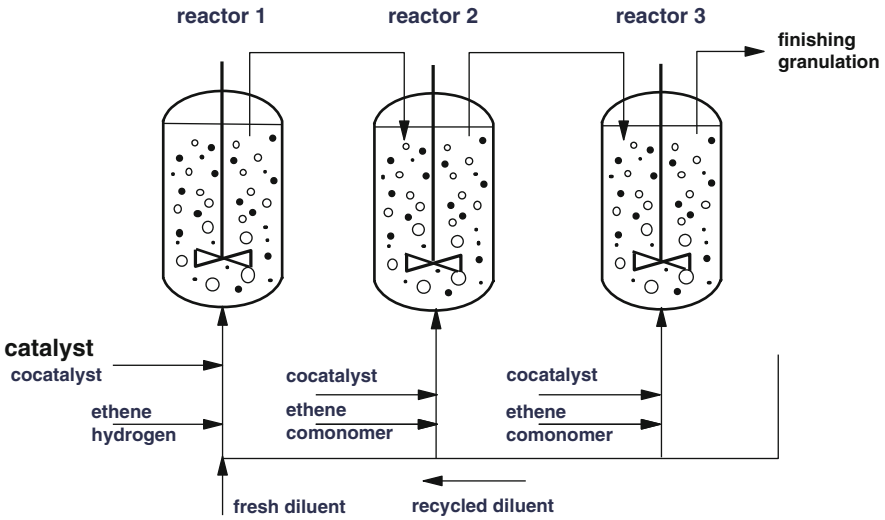

Fig. 12 Cascade process with three polymerization reactors in series (advanced cascade process)

Then it is easy to model the molecular mass distribution from narrow to very broad. With two polymerization reactors in series, the average molecular mass and commoner content can be varied in both reactors, and it is further possible to vary the mass fraction in one polymerization reactor. With three polymerization

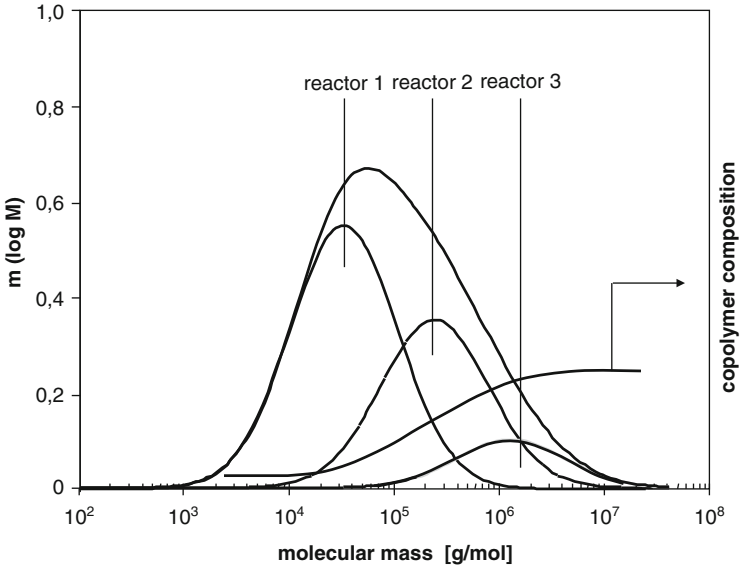

Fig. 13 Shaping molecular mass and comonomer distribution using the cascaded polymerization process

reactors in series, average molecular mass and comonomer content can again be varied in all three reactors together with the mass fraction in two polymerization reactors. This means that, in this case, there are eight variables to be changed independently, which gives room for product optimization in an outstanding way.

Figure 13 gives an example. In the first reactor, a high amount of a low molecular mass homopolymer is generated, followed by a minor amount of a medium molecular mass copolymer in the second reactor, and finished in the third reactor by a small amount of a very high molecular mass copolymer containing a high amount of comonomer. This leads to a polymer with a very broad molecular mass distribution combined with a heterogeneous comonomer distribution.

Therefore, it is not surprising that this cascaded process opens the door to products with combinations of properties so far not known [48–50]. It is important to underline that with this process design the polymer generated in all three polymerization reactors is finely divided in the final polymer particle. Each catalyst primary particle is enveloped with the polymer from reactors 1, 2, and 3. With this in-situ blend it is possible to obtain a homogeneous melt in the granulation facility; this is necessary to exploit the full potential of the product in the solid state. Mechanical blending of such three types of polyethylenes would never lead to a homogeneous melt.

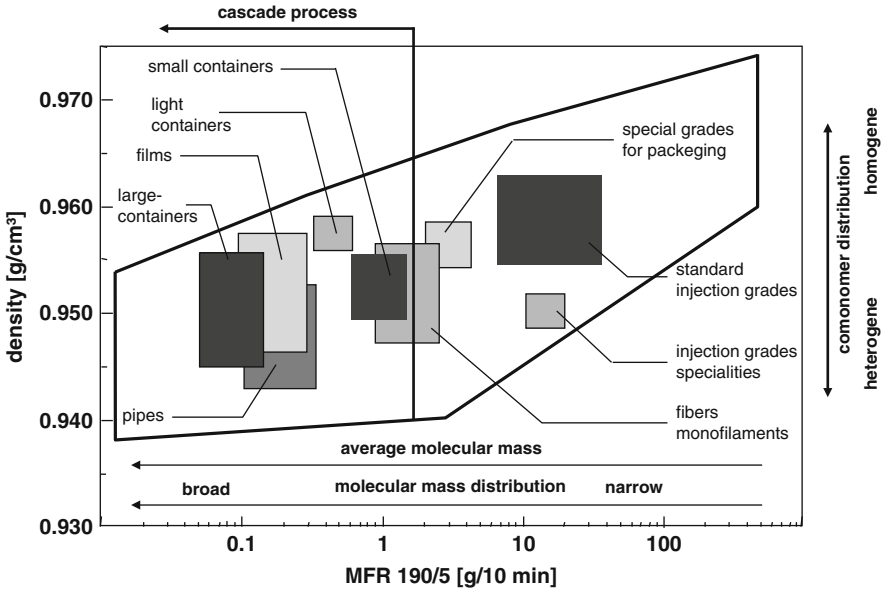

Fig. 14 Product portfolio of high-density polyethylene grades

5 Product Portfolio

Polyethylene products enjoy an outstanding position in the polymer market due to the ability of modern polymerization technologies like the cascaded process to offer tailor-made products with new combinations of properties with respect to processability and final product properties. The product portfolio for high-density polyethylene grades is shown in Fig. 14.

High-density polyethylenes (PE-HD) are used in a broad field of applications. Low molecular mass grades with low melt viscosities at high shear rates are used in injection molding (MFR 190/5 $>$ 5 g/10 min). In this field, the requested product properties are best achieved by products with narrow molecular mass distributions and uniform comonomer distributions for grades with lowered densities. To produce these products, the cascade process is not used. Only one polymerization reactor is operated to synthesize these grades, as discussed elsewhere [32, 33]. For medium high and very high molecular mass grades (MFR 190/5 $\leq$ 1.5 g/10 min) the molecular mass distribution must be broad or even very broad, and the commoner distribution must be non-uniform, meaning that a comonomer like 1-butene is mainly or only incorporated in the high molecular mass fraction. This normally varies from application to application, and it also depends on the final product density. To achieve good processability at high shear rates, the molecular mass distribution must become broader with increasing average molecular mass or decreasing MFR values. This is necessary to hold the melt temperature as low as possible, even at high throughputs on the processing machine. In some

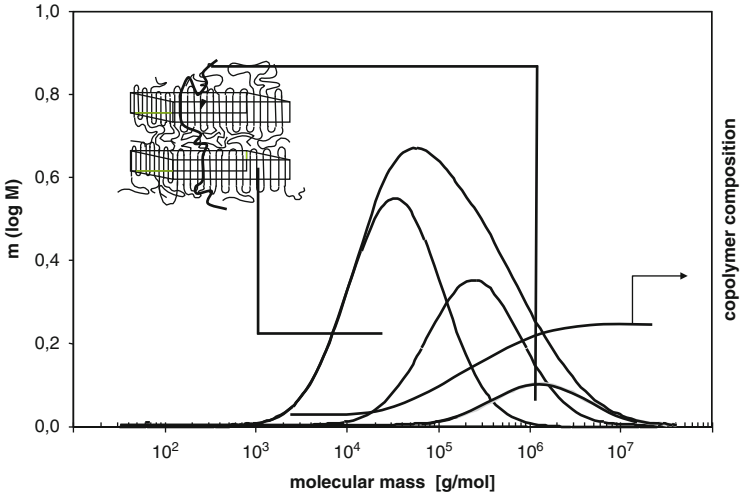

Fig. 15 Polymer composition and solid state structure

applications there are some further specific needs for good processability, like strain hardening for the film blowing process [54], high melt viscosity at low shear rates to avoid sagging in pipe extrusion [48], and high melt strength in the blow molding process of large containers. For pipe extrusion and for blow molding it is further of interest to influence melt elasticity [49]. Then, the die swell ratio increases with a favorable influence on surface structure and wall thickness for blown articles and pipes.

The final product properties mainly depend on average molecular mass and density. With increasing molecular mass, there is an increase in toughness and all other properties correlated with toughness [55]. With increasing density, stiffness increases. However, there are other important properties like stress crack resistance, rapid crack propagation behavior, and creeping under stress that depend on the solid state structure [48]. Polyethylene is a semicrystalline material built up by a crystalline hard phase and an amorphous soft phase. Both phases are interconnected by tie molecules. These are long polymer chains that bind the crystalline lamellae together across the amorphous phase. With the cascaded polymerization process, especially with the advanced cascade process (ACP), polyethylene compositions can be produced to form a polymer alloy in the solid state. This alloy is composed of the hard crystalline lamellae formed mainly by the low molecular mass homopolymers. These lamellae are tightly connected by the tie molecules, mainly formed by the high molecular mass copolymer fraction. This is schematically illustrated in Fig. 15.

One tie molecule is shown by the bold line passing through two crystalline lamellae. It is known that these tie molecules are fixed in the crystalline lamellae by short-chain branches of the comonomer molecules, meaning that they resist diffusing out of the lamellae under permanent stress [40–43, 56]. It is a unique

advantage of the cascaded process with three reactors in series that the polyethylene composition can be easily modified by changing the mass fractions as well as the average molecular mass and the copolymer composition in each reactor as needed. In this way, the structure of the solid product can be modified to achieve outstanding final properties for all applications [48–50]. The development of HD-PE pipe grades is an instructive example of how product development has been successfully carried out over a period of 60 years. The potential of HD-PE for this application was realized early. In 1959, Richard et al. reported on the use of HD-PE as a material for pipes of drinking water lines [57]. The main point to be clarified experimentally was the life-time under permanent pressure or permanent stress. The target was a life-time of 50 years at 20°C. It was found that this could be realized with a permanent pressure not higher than 8 bars. The first tests were started in 1955 and in 2005 these specimens were still under test, showing that such pipes can be used for over 50 years without failure by stress cracking [58, 59]. With the cascaded technology, a new pipe grade was accessible with so-far unknown properties with respect to the life-time under pressure. This new grade shows a longer life-time of up to 100 years at a higher hoop stress (comparison stress at 10 bars). This grade is classified as PE 100 [48]. By introducing the advanced cascade process this pipe grade could be further upgraded to be applied for pipes with even larger diameters and thick walls because the sagging problem could be solved. This grade shows a further favorable behavior in the rapid crack propagation test for its application in gas distribution systems [58]. Former polyethylene grades failed at a pressures below 2 bars; the new material can withstand pressures up to 25 bars. Resistance against slow and rapid crack growth is caused by the high amount of tie molecules interconnecting the crystalline lamellae. These tie molecules are further well fixed by having short-chain branches introduced into the long polymer chains by copolymerization with 1-olefins. The use and application of HD-PE pipe materials is an interesting example of product and process development to achieve outstanding qualities through unusual combinations of properties. A summary of these developments over 50 years can be found elsewhere [59].

Product development is a very complicated process that comprises scientific, technical, and commercial aspects as described above. The cascaded polymerization process offers unique possibilities because of the high flexibility to design the polyethylene structure with respect to average molecular mass, the shape of the molecular mass distribution, and the comonomer distribution. Although there is a widespread know-how available on how to design polyethylenes for different applications, product development is as always based on experimental work. With a well-designed cascaded pilot plant, product development can be successfully done within a short time because this process offers a broad range of opportunities for achieving the requirements.

6 Conclusions

The slurry polymerization process as first described by Ziegler et al. [1–4] is still operated in the same way today. However, there have been breakthrough inventions in the last 60 years that have improved this process considerably. This process is now running with super-active catalysts. The reactor volume has now reached around 200 m^3. There is a detailed understanding of all relevant processes on the microscale, mesoscale, and macroscale levels. Therefore, the process can be well controlled to be operated safely without shutdowns over long production times and to achieve excellent quality consistency for the full product range. The cascaded process, especially the advanced cascade process, allows the production of polyethylenes with an outstanding combination of properties for all fields of application. With this technology, products in the high molecular mass range for technical applications have now reached combinations of properties so far not known. These products for pipes and large containers can be regarded as polymer alloys, with a solid state structure of the hard crystalline phase interconnected across the amorphous softer phase via tie molecules anchored in the crystalline phase. The polymerization process allows the design of the composition of these in-situ blends to achieve the best combinations of properties. Furthermore, the cascaded process is very flexible in product development.

Today, the slurry polymerization process is being run all over the world with great success. The current installed capacity for the described process is around 6 million tons per year, which represents approximately one sixth of the worldwide PE-HD production. Other processes for PE-HD production are the Phillips process, operated with chromium-based catalysts, and other slurry processes also operated with Ziegler-type catalyst systems [60].

Acknowledgements This article summarizes the development over many years. I want to express my thanks to all colleagues who contributed to this development. I have also to thank DI Elke Damm for her very appreciated advice and help in writing this article.

References

1. Ziegler K, Holzkamp E, Breil H, Martin H (1955) Angew Chem 67:426
2. Ziegler K (1964) Angew Chem 76:545
3. Ziegler K, Breil H, Holzkamp E, Martin H (1953) Patent DE 973,626 [Chem Abstr 54:14794 (1960)]
4. Martin H (1995) In: Fink G, Mülhaupt R, Brintzinger HH (eds) Ziegler catalysts. Springer, Berlin, pp 15–34
5. Grams E, Gaube E (1955) Angew Chem 67:548
6. Schulz G, Mehnert K (1955) Kunststoffe 45:410, 589
7. Neumann IA, Bockhoff FJ (1955) Plastics 32:117
8. Richard K (1955) Kunststoffe 45:10
9. Kneip W (1955) Chem Ind 7:297
10. Sommer S, Wagener S, Ebner H (1959) Kunststoffe 49:500

11. Galli P, Susa E, Di Drusco G (1970) (Montecatini Edison S.p.A.), Patent DE 2,000,585 [Chem Abstr 73:53566 (1970)]
12. Mayr A, Susa E, Di Brusco G (1970) (Montecatini Edison S.p.A.) Patent DE 2,013,730 [Chem Abstr 73:121062 (1970)]
13. Galli P, Luciani L, Cecchin G (1981) Angew Makromol Chem 94:63
14. Barbé PC, Cecchin G, Noristi L (1986) Adv Polym Sci 81:1
15. Luciani L, Kashiwa N, Barbé P, Toyota A (1975) (Montedison, Mitsui Petrochemical) Patent US 4,226,714 [Chem Abstr 87:68693 (1977)]
16. Kashiwa N (1980) Polym J 12:603
17. Kashiwa N, Yoshitake J, Tsutsui T (1988) In: Kaminsky W, Sinn HJ (eds) Transition metals and orgnometallics as catalysts for olefin polymerization. Springer, Berlin, p 33
18. Ferraris M, Rosati F, Gianetti E, Motroni G, Albizzati E (1980) (Montedison S.p.A.) Patent DE 2,933,997 [Chem Abstr 92:199055 (1980)]
19. Thum G (1987) (Hoechst AG) Patent DE 3,620,060 [Chem Abstr 108:205257 (1988)]
20. Böhm L (1990) (Hoechst AG) Patent DE 4,017,661 [Chem Abstr 116:84398 (1992)]
21. Breuers W, Lecht R, Böhm L (1994) (Hoechst AG) Patent EP 0,613,909 [Chem Abstr 122:134146 (1995)]
22. Ray WH (1986) Ber Bunsenges Phys Chem 90:947
23. Cossee P (1964) J Catal 3:80
24. Arlman EJ (1964) J Catal 3:89
25. Arlman EJ, Cossee P (1964) J Catal 3:99
26. Böhm LL (1978) Polymer 19:545
27. Böhm LL, Franke R, Thum G (1988) In: Kaminsky W, Sinn HJ (eds) Transition metal and organometallics as catalysts for olefin polymerization. Springer, Berlin, p 391
28. Mc Kenna T, Mattioli V (2001) Macromol Symp 173:149
29. Wicke E, Padberg G (1968) Chem Ing Techn 40:1033
30. Fieguth P, Wicke E (1971) Chem Ing Techn 43:604
31. Wicke E (1974) Chem Ing Techn 46:365
32. Böhm LL (2003) Angew Chem 115:5162
33. Böhm LL (2003) Angew Chem Int Ed 42:5010
34. Kipke K (1979) Chem Ing Techn 51:430
35. Himmelbach W, Houlton D, Ortlieb D, Lavallo M (2006) Chem Eng Sci 61:3044
36. Himmelbach W, Houlton D, Keller W (2007) New advances in HDPE reactor technology in PEPP. Maack Business Services, Zürich
37. Böhm LL, Goebel P, Schöneborn P-R (1990) Angew Makromol Chem 174:189
38. Böhm LL, Göbel P, Schöneborn P-R, Tauchnitz T (1992) In: Proceedings of the 4th world congress of chemical engineering (Karlsruhe, 16–21 June 1991). DECHEMA, Frankfurt am Main, pp 605–619
39. Böhm LL, Göbel P, Lorenz O, Tauchnitz T (1992) DECHEMA Monographien 127:257
40. Böhm LL, Enderle HF, Fleißner M (1992) Adv Mater 4:234
41. Böhm LL, Bilda D, Breuers W, Enderle HF, Lecht R (1995) In: Fink G, Mülhaupt R, Brintzinger HH (eds) Ziegler catalysts. Springer, Berlin, p 387
42. Scheirs J, Böhm LL, Boot JC, Leevers PS (1996) Trends Polym Sci 4:408
43. Berthold J, Böhm LL, Enderle H-J, Göbel P, Lüker H, Lecht R, Schulte U (1996) Plast Rubber Compos Proc Appl 25:368
44. Böhm LL, Enderle HF, Fleissner M (1998) Plast Rubber Compos Proc Appl 27:25
45. Böhm L, Fischer D (2000) Kunststofftechnik. VDI Verlag GmbH, Düsseldorf, p 205
46. Böhm LL (2001) Macromol Symp 173:53
47. Alt P, Böhm LL, Enderle H-F, Berthold J (2001) Macromol Symp 163:135
48. Schulte U (2006) Kunststoffe 96:46
49. Sattel R (2008) Kunststoffe 9:115
50. Müller W, Damm E (2009) Kunststoffe Int 2009(10):28

51. Auriemma F, Talarico G, Corradini P (2000) In: Sano T, Uozumi T, Nakatani H, Terano M (eds) Progress and development of catalytic olefin polymerization. Technology and Education, Tokyo, p 7
52. Böhm LL (1978) Polymer 19:553
53. International Organization for Standardization (1981) ISO 1133:1981. Plastics – determination of the melt flow rate of thermoplastics. ISO, Geneva
54. Fleissner M (1988) Int Polym Process II:229
55. Fleißner M (1982) Angew Makromol Chem 105:167
56. Schmitt-Rohr K, Spieß HW (1991) Macromolecules 24:5288
57. Richard K, Gaube E, Diedrich G (1959) Kunststoffe 49:516
58. Schulte U (1997) Kunststoffe 87:203
59. Brömstrup H (ed) (2006) Wiesbadener Kunststoffrohrtage. Vulkan, Essen
60. Keim W (ed) (2006) Polyolefine in Kunststoffe. Wiley, Weinheim

Adv Polym Sci (2013) 257: 81–98
DOI: 10.1007/12_2013_224

Published online: 12 June 2013

The Use of Donors to Increase the Isotacticity of Polypropylene

Toshiaki Taniike and Minoru Terano

Abstract Since the discovery of electron donors for $MgCl_2$-supported Ziegler–Natta catalysts, donors have become key components for improving the stereospecificity and activity of these catalysts. Starting from benzoate for third-generation catalysts, the discovery of new donor structures has always updated the performance of Ziegler–Natta catalysts. Numerous efforts have been devoted since the early 1970s, in both industry and academy, not only for discovering new donors but also for understanding their roles in Zielger–Natta olefin polymerization. This chapter reviews the history of these efforts, especially after the twenty-first century. The first half of the chapter describes the history of catalyst developments, with special focus on industrialized donors, and then introduces recent trends in the development of new donors. The second half reviews historical progress in the mechanistic understanding of how donors improve the performance of Ziegler–Natta catalysts.

Keywords Donor · Heterogeneous Ziegler–Natta catalyst · Propylene polymerization

Contents

T. Taniike (✉) and M. Terano
School of Materials Science, Japan Advanced Institute of Science and Technology, 1-1 Asahidai, Nomi, Ishikawa 923-1292, Japan
e-mail: taniike@jaist.ac.jp; terano@jaist.ac.jp

1 History

Polypropylene (PP) is one of the most widely used plastics and features a wide range of advantages such as low cost, light weight, high melting temperature, good processability, balanced mechanical properties in terms of stiffness and impact resistance, etc. Moreover, PP is regarded as a clean material with respect to urgent environmental requirements, not only due to the halogen- and benzene-free structure but also due to the ease of reuse and recycle. The world production of PP in 2012 reached approximately 60 million tons per year, and is forecasted to stably grow in the future (Fig. 1). The diverse properties of PP enable its application in a variety of fields from commodity to specialty.

The immense growth of the polypropylene industry has been greatly driven by the continuous developments in catalyst technology (Table 1) [1, 2 and references therein]. The history of propylene polymerization started with the landmark discovery of a solid $TiCl_3$ pro-catalyst combined with diethylaluminum chloride (DEAC) by Natta in 1954 [3, 4]. This so-called first generation catalyst enabled the first catalytic isoselective propylene polymerization, but its poor activity and isospecificity necessitated additional processes to extract poorly isotactic products and violet catalyst residues from the obtained polymer. Significant efforts were then devoted to improving the activity and isospecificity of the catalyst. For the catalyst activity, there were two main directions of study in order to enhance the utilization efficiency of the Ti species: preparation of $TiCl_3$ with larger surface area and the search for an efficient support material for Ti halide species. The Solvay corporation invented the so-called Solvay-type $TiCl_3$ in the early 1970s, which was prepared by the reduction of $TiCl_4$ with DEAC followed by the removal of Al residues with the aid of ether [5]. The resultant catalyst, regarded as a second generation catalyst, achieved improved activity and isospecificity over the first generation of catalysts, but the level of the improvements was still insufficient to eliminate the above-mentioned purification processes for the obtained polymer. Regarding a support material, metal oxide (SiO_2, Al_2O_3) or hydroxide materials [$Mg(OH)_2$] were initially considered due to the ease of the immobilization of Ti species through covalent bonds. However, successful improvement in activity was not achieved until Montedison and Mitsui discovered $MgCl_2$ support, almost at the same time in 1968 [6, 7]. The catalysts, consisting of $TiCl_4$ active site precursor, $MgCl_2$ support, and triethylaluminum (TEA) activator, exhibited much higher activities than the former generation of catalysts, but their use was limited to ethylene polymerization due to poor isospecificity. That is the story before the appearance of "donors," i.e., the main topic of this chapter.

The first donors in Ziegler–Natta catalysis appeared as a result of collaborative efforts between Montedison and Mitsui to improve the isospecificity of the above-mentioned $MgCl_2$-supported catalyst [8, 9]. The developed catalyst, termed third generation, achieved not only high activity but also high isospecificity by adding benzoate to the $TiCl_4/MgCl_2$ catalyst. The term "donor" originates from the fact that additives to improve the catalyst isospecificity are Lewis bases with

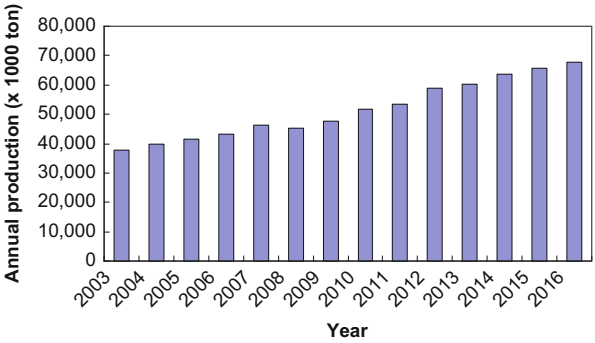

Fig. 1 Annual production of polypropylene (from Ministry of Economy, Trade and Industry, Japan, 2012)

Table 1 Propylene polymerization performance of Ziegler–Natta catalysts of different generations[a]

Generation	Pro-catalyst	External donor	Activity (g-PP/mmol-Ti h atm)	I.I.[b] (%)
First	$TiCl_3$	–	ca. 4	90
Second	Solvay-type $TiCl_3$	–	ca. 30	95
Third	$TiCl_4/MgCl_2$/benzoate	Benzoate	ca. 1,000	92–94
Fourth	$TiCl_4/MgCl_2$/phthalate	Alkoxysilane	ca. 1,000–3,000	>98
Fifth	$TiCl_4/MgCl_2$/1,3-diether	Alkoxysilane	ca. 3,000–5,000	>98

[a]Reproduced from [1]
[b]Insoluble fraction in boiling heptane

electron-donating ability. Usually, donors are classified into two types according to their roles: internal donors contained in the solid component ($TiCl_4/MgCl_2$) and external donors, which are added together with alkylaluminum in order to prevent the deterioration of the catalyst isospecificity during the course of polymerization. It should be noted that the idea to add Lewis bases already existed for $TiCl_3$-based catalysts, where the addition of some Lewis bases during polymerization improved the isotactic index (I.I.) by, at maximum, up to 10%. However, donors for $MgCl_2$-supported catalysts are totally different in terms of the dramatic improvements in the isospecificity; it is not exaggerating to say that donors "endow" isospecificity to $MgCl_2$-supported catalysts. The third generation catalyst typically combines ethylbenzoate (EB) as an internal donor with EB or *para*-substituted benzoate as an external donor (Fig. 2). The third generation catalysts achieved propylene polymerization activity of 100 times higher than the second generation (Table 1), and high isospecificity (I.I. of 92–94%). However, the remaining 6–8% of poorly isotactic fraction triggered further research, mainly focused on improvements in catalyst preparation procedures as well as on finding a more efficient combination of internal and external donors. The extraction process for poorly isotactic fraction was finally eliminated in 1977 by use of a catalyst employing a new donor combination. i.e., phthalic diester as an internal donor and alkoxysilane as an external donor (Fig. 2) [10, 11]. This catalyst, termed a fourth generation catalyst,

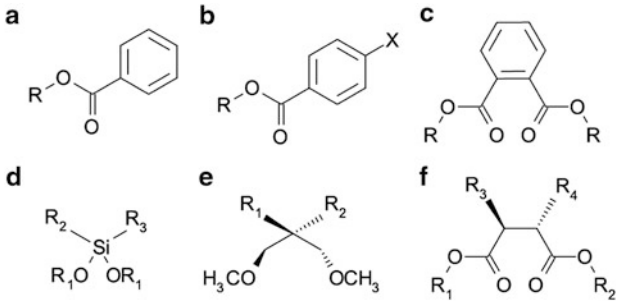

Fig. 2 Industrially developed internal and external donors: (**a**) benzoate, (**b**) *para*-substituted benzoate, (**c**) phthalate, (**d**) dialkoxysilane, (**e**) 1,3-substituted diether, and (**f**) 2,3-substituted succinate. Note that (**a**), (**c**), (**e**), and (**f**) are employed as internal donors, whereas (**a**), (**b**), and (**d**) are used as external donors

comprises $TiCl_4/MgCl_2$/phthalate and $AlEt_3$/alkoxysilane, and has been widely employed for the industrial production of polypropylene (PP) since its discovery.

From the late 1980s to 1990s, a series of 1,3-diether compounds were proposed as a new type of internal donor (Fig. 2) [12]. Catalysts containing 1,3-diether as an internal donor exhibit quite high activity and isospecificity without the addition of an external donor, whereas ester-type internal donors for the former generations require the addition of external donors to suppress or compensate for decreases in the activity and isospecificity during the course of polymerization. Furthermore, the new catalysts are generally characterized by a superior hydrogen response as well as narrower molecular weight distribution (M_w/M_n around 4) as compared with the former generation of catalysts. Owing to these distinct characteristics, the catalysts are recognized as fifth generation and are especially employed to produce PP grades suitable for unwoven fabric applications.

In the late 1990s, a research group from Ube Industries (later Grand Polymer) patented a series of unique nitrogen-containing alkoxysilane external donors [13–19]. In contrast to the original patent [10, 11] for the fourth generation catalyst, which specified external donors containing at least one Si-OR, Si-OCOR, or $SiNR_2$ group, the research group systematically explored external donors containing both Si-OR and $SiNR_2$ groups. They found that the addition of dialkoxysilane with N-containing polycyclic groups (examples are shown in Fig. 3) enables the production of highly isotactic PP featuring a molecular weight distribution as broad as that given by the $TiCl_3$-based catalysts [14]. The significance of their findings was twofold: they allowed broadening of the molecular weight distribution by means of external donors without sacrificing the activity and isospecificity of the fourth generation catalyst, and they opened up development of heteroatom-containing donors. Based on this trend, several N-containing external donors with much higher hydrogen response (i.e., better melt flowability of PP) were presented (examples are listed in Fig. 3) [19]. At present, the industrial application of N-containing donors is limited for several reasons, e.g., the absence of the highest molecular weight tail in

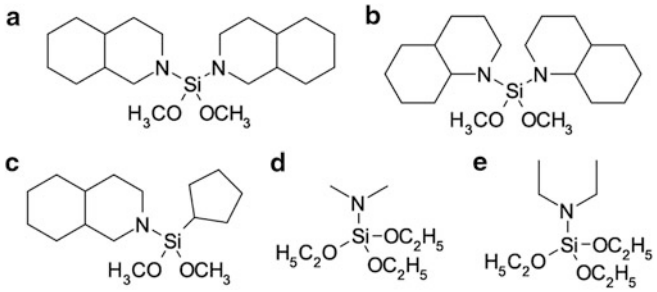

Fig. 3 Examples of nitrogen-containing external donors: (**a**) bis(perhydroisoquinolino) dimethoxysilane, (**b**) bis(perhydroquinolino)dimethoxysilane, and (**c**) cyclopentylisoquinolinodimethoxysilane for broad molecular weight distribution; (**d**) dimethylaminotriethoxysilane and (**e**) triethylaminotriethoxysilane for high hydrogen response

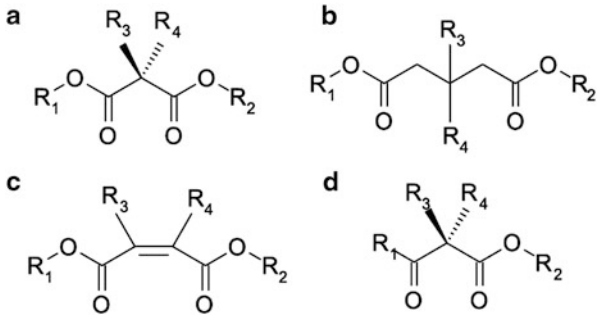

Fig. 4 Internal donors developed for catalysts equipping both high activity and high isospecificity: (**a**) malonate, (**b**) β,β-substituted glutarate, (**c**) 2,3-substituted maleate, and (**d**) β-ketoester

the molecular weight distribution of PP, an odor problem, and so on. However, heteroatom-containing donors are doubtless promising in order to facilitate unique properties.

Though the fifth generation catalysts achieved almost two times higher activity than the fourth generation catalysts, their application is limited to some special grades. This is mainly because of the lower isospecificity as well as the narrower molecular weight range, which is disadvantageous in terms of balanced solid stiffness and melt flowability of the resultant PP. Consequently, the decade after the late 1990s was devoted to the finding of new donor systems that facilitated not only high activity but also high isospecificity. For instance, malonate (1998) [20], β-substituted gultarate (2000) [21], maleate (2003) [22], and β-ketoester (2005) [23] are such internal donors (Fig. 4). Of these donors, 2,3-substituted succinate (2000) [24] not only achieved high isospecificity, but also offered broader molecular weight distribution of PP than that given by the fourth generation catalysts (Fig. 2). Because succinate enabled the first production of PP with broad molecular weight distribution without the above-mentioned problems of $TiCl_3$-based catalysts

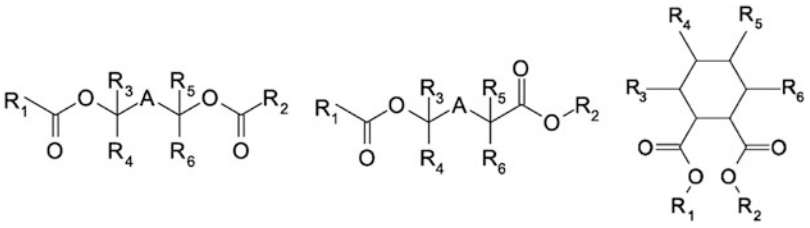

Fig. 5 Internal donors developed for broad molecular weight distribution of PP

and of N-containing external donors, the catalyst employing succinate as an internal donor is nominated as a sixth generation catalyst. The specific features of succinate are commonly attributed to the presence of chiral centers in the framework, which plausibly enables the coexistence of donors having different stereostructures. Figure 5 shows donors that have been developed on the basis of a similar idea [25–27].

Thus, it is not too much to say that the history of heterogeneous Ziegler–Natta catalysts is almost identical to the history of finding new donors since the third generation. This is because donors modify not only the catalyst activity but also physical properties of PP through isotacticity, molecular weight distribution, and comonomer incorporation. However, great modifications in the preparation of solid catalyst components must not be overlooked in terms of the historical improvements in the activity and isospecificity. This is reasonable when one considers that catalyst structures are affected not only by donors but also by preparative routes. In this sense, a seventh generation catalyst may appear as the result of synergistic combination between new donors and new preparative techniques.

2 Mechanistic Aspects

It is known that the addition of donors causes a variety of consequences in the performance of Ziegler–Natta catalysts such as activity enhancement, drastic improvement in the isospecificity, the elongation of molecular weight, and so on. Considering that olefin polymerization catalysis results from a catalytic function of active Ti species, these consequences must result from interactions of donors with active Ti species. Interactions can not only be direct but also indirect, whereby donors interact with other catalytic components that interact with Ti species, thus indirectly affecting its performance. This section briefly summarizes the mechanistic aspects of how donors interact with other catalytic components to modify the performance of Ziegler–Natta catalysts, especially focusing on progress since 2000. A reader who is interested in more details, especially before 2000, is referred to [2, 28, 29] together with references therein.

In principle, donors (Lewis basic compounds) can bind to catalytic components with Lewis acidic sites such as Ti of $TiCl_4$, undercoordinated Mg on $MgCl_2$ surfaces, and Al of alkylaluminum. The coordination of donors occurs through

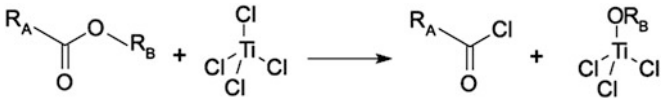

Scheme 1 Reaction of an ester-type donor with $TiCl_4$

the donation of an unshared electron pair. In the case of ester-based donors, the coordination accompanies a red-shift of the C=O vibrational frequency, whose degree depends on the chemical nature of the Lewis acidic sites. This fact has been frequently utilized to examine the state and location of ester-type donors in solid catalysts by means of IR spectroscopy. Terano et al. clarified with IR spectroscopy and thermal analysis that EB dominantly resides on $MgCl_2$ surfaces without forming a $TiCl_4$·EB complex [30]. This is in agreement with quantum chemical calculations, which concluded that the dissociative adsorption of $TiCl_4$·EB on $MgCl_2$ surfaces is energetically more advantageous than non-dissociative adsorption [31]. Similar IR results were obtained for dibutylphthalate (DBP), for example, by Arzoumanidis and Karayannis [32] They studied catalysts that were activated at different temperatures and found that DBP dominantly coordinated to surface Mg sites at any activation temperature. However, a residual amount of $TiCl_4$·DBP complex was detected only when a catalyst was activated at a too-low temperature (called under-activation), whereas activation at a too-high temperature led to the formation of carbonyl halides according to Scheme 1 [32, 33] (called over-activation [32]), both of which resulted in a clear reduction in propylene polymerization activity.

Thus, it is well accepted that donors are supported on $MgCl_2$ surfaces separately from $TiCl_4$ in solid catalysts. As a consequence, most research since the 1990s has been directed towards understanding how internal donors affect the formation of solid catalysts during preparation, which $MgCl_2$ surfaces the donors prefer to be located on, and how donors interact with $TiCl_4$ or active Ti species.

The preparation of highly active $MgCl_2$-supported Ziegler–Natta catalysts generally requires activation of the $MgCl_2$ support, which is typically performed by co-grinding $MgCl_2$ with an internal donor and/or $TiCl_4$, treating a $MgCl_2$·donor adduct with $TiCl_4$, or by chlorinating MgX_2 (X = R, OR, OCOR, etc.) into $MgCl_2$ followed by treatment with an internal donor. In contrast to α- and β-$MgCl_2$ with well-dissolved X-ray diffraction (XRD) patterns, activated $MgCl_2$ usually exhibits an XRD pattern typical for δ-$MgCl_2$, featuring very broad peaks centered at around 15°, 32°, and 50° [corresponding to (0 0 3), (1 0 l), and (1 1 0) reflections, respectively] (Fig. 6) [34]. These broad peaks are usually ascribed to a rotational disorder in the Cl–Mg–Cl tri-layer stacking along the (0 0 1) direction and reduced crystalline dimensions [35, 36]. Since donors strongly bind to undercoordinated Mg sites and stabilize the corresponding sites, internal donors might affect the structure of the activated $MgCl_2$ support. However, full understanding of its structure has been prevented by the structural irregularity of δ-$MgCl_2$, and great progress has only recently been made, especially regarding the surface structures of δ-$MgCl_2$.

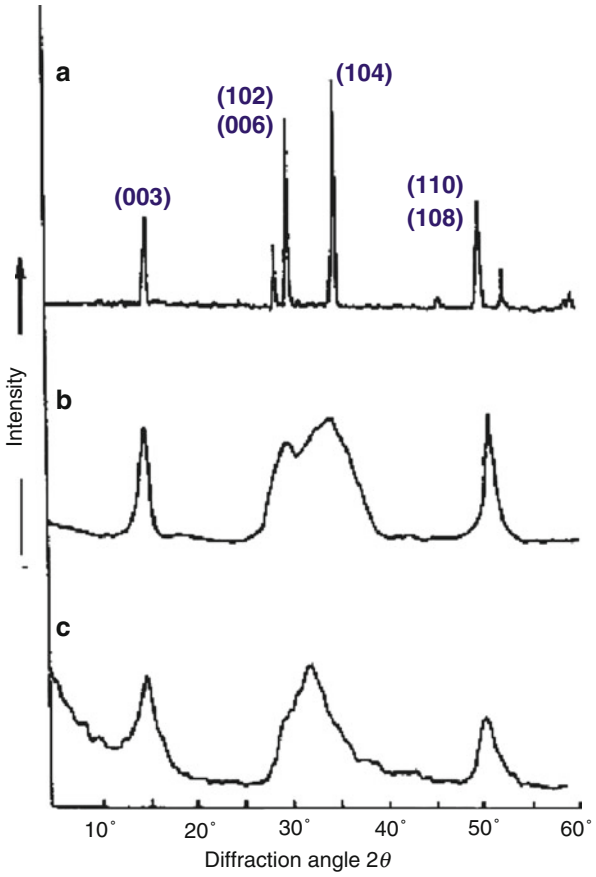

Fig. 6 X-ray diffraction patterns of (**a**) α-$MgCl_2$, (**b**) mechanically activated $MgCl_2$, and (**c**) chemically activated $MgCl_2$ (reproduced from [34]). The latter two show diffraction patterns characteristic for δ-$MgCl_2$

The most stable surface of $MgCl_2$ is the (0 0 1) basal plane, which is obtained by cleaving the $MgCl_2$ tri-layer stacking. The (0 0 1) plane is coordinatively saturated [37] and therefore inactive to the adsorption of $TiCl_4$ and donors [38, 39], i.e., it is catalytically irrelevant. Catalytically relevant surfaces are low-index planes that expose unsaturated Mg^{2+} ions. The (1 1 0) and (1 0 4) lateral planes have been long believed to be representative [35, 36], consistent with the diffraction peaks for these planes. Note that the (1 0 4) plane is sometimes expressed as the (1 0 0) plane [37, 40]. The (1 1 0) and (1 0 4) surfaces, respectively, expose four- and fivefold coordinated Mg^{2+} ions in comparison with sixfold coordination in the bulk and on the (0 0 1) basal plane (Fig. 7 [41]). Busico et al. recently used dispersion-corrected density functional theory (DFT-D) calculations to show that $MgCl_2$ mainly exposes the (0 0 1) and (1 0 4) surfaces at an equilibrium crystallographic morphology (Fig. 8) [37]. However, activated $MgCl_2$ can also expose the (1 1 0) lateral plane, as a result of the morphology formation under kinetically non-equilibrated conditions and/or a shifted equilibrium in the presence of adsorbates such as $TiCl_4$ and donors [37, 40]. For example, Mori, Terano et al. observed with

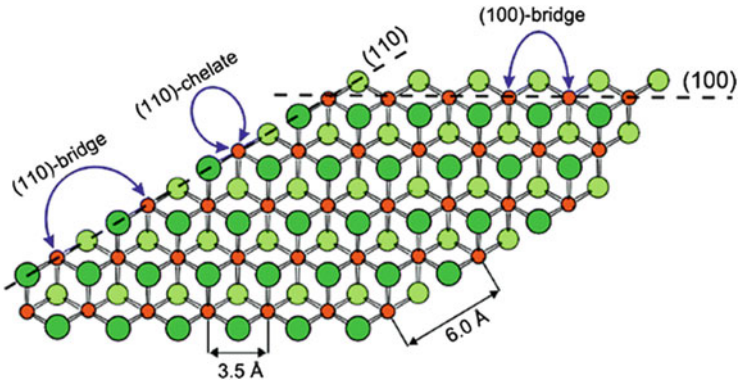

Fig. 7 Schematic view of a $MgCl_2$ monolayer with (1 1 0) and (1 0 0) terminations (reproduced from [41]). *Orange balls* represent Mg^{2+} ions, and *light* and *dark green balls* represent Cl^- ions. The top surface corresponds to the (0 0 1) basal plane without coordinative unsaturation

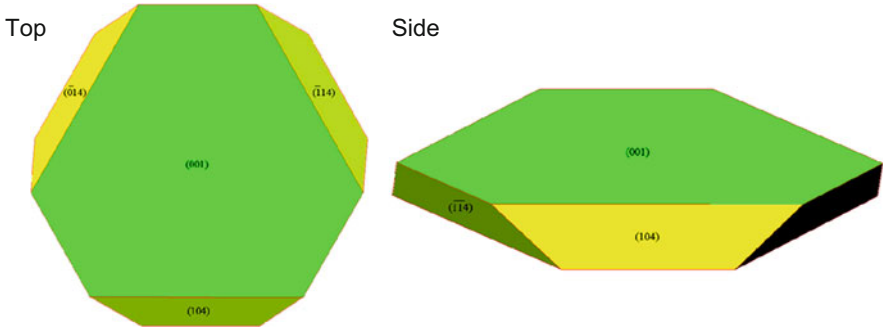

Fig. 8 Equilibrium crystallographic morphology of $MgCl_2$ estimated from surface energies of DFT-D calculations (reproduced from [37])

high-resolution transmission electron microscope (TEM) that lateral surfaces of mechanically activated $MgCl_2$ are dominantly composed of the (1 1 0) and (1 0 4) planes (Fig. 9) [42]. Andoni et al. reported preferential growth of $MgCl_2$ crystal along the (1 1 0) direction in the presence of 1,3-diether, while the growth occurred along both the (1 1 0) and (1 0 4) directions in the presence of DBP (Fig. 10) [43]. Recent DFT calculations by Credendino, Cavallo et al. pointed out that the equilibrium crystallographic morphology of $MgCl_2$ became completely different in the presence of a donor, where the (1 1 0) termination prevailed over the (1 0 4) termination in the presence of ether adsorbates [44].

Since donors bind to and stabilize undercoordinated Mg^{2+} ions during the formation of solid catalysts, their adsorption behaviors on $MgCl_2$ surfaces have been extensively studied, mainly based on IR spectroscopy and quantum chemical calculations. The adsorption structures of representative donors are summarized in Fig. 11 [40, 41]. In general, monoester-type donors for the third generation adsorb

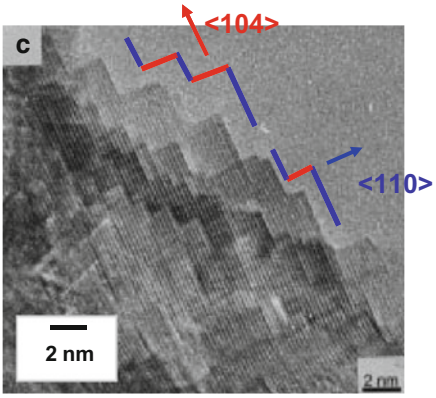

Fig. 9 High-resolution TEM image of milled $MgCl_2$, where the lateral cuts are mainly composed of the (1 1 0) and (1 0 4) surfaces (reproduced from [42])

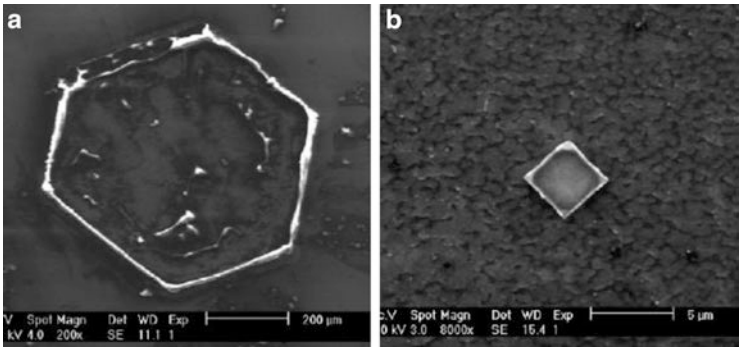

Fig. 10 Morphology of $MgCl_2$ grown from ethanol solution over silicon wafer in the presence of (**a**) 1,3-diether and (**b**) phthalate (reproduced from [43]). $MgCl_2$ formed in the presence of 1,3-diether exhibits only 120° corners, indicating the exposure of only one type of lateral cut, i.e., (1 1 0). On the other hand, 90° corners for phthalate indicate coexposure of the (1 1 0) and (1 0 4) lateral cuts

on $MgCl_2$ surfaces in a monodentate fashion through the carbonyl oxygen. Diester-type donors for the fourth and sixth generations can adsorb either in a bidentate fashion or in a bridging fashion. 1,3-Diethers (stereoregulating ones) and alkoxysilane preferentially adsorb in a bidentate fashion because the distance between two Lewis basic oxygens is not enough to bridge two neighboring Mg^{2+} ions on the $MgCl_2$ surfaces [45, 46]. In terms of the lateral planes, bidentate adsorption does not occur on the (1 0 4) surface with fivefold coordinated Mg^{2+} ions exposed. Namely, 1,3-diether poorly adsorbs on the (1 0 4) surface, i.e., hardly stabilizes the (1 0 4) surface as an internal donor. This is in contrast to ester-type donors, which can adsorb both on the (1 1 0) and (1 0 4) surfaces [40, 44]. This fact is consistent with the preferential growth of $MgCl_2$ crystal along the (1 1 0) direction in the presence of 1,3-diether [43] and with the narrow molecular weight

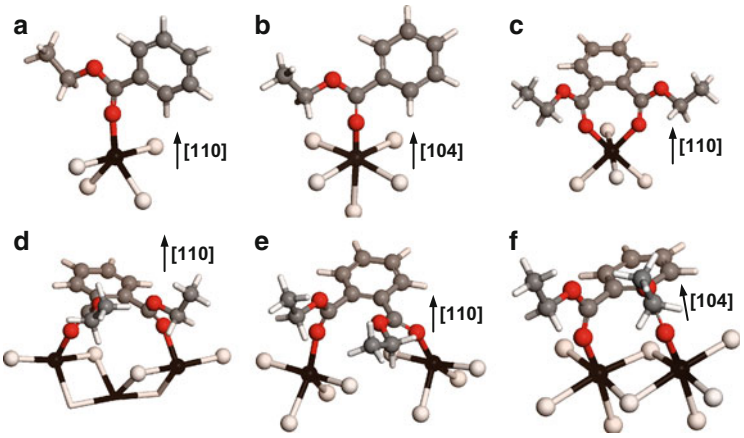

Fig. 11 Adsorption modes of donors on $MgCl_2$ surfaces (reproduced from [40]): (**a**, **b**) Benzoate adsorbed on the (1 1 0) and (1 0 4) surfaces in a monodentate fashion, (**c**–**e**) phthalate adsorbed on the (1 1 0) surface in bidentate, intra-bridging, and inter-bridging fashions, and (**f**) phthalate adsorbed on the (1 0 4) surface in an intra-bridging mode. *Black* Mg, *white* Cl (*balls*) and H (*sticks*), *gray* C, *red* O

distribution of PP produced by a 1,3-diether-containing catalyst. The number of adsorption modes for one donor may be important for the molecular weight distribution of PP [41]. Zakharov and coworkers conducted systematic IR studies to examine the adsorption states of benzoate and phthalate on $MgCl_2$ [47–50]. The carbonyl absorption bands of these donors were not only red-shifted but also broadened as compared with those of free (non-adsorbed) donors, which was explained by the adsorption of the donors at Mg^{2+} sites with different coordination vacancies. Brambilla et al. employed an advanced approach to identify the location of $TiCl_4$ or 1,3-diether in solid catalysts, where experimental Raman spectra were compared with simulated spectra by assuming molecular model structures [51, 52]. They found that the adsorption on the (1 1 0) surface led to better reproduction of the experimentally obtained spectra than that on the (1 0 4) surface.

The fact that donors adsorb on coordinatively unsaturated $MgCl_2$ surfaces is important in considering the state of $TiCl_4$ as active site precursor, since $TiCl_4$ competitively adsorbs on these surfaces. In fact, the treatment of donor/$MgCl_2$ by $TiCl_4$ or the treatment of $TiCl_4$/$MgCl_2$ by a donor at an elevated temperature generally reduces the content of the donor or $TiCl_4$, respectively. Consequently, mechanistic suggestions about how donors affect the catalytic performance, especially isospecificity, have been made on the basis of their competitive adsorption on $MgCl_2$ surfaces. The following paragraphs summarize the historical variation in academic consensuses on this subject from the late 1980s to the present.

The advantages of $MgCl_2$ as a catalytic support over the other halides are attributed to the facts that $MgCl_2$ has a similar crystallographic structure to violet $TiCl_3$ and that $TiCl_4$ can adsorb on unsaturated $MgCl_2$ surfaces in a epitactic manner due to resemblance between the atomic radii of Mg^{2+} and Ti^{4+} [28, 53]. When $TiCl_4$ adsorbs as mononuclear species on the (1 1 0) surface and

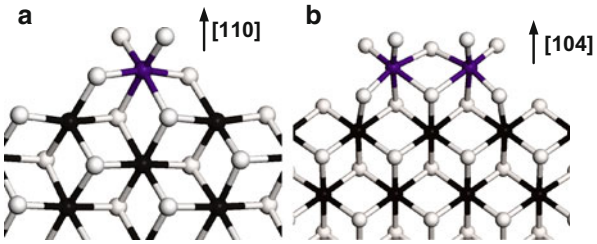

Fig. 12 $TiCl_4$ adsorbed on $MgCl_2$ surfaces: (**a**) mononuclear species on the (1 1 0) surface, and (**b**) dinuclear species on the (1 0 4) surface (reproduced from [40]). *Black* Mg, *white* Cl, *purple* Ti

as dinuclear species on the (1 0 4) surface , $TiCl_4$ can terminate these surfaces with Ti^{4+} ions located at positions that are supposed to be occupied by Mg^{2+} ions (Fig. 12) [53]. From structural analogy with active sites for $TiCl_3$-based catalysts, the mononuclear species on the (1 1 0) surface is regarded as precursor of an aspecific active site, while the dinuclear species on the (1 0 4) surface is regarded as precursor of an isospecific active site. The first persuading proposal on the mechanism for how donors improve the catalyst isospecificity was performed by Busico, Corradini, and coworkers: donors preferentially adsorb on the (1 1 0) surface with higher Lewis acidity, thus preventing the formation of the aspecific mononuclear species while increasing the ratio of the isospecific dinuclear species [53]. Corradini's model was widely accepted, but subsequent research progress posed several controversial points, two of which are:

- Not only the above-mentioned research by Brambilla et al. [51] but also most recent DFT calculations support the preferential adsorption of $TiCl_4$ on the (1 1 0) surface [31, 40, 54–58].
- Within Corradini's model, the isospecific active site always corresponds to the dinuclear species on the (1 0 4) surface, irrespective of the molecular structure of donors. However, microtacticity of isotactic PP produced in the presence of different donors was found to be sensitive to the molecular structure of donors (Fig. 13), clearly indicating that the active site structure and its nature are dependent on the structure of the donors [59–62].

Separately from their previous model [53], Busico et al. proposed a general active site model in Ziegler–Natta propylene polymerization, based on statistical analyses of polymer stereostructures acquired by high-resolution ^{13}C-NMR [63]. This so-called three-site model, after modification by Liu, Terano et al. [64], is at present widely accepted. As shown in Fig. 14, the stereospecificity of Ti species situated in an octahedral symmetry is described by the presence or absence of ligands $L_{1,2}$ at the neighboring metal centers, which are connected to the Ti center through chlorine bridges. $L_{1,2}$ sterically transfers underlying C_2 symmetry to the Ti center in a way that controls the configurational orientation of growing chain and propylene [40, 41, 63]. This model explicitly represents an active site that contain donors at the $L_{1,2}$ positions, where it is easy to imagine that the bulkiness of donors at $L_{1,2}$ affects the stereospecificity of the Ti center. Taniike and Terano conducted systematic DFT calculations on the coexistence of Ti species and donors on catalytic surfaces, and clarified that coadsorption of

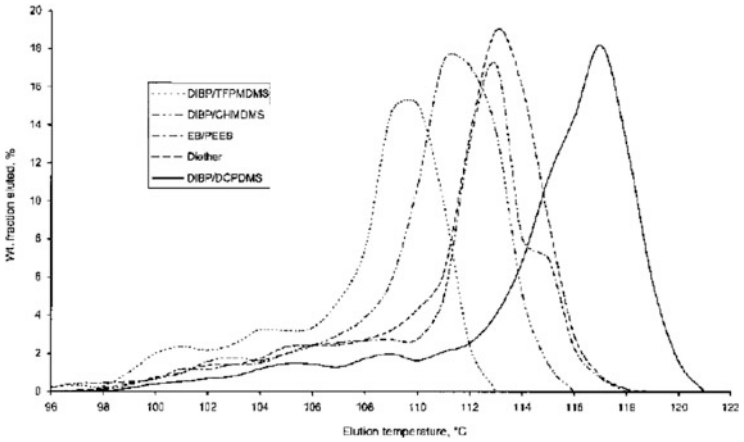

Fig. 13 Profiles of temperature rising elution fractionation of PP produced by catalysts with different internal and external donors (reproduced from [59]). *DIBP* disobutylphthalate, *TFPMDMS* 3,3,3-trifluoropropyl(methyl)dimethoxysilane, *CHMDMS* cyclohexyl(methyl)dimethoxysilane, *EB* ethylbenzoate, *PEEB* ethyl *p*-ethoxybenzoate, *DCPDMS* dicyclopentyldimethoxysilane. The deviation in the peak positions indicates that the isospecificity of the main active sites varies according to the combination of donors

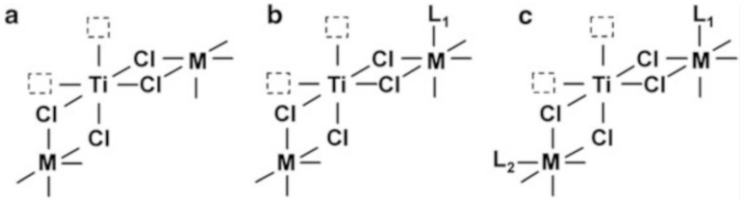

Fig. 14 Three-site model proposed by Busico et al. [63] (reproduced from [75]). Active site models relevant to the production of (**a**) syndiotactic (or atactic), (**b**) isotactoid (or isotactic), and (**c**) highly isotactic PP. A growing chain and propylene monomer occupy the chained squares. M = Ti, Mg, or Al; L = Cl, donor, or alkylaluminum moiety [64]

donors with $TiCl_4$ mononuclear species on the $MgCl_2$ (1 1 0) surface is the most plausible scenario from energetic, steric, and electronic points of views [40]. Thus, the proposed coadsorption model [40] succeeded in reproducing experimentally well-known results on the influences of donors on catalytic performance, such as improvements in isospecificity and regiospecificity, elongation of PP molecular weight, and so on [65–68].

Although the above paragraphs focused on the roles of donors in the formation of solid catalysts and the active sites thereon, the interaction between donors and alkylaluminum also plays a crucial role in catalysis. Lewis basic donors not only form a complex with alkylaluminum, but also react with highly reactive Al–R bonds: internal donors except 1,3-diether desorb from $MgCl_2$ surfaces through

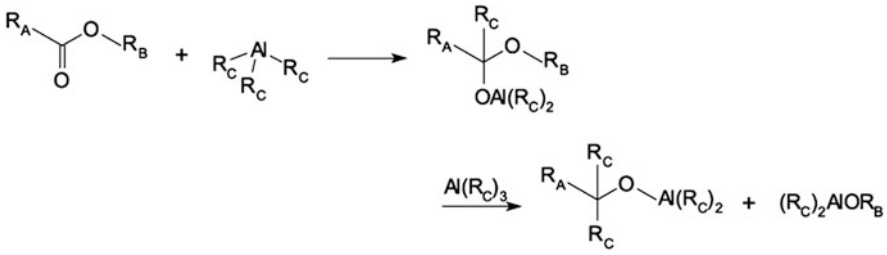

Scheme 2 Reaction of an ester-type donor with alkylaluminum

complexation with alkylaluminum and lose their functionality through the reaction with Al–R. For instance, ester-type donors are known to react with alkylaluminum according to Scheme 2 [28, 29, 69, 70].

On the other hand, 1,3-diether is known to be difficult to extract by alkylaluminum from surfaces and therefore can retain high isospecificity even without external donors [71]. The extraction of internal donors not only decreases the catalyst isospecificity but also the activity. To prevent these deteriorations, external donors are usually added during polymerization. As stated above, benzoate is employed for the third generation catalysts and alkoxysilane for the later generations. It is known that benzoate as an external donor prevents the extraction of internal donors, whereas alkoxysilane accelerates it, but the mechanistic origin is not clear. The most widely employed dialkoxysilane forms a one-to-one complex with alkylaluminum and goes through a slow ligand exchange equilibrium between an alkoxy group of dialkoxysilane and an alkyl group of alkylaluminum [72]. Wrong combination between internal and external donors, such as an alkoxysilane external donor for a third generation catalyst and a benzoate external donor for the later generation catalysts, usually exhibit much poorer performance compared with the correct combination. This is known as a key-hole relation between internal and external donors [73, 74], whose origin is also still unclarified. In this way, chemistry of the interaction between (internal and external) donors and alkylaluminum has hardly progressed since 2000; nonetheless, it is certain that a good external donor must not only be tolerant against alkylaluminum but also compatible with the employed internal donor.

In summary, the present chapter has briefly reviewed the historical development and state-of-the-art academic understanding of donors in Ziegler–Natta propylene polymerization. The roles of donors have been gradually uncovered due to advances in characterization techniques and computational chemistry, while their development still relies on conventional trial-and-error methodology, mainly because of poor understanding of their structure–performance relationships. The authors strongly wish that further advances in the molecular-level elucidation will finally enable us to reach a priori design of a new class of donors, something that has not yet been fully achieved even for other heterogeneous catalysts.

References

1. Matsunaga K (2008) Next generation polyolefins, vol 1. Sankeisha, Nagoya, p 84
2. Albizzati E, Giannini U, Collina G, Noristi L, Resconi L (1996) In: Moore EP Jr (ed) Polypropylene handbook. Hanser-Gardner, Cincinnati, p 11
3. Natta G (1995) J Polym Sci 16:143
4. Natta G (1955) J Am Chem Soc 77:1707
5. Hermans JP, Henrioulle P (1972) Process for the preparation of a Ziegler–Natta type catalyst. German Patent 2,213,086, to Solvay & CIE
6. Mayr A, Galli P, Susa E, Di Drusco G, Giachetti E (1968) Polymerization of olefins. British Patent 1,286,867, to Montedison
7. Kioka M, Kitani H, Kashiwa N (1971) Process for producing olefin polymers or copolymers. Japanese Patent 34,092, to Mitsui Petrochemical Industries
8. Giannini U, Cassata A, Longi P, Mazzoch R (1972) Procede pour la polymerisation stereoreguliere des alpha-olefines. Belgian Patents 785,332 and 785,334, to Montedison
9. Luciani L, Kashiwa N, Barbè PC, Toyota A (1977) Katalysatoren zur polymerisation von alpha-olefinen. German Patent 2,643,143, to Montedison and Mitsui Petrochemical Industries
10. Luciani L, Kashiwa N, Barbè C, Toyota A (1977) α-Olefin polymerization catalyst. Japanese Patent 151,691, to Montedison and Mitsui Petrochemical Industries
11. Parodi S, Nocci R, Giannini U, Barbè PC, Scata U (1982) Components and catalysts for the polymerization of olefins. European Patent 45,977, to Montedison
12. Albizzati E, Barbè PC, Noristi, Scordamaglia LR, Barino L, Giannini U, Morini G (1990) Components and catalysts for the polymerization of olefins. European Patent 361,494 A1, to Himont
13. Igai S, Ikeuchi H, Yamashita J (1997) Diaminoalkoxysilane. Japanese Patent H09-67,379, to Ube Industries
14. Igai S, Ikeuchi H, Sato H (1998) Polymerization of alpha-olefin. Japanese Patent 1998-218,926, to Grand Polymer
15. Ikeuchi H, Sato H, Igai S (1998) Propylene polymer. Japanese Patent 1998-237,127, to Grand Polymer
16. Ikeuchi H, Sato H, Igai S (1998) Process for producing alpha-olefin. Japanese Patent 1998-292,008, to Grand Polymer
17. Igai S, Ikeuchi H, Sato H (1999) Polymerization of alpha-olefin. Japanese Patents 1999-147,906, 1999-292,914, and 1999-322,830, to Grand Polymer
18. Ikeuchi H, Sato H, Igai S (1999) Polymerization of alpha-olefin. Japanese Patent 1999-349,620, to Grand Polymer
19. Fukunaga T, Ikeuchi H, Machida T, Sato H, Tanaka Y, Yano T, Yoshikiyo M (2004) Catalysts for polymerization or copolymerization of α-olefins, catalyst components thereof, and processes for polymerization of α-olefins with the catalysts. WO 2004/016,662 A1, to Ube Industries
20. Morini G, Balbontin G, Chadwick J, Cristofori A, Albizzati E (1998) Components and catalysts for the polymerization of olefins. WO 1998/056,830, to Montell Technology
21. Morini G, Balbontin G (2000) Components and catalysts for the polymerization of olefins. WO 2000/055,215, to Basell Technology
22. Morini G, Balbontin G, Gulevich YV, Vitale G (2003) Components and catalysts for the polymerization of olefins. WO 2003/022,894, to Basell Polyolefin Italia
23. Gulevich Y, Balbontin G, Morini G, Nifant'ev I (2005) Components and catalysts for the polymerization of olefins. WO 2005/097,841, to Basell Polyolefin Itralia
24. Morini G, Balbontin G, Gulevich YV, Kelder RT, Duijghuisen HPB, Klusener PAA, Kondorffer FM (2000) Components and catalysts for the polymerization of olefins. WO 2000/063,261, to Basell Technology

25. Gao M, Liu H, Li Z, Wang J, Yang J, Li T, Wang X, Li C, Ding C (2003) Solid catalyst component for polymerization of olefins, catalyst comprising the same and use thereof. WO 2003/068,828, to China Petroleum & Chemical
26. Gao M, Liu H, Li T, Li X, Li C, Li J, Xing L, Yang J, Ma J, Wang X, Ding C (2005) Catalyst component for olefin polymerization reaction and catalyst thereof. WO 2005/105,858, to China Petroleum & Chemical
27. Matsunaga K, Hashida H, Tsutsui T, Yamamoto K, Shibahara A, Shinozaki T (2006) Solid titanium catalyst component, catalyst for olefin polymerization, and process for producing olefin polymer. WO 2006/077,945, 077,946, to Mitsui Chemicals
28. Soga K, Shiono T (1997) Prog Polym Sci 22:1503
29. Barbé PC, Cecchin G, Noristi L (1986) Adv Polym Sci 81:1
30. Terano M, Kataoka T, Keii T (1987) Macromol Chem 188:1477
31. Taniike T, Terano M (2007) Macromol Rapid Commun 28:1918
32. Arzoumanidis GG, Karayannis NM (1991) Appl Catal 76:221
33. Yang CB, Hsu CC (1993) Makromol Chem Rapid Commun 14:387–393
34. Di Noto V, Bresadola S (1996) Macromol Chem Phys 197:3827
35. Giannini U (1981) Makromol Chem Suppl 5:216
36. Zannetti R, Marega C, Marigo A, Martorana A (1988) J Polym Sci B Polym Phys 26:2399
37. Busico V, Causà M, Cipullo R, Credendino R, Cutillo F, Friederichs N, Lamanna R, Segre A, Van Axel Castelli V (2008) J Phys Chem C 112:1081
38. Somorjai GA, Magni E (1995) Appl Surf Sci 89:187–195
39. Magni E, Somorjai GA (1995) Surf Sci 341:L1078–L1084
40. Taniike T, Terano M (2012) J Catal 293:39
41. Correa A, Piemontesi F, Morini G, Cavallo L (2007) Macromolecules 40:9181
42. Mori H, Sawada M, Higuchi T, Hasebe K, Otsuka N, Terano M (1999) Macromol Rapid Commun 20:245
43. Andoni A, Chadwick JC, Niemantsverdriet JW, Thüne PC (2008) J Catal 257:81
44. Credendino R, Pater JTM, Correa A, Morini G, Cavallo L (2011) J Phys Chem C 115:13322
45. Toto M, Morini G, Guerra G, Corradini P, Cavallo L (2000) Macromolecules 33:1134
46. Barino L, Scordamaglia R (1998) Macromol Theory Simul 7:407
47. Potapov AG, Bukatov GD, Zakharov VA (2006) J Mol Catal A Chem 246:248–253
48. Potapov AG, Bukatov GD, Zakharov VA (2009) J Mol Catal A Chem 301:18–23
49. Potapov AG, Bukatov GD, Zakharov VA (2010) J Mol Catal A Chem 316:95–99
50. Stukalov DV, Zakharov VA, Potapov AG, Bukatov GD (2009) J Catal 266:39
51. Brambilla L, Zerbi G, Piemontesi F, Nascetti S, Morini G (2007) J Mol Catal A Chem 263:103
52. Brambilla L, Zerbi G, Piemontesi F, Nascetti S, Morini G (2010) J Phys Chem C 114:11475
53. Busico V, Corradini P, De Martino L, Proto A, Savino V, Albizzati E (1985) Makromol Chem 186:1279
54. Monaco G, Toto M, Guerra G, Corradini P, Cavallo L (2000) Macromolecules 33:8953
55. Martinsky C, Minot C, Ricart JM (2001) Surf Sci 490:237
56. Stukalov DV, Zilberberg IL, Zakharov VA (2009) Macromolecules 42:8165
57. Boero M, Parrinello M, Weiss H, Hüffer S (2001) J Phys Chem A 105:5096
58. D'Amore M, Credendino R, Budzelaar PHM, Causà M, Busico V (2012) J Catal 286:103
59. Chadwick JC, Morini G, Balbontin G, Camurati I, Heere JJR, Mingozzi I, Testoni F (2001) Macromol Chem Phys 202:1995
60. Zambelli A, Ammendola P (1991) Prog Polym Sci 16:203
61. Sacchi MC, Tritto I, Locatelli P (1991) Prog Polym Sci 16:331
62. Wada T, Taniike T, Kouzai I, Takahashi S, Terano M (2009) Macromol Rapid Commun 30:887
63. Busico V, Cipullo R, Monaco G, Talarico G, Vacatello M, Chadwick JC, Segre AL, Sudmeijer O (1999) Macromolecules 32:4173
64. Liu B, Nitta T, Nakatani H, Terano M (2003) Macromol Chem Phys 204:395
65. Busico V, Cipullo R, Polzone C, Talarico G, Chadwick JC (2003) Macromolecules 36:2616

66. Busico V, Chadwick JC, Cipullo R, Ronca S, Talarico G (2004) Macromolecules 37:7437
67. Yang CB, Hsu CC (1995) J Appl Polym Sci 58:1245
68. Sacchi MC, Forlini F, Tritto I, Mendichi R, Zannoni G, Noristi L (1992) Macromolecules 25:5914
69. Spitz R, Duranel L, Guyot A (1988) Makromol Chem 189:549
70. Jeong YT, Lee DH, Soga K (1991) Makromol Chem Rapid Commun 12:5
71. Albizzati E, Giannini U, Morini G, Smith CA, Zeigler R (1995) In: Fink G, Mulhaupt R, Brintzinger HH (eds) Ziegler catalysts. Recent scientific innovations and technological improvements. Springer, Berlin, p 413
72. Spitz R, Bobichon C, Guyot A (1989) Makromol Chem 190:707
73. Albizzati E, Galimberti M, Giannini U, Morini G (1991) Makromol Chem Makromol Symp 48/49:223
74. Vähäsarja E, Pakkanen TT, Pakkanen TA, Iiskola E, Sormunen P (1987) J Polym Sci A Polym Chem 25:3241
75. Taniike T, Terano M (2008) Macromol Rapid Commun 29:1472

Adv Polym Sci (2013) 257: 99–134
DOI: 10.1007/12_2013_227

Published online: 14 July 2013

Kinetics of Olefin Polymerization and Active Sites of Heterogeneous Ziegler–Natta Catalysts

Lyudmila A. Novokshonova and Vladimir A. Zakharov

Abstract Kinetic investigations of olefin polymerization with Ziegler–Natta (ZN) catalysts provide information for understanding the mechanism of these reactions and are also necessary for development of industrial productions of polyolefins. In this chapter, the main kinetic features of olefin polymerization with heterogeneous ZN catalysts are considered as well as problems such as a deviation from the linear dependence of the rate of polymerization on monomer concentration, the hydrogen effect in ethene and propene polymerizations, and the comonomer effect, the natures of which are not yet completely clear and are discussed in the literature. For analysis of the kinetics and mechanism of olefin polymerization, data on the number of active centers and propagation rate constants are important. The main methods for determination of these kinetic parameters are discussed in this chapter. Data on the number of active centers in ZN catalysts of different composition are presented. On the base of these kinetic data, the hydrogen effect and the heterogeneity of active centers at propylene polymerization over ZN catalysts are analyzed.

Keywords Active site number · Kinetic features · Mechanism · Metallorganic catalysts · Olefin polymerization

L.A. Novokshonova (✉)
Semenov Institute of Chemical Physics, RAS, Moscow, Russia
e-mail: lnov@chph.ras.ru

V.A. Zakharov
Boreskov Institute of Catalysis, RAS, Novosibirsk, Russia

Contents

Kinetic investigations of olefin polymerization with Ziegler–Natta (ZN) catalysts provide information for understanding the mechanism of these reactions. Knowledge of kinetic regularities is also necessary for development of industrial productions of polyolefins.

The complex nature of ZN catalysts, the chemical interaction between the components of the catalyst during polymerization, the decay in activity during polymerization, and the heterogeneity of active centers make it difficult to study the kinetics of olefin polymerization processes and to interpret the results.

For analysis of the kinetics and mechanism of olefin polymerization it is important to know the number of active centers, which depends on the structure and composition of the catalyst and on the polymerization conditions. Properties of catalysts are also determined by the characteristics of the main reactions of the polymerization process, including initiation of active centers, propagation of polymer chain, transfer of the growing polymer chain with the subsequent reactivation of active centers, and deactivation of active centers.

In this review, the conventional heterogeneous ZN catalysts and modern highly active $MgCl_2$-supported catalysts, modified by electron donor stereoregulating compounds, are considered.

The review includes two parts, in which the main features of the kinetics of olefin polymerization with heterogeneous ZN catalysts (Sect. 1) and data on the number of active centers and the propagation rate constants depending on the nature of these catalysts (Sect. 2) are considered.

1 Kinetics of Olefin Polymerization

Olefin polymerization kinetics are considered and discussed in many reviews [1–6]. In this section, the influence of the main parameters such as the concentrations of catalysts and cocatalysts and time of polymerization on polymerization rate, and the main reactions in the olefin polymerization process will be briefly reviewed. We also consider the problems of deviation from the linear law of polymerization rate with changing monomer concentration, the effect of hydrogen in the ethene and propene polymerizations, as well as the nature of the comonomer effect, which are under discussion in the literature and the natures of which are not yet completely clear.

To describe the kinetics of olefin polymerization with heterogeneous catalysts, kinetic models based on adsorption isotherm theories have been proposed [7–10]. The most accepted two-step mechanism of ZN polymerization, proposed by Cossee [10–12], includes olefin coordination and migratory insertion of coordinated monomer into a metal–carbon bond of the growing polymer chain.

1.1 Influence of Catalyst and Cocatalyst Concentrations

The olefin polymerization rate with heterogeneous catalysts is directly proportional to catalyst concentration [5, 13–15]. The concentration of metallorganic cocatalyst does not affect the polymerization rate with $TiCl_3$ unless a too-high Al-alkyl concentration is used [15, 16]. The catalysts based on VCl_3 are more sensitive to the concentration and type of AlR_3 [17]. According to many observations, in the case of $MgCl_2$-supported catalyst, increasing the Al-alkyl concentration leads to an increase in the maximum rate of polymerization and an increase in the polymerization rate decay [5, 18, 19].

1.2 Main Reactions of Olefin Polymerization

Chain propagation:

$$Mt–CH_2–CH(CH_3)–Polymer + CH_2{=}CH(CH_3) \rightarrow Mt–CH_2–CH(CH_3)–CH_2–CH(CH_3)–Polymer$$

Polymer chain termination occurs mainly through the following reactions:

1. Transfer with monomer:
   $$Mt–CH_2–CH(CH_3)–Polymer + CH_2{=}CH(CH_3) \rightarrow Mt–CH_2–CH_2CH_3 + CH_2{=}C(CH_3)–Polymer$$

2. Transfer with cocatalyst:
   $Mt–CH_2–CH(CH_3)–Polymer + AlR_3 \rightarrow Mt–R + R_2Al–CH_2–CH(CH_3)–Polymer$
3. β-Hydride elimination:
   $Mt–CH_2–CH(CH_3)–Polymer \rightarrow Mt–H + CH_2{=}C(CH_3)–Polymer$
4. Transfer with hydrogen:
   $Mt–CH_2–CH(CH_3)–Polymer + H_2 \rightarrow Mt–H + CH_3–CH(CH_3)–Polymer$

1.3 Kinetic Profile of Polymerization Reactions

The kinetic profile of the polymerization reaction depends on many factors, including the nature of monomer, pre-catalyst (transition metal compound), and cocatalyst (aluminum organic compound), their concentrations and molar ratios, the temperature, and the presence of modifying agents. The polymerization process can occur at a constant rate for a long time after an initial acceleration period [15, 20, 21], which may continue from several minutes to some hours and is increased at lower temperatures, or the polymerization can proceed with a decay of activity with time. The latter type of kinetics is characteristic for propene polymerization with highly active $MgCl_2$-supported catalysts [18, 22]. The rate of catalyst decay depends on the catalyst type and usually increases with temperature. One of the possible reasons for catalyst deactivation is the reduction of active Ti^{3+} to Ti^{2+} (or V^{3+} to V^{2+}) [17, 18]. According to [22, 23], in the case of $MgCl_2/TiCl_4$ catalysts, the deactivation can be connected to the formation of complexes between electron donors and the active site, and with their chemical interaction. As shown [18, 24], the rate decay is not associated with diffusion limitation of monomer to the active sites of a heterogeneous catalyst.

1.4 Dependence of Polymerization Rate Order on Monomer Concentration

One of the most important characteristics of the polymerization process is the dependence of the polymerization rate on monomer concentration. A number of investigations have shown a first order reaction rate with respect to monomer concentration for ethene, propene, and other olefins over a broad concentration range, and the overall rate of olefin polymerization is generally described by the equation:

$$R_p = k_p C_p C_M \tag{1}$$

where k_p is the propagation rate constant, C_p the number of active sites, and C_M the monomer concentration.

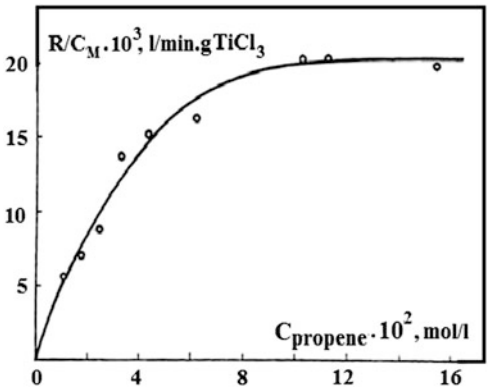

Fig. 1 Dependence of specific stationary rate of propene polymerization on the monomer concentration with $TiCl_3$–$Be(C_2H_5)_2$ in *n*-heptane at 70°C [29]

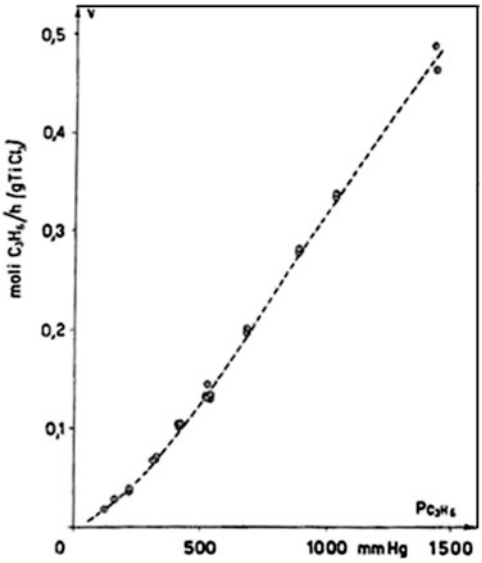

Fig. 2 Dependence of stationary rate of propene polymerization on the monomer pressure with $TiCl_3$–$Al(C_2H_5)_3$ in toluene at 72°C [30]

However, there are now many observations that show a higher rate law order dependence on monomer concentration (up to 2) for ethene [2, 25–27], propene [2, 28–39], styrene [40], and diene [41] using heterogeneous ZN catalysts as well as homogeneous and supported metallocene systems of different kinds.

This was first detected in 1962 by Firsov et al. [28, 29] and Natta at al. [30] in studies of propene polymerization with $TiCl_3$ at low propene concentrations (propene pressure <1 atm). Polymerization proceeded with an initial acceleration to a constant rate, and the effect of propene concentration on the polymerization rate was tested during the steady state phase of the process. It was shown that the dependence of polymerization rate order on monomer concentration increases from first order to some intermediate between first and second order with a reduction in monomer concentration (Figs. 1 and 2).

For an explanation of this effect, authors of works [28–30] proposed similar kinetic models in which the chain propagation includes two reactions of the active site with monomer molecules that differ in the value of the rate constant. The slower reaction is the insertion of the first monomer molecule (the initiation/activation of the active site), the faster reactions are the subsequent insertions of monomer molecules into activated sites (chain propagation). For a description of the stationary rate of polymerization, Eq. (2) was proposed, which takes into account the reactions of initiation (re-initiation after the chain terminations), propagation, and termination:

$$R = \frac{k_p k_i C^* C_M^2}{k_i C_M + k_{tM} C_M + \sum_j k_{tj} C_j^{\alpha j}} \tag{2}$$

or in form (3):

$$R = \frac{k_p C^* C_M}{1 + k_{tM}/k_{iM} + \sum_j (k_{tj} C_{tj}/k_{ij} C_M)} \tag{3}$$

where C^* is the total number of active sites and is equal to the sum of initiation sites (C_i) and propagation sites (C_p), k_{ij} is the constant rate of active center initiation and re-initiation after termination by agent j, $C_м$ is the monomer concentration, k_{tj} is the constant rate of termination with agent j (metallorganic cocatalyst, hydrogen, β-hydride elimination), and C_j is the concentration of appropriate termination agent.

According to these equations, depending on the conditions of polymerization, one can observe a first order rate, an intermediate between first and second order, or a second order rate with respect to the monomer concentration.

On the base of this kinetic scheme, Novokshonova et al. [17] proposed equations for the description of polymerization rate as a function of time, including the initial period of rate acceleration (4) and the possible deactivation of active sites (5):

$$R = \frac{k_p k_i C^* C_M^2}{k_i C_M + \sum_j k_{tj} C_{tj}} \left(1 - e^{-(k_i C_M + \sum_j k_{tj} C_{tj})t}\right) \tag{4}$$

$$R = \frac{k_p k_i C^* C_M^2}{k_i C_M + \sum_j k_{tj} C_{tj}} \left(1 - e^{-(k_i C_M + \sum_j k_{tj} C_{tj})t}\right) e^{-k_d C_A t} \tag{5}$$

where k_d is the rate constant of active site deactivation by cocatalyst, and C_A is the cocatalyst concentration.

Experimental data obtained for the stationary rate of polymerization with VCl_3–Al*i*Bu_3 [17, 31, 32] both for propene and ethene, depending on monomer concentration, support Eqs. (2) and (3): there was an increase in the reaction order

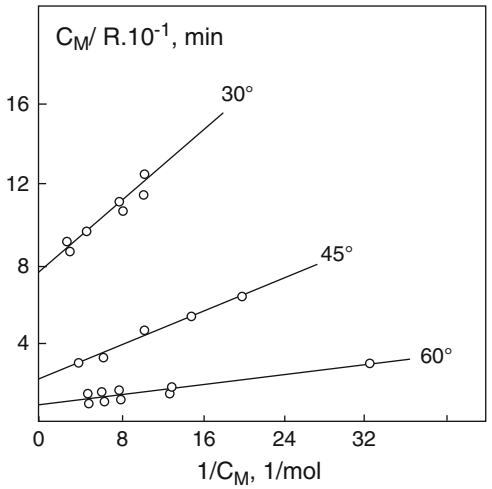

Fig. 3 Dependence of specific stationary rate of propene polymerization on the monomer concentration with VCl_3–Al(*i*-Bu)$_3$ in *n*-heptane at temperatures of 30°C, 45°C and 60°C. The graph plots C_M/R against $1/C_M$, where C_M is the monomer concentration [31]

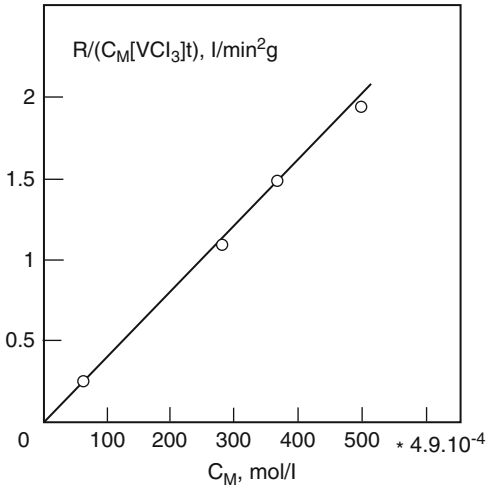

Fig. 4 The rate at initial acceleration period of propene polymerization as a function of the monomer concentration. Catalyst is VCl_3–Al(*i*-Bu)$_3$, temperature 60°C [17]

with respect to monomer with lowering the monomer concentration, and a linear relationship of C_M/R with $1/C_M$ (Fig. 3).

The series expansion of the exponent in Eq. (4) gives at small times t the Eq. (6), which describes the acceleration period on the kinetic curve for polymerization without deactivation of catalyst:

$$R = k_p k_i C^* C_m{}^2 t \tag{6}$$

According to experimental data (Fig. 4) [17], the rate of polymerization at the acceleration stage of propene polymerization is second order with respect to monomer concentration, which fits Eq. (6). It was found from the kinetic results for propene polymerization [17], that the rate constant of initiation is several orders

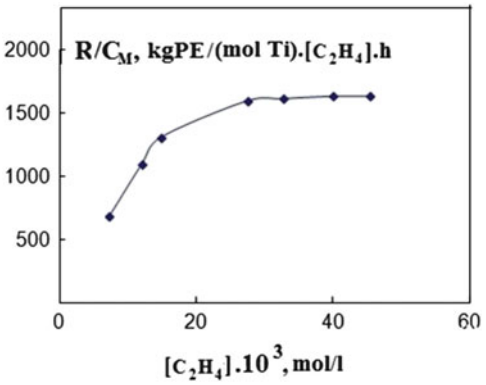

Fig. 5 The specific rate of ethene polymerization at steady state as a function of the monomer concentration with $MgCl_2/D_1/TiCl_4/Al(C_2H_5)_3$ at 50°C [26]

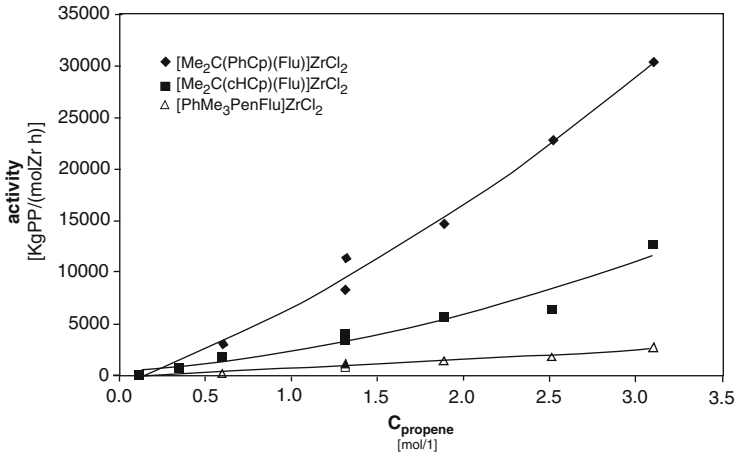

Fig. 6 Activity of metallocene catalysts in propene polymerization as a function of the monomer concentration [39]

of magnitude lower than the propagation rate constant, and that the activation energy of initiation (slow monomer insertion stage) is much higher than the activation energy of chain propagation (fast monomer insertion stage).

A reaction rate order higher than one has also been reported for olefin polymerization with $MgCl_2/TiCl_4$ [26, 38] (Fig. 5) and with homogeneous and supported metallocene catalysts of different types [27, 35–37, 39, 42] (Fig. 6).

At the steady state, the change in the specific rate of polymerization with an alteration of monomer concentration is fully reversible, as has been shown in studies performed during the course of a single experiment for propene polymerization with $MgCl_2/TiCl_4$ catalyst [26] (Fig. 7).

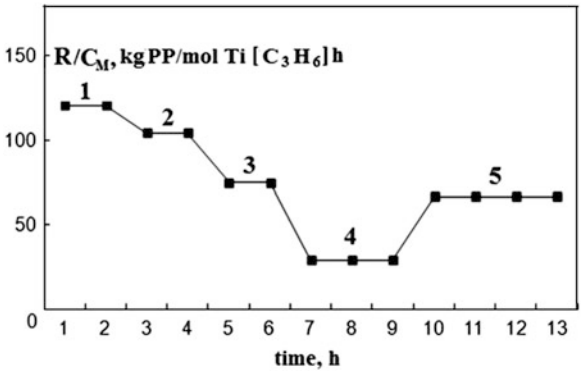

Fig. 7 The specific rate of propene polymerization with an alteration of the monomer concentration in the course of single experiment at steady state with $MgCl_2/D_1/TiCl_4/D_2–Al(C_2H_5)_3$ at 50°C [26]. Monomer concentration, mol/l: 1 – 0.12; 2 – 0.10; 3 – 0.073, 4 – 0.028; 5 – 0.065

It should be noted that when comparing the polymerization rates at different monomer concentrations, the complicated change of rate with time is not always taken into account, so the appropriate concentration range is not always chosen.

To date, besides the above kinetic model, a number of other approaches have been proposed in the literature to explain the deviation from a linear law of olefin polymerization rate with changing monomer concentration. Most recent studies have been carried out on metallocene catalysts.

Some authors have postulated that the active centers can coordinate two monomer molecules [33, 43]. Ystenes [44, 45] suggested the "trigger mechanism" according to which the insertion of coordinated monomer is triggered by a second monomer molecule. The main assumptions of this mechanism are as follows: the active site is never free because a new monomer enters the site at the same time as the first monomer is inserted; the insertion of the first monomer will not proceed (or will proceed very slowly) if no new monomer is available; in the transition state, two monomer molecules interact with each other and with the central metal atom. Brintzinger et al. [46] analyzed the consistency of "trigger mechanism" by DFT studies.

Resconi et al. [34, 47–49] proposed a model in which, at the steady state, the active site can exist in two active states, having different propagation rate constants (a faster propagation state and a slower one), that can interconvert without monomer assistance. The monomer insertion transforms a slow center into a fast one (see Scheme 1 [47]).

According to this kinetic scheme, the propagation rate R_p can be presented as:

$$\frac{R_p|}{[C]} = \frac{\left(k_{f\to s}\frac{k_{p,fast}k_{s\to f}}{k_{p,slow}}\right)[M] + k_{p,fast}[M]^2}{\left(\frac{k_{f\to s}+k_{s\to f}}{k_{p,slow}}[M]\right)} \tag{7}$$

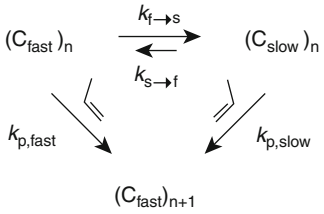

Scheme 1 Transformation of a slow center into a fast one

In this case, a reaction rate order with respect to monomer concentration higher than 1 is due to the decrease in the concentration of the slower state as the monomer concentration increases. The authors suggest that the distinction between the fast and slow states of the active center is in the conformation of the growing chain. Some theoretical calculations show that the kinetic product of monomer insertion is a γ-hydrogen agostic intermediate, whereas the resting (slow) state has the β-hydrogen agostic interaction.

Busico et al. [50–52] proposed a microstructural approach to propene polymerization. It is stated that the regioirregular 2,1-insertion slows chain propagation. The active center with a secondary growing chain enters into a dormant state because of higher steric hindrance for subsequent monomer insertion. However, this approach cannot be considered general because an order higher than 1 is also observed in ethene polymerization.

The physical reasons (mass and heat transfer) for the deviation from a linear law of polymerization rate with changing monomer concentration in propene polymerization have been analyzed and outlined by Mülhaupt et al. [37]. Some aspects of chain propagation steps are also considered in other works [53–55].

Thus, the nature of the two states of active center responsible for the slow and fast insertions of monomer, leading to the nonlinear relationship between activity and monomer concentration, is not yet fully clarified.

1.5 Concentration of Monomer Near the Active Centers

For the calculation of the rate constants of olefin polymerization as well as the constants of copolymerization, it is necessary to know the actual concentration of monomer near the active centers [56]. According to the known schemes [57–59], polyolefin is formed on the surface of the catalyst particles as a polymer shell, and monomer access to the active centers is by diffusion through this polymer shell. As shown [60], the crystallites in polyethylene are impenetrable and are randomly distributed on a macroscopic scale with respect to the diffusion and dissolution processes; the amorphous phase of polymer behaves as a homogeneous liquid. That is, monomer access to the active centers occurs by monomer dissolution in

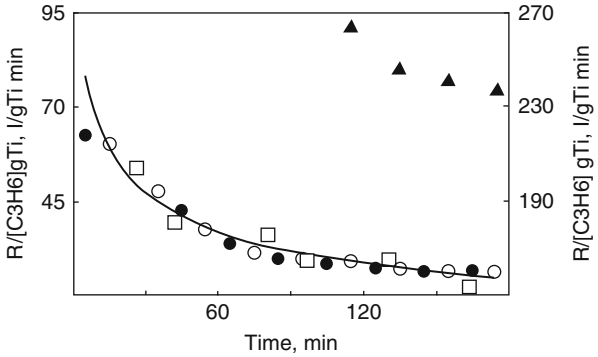

Fig. 8 Kinetic curves of propene polymerization with $MgCl_2/D_1/TiCl_4/D_2$–$AlEt_3$, 70°C. (*Open circles*) polymerization of propylene in *n*-heptane $p_{C_3H_6} = 2.5\,\text{atm}$, $K_H = 0.325$ mol/(l atm); (*closed circles*) polymerization in liquid propene $[C_3H_6] = 10.5$ mol/L; (*open squares*) gas-phase polymerization of propylene, $p_{C_3H_6} = 2.5\,\text{atm}$, $K_H^{C_3H_6/PP} = 0.13\,\text{mol}/(1\ \text{atm})$; (*closed triangles*) gas-phase polymerization of propylene, $p_{C_3H_6} = 2.5\,\text{atm}$, $[C_3H_6] = p_{C_3H_6}/RT\,\text{mol/L}$ [61]

Table 1 Reactivity ratios of ethene and propene in gas-phase and suspension copolymerizations with $MgCl_2/TiCl_4$ catalyst at 70°C [61]

Copolymerization mode	r_1^*	r_1	r_2^*	r_2
Gas phase	2.26 ± 0.04	7.3 ± 0.2	0.55 ± 0.04	0.141 ± 0.004
Suspension in *n*-heptane	–	7.3 ± 0.2	–	0.141 ± 0.004

Copolymerization constants were determined by kinetic method [63] and calculated by the Fineman–Ross equation [64]

r_1^* and r_2^* were calculated using the concentrations of comonomers in the gas phase; r_1 and r_2 were calculated using the concentrations of comonomers in the polymer shell

the amorphous regions of polymer shells for polymerization in both the slurry and gas phase. This means that for estimation of monomer concentration near the active centers, the solubility constants in the polymer should be used. Use of the monomer concentration in the gas phase for the calculation of the specific rate of polymerization and of the copolymerization constants in the gas-phase processes gives incorrect (anomalous) results. As shown in Fig. 8 [61], the specific rates of propene polymerization in *n*-heptane, in bulk, and in the gas phase on $MgCl_4/TiCl_4$ under identical conditions are the same, using the monomer solubility constants in polymer. Use of the monomer concentration in the gas phase for the calculation of gas-phase homopolymerization specific rate and calculation of reactivity ratios (r_1 and r_2) in gas-phase copolymerization gives the higher value for the specific rate and values of r_1 and r_2 that are not typical for ZN catalysts [61, 62] (see Table 1).

The temperature dependence of solubility constants for ethene and propene in nascent UHMWPE and isotactic PP (in dry powder-like state and swollen in heptane) were determined in the range of 20–70°C [61]. Solubility constants (Henry constants, K_H) were calculated taking into account the fact that the solubility of gases in the

semicrystalline polymers is directly proportional to the content of the amorphous phase: $K_H = 20\times10^{-3}\ e^{730/RT}$, $2.5\times10^{-3}\ e^{1,700/RT}$, $25\times10^{-3}\ e^{1,330/RT}$, and $1.3\times10^{-3}\ e^{3,100/RT}$ for ethene in PE, ethene in PP, propene in PE, and propene in PP, respectively. The constants for ethene and propene solubility in PE and PP, and swollen in *n*-heptane, are close to the constants for their solubility in *n*-heptane [65–67].

1.6 Hydrogen Effect

Hydrogen is the most used molecular weight regulator in polyolefin production. There are many publications describing the effect of hydrogen on olefin polymerization. The dependence of catalyst activity on the presence of hydrogen varies with the nature of the monomer and catalyst.

Usually, hydrogen significantly reduces the activity of the catalyst in the ethene polymerization [22, 68–71]. The character of the kinetic curves of ethene polymerization in the presence of hydrogen is practically unchanged [71, 72]. It is also noted [73, 74] that the effect of hydrogen is reversible. The removal of hydrogen from the reaction medium is accompanied by recovery of the original activity level. These facts indicate that the hydrogen does not affect the stability of the active centers. According to Natta [68] and Grieveson [75], the reason for the reduction in the rate of ethene polymerization in the presence of hydrogen is connected to the slower insertion of monomer into the Ti–H bonds, which are formed by reaction of active centers with H_2:

$$\mathrm{Mt-CH_2-CH_2-Pol + H_2 \rightarrow\ Mt-H + CH_3-CH-Pol} \qquad (8)$$

Kissin et al. [72, 73, 76, 77] explain the reduction in activity by the formation of Ti–CH_2–CH_3 structures after the insertion of ethene into Ti–H bonds, and these structures are the low-activity (or dormant) centers in polymerization because of the β-hydrogen agostic interaction.

Published data [78–81] show that a first order rate of chain transfer to hydrogen in the polymerization of ethylene with a ZN catalyst is usually observed; on the other hand, a number of studies [82] show a rate order of 0.5.

In propylene polymerization, the activating effect of hydrogen, i.e., an increase in initial polymerization rate as well as in overall activity, is observed [83–90] (Fig. 9). This activation is reversible and the polymerization rate decreases after the removal of hydrogen from the reaction zone [89, 90]. The degree of increase in the activity and change of the polymerization rate with time, in comparison with polymerization without hydrogen, depend on the catalyst nature and the hydrogen concentration.

A number of explanations of this effect have been proposed. The most accepted hypotheses for the activation effect are based on the capability of active centers of ZN and metallocene catalysts for regioirregular 2,1-insertion of propene into

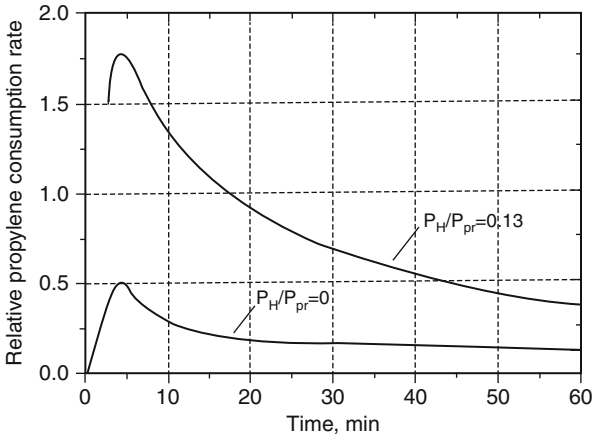

Fig. 9 Kinetics of propene polymerization at 70°C with $MgCl_2$/dibutylphtalate/$TiCl_4$/PhSi$(OEt)_3$–$AlEt_3$ without hydrogen (p_H/p_{pr}=0) and in the presence of hydrogen (p_H/p_{pr}=0.13) [76]

the growing chain, resulting in the formation of the low-activity or dormant active centers, Mt–$CH(CH_3)$–CH_2–Pol:

$$\begin{aligned} &\mathrm{Mt-CH_2-CH(CH_3)-Pol+CH(CH_3)=CH_2\rightarrow}\\ &\mathrm{Mt-CH(CH_3)-CH_2-CH_2-CH(CH_3)-Pol} \end{aligned} \tag{9}$$

Chain transfer in the presence of hydrogen reactivates such dormant centers:

$$\begin{aligned} &\mathrm{Mt-CH(CH_3)-CH_2-CH_2-CH(CH_3)-Pol+H_2}\\ &\rightarrow\ \mathrm{Mt-H+CH_3-CH_2-CH_2-CH_2-CH(CH_3)-Pol} \end{aligned} \tag{10}$$

The presence of *n*-butyl end groups in polymer chains formed during propene polymerization in the presence of hydrogen supports this hypothesis [85, 91–93]. The possibility of formation of the inactive centers Mt–$CH(CH_3)_2$ by the reaction of chain transfer with the monomer in a secondary 2,1-orientation or by a secondary insertion in the Mt–H bond, formed as a result of chain transfer to hydrogen, has been considered [76]:

$$\begin{aligned} &\mathrm{Mt-CH_2-CH(CH_3)-Pol+CH(CH_3)=CH_2}\\ &\rightarrow\ \mathrm{Mt-CH(CH_3)_2+CH_2=C(CH_3)-Pol} \end{aligned} \tag{11}$$

$$\mathrm{Mt-H+CH(CH_3)=CH_2\rightarrow\ Mt-CH(CH_3)_2} \tag{12}$$

The chain transfer with hydrogen reactivates inactive centers Mt–$CH(CH_3)_2$ with the formation of a Ti–H bond, followed by a primary propene insertion. Another explanation is related to the reactivation of Ti^{2+} sites, which are inactive

in propene polymerization, by hydrogen oxidative addition [94]; indeed, the concentration of active sites is noticeably increased in the presence of hydrogen [87, 95] due to hydrogenation of inactive Ti-allyl centers [95].

Thus, the mechanism of the activating action of hydrogen in propene polymerization, as well as the mechanism of reduction of catalyst activity in ethene polymerization in the presence of hydrogen, are still not completely clear and need further confirmation.

1.7 Heterogeneity of Active Centers

The distinctive property of heterogeneous ZN catalysts is a heterogeneity of active centers. This influences the kinetics of olefin polymerization and the characteristics of the polymers obtained. The multicenter nature of heterogeneous catalysts manifests itself in broadening of molecular weight distribution (MWD), formation of polymer fractions of different stereoregularity, compositional non-uniformity of copolymers of ethene and propene with α-olefins, and the complicated order of catalyst deactivation reactions. Non-uniformity of active sites is related, obviously, to the chemical, structural, and energy non-uniformity of the catalyst surface. The presence on the catalyst surface of active centers of various types, differing in the magnitude of propagation rate constants, has been reported in a number of publications [18, 96–98]. This fact has been proposed [99] as a cause of MWD broadening. Floyd et al. [100] found that the unimodal MWD curves for polypropylene obtained with heterogeneous ZN catalysts can be simulated only by assuming the presence of at least three or four types of active sites, each of which follows Flory's most probable distribution. The MWD of the polymer depends on the type of heterogeneous catalyst, nature of the donors in $MgCl_2$-supported catalysts, comonomer presence, and the conditions of polymerization.

For investigation of active site non-uniformity, a method was proposed [101, 102] based on mass-spectrometric study of temperature-programmed desorption (TPD) products from the catalyst surface at the most initial stage of olefin polymerization (up to 10–15 monomer units in chain). The method allows one to obtain information concerning the energy non-uniformity of active sites in terms of a distribution of active sites over the activation energy of active Mt–C bond thermal destruction in active sites. So, it was shown for ethene polymerization with $SiO_2/TiCl_4/AlEt_2Cl$ and $SiO_2/AlEt_2Cl/TiCl_4$ catalysts that there are at least two groups of active sites in these catalysts, varying in the activation energy of thermal destruction of active Ti–C bonds (Fig. 10), and that the distribution depends on the catalyst type.

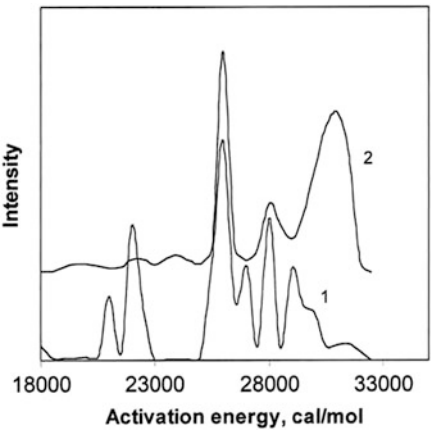

Fig. 10 Energy spectra of active sites for $SiO_2/TiCl_4/Al(C_2H_5)_2Cl$ (*1*) and $SiO_2/Al(C_2H_5)_3/TiCl_4$ (*2*) catalysts calculated on the basis of TPD experiments in the terms of active site distribution over activation energy of thermal destruction of Ti–C bonds [102]

1.8 Copolymerization

Processes of ethene/α-olefin copolymerization are of great practical importance. Copolymerization of ethene with small amounts of highest α-olefins (1-butene, 1-hexene, 1-octene) allows one to produce linear low density polyethylene (LLDPE), which is one of the most widely used large-scale polyolefin products. Polypropylene, modified with small amounts of ethene, exhibits higher impact strength compared to isotactic homopolypropylene. Copolymerization of propene with large amounts of ethene and terpolymerization of ethene/propene/diene result in amorphous elastomer materials (rubbers) [103].

The properties of olefin copolymers depend on the nature and content of comonomer and on the comonomer distribution in the polymer chain. If monomers are distributed as long sequences, crystalline copolymers are formed. The random distribution of comonomers gives amorphous polymer materials. The conventional ZN systems, such as heterogeneous Ti- or V-based catalysts and homogeneous V-based catalysts, are used for industrial production of olefin copolymers. The application of metallocene catalysts [104] has allowed an increase in the comonomer content in copolymers, more uniform comonomer distribution in the polymer chains, and broadening of the range of comonomers used [104–106]. Several examples of reactivity ratios r_1 and r_2 and their product r_1r_2 for ethene/propene copolymerization are given in Table 2. For most heterogeneous titanium catalysts, the product r_1r_2 is usually close to 1 or greater, which corresponds to the tendency for this catalysts to form copolymers with long crystallizable ethene sequences. In the case of V-based systems, the r_1r_2 value is lower and they give a more random comonomer distribution in the chain [107–109, 112]. For metallocene catalysts, the product r_1r_2 is smaller than 1, which is reflected in the alternation of ethene and propene units in copolymer chains [110, 111].

Table 2 Reactivity ratios of ethene/propene copolymerization

Catalyst	Temperature (°C)	r_1	r_2	r_1r_2	References
δ-$TiCl_3$−$Al(C_2H_5)_2Cl$	70	11.6	0.35	4.1	[107]
VCl_3−$Al(n\text{-}C_6H_{13})_3$	25	5.6	0.15	0.81	[108]
$VOCl_3$−$Al(n\text{-}C_6H_{13})_3$	25	18	0.07	1.2	[108]
$MgCl_2/TiCl_4$/ethylbenzoate/$Al(C_2H_5)_3$	70	5.5	0.36	2.0	[107]
$MgCl_2/TiCl_4/Al(i\text{-}C_4H_9)_3$	70	15.8	0.03	0.5	[109]
$MgCl_2/VCl_4/Al(i\text{-}C_4H_9)_3$	70	3.4	0.06	1.9	[109]
EBI$ZrCl_2$/MAO	50	6.61	0.06	0.4	[110]
EBI$ZrCl_2$/MAO	25	6.26	0.11	0.69	[110]
Me_2C(Cp)(Flu)$ZrCl_2$/MAO	25	1.3	0.2	0.26	[111]

1.9 Comonomer Effect in Olefin Copolymerization Reactions

One of the features of olefin copolymerization kinetics is the effect of comonomer on the rate of ethene or propene polymerization during ethene/α-olefin or propene/α-olefin copolymerization, i.e., the so-called comonomer effect (CEF). The rate enhancement of ethene or propene polymerization in the presence of a comonomer is observed for conventional ZN catalysts [80, 113–123] and for homogeneous [124–133] and supported metallocenes [134–136] and post-metallocenes catalysts [137–140]. The increase in activity was remarked in the presence of such comonomers as propene, 2-methylpropene, 1-butene, 3-methylbutene, 4-methylpentene-1, 1-hexene, 1-octene,1-decene, cyclopentene, styrene, and dienes.

Numerous studies have shown that the magnitude of effect depends on the catalyst nature, the comonomer type, and the experimental conditions. Examples of the comonomer effect for various catalysts and comonomers are shown in Tables 3, 4, and 5 as the ratio of copolymerization rate to the ethylene (or propylene) homopolymerization rate.

The effect is generally higher for heterogeneous catalysts, and for supported metallocenes it is higher than for homogeneous catalysts. The length of the α-olefin chain is also important. The higher the comonomer chain length, the smaller the effect. The negative effect of comonomer on the rate was found for ethylene/norbornene copolymerization [126] and for copolymerization of propene with 1-octene for metallocene catalysts [136].

For understanding the nature of the comonomer effect, it is also very important that the rate enhancement takes place in the sequential processes of homo- and copolymerization, i.e., when the ethene homopolymerization is carried out after the α-olefin homopolymerization or ethene/α-olefin copolymerization [122, 123] (Table 6).

The nature of this phenomenon is widely discussed in the literature. Several reasons (physical and chemical) have been proposed:

1. Monomer access to active centers through the polymer film becomes easier with higher amorphous phase content in the copolymer [116, 119, 121–123] or with dissolving of the polymer in the reaction medium [126, 130, 131]

Table 3 Comonomer effect in ethene/α-olefin copolymerization using heterogeneous and supported ZN catalyst systems

Catalyst	Comonomer	CEF (R_{cop}/R_{pol})	References
δ-$TiCl_3$ × 0.33 $AlCl_3$ + $AlEt_3$	4-MP-1	15.8–4.7	[113]
	1-Hexene	14–10	
$TiCl_4/MgCl_2$ + $AlEt_3$	1-Hexene	2–4	[114]
$TiCl_4/MgCl_2$/EB + Al(*n*-oct)$_3$	4-MP-1	6.9–9.5	[113]
$TiCl_4/MgCl_2$/DIBP + $AlEt_3$	Propene	2.0	[116]
VCl_3(THF)/SiO_2 + $AlEt_3$	Propene	5.8	[141]
	1-Butene	3.4	
	1-Hexene	2.0	

CEF – comonomer effect, Rcop – rate of ethene insertion in ethene/α-olefin copolymerization Rpol –rate of ethene homopolymerization

Table 4 Comonomer effect in ethene/α-olefin copolymerization using homogeneous metallocene catalysts

Catalyst	Comonomer	Temperature (°C)	CEF (R_{cop}/R_{pol})	References
Cp_2ZrCl_2/MAO	Propylene	30	1.65	[124]
	1-Hexene	30	2.30	
Cp_2ZrCl_2/MAO	1-Hexene	50	2.3	[127]
		95	Not observed	
Et(IndH_4)$_2ZrCl_2$/MAO	Propene	40	2	[129]
	1-Hexene	40	1.8	
*i*Pr(Cp)(Flu)ZrCl2	Propene	40	Not observed	[129]
	1-Hexene	40	Not observed	
(*tert*-Butanamide)Me(Me$_4$-η^5-Cp) silane-$TiCl_2$/MAO	Poly(propylene) macromonomer	40	3.2	[130]
		90	Not observed	
*i*Pr[FluCp]$ZrCl_2$/MAO	1-Hexene	25	6	[126]
Me_2Si[Ind]$_2ZrCl_2$/MAO	1-Hexene	25	2.6	[126]

2. The increase in the number of active centers can be achieved as a result of heterogeneous catalyst fragmentation [122, 123], deagglomeration of the growing polymer particles during copolymerization with homogeneous catalysts [126, 130, 131], or by activation of dormant active centers [113]
3. Modification of active centers by comonomer, with variation in the propagation rate constant [118, 119, 124, 125, 127, 132, 141]
4. Diffusion effects and the related increase in monomer concentration near the active site [134, 145]

Due to the diversity and complexity of the considered polymerization processes, the different causes for manifestation of the comonomer effect or their combination may appear, depending on conditions.

Table 5 Comonomer effect in propene/α-olefin copolymerization using heterogeneous ZN catalyst and homogeneous and supported metallocene catalyst systems

Catalyst	Comonomer	Copolymerization conditions	CEF (Q_{cop}/Q_{pol})[a]	References
$MgCl_2$/DIBP/$TiCl_4$ + $AlEt_3$ + D_2 with no external donor	1-Hexene	60°C, in *n*-heptane, 30 min	1.2	[142]
$MgCl_2$/DIBP/$TiCl_4$ + $AlEt_3$ + D_2 with PTES (triethoxyphenylsilane)			1.02	
$MgCl_2$/DIBP/$TiCl_4$ + $AlEt_3$ + D_2 with DTBDMS(dimethoxydi-*tert*-butylsilane)			1.63	
rac-$Me_2Si(Ind)_2ZrCl_2$/MAO	1-Hexene	30°C, in toluene, 120 min	2.38	[143]
rac-Me_2Si(4-Ph-2Me-Ind)$_2$ $ZrCl_2$/MAO			1.60	
$Ph_2C(Cp)(Flu)ZrCl_2$/MAO			0.21	
rac-Me_2Si(4-Ph-2Me-Ind)$_2$ $ZrCl_2$/MAO	1-Butene	60°C, in liquid propene, 10/11 min	4.87	[144]
rac-Me_2Si(4-Ph-2Me-Ind)$_2$ $ZrCl_2$/MAO	1-Octene	60°C, in liquid propene, 40/29 min	0.57	[136]
SiO_2/MAO/*rac*-Me_2Si (4-Ph-2Me-Ind)$_2ZrCl_2$/Al*i*Bu_3	1-Octene	60°C, in liquid propene, 50 min	1.69	[136]

[a]Q_{cop} and Q_{pol} are polymer and copolymer yields

Table 6 Comonomer effect in the two-step process of homo- and copolymerization of ethene and α-olefin using different types of catalyst [133]

Catalyst	Process	R_2/R_1
$TiCl_4/MgCl_2/D_1$[a]–D_2[b]–$AlEt_3$	$C_3 \rightarrow C_2$	3.0
$VCl_3/Al(OH)_3$–Al(*i*-Bu)$_3$	$C_2 + C_3 \rightarrow C_2$	3.3
Cp_2ZrCl_2–MAO	$C_3 \rightarrow C_2$	1.5
Et(Ind)$_2ZrCl_2$–ZSM-5(H_2O)–$AlMe_3$	$C_3 \rightarrow C_2$	5.3

R_1 is the specific rate of ethene homopolymerization and R_2 the specific rate of ethene homopolymerization on the second step of the two-step process
[a]Mixture of dibutylphthalate and ethylbenzoate
[b]Phenyltriethoxysilane

2 Number of Active Centers and Propagation Rate Constants for Olefin Polymerization on ZN Catalysts

For catalytic olefin polymerization on heterogeneous ZN catalysts, it is accepted that surface alkyl compounds of transition metals should be considered as the active centers. These species contain a growing polymer chain as an alkyl group. For analysis of the kinetics and mechanism of polymerization on ZN catalysts, it is all-important to have data on the number of active centers (C_p). The number of

active centers depends on the composition and conditions of preparation of the catalysts and on the conditions of polymerization and is usually a small fraction of the total number of surface transition metal compounds in the catalyst. Thus, the rate of polymerization, which is equal to the rate of propagation of the olefin polymer chain, is defined by a simple equation (1).

The problem of determination of the number of active centers as the number of titanium–polymer bonds was formulated for the first time in the pioneering works of Natta [15, 146] for propylene polymerization on catalyst $TiCl_3 + AlEt_3$. He used for this purpose cocatalyst $AlEt_3$ labeled by a radioactive isotope ^{14}C in the ethyl group. Active centers of type $Cl_xTi–^{14}CH_2CH_3$ are formed in this case and polymer with a radioactive label obtained on these centers. The number of active centers can be calculated from these data.

In this review, data on the number of active centers and values of propagation rate constants (k_p) for olefin polymerization on traditional ZN catalysts (mainly $TiCl_3/AlEt_xCl_y$) and highly active supported ZN catalysts containing titanium chlorides on activated magnesium dichloride will be presented.

Different methods for determination of the number of active centers during catalytic olefin polymerization are proposed. There are two basic groups of method applied to determine the kinetic characteristics of propagation reactions and transfer reactions of polymer chains (values of C_p, k_p, and K_{tr}) for catalytic olefin polymerization.

1. Methods based on the analysis of dependences of polymerization rate and molecular weight on the time and conditions of polymerization. We will name them conditionally "kinetic methods."
2. Methods based on introduction of a radioactive label in the growing polymer molecule.

2.1 Kinetic Methods

The method of calculation of rate constants of the separate reactions proceeding in the course of polymerization and based on the analysis of dependences of polymerization rate (R_p) and polymerization degree (P_n) on the concentration of reagents was used for the first time in the works of Natta [15, 146] and Chirkov [28, 29]. This method allows calculation of values for the products of rate constants of separate reactions and the number of active centers, but does not allow calculation of separate values for rate constants and the number of active centers.

Another kinetic method has been proposed [17]. This method allows one to determine the k_p value and the number of active sites using the dependence on monomer concentration of the stationary polymerization rate and of the polymerization rate during the acceleration period of the kinetic curve, according to Eqs. (2) and (6). The method has been applied for determination of these kinetic parameters in the polymerization of propylene and ethylene with $VCl_3/Al(i\text{-}Bu)_3$ catalyst.

Calculation of rate constants of separate reactions for the stationary phase of polymerization, when the number of the active centers does not change with polymerization time, is possible by use the dependence of the molecular weight of polymer (polymerization degree) on polymerization time [147, 148]:

$$\frac{1}{P_n} = \frac{1}{k_p C_m} \cdot \frac{1}{\tau} + \frac{\sum k_{tr}^i \cdot C_i^i}{k_p C_m} \tag{13}$$

where P_n is the average polymerization degree, k_p is the propagation rate constant, C_m is the concentration of monomer, τ is polymerization time, K_{tr}^i is the rate constant for the transfer of polymer chain reaction with a component i, and C_i is the concentration of component i.

This method has been used [147, 148] for determination of k_p values for polymerization of butene-1 on a ZN catalyst based on $TiCl_3$ and VCl_3. The k_p value greatly increases at transition from $TiCl_3$ to VCl_3. The same method has also been used [149, 150] for study of propylene polymerization on the catalyst α-$TiCl_3$ + $AlEt_3$, and also for study of ethylene polymerization on the catalyst γ-$TiCl_3$ + $AlEt_3Cl$ [151, 152]. However, in the latter cases the condition of polymerization stability was not met. It is necessary to notice also that in works [147–152], P_n values were calculated from polymer viscosity data in the assumption that polydispersity of the polymer does not depend on polymerization time. These assumptions are not always met and therefore reduces the reliability of results obtained by this method.

A new and more effective and reliable variant of the kinetic method is the stopped flow method (SF method), which has been offered by Keii and Terano [153] for determination of the number of active centers and the propagation rate constant in olefin polymerization on ZN catalysts. The main feature of this method is determination of C_p and k_p values in conditions of quasi-living polymerization, when transfer reactions of a polymer chain practically do not proceed and linear dependences of molecular weight of formed polymer and yield of polymer on polymerization time are observed. It has been shown that these conditions are obtained for propylene polymerization on supported titanium-magnesium catalysts (TMC) at low temperature (30°C) and at times of polymerization less than 0.2 s; in these cases, values of C_p and k_p can be calculated from Eqs. (14) and (15):

$$M_n = M_0 k_p C_m \tau \tag{14}$$

$$Y = k_p C_p C_m \tau \tag{15}$$

where M_n is the average number molecular weight of polymer, M_0 the molecular weight of monomer, C_m the concentration of monomer, Y the polymer yield, and τ the polymerization time.

To make these calculations, some conditions are necessary:

1. Active centers should be formed instantly at interaction of the catalyst with cocatalyst and the time necessary for formation of the active centers should be less than the time of quasi-living polymerization
2. The number of active centers and polymerization rate should be constant at the stage of quasi-living polymerization

2.2 Radiochemical Methods

In these methods, the number of active centers is defined by introduction of a radioactive label in a growing polymeric chain. The label can be entered at an initiation stage by use of an organoaluminum cocatalyst, containing alkyl group with a radioactive label. This method has been used Natta [15, 146] and Chien [154] in a study of propylene polymerization on the $TiCl_3$ catalyst in a combination with cocatalysts $Al(Et)_3$ or $Al(Et)_2Cl$ labeled by radioactive isotope ^{14}C.

Another method is based on introduction into polymerization of compounds (quenching agents) labeled by a radioactive isotope and by termination of polymerization in such a manner that this compound or its part joins a growing polymer chain (QR method). In the case of olefin polymerization on ZN catalysts, alcohol labeled with ^3H in the hydroxyl group was used as a quenching agent (QR RO^3H method):

$$Cl_xTi - CH_2R + RO^3H \rightarrow Cl_xTi - OR + {}^3HCH_2R \tag{16}$$

For the first time, this method was used [155] for study of ethylene polymerization on catalyst $TiCl_4 + AlEt_3$. Further, a number of works on definition of C_p and k_p values have been published for olefin polymerization on ZN catalysts using this method [156–162]. The basic difficulty of quantitative definition of the number of active centers at polymerization on ZN catalysts by this method is connected with the formation of inactive aluminum–polymer bonds during the course of polymerization. These bonds appear as a result of transfer reaction of a growing polymer chain with organoaluminum cocatalyst. The presence of this reaction was shown in the early works of Natta [15, 146] and confirmed experimentally for all ZN catalysts. For this reason, an increase in the number of metal–polymer bonds is observed with increasing polymerization time although polymerization rate can decrease [162] or remain constant [156]. To account for the effect of inactive aluminum–polymer bonds, the number of active centers is defined by extrapolation of the total number of metal–polymer bonds to zero time of polymerization. However, according to Coover et al. [156], the rate of formation of aluminum–polymer bonds sharply decreases during the course of polymerizations and this effect should be accounted for in calculation of the number of active centers. The authors [156] believe that this effect is connected with a reduction in the

concentration of organoaluminum compound on a surface of the catalyst owing to its slow diffusion through a layer of formed polymer.

More reliable data on the number of active centers can be obtained by this method for cases where the contribution of the transfer reaction with organoaluminum cocatalyst is very small. Such a case is the polymerization of 4-methylpentene-1 on catalyst $VCl_3/Al(i\text{-}Bu)_3$ [163].

Later, for definition of the number of active centers at polymerization on ZN catalysts, it was suggested that the "selective" quenching agent (^{14}CO), interacting only with titanium–polymer bonds [164–166], (QR ^{14}CO method) be used. The use of carbon monoxide for this purpose is based on the well-known metallorganic chemistry reaction of CO insertion into δ-bond transition metal-alkyl:

$$L_xM{-}CH_2R \xrightarrow{CO} L_xM{-}\underset{\underset{O}{\|}}{C}{-}CH_2R \qquad (17)$$

Examples of irreversible CO insertion into a titanium-alkyl bond are described [167] for CO reaction with a complex Cp_2TiClR, with formation of acyl complex $Cp_2Ti(Cl)COR$. There are examples of CO insertion into vanadium-alkyl and titanium-alkyl bonds, formed in ZN catalysts [168, 169]. In particular [168], it is shown that CO is attached irreversibly with "living" polypropylene molecules formed during propylene polymerization on soluble catalyst $V(acac)_3/AlEt_2Cl$ at a temperature of −78°C. Introduction of CO terminates polymerization and after that each polymer molecule contains one terminal group R(C═O)H. Thus, CO interacts quantitatively with growing polymer molecules by insertion into active vanadium–polymer bonds. Similar research [169] has been performed for ethylene polymerization on TMC catalysts in the conditions of "living" polymerization, with the subsequent interaction of growing polymer chains with CO. It was also confirmed that CO insertion into titanium–polymer bonds results mainly in formation of structures R (CO)R′.

Details of the interaction of ^{14}CO with ZN catalysts during olefin polymerization and the use of this technique for definition of the number of active centers are presented in works [166, 170–173] and the review [174]. In particular, it is necessary to note the necessity of additional clearing of polymer from the low molecular weight by-products containing a radioactive label [173]. These by-products are formed through interaction of ^{14}CO with titanium-alkyl bonds like the Ti–Et present in the catalyst as a result of alkylation of titanium chlorides by AlR_3 and transfer reactions of the growing polymer chain with $AlEt_3$ cocatalyst or with monomer.

We have listed the advantages and some limitations of the SF method. In the case of QR, it is possible to study polymerization kinetics at a wide variation of composition and morphology of the catalysts, leading to change in the rates of formation and deactivation of the active centers during the course of polymerization. It is also possible to study polymerization with more reactive monomers like ethylene, and in the presence of an additional effective chain transfer agent such as hydrogen.

Data on the number of active centers and propagation rate constants for olefin polymerization on traditional ZN catalysts and highly active supported ZN catalysts, obtained by use of SF and QR methods, will be presented and discussed below.

2.3 Number of Active Centers in Ethylene and Propylene Polymerization on Traditional ZN Catalysts and Supported Titanium–Magnesium Catalysts

It is known that the activity of catalysts changes very much depending on their composition, preparation and activation methods, and polymerization conditions. The most plausible reason for this is a change in the number of active centers. From the data obtained using a QR RO^3H method [155, 157, 161, 162] or using labeled cocatalyst $Al(^{14}C_2H_5)_3$ [15, 146, 154] for ethylene and propylene polymerization on $TiCl_3/AlR_xCl_y$ catalysts, the number of active centers is $(1–10) \times 10^{-2}$ mol/mol Ti. However, in work [156] it has been shown that the rate of transfer reaction of polymer chain with AlR_3 decreases sharply with increasing polymerization time (polymer yield). Taking into account this effect, it was found [156] that the C_p values for propylene polymerization on $TiCl_3/AlEt_2Cl$ ($AlEt_3$) catalyst are lower and only $(0.1–0.3) \times 10^{-2}$ mol/mol Ti. This value is close to the number of active centers, $(0.1–0.5) \times 10^{-2}$ mol/mol Ti, found later with use of the QR ^{14}CO method for ethylene and propylene polymerization on similar catalysts, $TiCl_3/AlEt_2Cl$ ($AlEt_3$, $Al\textit{i}Bu)_3$ [21, 165, 166, 174, 175]. Thus, the number of active centers for traditional ZN catalysts based on $TiCl_3$ is very low and, according to works [21, 59, 166, 175] (QR methods), makes up no more than 0.8 mol% of the total content of Ti in catalysts. By estimation [174], this value can correspond to the number of titanium chlorides located on the lateral sides of crystals, making microparticles of δ-$TiCl_3$ with a surface of 70–100 m^2/g.

A great increase in activity of ZN catalysts is reached by supporting $TiCl_4$ on "activated" magnesium dichloride, having a high surface and disordered crystal structure (supported TMC catalysts) [176, 177]. The activity of these catalysts in ethylene and propylene polymerization is usually 30–150 kg/g Ti h atm, which exceeds the activity of traditional ZN catalysts based on δ-$TiCl_3$ by approximately two orders of magnitude. According to works [74, 165, 173, 178–180] (QR ^{14}CO method) and works [181, 182] (QR RO^3H method), such an increase in activity is connected with a great increase in the number of active centers, which for these catalysts is 1–7 mol% of the total Ti content. Further, in works [153, 183–192] with use of the SF method in the case of propylene polymerization on TMC, C_p values of the same order (0.5–11 mol%) have been obtained. It is necessary to notice that the number of active centers changes considerably with variation in the composition and conditions of catalyst preparation. For example, in work [183] for three types of TMC with different activities, C_p values from 0.8 to 9.9 mol% were obtained by the SF method.

Thus, the results of definition of the number of active centers for propylene polymerization on TMC, obtained by independent methods (SF and QR methods), show the following:

1. The great increase in activity of TMC in comparison with traditional ZN catalysts is defined, mainly, by an increase in the number of active centers
2. The number of active centers is less than 10 mol% of the total titanium content in the catalysts (usually in limits from 1% to 10%) and depends on the composition and procedure of TMC preparation; most of the titanium is in the inactive form and does not participate in polymerization

It has been found [80, 193] that a great increase in activity of TMC in ethylene polymerization (from 50–100 kg/g Ti h atm to 400–600 kg/g Ti h atm) is observed with a decrease in titanium content in the catalyst from 1–4 wt% of Ti to values less than 0.1 wt% of Ti. In this case, it is possible to expect that the number of the active centers increases to 30–40 mol% of the total content of titanium [194].

The number of active centers at polymerization on ZN catalysts essentially depends on the conditions of polymerization, in particular on the composition of the organoaluminum cocatalyst and its concentration, the temperature of polymerization, and the presence of additional components added for regulation of activity and the molecular weight of polymer.

Data on the effect of hydrogen on the number of the active centers and propagation rate constants for polymerization of propylene and ethylene on ZN catalysts of various compositions will be presented and discussed in the next section.

2.4 Number of the Active Centers and Propagation Rate Constants in Polymerization in the Presence of Hydrogen

Hydrogen is the most effective chain transfer agent for olefin polymerization on ZN catalysts and is widely used for polyolefin production in industry and in laboratory research for control of molecular weight of polymers. The presence of hydrogen during the polymerization influences the polymerization kinetics. In the case of ethylene polymerization, addition of hydrogen into polymerization usually decreases the polymerization rate. In work [195] for the first time it was shown that addition of hydrogen during propylene polymerization on ZN catalysts leads to an appreciable increase in polymerization rate. This phenomenon has been confirmed in a number of other works [22, 89, 196–198]. To reveal the reasons for the activating effect of hydrogen (the "hydrogen effect"), data on the influence of hydrogen on the number of active centers and propagation rate constants can be the useful. In work [199] it was found that in the presence of hydrogen during propylene polymerization on TMC the number of active centers increases considerably (QR ^{14}CO method). However, according to data presented in [184], the presence of hydrogen at a quasi-living polymerization for 0.2 s does

Table 7 Data on the hydrogen effect on C_p and k_p values for propylene polymerization over ZN catalysts (QR ^{14}CO method) [74, 180]

Catalyst[a]	H_2	Temperature[b] (°C)	R_p[c] (kg/g Ti h atm)	C_p[d] ($\times 10^2$ mol/mol Ti)	k_p[d] (L/mol s)
I	–	70	9.0	1.4	650
I	+[e]	70	20.2	0.72	2,750
III	–	70	1.1	0.27	640
III	+[e]	70	1.6	0.23	1,580
II	–	40	26.0	4.1	350
II	+[e]	40	33.6	1.5	1,200

[a]Catalyst I: $TiCl_4/MgCl_2$/dibutylphtalate + $AlEt_3$/phenyltriethoxysilane; catalyst II: $TiCl_4/MgCl_2$/ethylbenzoate + Al(*i*-Bu)$_3$/ethylanizate; catalyst III: $TiCl_3$ + $AlEt_3$
[b]Polymerization temperature
[c]Polymerization rate at the moment of ^{14}CO addition
[d]Data for PP insoluble in boiling heptane (isotactic fraction)
[e]The ratio $H_2/C_3H_6 = 0.16$ (in gas phase)

not influence the number of active centers nor the propagation rate constant, and the hydrogen effect is not observed in conditions of quasi-living polymerization. Later [185], it was shown that in these conditions hydrogen does not influence the molecular weight of formed polymer. In works [74, 180], the hydrogen effect on propylene polymerization on TMC of various compositions and titanium trichloride has been studied (using QR ^{14}CO method) for definition of the number of active centers and propagation rate constants. It was found that the hydrogen effect is reversible and that removal of hydrogen from polymerization decreases the polymerization rate to the value observed for polymerization without hydrogen.

In Table 7, data on the influence of hydrogen on C_p and k_p values at propylene polymerization on catalysts with various compositions are presented. It is seen that hydrogen addition leads to a decrease in the number of active centers and an increase in k_p values calculated from data on the rate of polymerization and C_p. It is necessary to note that data in Table 7 are obtained for the isotactic PP fraction insoluble in boiling heptane. In work [199], with use of the same method (QR ^{14}CO), it was found that the number of active centers (radioactive labels in polymer) increases for polymerization in the presence of hydrogen. These data, unlike those in work [180], were obtained for the total polymer including the fraction soluble in boiling heptane. However, according to works [173, 180], this fraction after quenching polymerization with ^{14}CO contains low molecular weight by-products labeled with ^{14}C, and special techniques are required for their separation from polymer [173, 180]. The presence of these by-products can cause the raised number of radioactive labels in polymer, and accordingly leads to an increase in the calculated C_p value [199]. At the same time, it is improbable to expect an increase in reactivity of the active center (k_p value) after interaction of the active center with hydrogen. In [180], the possibility of formation of "dormant" centers is used to explain the increase in k_p values. These representations have been offered earlier [90, 200]. According to [90, 200], these centers are formed during propylene polymerization as a result of propylene 2,1-addition into an active titanium–polymer bond in the active center. In this case, two types of centers are formed during propylene polymerization on ZN catalysts without hydrogen:

1. Active centers (C_p), functioning in the conditions of 1,2-insertion of propylene into titanium–polymer bonds in the active center

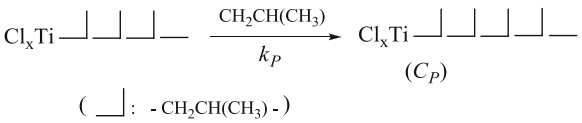

(18)

2. Dormant centers (C_d), formed after propylene 2,1-insertion into titanium–polymer bonds

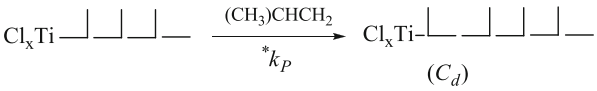

(19)

Dormant centers (C_d), do not attach propylene for steric reasons, but interact with ^{14}CO the same as the active centers C_p. In this case, the QR^{14}CO method can define the total number of the centers ($C_p + C_d$), containing titanium–polymer bonds.

Dormant centers can be transformed to an active state by interaction with hydrogen as a result of reactions (20) and (21):

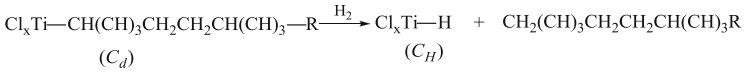

(20)

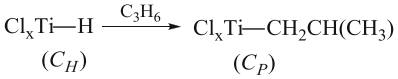

(21)

As a result of reactions (20) and (21) during polymerization in the presence of hydrogen, the share of active centers (C_p) increases, leading to an increase in polymerization rate and, accordingly, to an increase in the calculated values of k_p:

$$k_p = R_p/(C_p + C_d)C_m \tag{22}$$

The values of k_p concerning reactivity of the active center in the propagation reaction can be calculated if $C_p \gg C_d$, which is reached only for polymerization in the presence of hydrogen.

Surface titanium hydrides (Cl_xTi–H) are highly reactive compounds and can be partially deactivated in side reactions by interaction with components of the catalytic system. As a result of these side reactions, the number of active centers for polymerization in the presence of hydrogen is as a rule lower than the total number of the centers containing titanium–polymer bonds ($C_p + C_d$) during polymerization without hydrogen (Table 7). In the case of ethylene polymerization, dormant centers (C_d) are not formed. But, for polymerization in the presence of hydrogen,

the centers C_H (surface hydrides of titanium) are deactivated by interaction with components of the catalytic system the same as and at propylene polymerization. These reactions lead to a decrease in the number of active centers (C_p) and to a decrease in ethylene polymerization rate. Thus, the values of the propagation rate constant are the same for ethylene polymerization with hydrogen and without hydrogen [201].

So, in the case of propylene polymerization in the presence of hydrogen, the proportion of the centers participating in the propagation reaction (C_p) is essentially higher than for polymerization without hydrogen, when some of the centers are in a "sleeping" condition, C_d. Therefore, k_p values calculated for experiments in the presence of hydrogen more precisely correspond to the real reactivity of active centers in the propagation reaction. These values (see Table 7) of $(1.6–2.8)\times10^3$ L/mol s at 70°C and $(1.2–1.6)\times10^3$ L/mol s at 40°C are close to the k_p values found for propylene polymerization on TMC by the SF method, $(1.0–5.0)\times10^3$ L/mol s at 30°C [149, 153, 183–185].

2.5 *Heterogeneity of Active Centers of ZN Catalysts, Taking into Account Data on the Distribution of Active Centers on Propagation Rate Constants and Their Stereospecificity*

It is known that ZN catalysts are multisite catalytic systems containing active centers that differ in their k_p values and stereospecificity. This is apparent in the formation of polymers with broad molecular mass distribution (MMD, $M_w/M_n > 2$) and polyolefins containing separate fractions with varying stereoregularity. Data on the reactivity (k_p values) of separate groups of the active centers and their transformations with the variation in the composition of catalysts and polymerization conditions have an undoubtedly important role in analysis of this phenomenon.

In the literature, various reasons for formation of polymers with broad MMD on heterogeneous ZN catalysts are discussed. Convincing evidence has been obtained using the SF method that the reason is heterogeneity of the active centers on a surface of the catalyst [186]. In conditions of quasi-living polymerization there are no transfer reactions of the growing polymer chain and polymer is formed on the surface of catalyst in very small quantities. This polymer cannot cause diffusion restrictions, but nevertheless polymer with broad MMD ($M_w/M_n = 3.2–4.3$) is formed. The further increase in time of polymerization does not influence the width of MMD ($M_w/M_n = 3.6$).

In works [187, 188], using the SF method, the tendency for increased k_p values with increase in stereospecificity of the catalyst has been noted (Table 8, experiments 1–3). It is supposed that an external donor mainly deactivates

Table 8 Data on the effect of internal and external donors on C_p and k_p values for propylene polymerization [183, 187, 188] (SF method)

Experiment number	Catalyst	Isotacticity, mmmm (mol%)	C_p (mol/mol Ti)	k_p (L/mol s)
1	$TiCl_4/MgCl_2 + AlEt_3$ (I)	56	0.1	1,100
2	I + $Me_2Si(OEt)_2$	66	0.064	1,500
3	I + CMDMS[a]	66	0.038	1,600
4	$TiCl_4/MgCl_2 \cdot n$DBP[b] + $AlEt_3$ (II-A)	94	0.008	3,000
5	II-B[c]	85	0.0075	2,500
6	II-C[c]	78	0.0072	2,300

[a]External donor, *CMDMS* cyclohexyl(methyl)dimethoxysilane
[b]Internal donor, *DBP* dibutylphtalate
[c]Catalysts II-B and II-C were prepared by pretreatment of catalyst II-A by $AlEt_3$ at 30°C for 5 and 30 min, respectively, to remove DBP from catalyst II-A

Table 9 Data on the effect of AlR_3 cocatalysts on the C_p and k_p values for propylene polymerization over catalyst $TiCl_4/MgCl_2$/DBP [189] (SF method)

	Cocatalyst				
Parameter	TEA	TNBA	TNHA	TNOA	TIBA
C_p^{tot} (mol/mol Ti)	0.056	0.036	0.027	0.016	0.02
K_p^{tot} (L/mol s)	3,900	4,000	3,700	3,400	2,800
mmmm (mol%)	92.8	92.9	91.8	89.3	87.8
C_p^i (mol/mol Ti)	0.03	0.028	0.016	0.008	0.008
K_p^i (L/mol s)	4,700	4,800	4,900	4,900	4,900

TEA $AlEt_3$, *TNBA* Al(*n*-Bu)$_3$, *TNHA* Al(*n*-hexyl)$_3$, *TNOA* Al(*n*-oktyl)$_3$, *TIBA* Al(*i*-Bu)$_3$

nonstereospecific centers. This leads to an increase in polymer isotacticity and to a decrease in polymerization rate. The k_p value increases because of an increase in the proportion of stereospecific active centers with higher reactivity. A similar effect of the influence of stereospecificity of the catalyst on k_p values has been found [183] using a catalyst containing an internal donor (dibutylphtalate, DBP) (see Table 8, experiments 4–6). In this case, the stereospecificity of the catalyst was changed by its preliminary treatment with triethylaluminum, which leads to partial removal of DBP from the catalyst. It is seen that in this case the k_p values also increase with an increase in stereospecificity of the catalyst (i.e., in the content of *meso*-pentads in polypropylene).

In work [189], data on the influence of the composition of organoaluminum cocatalyst on C_p and k_p values were obtained for propylene polymerization on TMC containing an internal donor (Table 9, SF method). In Table 9, the data both for total polymer and the isotactic fraction insoluble in boiling heptane are presented. The values calculated for total polymer (K_p^{tot}) depend on AlR_3 composition and this dependence correlates with changes in isotacticity of polypropylene (the content of

Table 10 Data on C_p and k_p values for separate fractions of PP with different isotacticity [190–192] (SF method)

Parameter	Catalyst A: $TiCl_4/MgCl_2 + AlEt_3$	Catalyst B: $TiCl_4/MgCl_2 + AlEt_3ED$[a]
Total		
C_p^{tot} (mol/mol Ti)	0.1	0.038
K_p^{tot} (L/mol s)	1,100	1,600
Fraction III[b] (100–110°C by TREF)		
C_p^{III} (mol/mol Ti)	0.0063	0.080
K_p^{III} (L/mol s)	4,170	4,830
Fraction IV[c] (110–140°C by TREF)		
C_p^{IV} (mol/mol Ti)	0.00041	0.00038
K_p^{IV} (L/mol s)	9,300	9,270

[a]*ED* external donor, cyclohexyl(methyl)dimethoxysilane
[b]Fraction III: $M_n \cong 20\times10^3$ g/mol, $M_w/M_n = 1.8$ mmmm $\cong$ 95 mol% for catalysts A and B
[c]Fraction IV: $M_n \cong 41.5\times10^3$ g/mol, $M_w/M_n = 1.8$ mmmm $\cong$ 98.5 mol% for catalysts A and B

meso-pentads). At the same time, values calculated for the isotactic fraction (K_p^i), which contains 99% of *meso*-pentads, do not depend on AlR_3 composition. Thus, the composition of AlR_3 does not influence the reactivity of stereospecific active centers but considerably influences both the total number of active centers (C_p^{tot}), and the number of stereospecific active centers (C_p^i).

New important information on the distribution of the active centers was obtained using a combination of the SF method and temperature rising elution fractionation (TREF) [190–192]. According to the TREF data, polypropylene obtained for 0.15 s on catalysts $TiCl_4/MgCl_2 + AlEt_3$ (catalyst A) and $TiCl_4/MgCl_2 + AlEt_3$/ED (catalyst B) contains four fractions liberated at temperatures of approximately 20°C (I), 20–100°C (II), 100–110°C (III), and 110–140°C (IV). Fraction I is atactic polymer, fraction II is polymer with low isotacticity, fractions III and IV are isotactic polymers, and fraction IV has the highest isotacticity (98.5 mol% of *meso*-pentads). Table 10 presents data on the number of the active centers making fractions III and IV (C_p^{III} and C_p^{IV}) and the propagation rate constants for these centers (K_p^{III} and K_p^{IV}). It is seen that the isospecific centers III and highly isospecific centers IV have higher propagation rate constants in comparison with the average propagation rate constant for the total polymer. However, the proportion of isospecific active centers is insignificant and is only 6% for the centers III and 0.4% for the centers IV of the total number of active centers of catalyst A. In the case of catalyst B, the share of the isospecific active centers III and IV is considerably higher and is 21% for the centers III and 1% for the centers IV of the total number of active centers. It is necessary to notice that fractions III and IV have narrow MMD ($M_w/M_n \cong 2$), but various molecular weights. A difference in M_n for these fractions (approximately twofold) is defined

Table 11 Data on C_p and k_p values for different fractions of PP prepared with ZN catalysts of different composition [202] (QR ^{14}CO method)

Parameter		$TiCl_3$	TMC-1	TMC-2	TMC-3	TMC-4
R_p[a] (kg/g Ti h atm)		1.6	16.8	26.0	25.7	37.2
Content of PP fraction (wt%)	PP5[b]	17.1	43	10.6	3.1	1.9
	PP7[b]	10.5	27	14.7	6.9	2.7
	IPP[b]	72.4	30	74.7	90	95.4
Total C_p (mmol/mol Ti)		2.34	11.5	23.3	18.4	21.6
Portion of C_p (%) for fraction	PP5	45	50	41	25	14
	PP7	25	34	25	32	23
	IPP	30	16	34	43	63
k_p (L/mol s) for fraction	PP5	250	1,230	280	170	220
	PP7	270	1,120	660	300	190
	IPP	1,580	2,590	2,480	2,820	2,560

Polymerization conditions: 70°C, $AlEt_3$ as cocatalyst, with hydrogen presence at ratio $H_2/C_3H_6 = 0.15$ in gas phase

TMC-1 $TiCl_4/MgCl_2$, *TMC-2* $TiCl_4/MgCl_2{\cdot}n$DBPh, *TMC-3* $TiCl_4/MgCl_2{\cdot}n$DBDMP, *TMC-4* $TiCl_4/MgCl_2{\cdot}n$DBPh + DCPDMS, *DCPDMS* dicyclopentyldimethoxysilane as an external donor

[a]Polymerization rate at the moment of ^{14}CO addition

[b]*PP5* atactic fraction soluble in boiling pentane, *PP7* stereoblock fraction soluble in boiling heptane, *IPP* isotactic fraction insoluble in boiling heptane

by the twofold increase in k_p values for active centers IV. k_p values for active centers III and IV are similar for catalysts A and B. So, the presence of internal donor in TMC does not affect the k_p values of isospecific active centers III and IV.

Thus, the SF method gives valuable information on the quantity of active centers and their reactivity in the propagation reaction, the influence of catalyst composition on these kinetic parameters, and on the distribution of the active centers and their reactivity for the centers with various isospecificities. Of course, these data only concern the initial stage of polymerization for time of polymerization less than 0.2 s. But, ZN catalysts undergo essential changes in the conditions of the real process of polymerization because of interaction of the components of the catalytic system with each other and with components of the reaction environment. These interactions can lead to changes in the number of active centers and in the distribution of the active centers with different reactivities. Some reversible interactions can also occur between active centers and different components of the catalyst and polymerization environment. These interactions can be studied only for polymerization at different polymerization times. Therefore, it is necessary to also have data on the number of active centers and propagation rate constants at various stages of polymerization. As noted above, such data can be obtained by the QR method. Some results obtained in works [180, 202] by the QR ^{14}CO method for propylene polymerization on ZN catalysts are presented in Table 11. These data were obtained for polymerization on the traditional ZN catalyst based on $TiCl_3$ and on supported titanium–magnesium catalysts with different compositions, i.e., catalyst not containing electron donor stereoregulating additives (TMC-1), catalysts containing internal donors of various structures

(TMC-2 and TMC-3), and catalyst containing an internal and external donor (TMC-4). Polymers obtained with these catalysts have been fractionated into three fractions: PP5, atactic fraction soluble in boiling pentane; PP7, stereoblock fraction soluble in boiling heptane; and IPP, isotactic fraction insoluble in boiling heptane. C_p and k_p values have been calculated for separate fractions to account for the content of every fraction in the total polymer.

Following conclusions can be made from results presented in Table 11:

1. For all catalysts, k_p values increase considerably at transition from aspecific active centers (PP5 and PP7 fractions) to isospecific centers (IPP fraction) and reach values of $(2.5–2.8)\times10^3$ L/mol s.
2. k_p values for isospecific centers (IPP fraction) are close for TMC of various compositions.

   Conclusions (1) and (2) agree with results obtained by the SF method in works [190–192].
3. The proportion of aspecific and low specificity centers (PP5 and PP7 fractions) in the catalysts that do not contain internal or external donors ($TiCl_3$, TMC-1) is great enough (70–84%).
4. Addition of the external donor to TMC, containing the internal donor, has little effect on the total number of active centers (catalysts TMC-2 and TMC-4). However, the proportion of isospecific active centers increases considerably from 34% to 63%. This is possibly because aspecific centers in TMC-2 (PP5 fraction) transform into isospecific centers (IPP fraction).

The results presented show that data on the number of active centers and the propagation rate constants allow us to explain many questions connected with the role of the separate components of catalysts in the formation of active centers and their transformations during polymerization, revealing the factors that define the activity and stereospecificity of catalysts.

The information about the number of active centers and the propagation rate constants is also important for analysis of some kinetic features of olefin polymerization:

– The causes of heterogeneity of the catalyst active centers
– Exact estimation of activation energy of reactions of propagation and transfer of polymer chain is impossible without data on the effect of temperature on the number of active centers
– The reasons for the widespread comonomer effect in ZN catalysis
– Data on the dependence of active site number on monomer concentration might help in understanding the deviation from the low linear rate of polymerization with changing monomer concentration

References

1. Keii T (1972) Kinetics of Ziegler-Natta polymerization. Kodansha, Tokyo
2. Chirkov NM (1969) Proceedings IUPAC international symposium on macromolecular chemistry, Budapest, p 387
3. Tait PJT (1975) Coordination polymerization. Academic, London
4. Zakharov VA, Ermakov YI (1979) Catal Rev Sci Eng 19:67
5. Barbe PC, Ceecchin G, Noristi L (1986) Adv Polym Sci 81:1
6. Kissin YV (1985) Isospecific polymerization of olefins. Springer, New York
7. Keii T (1972) Kinetics of Ziegler-Natta polymerization. Kodansha, Tokyo, p 61
8. Böhm LL (1978) Polymer 19:545–553
9. Burfield DR, Mc Kenzie ID, Tait PJT (1972) Polymer 13:302
10. Cossee P (1964) J Catal 13:80
11. Arlman EJ, Cossee P (1964) J Catal 3:99
12. Cossee P (1966) Recueil Trav Chim 85:1151
13. Burfield DR (1984) Polymer 25:1645
14. Mejzlik J, Lesna M, Kratochvila J (1987) Adv Polym Sci 81:83
15. Natta G, Pasquon I (1959) Adv Catal 11:1
16. Schneko H, Dost W, Kern W (1969) Macromol Chem 121:159
17. Novokshonova LA, Berseneva GP, Tsvetkova VI, Chirkov NM (1967) Vysokomolek Soedin A 9:562
18. Keii T, Suzuki E, Tamura M, Doi Y (1982) Macromol Chem 183:2285
19. Zakharov VA, Makhtarulin SI, Yermakov YI (1978) React Kinet Catal Lett 9:137
20. Novokshonova LA, Tsvetkova VI, Chirkov NM (1963) Vysokomolek Soedin, Sbornik Karbotcep Soedin No 4, 48
21. Zakharov VA, Chumaevskii NR, Bukatov GD, Ermakov YI (1976) Macromol Chem 177:763
22. Albizzati E, Galimberti M, Giannini U, Morini G (1991) Macromol Chem Macromol Symp 48/49:223
23. Spitz R, Lacombe JL, Guyot A (1984) J Polym Sci A Polym Chem 22:2641
24. Galli P, Luciani L, Cecchin G (1981) Angew Macromol Chem 94:63
25. Chien JCW, Yu Z, Marques MM, Flores JC, Rausch MD (1998) J Polym Sci A Polym Chem 36:319
26. Novokshonova LA, Meshkova IN, Fushman EA (2013) Kinet Katal (in press)
27. Meshkova IN, Ladygina TA, Ushakova TM, Novokshonova LA (2002) Polym Sci A 44:1310
28. Tsvetkova VI, Firsov AP, Chirkov NM (1962) Dokl Akad Nauk SSSR 142(1):149
29. Firsov AP, Tsvetkova VI, Chirkov NM (1964) Izv Akad Nauk Ser Khim N 11:1956
30. Natta G, Pasquon I, Svab J, Zambelli A (1962) Chim Ind 44(6):621
31. Novokshonova LA, Tsvetkova VI, Chirkov (1967) J. Polym Sci (1967) Part C, No 16, 2659
32. Novokshonova LA, Berseneva GP, Tsvetkova VI, Chirkov NM (1965) Vysokomolek Soedin 7:898
33. Ewen JA, Elder MJ, Jones RL, Curtis S, Cheng HN (1990) In: Keii T, Soga K (eds) Catalytic olefin polymerization, studies in surface science and catalysis. Elsevier, New York, p 439
34. Resconi L, Fait A, Piemontesi F, Colonnesi M, Rychlicki H, Zeigler R (1995) Macromolecules 28:6667
35. Fink G, Herfert N, Montag P (1995) In: Fink G, Mülhaupt R, Brintzinger H-H (eds) Ziegler catalysts. Springer, Berlin, p 159
36. Herfert N, Fink G (1993) Makromol Chem Macromol Symp 66:157
37. Jungling S, Mulhaupt R, Stehling U, Brintzinger H-H, Fischer D, Langhauser F (1995) J Polym Sci A Polym Chem 33:1305
38. Pino P, Rotzinger B, von Achenbach E (1985) Makromol Chem Suppl 13:105
39. Kaminsky W, Werner R (1999) In: Kaminsky W (ed) Metalorganic catalysts for synthesis and polymerization. Springer, Berlin, p 170

40. Oliva L, Pellecchia C, Cinquina P, Zambeiii A (1989) Macromolecules 22:1642
41. Novikova ES, Parenago OP, Frolov VM, Dolgoplosk BA (1976) Kinet Katal 17:928
42. Frauenrath H, Keul H, Höcker H (2001) Macromol Chem Phys 202:3543
43. Chien JCW, Yu Z, Marques MM, Flores JC, Rausch MDJ (1998) Polym Sci A Polym Chem 36:319
44. Ystenes M (1991) J Catal 129:383
45. Ystenes M (1993) Makromol Chem Macromol Symp 66:71
46. Prosenc M-H, Schaper F, Brintzinger H-H (1999) In: Kaminsky W (ed) Metalorganic catalysts for synthesis and polymerization. Springer, Berlin, p 223
47. Fait A, Resconi L, Guerra G, Corradini P (1999) Macromolecules 32:2104
48. Resconi L, Cavallo L, Fait A, Piemontasi F (2000) Chem Rev 100:1331
49. Moscardi G, Resconi L (2001) Organometallics 20:1918
50. Busico V, Cipullo R Corradini P (1993) Makromol Chem Rapid Commun 14:97
51. Busico V, Cipullo R, Chadwick JC, Modder JF, Sudmeijer O (1994) Macromolecules 27:7538
52. Busico V, Cipullo R, Cutillo F, Vacatello M (2002) Macromolecules 35:349
53. Richardson DE, Alameddin NG, Ryan MF, Hayes T, Eyler JR, Siedle AR (1996) J Am Chem Soc 118:11244
54. Silanes I, Ugalde JM (2005) Organometallics 24:3233
55. Jensen VR, Kolev D, Jagadeesh MN, Thiel W (2005) Macromolecules 38:10266
56. Keii T (2003) Proceedings of 3rd international workshop on heterogeneous Z-N catalysts. JAIST, Japan, p 19
57. Wristers J (1973) J Polym Sci B Polym Phys 11:1601
58. Hamba M, Han-Adebekun GC, Ray WH (1997) J Polym Sci A Polym Chem 35:2075
59. Bukatov GD, Zaikovskii VP, Zakharov VA, Kryukova GN, Fenelonov VB, Zhagrafskaya RV (1982) Vysokomol Soedin 24(3):542
60. Michaels AS, Bixler HJ (1961) J Polym Sci 50:393
61. Meshkova IN, Ushakova TM, Gul'tseva NM (2004) Polym Sci A 46:1213
62. Zakharov VA, Yechevskaya LG, Bukatov GD (1989) Makromol Chem 190(3):559
63. Firsov AP, Meshkova IN, Kostrova ND, Chirkov NM (1966) Vysokomol Soedin 8(11):1860
64. Fineman M, Ross SD (1950) J Polym Sci 5(14):269
65. Meshkova IN, Tzvetkova VI, Chirkov NM (1961) Vysokomol Soedin 3:1516
66. Natta G, Pasquon I, Giachetti E (1957) Angew Chem 69:213
67. Novokshonova LA, Tzvetkova VI, Chirkov NM (1963) Izv Akad Nauk Ser Khim 7:1176
68. Natta G, Mazzanti P, Longi P, Bernardini F (1959) Chim Ind 41:519
69. Keii T (1972) Kinetics of Ziegler-Natta polymerization. Kodansha, Tokyo, p 142
70. Zakharov VA, Chumaevskii NB, Bukatov GD, Yermakov YuI (1975) React Kinet Catal Lett 2:329
71. Kissin YV, Mink RI, Nowlin TE (1999) J Polym Sci A Polym Chem 37:4255
72. Kissin YV (2001) J Polym Sci A Polym Chem 39:1681
73. Spitz R, Pasquet V, Patin M, Guyot A (1995) In: Fink G, Multhaupt R (eds) Ziegler catalysts. Springer, Berlin, p 401
74. Bukatov GD, Goncharov VS, Zakharov VA (1995) Macromol Chem Phys 196(1751)
75. Grieveson BM (1965) Macromol Chem 84:93
76. Kissin YuV, Rishina LA (2008) Polym Sci A 50:1101
77. Kissin YV, Mink RI, Nowlin TE, Brandolini AJ (1999) Top Catal 7:69
78. Böhm LL (1978) Polymer 5:562
79. Zakharov VA, Echevskaya LG, Mikenas TB (1991) Vysokomol Soedin B 32:101
80. Echevskaya LG, Matsko MA, Mikenas TB, Zakharov VA (2006) J Appl Polym Sci 102: 5436–5442
81. Nikolaeva MI, Mikenas TB, Matsko MA, Zakharov VA (2011) J Appl Polym Sci 122:3092
82. Margues MMV, Nunes CP, Tait PJT, Dias AR (1993) J Polym Sci A Polym Chem 31:209
83. Guastalia G, Giannini U (1983) Makromol Chem Rapid Commun 4:519

84. Spitz R, Masson P, Bobichon C, Guyot A (1989) Makromol Chem 190:717
85. Tsutsui T, Kashiwa N, Mizuno A (1990) Makromol Chem Rapid Commun 11:565
86. Albizzati E, Giannini U, Morini G, Galimberti M, Barino I, Scardamaglia R (1995) Macromol Symp 89:73
87. Bukatov GD, Goncharov VS, Zakharov VA (1994) Kinet Katal 35(392)
88. Soares JBP, Hamielec AE (1996) Polymer 37:4607
89. Kioka M, Kashiwa N (1991) J Macromol Sci Chem 28:865
90. Chadwick JC (2001) Macromol Symp 172:21
91. Mori H, Tashino K, Terano M (1995) Macromol Chem Phys 196:651
92. Chadwick JC, Miedema A, Sudmeijer O (1994) Makromol Chem 195:167
93. Busico V, Cipullo P, Corradini P (1992) Macromol Chem Rapid Commun 13:15
94. Chien JCW, Nozaki T (1991) J Polym Sci A Polym Chem 27(1499)
95. Parsons IW, Al-Turki TM (1989) Polym Commun 30(72)
96. Chien JCW, Kuo C (1985) J Polym Sci Polym Chem 23:761
97. Rishina LA, Vizen EI (1980) Eur Polym J 16:965
98. Kashiwa N, Yashitake J (1984) J Polym Bull 12:99
99. Keii T, Doi Y, Suzuki E, Tamura M, Murata M, Soga K (1984) Macromol Chem 185:1537
100. Floyd S, Heiskanen T, Taylor TW (1987) J Appl Polym 33:1021
101. Novokshonova LA, Kovaleva NYu, Gavrilov YuA, Krasheninnikov VG, Leipunskii IO (1997) Polym Bull 39:59
102. Novokshonova LA, Kovaleva NYu, Gavrilov YuA, Krasheninnikov VG, Leipunskii (1999) In: Kaminsky W (ed) Metallorganic catalysts for synthesis and polymerization. Springer, Berlin, p 89
103. Galli P, Vecellio G (2004) J Polym Sci 42:396
104. Kaminsky W, Piel C, Scharlach K (2005) Macromol Symp 226:25
105. Capacchione C, Proto A, Ebeling H, Mülhaupt R, Okuda J (2006) J Polym Sci A Polym Chem 44(1908)
106. Kaminsky W, Tran PD, Werner R (2004) Macromol Symp 213:101
107. Kashiwa N, Mizuno A, Minami S (1984) Polym Bull 12:105
108. Natta G, Mazzanti G, Valvassori A, Sartori G, Barbagallo A (1961) J Polym Sci 51(429)
109. Echevskaya LG, Bukatov GD, Zakharov VA (1987) Makromol Chem 188:2573
110. Drogemuller H, Heiland K, Kaminsky W (1988) In: Kaminsky W, Sinn H (eds) Transition metals and organometallics as catalysts for olefin polymerization. Springer, Berlin, p 303
111. Zambell A, Grassi A, Galimbert M, Mazzochi R, Piemontesi F (1991) Makromol Chem Rapid Commun 12:523
112. Zakharov VA, Echevskaya LG, Bukatov GD (1991) Makromol Chem 192:2865
113. Tait PJT (1988) In: Kaminsky W, Sinn H (eds) Transition metals and organometallics as catalysts for olefin polymerization. Springer, Berlin, p 310
114. Finogenova LT, Zakharov VA, Buniyat-Zade AA, Bukatov GD, Plaksunov TK (1980) Vysokomol Soedin A 22:404
115. Vindstad BK, Solli K-A, Ystenes M (1992) Makromol Chem Rapid Commun 13:471
116. Gul'tseva NM, Ushakova TM, Aladyshev AM, Raspopov LN, Meshkova IN (1991) Vysokomol Soedin A 33:1074
117. Bobrov BI, Yechevskaya LG, Kleyiner VI, Zakharov VA, Krenzel BA (1990) Vysokomol Soedin B 3:457
118. Wester Thale S, Ystenes M (1997) Makromol Chem Macromol Chem Phys 198:1623
119. Jaber IA, Ray WH (1993) J Appl Polym 49:1709
120. Koivumaki J, Seppala JV (1994) Macromolecules 27:2008
121. Gul'tseva NM, Ushakova TM, Aladyshev AM, Raspopov LN, Meshkova IN (1992) Polym Bull 29:639
122. Meshkova IN, Ushakova TM, Gul'tseva NM, Larichev MN, Ladygina TA, Kudinova OI (1997) Polym Bull 38(419)
123. Ushakova TM, Gul'tseva NM, Meshkova IN, Gavrilov YuA (1994) Polimery 39:102

124. Tsutsui T, Kashiwa N (1988) Polym Commun 29:180
125. Kravchenko R, Waymouth RM (1998) Macromolecules 31:1
126. Herfert N, Montag P, Fink G (1993) Makromol Chem Macromol Chem Phys 194:3167
127. Seppala JV, Koivumaki J (1993) Macromolecules 26:5535
128. Kaminsky W, Kulper K, Nieboda S (1986) Makromol Chem Macromol Symp 3:377
129. Uozumi T, Soga K (1992) Makromol Chem 193:823
130. Shiono T, Moriki Yu, Ikeda T, Soga K (1997) Makromol Chem Macromol Chem Phys 198:3229
131. Ushakova TM, Meshkova IN, Grinev VG, Ladyigina TA, Arutyunov IA, Novokshonova LA (2002) Vysokomol Soedin A 44:197
132. Cruz VL, Munoz-Escalone A, Martinez-Salazar J (1998) J Polym Sci A Polym Chem 36 (1357)
133. Meshkova IN, Ushakova TM, Gul'tseva NM, Grinev VG, Ladygina TA, Novokshonova LA (2008) Polym Sci A 50(11):1161
134. Jungling S, Koltzenburg S, Multhaupt R (1997) J Polym Sci A Polym Chem 35(1)
135. Awudza JAM, Tait PJT (2008) J Polym Sci A Polym Chem 46(267)
136. Nedorezova PM, Chapurina AV, Koval'chuk AA, Klyamkina AN, Aladyshev AM, Optov VA, Shklyaruk BF (2010) Polym Sci B 52(1–2):1525
137. Tang L-M, Li Y-G, Ye W-P, Li Y-S (2006) J Polym Sci A Polym Chem 44:5846
138. Tang L-M, Hu T, Li P, Li Y-S (2005) J Polym Sci A Polym Chem 43:6323
139. Gibson VC, Spitzmesser SK (2003) Chem Rev 103:283
140. Coates GW, Hustad PD, Reinartz S (2002) Angew Chem Int Ed 41:2236
141. Karol FJ, Kao S-C, Cann KJ (1993) J Polym Sci A Polym Chem 31:2541
142. Zhi-Qiang Fan, Forlini F, Tritto I, Locatelli P, Sacchi MC (1994) Macromol Chem Phys 195:3889
143. Rishina LA, Galashina NM, Nedorezova PM, Klyamkina AN, Aladyshev AM, Tsvetkova VI, Baranov AO, Optov VA, Kissin YuV (2004) Polym Sci A 46(9):911
144. Nedorezova PM, Chapurina AV, Koval'chuk AA, Klyamkina AN, Aladyshev AM, Baranov AO, Shklyaruk BF (2012) Polym Sci B 54(1–2):1
145. Spitz R, Pasquet V, Guyot AB (1988) In: Kaminsky W, Sinn H (eds) Transition metals and organometallics as catalysts for olefin polymerization. Springer, Berlin, p 405
146. Natta G, Pasquon I (1958) Chim Ind 40:556
147. Natta G, Zambelli A, Pasquon I, Giongo GM (1966) Chim Ind 48:1298
148. Zambelli A, Pasquon I, Siqnorini R, Natta G (1968) Makromol Chem 112:160
149. Tanaka S, Morikava H (1965) J Polym Sci A3:3147
150. Murayama V, Keii T (1963) Shokubai (Catalyst) 5:247
151. Berger MN, Grievson BM (1965) Macromol Chem 83:80
152. Grievson BM (1965) Makromol Chem 84:93
153. Keii T, Terano M, Kimura K, Ishii K (1987) Macromol Chem Rapid Commun 8:583
154. Chien CW (1963) J Polym Sci A1(425)
155. Feldman GF, Perry E (1960) J Polym Sci 46:217
156. Coover HW, Gullet J, Gombs R, Joyner FB (1962) J Polym Sci 58:681
157. Lehman G, Gumboldt A (1964) Macromol Chem 70:23
158. Yuongman EA, Boor J (1966) J Polym Sci B4:913
159. Cooper W, Eaves DE, Owen G, Vanqhan G (1964) J Polym Sci C4:218
160. Bier G (1964) Makromol Chem 70:44
161. Bier G, Toffman W, Lehmann G, Seydel G (1962) Makromol Chem 58:1
162. Kohn, Shuurmans H, Cavender JV, Mendelson RA (1962) J Polym Sci 58:681
163. Tait PJT (1975) In: Chien JCW (ed) Coordination polymerization. Academic, New York, p 155
164. Yermakov YuI, Zakharov VA (1975) In: Chien JCW (ed) Coordination polymerization. Academic, New York, p 91
165. Zakharov VA, Bukatov GD, Yermakov YI (1977) Kinet i Katal 18:848

166. Bukatov GD, Zakharov VA, Yermakov YI (1978) Macromol Chem 179:2097
167. Fachinetti G, Floriani C, Soeckii-Evans H (1977) J Chem Soc Dalton Trans 1977:2297
168. Doi Y, Murata M, Soga K (1984) Macromol Chem Rapid Commun 5:811
169. Shiono T, Ohigizawa M, Soga K (1993) Macromol Chem 194:2075
170. Zakharov VA, Bukatov GD, Yermakov YuI (1975) Kinet i Katal (Russ) 16:417
171. Chumaevskii NB, Zakharov VA, Bukatov GD, Yermakov YI (1976) Macromol Chem 177: 747
172. Bukatov GD, Zakharov VA, Yermakov YI (1984) Polym Bull 11:89–90
173. Bukatov GD, Goncharov VS, Zakharov VA (1986) Macromol Chem Phys 187:1041
174. Zakharov VA, Bukatov GD, Yermakov YI (1983) On the mechanism of olefin polymerization by Ziegler-Natta catalysts. Adv Polym Sci 51:61
175. Zakharov VA, Bukatov GD, Chumaevskii NB, Yermakov YI (1977) Macromol Chem 178: 967
176. Pino P, Mulhaupt R (1980) Angew Chem Int 19(2):857
177. Galli R, Luciani L, Cecchin G (1981) Angew Macromol Chem 94:63–89
178. Bukatov GD, Zakharov VA, Yermakov YI (1982) Macromol Chem 183:2657
179. Zakharov VA, Shepelev SN, Bukatov GD, Yermakov YuI (1981) Kinet i Katal (Russ) 22:258
180. Bukatov GD, Zakharov VA (2001) Macromol Chem Phys 202:2003
181. Tait PJ, Zohuri GH, Kells AM, McKenzie ID (1995) In: Fink G, Mulhaupt R, Brintzinger HH (eds) Ziegler catalysts. Recent scientific innovations and technological improvements. Springer, Berlin, pp 343–362
182. Yaluma AK, Tait PJ, Chadwick JC (2006) J Polym Sci A Polym Chem 44:1635
183. Matsuoka H, Liu B, Nakatani H, Nishiyama I, Terano M (2002) Polym Int 51:781
184. Imaoka K, Ikai S, Tamura M, Yoshikiyo M, Yano T (1993) J Mol Catal 82:37
185. Liu B, Nitta T, Matsuoka H, Terano M (2001) Macromol Chem Phys 165:3–10
186. Terano M, Kataoka T, Keii T (1989) J Mol Catal 56:203
187. Mori H, Saito H, Terano M (1998) Macromol Chem Phys 199:55
188. Mori H, Saito H, Yamahiro M, Kono H, Terano M (1998) Macromol Chem Phys 199:613
189. Mori H, Iguchi H, Hasebe K, Terano M (1997) Macromol Chem Phys 198:1249
190. Liu B, Matsuoko H, Terano M (2001) Macromol Rapid Commun 22:1
191. Matsuoka H, Liu B, Nakatani H, Terano M (2001) Macromol Rapid Commun 22:326
192. Liu B, Nitta T, Nakatani H, Terano M (2002) Macromol Chem Phys 203:2412
193. Zakharov VA, Mikenas TB, Makhtarullin SI, Poluboyarov VA, Pankratyev YD (1988) Kinet Catal 29:1267
194. Zakharov VA, Bukatov GD, Barabanov AA (2004) Macromol Symp 19:213
195. Guastalla G, Ciannini U (1983) Makromol Chem Rapid Commun 4:519
196. Spitz R, Masson P, Bobichon C, Guyot A (1989) Macromol Chem 190:717
197. Kioka M, Kashiwa N (1991) J Macromol Sci Chem A 28:865
198. Guyot A, Spitz R, Dassaud JP, Gomez C (1993) J Mol Catal 82:29
199. Parsons IW, Al-Turki TM (1989) Polym Commun 30:72
200. Busico V, Cipullo R, Corradini P (1992) Macromol Chem Rapid Commun 13:15
201. Zakharov VA, Bukatov GD, Barabanov AA, Mikenas TB, Echevskaya LG (2004) In: Terano M (ed) Current achievements on heterogeneous olefin polymerization catalysts. Sankeisha Co., Nagoya
202. Zakharov VA, Bukatov GD, Barabanov AA (2004) Macromol Symp 213:19

Adv Polym Sci (2013) 257: 135–202
DOI: 10.1007/12_2013_222

Published online: 7 July 2013

Phillips Cr/Silica Catalyst for Ethylene Polymerization

Ruihua Cheng, Zhen Liu, Lei Zhong, Xuelian He, Pengyuan Qiu, Minoru Terano, Moris S. Eisen, Susannah L. Scott, and Boping Liu

Abstract The Phillips Cr/silica catalyst, discovered by Hogan and Banks at the Phillips Petroleum Company in the early 1950s, is one of the most important industrial catalysts for polyethylene production. In contrast to its great commercial success during the past half-century, academic progress regarding a basic understanding of the nature of the active sites and polymerization mechanisms is lagging far behind. During the last decade, increasing research efforts have been performed on the Phillips catalyst through various approaches, including spectroscopic methods, polymerization kinetics, heterogeneous model catalysts, homogeneous model catalysts, and molecular modeling. Much deeper mechanistic understanding, together with successive catalyst innovations through modifications of the Phillips catalyst, has been achieved.

Keywords Ethylene polymerization mechanisms · Heterogeneous model catalysts · Homogeneous model catalysts · Molecular modeling · Phillips Cr/silica catalyst · Polyethylene · Polymerization kinetics

R. Cheng, Z. Liu, L. Zhong, X. He, P. Qiu, and B. Liu (✉)
State Key Laboratory of Chemical Engineering, East China University of Science and Technology, Meilong Road 130, Shanghai 200237, PR China
e-mail: boping@ecust.edu.cn

M. Terano
School of Materials Science, Japan Advanced Institute of Science and Technology, 1-1 Asahidai, Nomi, Ishikawa 923-1292, Japan

M.S. Eisen
Schulich Faculty of Chemistry, Technion-Israel Institute of Technology, Technion City, Haifa 32000, Israel

S.L. Scott
Department of Chemical Engineering, University of California, Santa Barbara, CA 93106-5080, USA

Contents

Abbreviations

AFM	Atomic force microscope
BC	Bis(triphenylsilyl) chromate
BE	Binding energy
Cp	Cyclopentadienyl
DCB-d_4	1,2-dichlorobenzene-d_4
DEAE	Diethylaluminum ethoxide
DFT	Density functional theory
DRIFTS	Diffuse reflectance infrared Fourier transform spectroscopy
DRS	Diffuse reflectance spectroscopy
DSC	Differential scanning calorimetry
EDS	Energy dispersive spectrometer
EPMA	Electron probe microanalysis
EPR	Electron paramagnetic resonance
ESR	Electron spin resonance
EXAFS	Extended X-ray absorption fine structure
FTIR	Fourier transform infrared
FWHM	Full width at half maximum
GC-MS	Gas chromatography–mass spectrometry
GPC	Gel permeation chromatography
HDPE	High density polyethylene
HMDS	Hexamethyldisilazane

LA-MS	Laser ablation–mass spectrometry
LDI-MS	Laser desorption/ionization–mass spectrometry
m/z	Mass to charge ratio
MALDI-TOF	Matrix-assisted laser desorption/ionization time of flight
MAO	Methylaluminoxane
MAS	Magic angle spin
MECP	Minimum energy crossing point
MW	Molecular weight
M_W	Weight average molecular weight
MWD	Molecular weight distribution
NMR	Nuclear magnetic resonance
ONIOM	Our own *n*-layered integrated molecular orbital and molecular mechanics
PDI	Polydispersity index
PE	Polyethylene
Ph	Phenyl
PIXE	Proton induced X-ray emission
POSS	Polyhedral oligomeric silsesquioxanes
RBS	Rutherford backscattering spectrometry
RT	Room temperature
SCB	Short-chain branch
SEM	Scanning electron microscopy
SIMS	Secondary ion mass spectroscopy
SSA	Successive self-nucleation and annealing
TCB	1,2,4-Trichlorobenzene
TEA	Triethylaluminum
TEB	Triethylborane
TEMPO	2,2,6,6-Tetramethylpiperidine-*N*-oxyl
TG-DTA	Thermogravimetry–differential thermal analysis
THF	Tetrahydrofuran
TiBA	Triisobutylaluminum
T_m	Melting temperature
TPD-MS	Temperature-programmed desorption–mass spectrometry
TPR	Temperature-programmed reduction
TPS	Triphenylsilanol
TREF	Temperature rising elution fractionation
UV-vis	Ultraviolet–visible
XANES	X-ray absorption near edge structure
XAS	X-ray absorption spectroscopy
XPS	X-ray photoelectron spectroscopy
XRD	X-ray diffraction

1 Introduction

The discovery of Ziegler–Natta catalysts for olefin polymerization in 1953 was one of the most important achievements in the field of synthetic polymer chemistry during the past 60 years. Parallel to the discovery, another important catalyst for polyethylene production, SiO_2-supported inorganic chromium oxide, known as Phillips catalyst, was also discovered and commercially applied on a large scale [1–4]. Nowadays, this catalyst is used to produce over 10 million tons of high-density polyethylene (HDPE), accounting for about half of the world's market. Compared with the Ziegler–Natta and metallocene catalysts, the Phillips catalyst exhibits unique polymerization behaviors and can produce PE with distinctive polymer chain microstructures. The catalyst is known to be highly active for ethylene polymerization with or without using organometallic cocatalysts or a preliminary activation step using organometallic cocatalysts or any other reducing agents (such as CO or H_2). Its HDPE products feature an ultrabroad molecular weight distribution (MWD; the typical polydispersity index is larger than 10), small amount of long chain branches and a vinyl end-group for each PE chain. The products show high melt strength and are especially applicable for blow molding products like hollow containers. In the last few decades, the applications for exclusive Phillips HDPE products, including gasoline tanks for the automobile industry and ultralarge plastic containers and pipes, have experienced a successively increasing market demand.

Compared with the great success in commercial applications, academic progress on the Phillips catalyst is lagging far behind, in spite of numerous research efforts during the past 60 years. Aspects of the Phillips catalyst concerning the formation, structure, oxidation state of active sites, and polymerization mechanisms, especially the initiation mechanism, are still mysterious. The difficulties for basic studies on this important industrial catalyst system are mainly derived from the low percentage of active Cr species, the complexity of heterogeneous catalyst systems, the multiple valence states of Cr, the instant encapsulation of active sites by produced polymer, and the ultrafast polymerization rate.

Application of the Phillips catalyst in ethylene polymerization includes two important processes: catalyst preparation and catalyst activation through reduction. The catalyst is usually prepared by impregnation of an aqueous solution of chromium compound, such as chromate acetate, on porous amorphous silica gel, and subsequent calcination at high temperatures between 300 and 900°C in oxygen or dry air. It is generally accepted that chromate acetate first decomposes and is oxidized into bulk CrO_3. This is followed by a reaction with surface hydroxyl groups on silica gel during the calcination process, through which chromium compound could be highly dispersed and stabilized as surface hexavalent chromate species, i.e., monochromate, dichromate, and sometimes even polychromate, as illustrated in Scheme 1 [2, 5–9]. As for the reductive activation process for ethylene polymerization, the hexavalent chromate species is transferred into a lower oxidation state, i.e., divalent Cr(II) species, as the final active precursor for ethylene polymerization by ethylene monomer (C_2H_4), carbon monoxide (CO), Al-alkyl cocatalysts (e.g., TEA), or even other reducing agents.

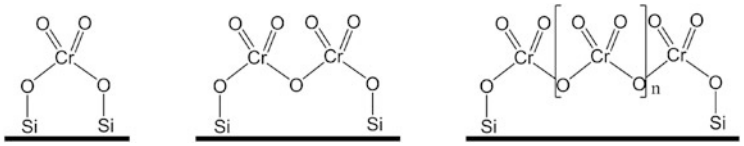

Scheme 1 Plausible structures of surface-stabilized hexavalent chromate species $Cr(VI)O_{x,surf}$ on the silica surface of the Phillips Cr/silica catalyst ($n \geq 1$)

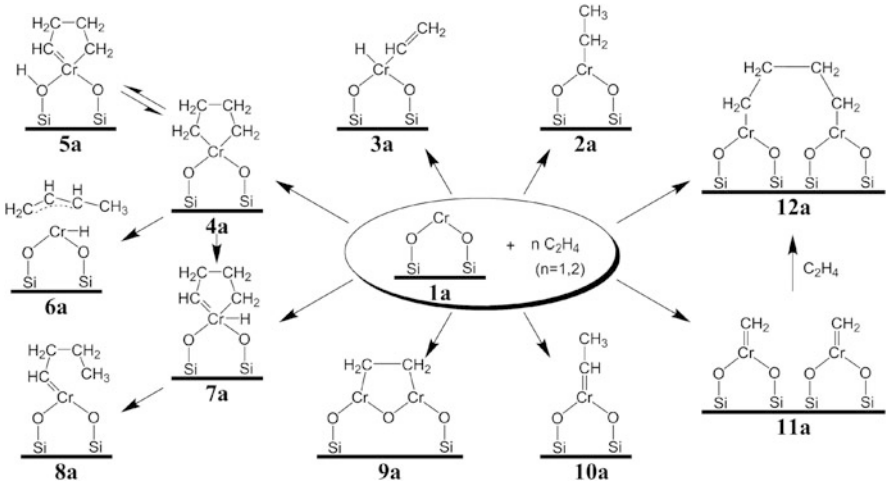

Scheme 2 Various initiation mechanisms proposed in the literature for ethylene polymerization over the pre-reduced Phillips $Cr(II)O_x/SiO_2$ catalyst

Because the Phillips catalyst is unique for its metal-alkyl-free feature in both the catalyst preparation and subsequent polymerization processes, ethylene monomer could play a key role in the activation through reduction of the hexavalent chromate species into surface-stabilized Cr(II) species [$Cr(II)O_{x,surf}$] as the final active precursor, followed by initiation of ethylene polymerization through alkylation of the Cr(II) center during the initial stage, in which an induction period is usually observed after the introduction of ethylene monomer at usual operating temperatures (lower than 150°C) [2, 6, 10]. The initiation mechanism in terms of an alkylation of the Cr(II) center by ethylene monomer, followed by the propagation of the first polyethylene chain is the most interesting and important academic question awaiting further exploration [2, 11]. Scheme 2 shows various initiation mechanisms that have been proposed on the basis of either pure speculation or controversial evidence:

1. Arguments on Cr-alkylidene species (Cr-carbene) [12, 13] and contradictory IR band assignments of the C–H bond vibration in a possible Cr-alkylidene species [14, 15] are still continuing. Therefore, the active sites concerned with Cr-alkylidene species (**5a**, **7a**, **8a**, **10a**, **11a**) [12, 14, 16, 17] under a supposed modified Ivin–Rooney–Green chain propagation [13, 18] still lack conclusive evidence.

2. The low IR detectability of any possible methyl end groups in the initial growing polymer chains [17, 19–21] on the active sites also sheds great doubts on those proposed active sites relating to metallacyclic species (**4a**, **9a**, **12a**) [16–18, 22, 23].
3. The models (**2a**, **3a**, **6a**) [24] involving a proposed Cossee–Arlman chain propagation [25], with either Cr–C or Cr–H as active sites similar to conventional Ziegler–Natta catalysts, still hold the most popularity [2, 11], although the origin of the first hydride scrambling is still obscure (e.g., for **2a**). These models are mainly speculated from the chain configuration of Phillips polyethylene chains featuring one vinyl and one methyl group on each chain end. The vinyl chain end is thought to be derived from chain transfer through β-hydride elimination during a Cossee–Arlman chain propagation.

In the polyolefin industry, there exists a strong driving force for development of new catalysts with better performance and improvements in the structures and properties of PE products through successive catalyst innovations of the traditional Phillips catalyst [2–4, 11]. During the past 60 years, several modified Phillips catalysts have been successfully developed and commercialized through surface modification of the silica support and catalyst with Ti, F, Al, or B compounds, more or less based on the progress in the academic field, although innovation regarding this catalyst is very limited. Another important commercial silica-supported Cr-based HDPE catalyst is Union Carbide's silyl chromate S-2 catalyst, which is solely applied in the gas phase UNIPOL polymerization processes [26]. This catalyst is usually prepared by chemisorption of bis (triphenylsilyl) chromate (BC) on partially dehydrated silica gel at around 600°C. Due to its similar structure and performance compared with the Phillips catalyst, in our opinion it could be considered as a heterogeneous model of the Phillips catalyst. Due to the presence of an electron-donating triphenylsilyl ligand, a much longer induction period exists without using any organometallic cocatalyst for ethylene polymerization. This catalyst combined with Al-alkyl cocatalyst usually produces polyethylene with broader MWD at both ends of the high and low molecular weight fractions than the Phillips catalyst without using cocatalyst [26]. Almost no improvement of this silica-supported silyl chromate S-2 catalyst has been reported, apart from a modified preparation procedure through transformation from Phillips catalyst by addition of triphenylsilanol (TPS) to avoid the use of highly toxic and expensive BC compound [27, 28]. Another Union Carbide Cr-based polymerization catalyst, formed upon treating partially dehydrated silica with chromocene (Cp_2Cr) and named S-9 catalyst, is not used industrially at present [29]. It is a supported metallocene catalyst featuring very poor ability of α-olefin incorporation in copolymerization with ethylene and produces polyethylenes with narrow MWD. It is very clear that further catalyst innovations through modifications of the traditional Cr-based industrial catalysts are still highly demanded [30].

During the last decade, increasing research efforts have been performed on Phillips catalysts through various approaches including spectroscopic methods, polymerization kinetics, heterogeneous model catalysts, homogeneous model

catalysts, and molecular modeling. Much deeper mechanistic understanding, together with successive catalyst innovations through modifications of the Phillips catalyst, has been achieved. The advances in the field of Phillips catalysts during the past half-century have been reviewed in depth by McDaniel in 1985 [2], Zecchina and coworkers in 2005 [11], and McDaniel in 2008 and 2010 [3, 4]. This present contribution aims at an overview of the achievements of the last decade, unraveling the mechanistic aspects of the activation, the nature of the active chromium species, and the polymerization mechanisms through both experimental and computational approaches, as well as catalyst innovation through modification of the Phillips catalyst with particular emphasis on the studies undertaken in the authors' laboratory.

2 Approaches Using Spectroscopic Methods

The state of surface Cr species, which is closely related to the molecular structure, texture, and orientation of the chromium oxide on the catalyst surface, is crucial for a deeper understanding of the Phillips catalyst. Many modern analytical methods [8, 11, 31], such as oxygen chemisorptions [32], magnetic susceptibility measurement [33], XRD [5, 34–36], EPR [33, 37–41], SIMS [42], Raman [35, 43–50], UV-vis DRS [33, 39, 43, 50], XAS (EXAFS-XANES) [48, 51–55], PIXE [56], TPR [36, 39], SEM/EDS [57], FTIR [11, 22, 50, 54, 55, 58–63], XPS [6, 8, 56, 64–71], NMR [41, 71, 72], AFM [73], EPMA [8], TPD-MS [67], TG-DTA [10], RBS [74], LA-MS, and LDI-MS [75], have been used separately or jointly to characterize the physico-chemical state of Cr species on Phillips catalysts [11, 31]. These approaches attempt to provide direct or indirect evidence for the anchoring of chromate species at the surface during activation and the ability of the catalyst to polymerize ethylene, especially at the early stage of polymer chain formation. For example, based on the combination of the FTIR, Raman, and UV-vis spectroscopic results, monochromate species were identified anchored on the surface of the Cr/silica catalyst at low chromium loadings [47]. The monochromate structure on a highly diluted $Cr/SiO_2/Si(100)$ system was also confirmed by EXAFS results [53]. In the polymerization mechanism study, the in-situ FTIR spectroscopy suggested that the initiation mechanism followed a metallacycle route [23]. Very recently, Groppo and coworkers [76, 77] reviewed the spectroscopic investigations into the Phillips catalyst. However, the lower concentration of the Cr species, diversity of the amorphous silica gel surface, and high sensitivity to moisture and air are major obstacles for exploring the structure of Cr species in relation to polymerization activities. At the same time, these obstacles have led to difficulty in combining different experimental findings from different groups into one unifying picture. Although a definite explanation of the nature of the active site relating to the polymerization mechanism has not yet been achieved, it will be demonstrated in the following sections that valuable understanding has been

achieved through various spectroscopic methods concerning thermal activation of the Phillips catalyst, activation of the Phillips catalyst by CO or Al-alkyl cocatalysts, activation of the Phillips catalyst by ethylene monomer, and modification of the Phillips catalyst by Ti.

2.1 Thermal Activation of the Phillips Catalyst

During the preparation of Phillips catalyst, thermal activation is a crucial stage in which the chromium oxide is anchored into surface-stabilized chromate species. In this calcination process, a highly dispersed state of surface-stabilized chromate species, including mono-, di-, and polychromate, can be achieved through the redispersion cycles of sublimation, volatilization, spreading, deposition, and stabilization of bulk CrO_3 on a silica support surface [2]. By measurement of molar ratios of Δ[OH]/[Cr], McDaniel [5] suggested that the initial bonding was monochromate at 200°C (Δ[OH]/[Cr] = 2), but that the dichromate became dominant at 500°C (Δ[OH]/[Cr] = 1), while polychromates might be formed above 800°C (Δ[OH]/[Cr] < 1). On the basis of DRIFTS and DRS results, Panchenko et al. [78] confirmed that the reactions of CrO_3 with the silica calcined at 250°C, 400°C, and 800°C dominantly yield monochromates, dichromates, and polychromates, respectively. However, two unfavorable problems might occur during the thermal activation process: the calcination-induced reduction of surface-stabilized Cr(VI) species into lower valence state (+5, +4, or +3) and the creation of aggregated Cr_2O_3 (usually in crystallized form) even in an oxidizing atmosphere (O_2 or dry air). These affect to a great extent the physico-chemical state of the surface Cr species and thus the properties and performance of the catalyst. High resolution XPS, which has been demonstrated to be a very powerful method for a better understanding of the physico-chemical nature of surface chromium species through monitoring their transformation on Phillips catalysts calcined at various conditions, has benefitted the investigation of the origins of these two problems [8, 67, 68, 70, 79, 80].

For the Phillips catalyst calcined in dry air at 800°C for 20 h with 0.4 Cr nm^{-2} loading, two oxidation states were found in the XPS measurement [8]. The first, with a binding energy (BE) of 581.81 eV and a full width at half maximum (FWHM) of 9.62 eV, was assigned as the surface-stabilized chromate $Cr(VI)O_{x,surf}$ species with an oxidation state of +6 (atomic concentration 70.4%). The second, with a BE of 577.21 eV and a FWHM of 4.43 eV, was assigned as an oxidation state of +3 (atomic concentration 29.6%), which was quite different from the typical values of the bulk Cr_2O_3, strongly suggesting a surface-stabilized and highly dispersed characteristic of trivalent Cr species chemically bonded to silica surface [$Cr(III)O_{x,surf}$]. Compared with bulk Cr_2O_3, the higher BE of $Cr(III)O_{x,surf}$ species might result from the stabilizing effect of the silica as well as the environmental effect of neighboring chromate species. The larger FWHM value could be ascribed to its variety in molecule structure and the heterogeneity of the silica surface. The

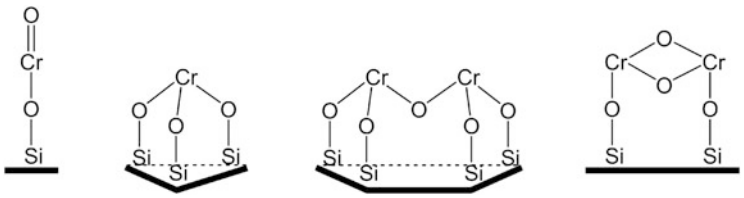

Scheme 3 Plausible structures of surface-stabilized trivalent chromium species $Cr(III)O_{x,surf}$ on the silica surface of the Phillips Cr/silica catalyst

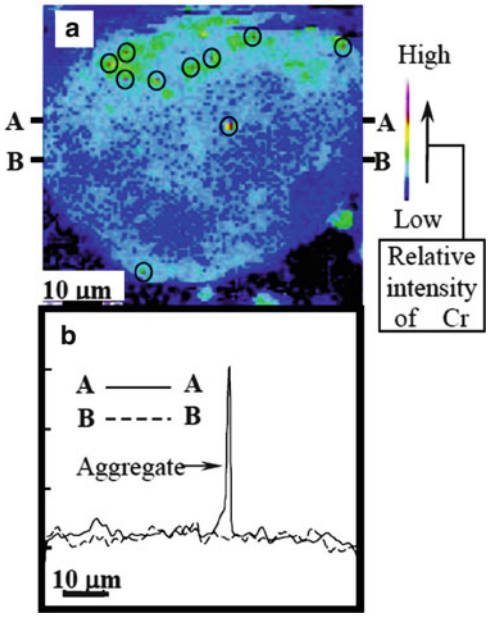

Fig. 1 EPMA map (**a**) and line curves (**b**) of the chromium distribution on the Phillips Cr/silica catalyst. The line curves of *A–A* and *B–B* in (**b**) correspond to the chromium distribution at the straight-line positions of *A–A* and *B–B* in (**a**), respectively. The *red patches* marked in *circles* in (**a**) correspond to small aggregates of surface Cr species

surface-stabilized $Cr(III)O_{x,surf}$ species on Phillips catalysts have been frequently reported by other researchers [33, 81]. Although its specific molecular structure still remains ambiguous, four plausible structure models (illustrated in Scheme 3) have been proposed. The formation of this $Cr(III)O_{x,surf}$ species was thought to originate from calcination-induced reduction of the chromate $Cr(VI)O_{x,surf}$ species and to increase with calcination temperature and time.

Figure 1 shows typical results of an electron probe microanalysis (EPMA) map and line curves of the Cr distribution on the calcined catalyst [8]. As can be seen, the Cr species mostly dispersed uniformly on the surface of each catalyst particle. However, the heterogeneity of Cr distribution on individual catalyst particles

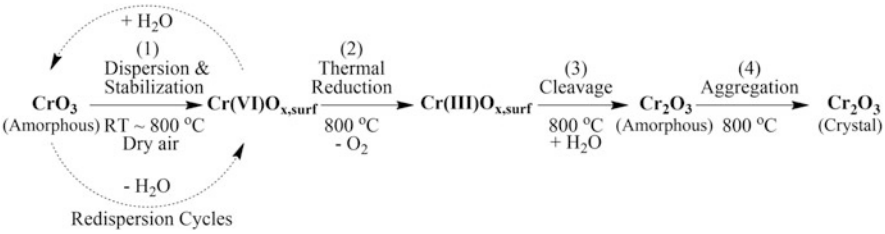

Scheme 4 Plausible mechanism of formation of aggregated Cr_2O_3 on the Phillips catalyst with 0.4 Cr nm^{-2} loading during calcination in the preparation process

revealed local aggregates of Cr species sized 200–300 nm. These aggregates, corresponding to the red patches in the map image (marked in circles) in Fig. 1a and to a sharp peak in the line curves in Fig. 1b, were suggested to be microcrystal particles of Cr_2O_3.

The irreversible formation of chromium oxide clusters, in the form of α-Cr_2O_3, is a well-known phenomenon occurring on the Cr/silica catalyst for Cr loadings higher than 1 wt% and/or in the presence of water poisoning. According to previous reports [33, 56, 64, 82], the formation of aggregated Cr_2O_3 on catalysts with a low level of Cr loading usually occurred in the later stage of calcination, followed by the full stabilization of bulk CrO_3 as chromate species and a consequent calcination-induced reduction into $Cr(III)O_{x,surf}$ species. Previously, the formation of aggregated Cr_2O_3 was usually thought to be related to the thermal decomposition (or reduction) of bulk CrO_3, as illustrated in (1). The XPS measurement [8] showed that the purposely introduced moisture induced the transformation of all the $Cr(III)O_{x,surf}$ species and one-seventh of the $Cr(VI)O_{x,surf}$ species into aggregates of Cr_2O_3 at high temperature, regardless of the oxidizing or inert atmosphere. Considering the traces of moisture from the simultaneous dehydroxylation of residual hydroxyl groups on the silica surface, the formation of aggregated Cr_2O_3 microcrystals might be induced by traces of moisture through cleavage of the $Cr(III)O_{x,surf}$ species during the calcination. The mechanism is illustrated in (2):

$$Cr(VI)O_{x,surf} + H_2O \underset{\text{dry air}}{\overset{800^\circ C}{\rightleftharpoons}} CrO_3 \xrightarrow[\text{dry air}]{800^\circ C} Cr_2O_3 + O_2 \quad (1)$$

$$Cr(III)O_{x,surf} + H_2O \xrightarrow[\text{dry air}]{800^\circ C} Cr_2O_3 \quad (2)$$

Thus, a plausible mechanism concerning the formation of Cr_2O_3 microcrystals during calcination in the preparation of Phillips catalyst was speculated (Scheme 4). At the first stage, the bulk CrO_3 was dispersed and stabilized as surface chromate species through the reaction with the hydroxyl groups on silica during the calcination process from room temperature (RT) to 800°C in dry air. Gradually, a highly dispersed state of chromate species can be achieved through many redispersion cycles of sublimation, volatilization, spreading, deposition, and stabilization of bulk CrO_3, as well as hydrolysis, re-spreading, re-deposition, and re-stabilization

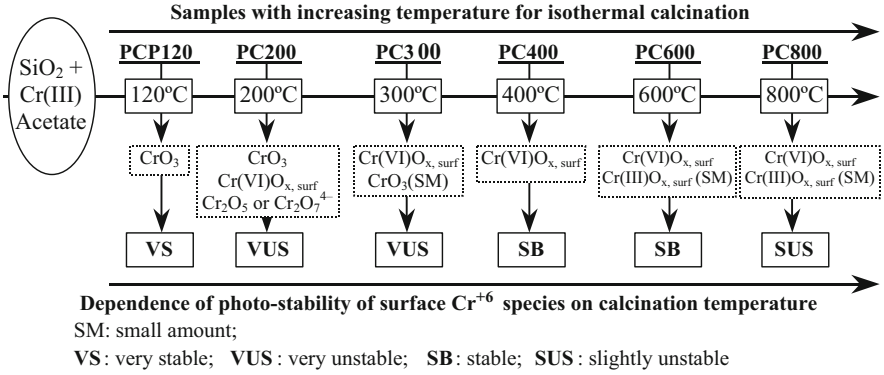

Fig. 2 Dependence of surface components of various Phillips catalyst samples on calcination temperature under isothermal conditions. *SM* small amount, *VS* very stable, *VUS* very unstable, *SB* stable, *SUS* slightly unstable

of chromate species on the support surface. These cycles may be facilitated in the presence of traces of moisture generating from the successive dehydroxylation of silica in the early stage of dispersion and support of bulk CrO_3 during calcination. During this period, the thermal decomposition of bulk CrO_3 can also be sufficiently inhibited by the presence of oxidizing gas (dry air or O_2). At the same time, the dehydroxylation also results in increasing strain in surface siloxane groups and in increasing reduction potential of the surface chromate species. At a certain critical point, the calcination-induced reduction of chromate species into $Cr(III)O_{x,surf}$ species would be expected (Scheme 4, reaction 2). Thereafter, traces of low moisture from dehydroxylation might split some $Cr(III)O_{x,surf}$ species, leading to the formation of Cr_2O_3 microcrystals (Scheme 4, reactions 3 and 4). Higher temperature, longer duration, and higher content of moisture in the last stage of the calcination process can lead to more serious aggregation of surface Cr species.

In order to further understand the specific transformation procedure of surface chromium species during the thermal activation process, Phillips catalysts isothermally calcined at various temperatures were prepared and characterized by XPS. The substantial dependence of surface Cr components of Phillips catalysts in terms of the calcination temperature in isothermal preparation is summarized in Fig. 2 [68, 70]. These catalysts (with Cr 1.0 wt% loading) isothermally calcined at 200°C, 300°C, 400°C, 600°C, and 800°C were designated PCX, where X is the calcination temperature. PCP120 was the silica support impregnated with chromium acetate and subsequently dried at 120°C, and all the other PCX catalysts were derived from PCP120. The specific surface Cr components of various catalyst samples versus calcination temperatures were clarified. The bulky CrO_3 started to be transformed into supported chromate species at 200°C and could be completely stabilized on silica gel surface as chromate species at 400°C. Partial thermal decomposition of bulky CrO_3 into bulky pentavalent Cr oxide [e.g., Cr_2O_5 or $(Cr_2O_7)^{4-}$] was only observed on samples calcined at 200°C due to the incomplete stabilization of bulky CrO_3 into chromate species. Only a slight thermally induced partial reduction of chromate species into $Cr(III)O_{x,surf}$ was observed at high temperatures (600–800°C).

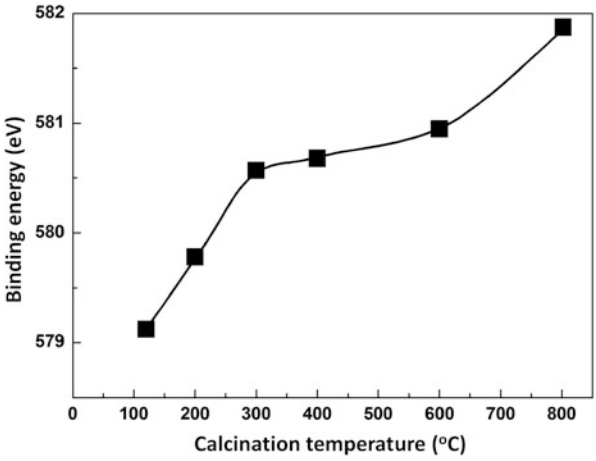

Fig. 3 Dependence of binding energy [Cr 2p (3/2)] of surface Cr^{6+} species of various Phillips catalysts on calcination temperature for preparation of the catalysts from PCP120 precursor

The successive increase in BE values of hexavalent chromium species with increasing calcination temperature from PCP120 to PC800 is plotted in Fig. 3. The chromate species [$Cr(VI)O_{x,surf}$] on the catalyst became more and more electron deficient with increased calcination temperatures from 200°C to 800°C. This correlates well with the typical polymerization behavior of Phillips catalysts, i.e., that the polymerization activity increases with an increase in calcination temperature. The dominant supporting of bulky CrO_3 on a silica gel surface and simultaneous dehydroxylation of the silica gel surface at 120–300°C account for the drastic increase in BE values of hexavalent chromate species in this temperature range for isothermal calcination. The slowly increasing of BE values of chromate species from 300°C to 600°C was solely derived from dehydroxylating residual surface hydroxyl groups. Another enhancement of the increase in BE values of chromate species from 600°C to 800°C might come from further dehydroxylation of residual hydroxyl groups, as well as enhancement of surface tension from easier relaxation of surface siloxane groups induced by high temperature.

The dependence of BE values on the XPS acquisition time during the XPS measurement indicated that further increasing the XPS acquisition from 10 to 30 or 120 min may lead to the catalyst being reduced by the soft X-ray irradiation during the XPS measurement, which provides a good method for evaluation of the photostability of Phillips catalysts prepared under different conditions. The photostability of surface chromate species on Phillips catalysts was found to be significantly dependent on the calcination temperature used for catalyst preparation (see Fig. 2); the sample calcined at moderate temperatures (400–600°C) showed the highest photostability [70].

2.2 Activation of Phillips Catalysts by CO or Al-alkyl Cocatalysts

The reduction of Cr(VI) to lower oxidation state is the first step in the induction period in the ethylene polymerization process. Active site precursors for polymerization can be formed after reduction of the chromate species by CO (usually at 350°C) or Al-alkyl cocatalyst (e.g., TEA) in a separated pre-activation step, or by ethylene monomer itself during the initial stage of polymerization [2]. Activation by ethylene monomer is most frequently used in the commercial processes. The use of CO or Al-alkyl cocatalyst as reduction agent may shorten or remove the induction period, which is frequently used at the laboratory scale. The effect of activation using different reducing agents for the Phillips catalyst was systematically investigated by XPS characterization.

Phillips catalyst reduced by CO at 350°C can exhibit instantaneous polymerization activity upon contact with ethylene [2] and is generally considered as an ideal catalyst system in spectroscopic investigations of the early stages of ethylene polymerization [11]. Comparison of the oxidation states of surface Cr species on PC600 (calcined) and PC600/CO (PC600 pre-reduced by CO at 350°C for 1 h) catalysts measured by XPS method suggested that about 63% of surface Cr species were reduced into surface-stabilized Cr(II) species by CO, leaving a certain amount of residual chromate species on PC600/CO [80]. The DRS results [83] showed that the Cr active sites could be fully available for reduction at higher reduction temperature (600°C).

The activation of the Phillips catalyst by Al-alkyl cocatalyst was also systematically studied by XPS and solid state NMR [69, 84]. XPS quantified the existence of four oxidation states, including +2, +3, +5, and +6, of surface Cr species on TEA-modified catalysts. It was found that the relative concentration of active sites was around 14.4–24.9 mol% Cr for the TEA-modified Phillips catalysts depending on the calcination temperature and Al/Cr molar ratio. The correlation of polymerization activities as well as the oxidation states of surface chromium species with the molar ratio of Al/Cr is shown in Fig. 4. It seemed that only the surface chromium species in oxidation states of +2 and +6 were possibly related with the activity of the ethylene polymerization catalysts. The correlation suggested that the active precursor of the chromium cluster can be named as a $Cr^{2+}{\cdot}2Cr^{6+}$ cluster composed of one $Cr(II)O_{x,surf}$ species and two $Cr(VI)O_{x,surf}$ species, in which the $Cr(II)O_{x,surf}$ species act as the real center of active chromium precursor and the residual $Cr(VI)O_{x,surf}$ species are also necessary components acting as the neighboring ligand environment with electronic and steric effects. Three plausible chemical structural models of the $Cr^{2+}{\cdot}2Cr^{6+}$ cluster are proposed in Scheme 5, based on the correlation between XPS and polymerization results and our previous understanding of the surface chemical nature of calcined Phillips $Cr(VI)O_x/SiO_2$ catalysts and pre-reduced $Cr(II)O_x/SiO_2$ catalysts.

The ^{1}H and ^{27}Al MAS solid state NMR spectra clearly demonstrated that the existing states of surface Al species in the TEA-modified Phillips catalysts strongly

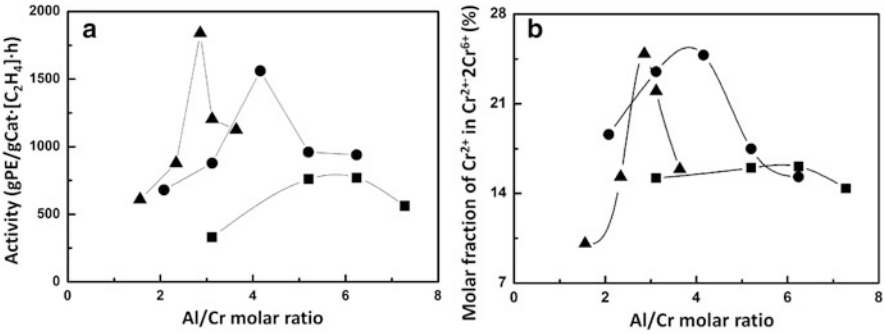

Fig. 4 Al/Cr molar ratios versus polymerization activity (**a**) and the molar fraction of Cr^{2+} (**b**) in $Cr^{2+}{\cdot}2Cr^{6+}$ cluster on the TEA-modified Phillips catalyst calcined at 400°C (*filled squares*), 600°C (*filled circles*), and 800°C (*filled triangles*)

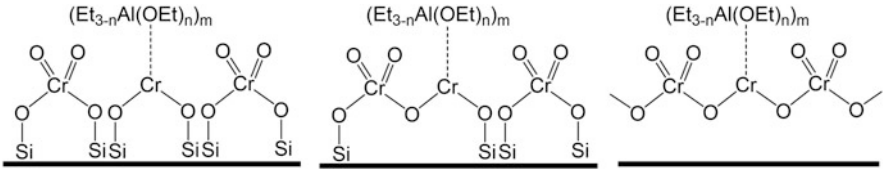

Scheme 5 Three plausible structure models of the active Cr^{2+} precursors existing as a $Cr^{2+}{\cdot}2Cr^{6+}$ cluster on the TEA-modified Phillips catalyst; $n = 1$ or 2; $m = 1$ or 2

depended on the concentration of TEA and the calcination temperature used during the catalyst preparation process [84]. In Fig. 5, three kinds of Al species with 6-, 5-, and 4-coordination states are distinguished for the PC400, PC600, and PC800 catalysts modified by TEA at various Al/Cr molar ratios. For PC400/TEA catalysts, the profiles were only slightly changed with various Al/Cr molar ratios, and the 6-coordinated Al species was dominant. For the PC600/TEA, the peak intensity of the 4-coordinated Al species significantly increased with increasing Al/Cr molar ratios, resulting in a dramatic change in the relative amounts of 6-, 5-, and 4-coordinated Al species. For higher Al/Cr molar ratios, the spectra completely changed, and the 5- and 4-coordination states of the surface Al species could not be clearly distinguished and the 6-coordinated Al species became dominant again. For PC800/TEA, it was observed that the 6-coordinated Al species was still predominant in a narrow range of Al/Cr molar ratio, except the sharp and strong peak of 4-coordianted Al species at the Al/Cr ratio of 2.34.

A relationship between the Al/Cr molar ratio and relative amount of 4-coordinated Al species on the PC400/TEA, PC600/TEA, and PC800/TEA catalysts is illustrated in Fig. 6 [84]. For PC400/TEA catalysts, the relative amounts of 4-coordinated Al species increased only slightly with the increase in Al/Cr ratios. For PC600/TEA and PC800/TEA catalysts, the relative amounts of 4-coordinated Al species firstly increased with an increase in Al/Cr ratios then reached a

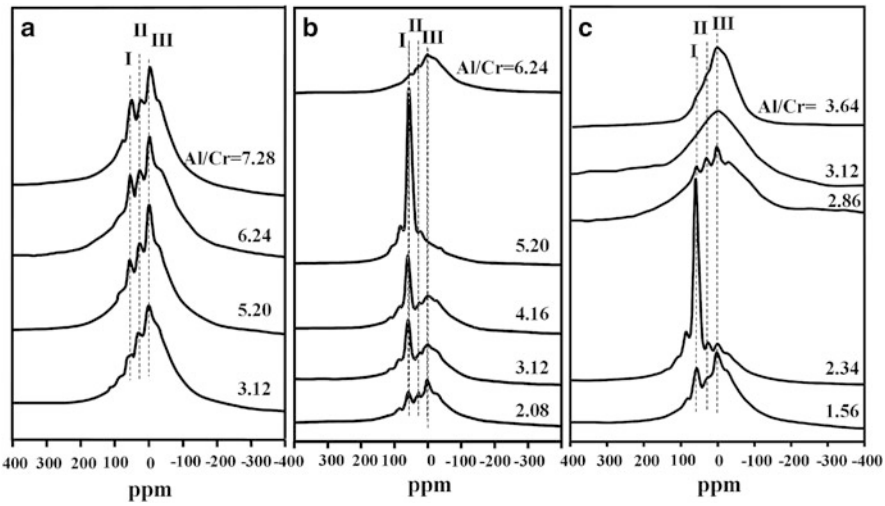

Fig. 5 ^{27}Al MAS NMR spectra of (**a**) PC400, (**b**) PC600, and (**c**) PC800 catalysts modified by TEA at the Al/Cr molar ratios listed; *I* 4-coordinated Al, *II* 5-coordinated Al, *III* 6-coordinated Al

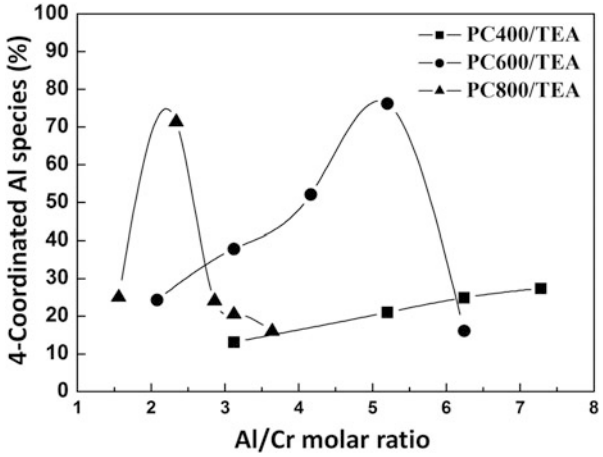

Fig. 6 Correlation between the Al/Cr molar ratio and the relative amount of 4-coordinated Al species on the PC400/TEA, PC600/TEA, and PC800/TEA catalysts

maximum value. With the further increase in Al/Cr ratios, the 4-coordinated Al species decreased. It was interesting to find that with an increase in Al/Cr molar ratio, the activities of the three types of catalysts (PC400/TEA, PC600/TEA, and PC800/TEA) first increased to a maximum value then decreased as shown in Fig. 4. The similar trend in Figs. 4 and 6 inspired us to consider that only the 4-coordinated Al species on the surface of the TEA-modified Phillips catalyst was directly related to the active Cr sites for ethylene polymerization.

Table 1 Evolution of alkenes and formaldehyde from the ethylene-treated Phillips catalyst under various conditions

	HCHO	C_2H_4	C_3H_6	C_4H_8	C_5H_{10}	C_6H_{12}	C_7H_{14}
	m/z						
Samples	30	28	42	56	70	84	98
RT/2 h	+	+	+	+	−	−	−
RT/5 h	+	+	+	+	−	−	−
RT/10 h	+	+	+	+	−	−	−
50°C/2 h	+	+	+	+	−	−	−
100°C/0.5 h	+	+	+	+	+	−	−
100°C/1 h[a]	+	+	+	+	+	+	+
150°C/0.5 h[a]	+	+	+	+	+	+	+

+, detected; −, not detected

[a]Polyethylene was confirmed by IR

2.3 Activation of the Phillips Catalyst by Ethylene Monomer

Activation of the Phillips catalyst directly by ethylene monomer was further investigated by XPS and TPD-MS methods in order to shed some light on the reaction mechanisms during the induction period. Deconvolution of the XPS spectra for industrial Phillips Cr/silica catalysts treated in ethylene atmosphere at RT for 2 h revealed that surface chromium species presented in three oxidation states: surface chromate $Cr(VI)O_{x,surf}$ species; surface-stabilized trivalent Cr(III) species; and surface-stabilized Cr(II) species. Compared to the original catalyst before ethylene treatment, about one-third of chromate $Cr(VI)O_{x,surf}$ species (i.e., ca. 22.6% of the whole surface Cr) was reduced to Cr species in lower oxidation states during the ethylene treatment, even under ambient conditions [67].

TPD-MS characterization of the calcined Phillips catalyst before and after treatment within ethylene atmosphere for 2 h under ambient conditions confirmed the evolution of three species: formaldehyde ($m/z = 30$); olefins with an odd number of carbon atoms, i.e., propylene ($m/z = 42$); and olefins with an even number of carbon atoms, i.e., butene ($m/z = 56$) [79]. As shown in Table 1, various new olefin species with pentene ($m/z = 70$), hexene ($m/z = 84$), and heptene ($m/z = 98$) also appeared under various catalyst treatment conditions in ethylene atmosphere [85]. Higher temperature led to the formation of olefins with higher carbon number. Moreover, the formation of polyethylene was also confirmed by IR characterization over catalyst samples treated at 100°C/1 h or 150°C/0.5 h in ethylene.

Formaldehyde is a by-product of the redox reaction between ethylene and hexavalent chromate species, resulting in the formation of divalent chromium species. Subsequently, the Cr(II) species coordinated with formaldehyde might act as the active precursor at lower temperatures to produce the new short olefins with both odd and even numbers of carbon atom. The experimental evidence obtained from the early stage of ethylene polymerization cannot be rationalized

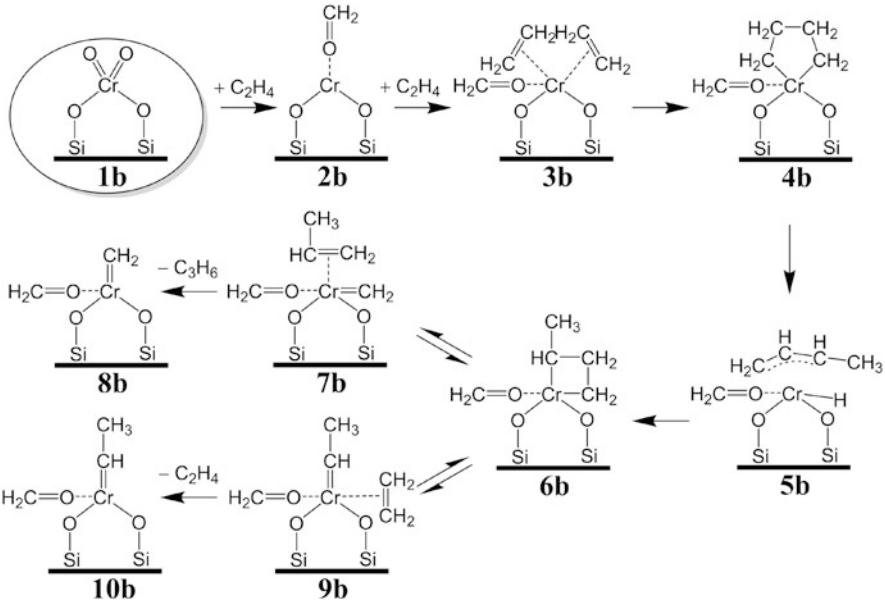

Scheme 6 Plausible mechanistic routes for the formation of the first hydrocarbon species, propylene, during the induction period over the non-pre-reduced Phillips Cr/silica catalyst through interaction with ethylene under various conditions

by the Cossee–Arlman mechanism [25]. It should be mentioned that the conversion of ethylene into higher olefins with both odd and even numbers of carbon atoms is a well-established phenomenon that was believed to proceed by metathesis over metal alkylidene species [86]. This indicated that the coordination of formaldehyde on surface-stabilized divalent chromium species results in the formation of active precursor for olefin metathesis rather than polymerization. The active sites in heterogeneous transition metal-catalyzed olefin metathesis are generally thought to be a transition metal alkylidene species, as for their well-defined homogeneous analogues [87]. In our work, the signal for Cr-alkylidene species for the sample treated at 100°C for 0.5 h was firstly observed in XPS measurement [85]. At the same time, the evolution of the Cr-metallacyclic species can be considered to be prior to that of the Cr-alkylidene species after gradual increase in ethylene treatment time. Thus, a metathesis initiation mechanism based on the experiment was speculated and is shown in Scheme 6. The π-allyl Cr(II)-hydride species **5b**, which formed through the metallacyclopentane **4b**, was converted into metallacyclobutane **6b** [88]. The metallacyclobutane species (**6b**) was subsequently subjected to metathesis, generating either Cr(IV)-methylidene **7b** and the first hydrocarbon species propylene or Cr(IV)-ethylidene **9b** and a new ethylene monomer [87]. The subsequent metathesis of the first hydrocarbon species propylene on Cr(IV)-ethylidene **8b** and/or Cr(IV)-methylidene **10b** led to the formation of the second hydrocarbon species butene during the induction period [86, 87, 89].

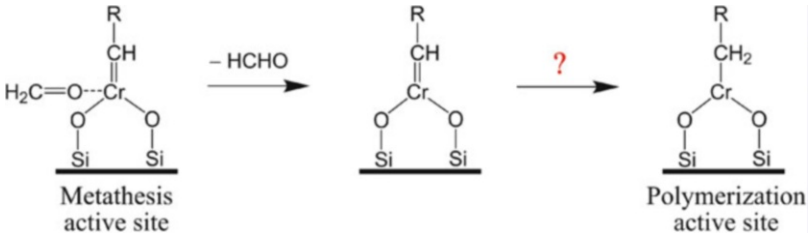

Scheme 7 Plausible transformation of metathesis site into polymerization site from induction period to polymerization period on the Phillips catalyst

It is made clear that the Cr(II) species adsorbed with formaldehyde during the induction period could serve as active site precursor for ethylene metathesis, and the gradual desorption of formaldehyde at higher temperatures transforms the ethylene metathesis site into an ethylene polymerization site resulting in accelerating-type kinetics (as shown in Scheme 7). The question is how the ethylene polymerization reaction occurred starting from the Cr-carbene species formed during the induction period. Scott and coworkers reported the SiO_2-supported Cr-alkylidene catalyst to be highly active for ethylene polymerization, producing HDPE with similar chain conformation as that produced by Phillips catalyst [90–94]. The analyzing of the microstructures of two polyethylenes obtained by industrial Phillips catalysts might give some clues. Firstly, two ethylene homopolymers from both calcined and Al-alkyl pre-reduced Phillips catalysts were analyzed. The ^{13}C NMR spectra showed that the peak intensity of methyl branches was always strongest in the methyl, ethyl, and butyl branches [85], suggesting that propylene was the first and dominant olefin formed from ethylene metathesis. The generated propylene subsequently inserted into growing polyethylene chains to form methyl braches. Due to the coexistence of ethylene metathesis active sites with polymerization sites, the formation of short chain branches (SCBs) over the Phillips catalyst during ethylene homopolymerization can be rationalized well by the in-situ formation of various short olefins with both even and odd number of carbon atoms from ethylene metathesis sites and subsequent in-situ copolymerization with ethylene monomer over the ethylene polymerization sites.

Another example came from the polymer produced by copolymerization of ethylene and cyclopentene over Phillips catalyst [95]. As shown in Fig. 7, the 1,2-insertion and 1,3-insertion of cyclopentene into the polyethylene chain were confirmed. The absence of any internal double bond (C=C) in the copolymer ruled out the ring-opening metathesis polymerization mechanism. This evidence strongly implied that Cr=C might not be an active site for polymerization. Cr–C active sites under the Cossee–Arlman mechanism should be responsible for the chain propagation. From analysis of the structure of the polymer produced by copolymerization of the isotope-labeled monomer, McGuinness et al. also provided unambiguous support for chain growth via a Cossee–Arlman process on Phillips catalyst [96]. Based on the above-mentioned experimental evidence, during the induction period the

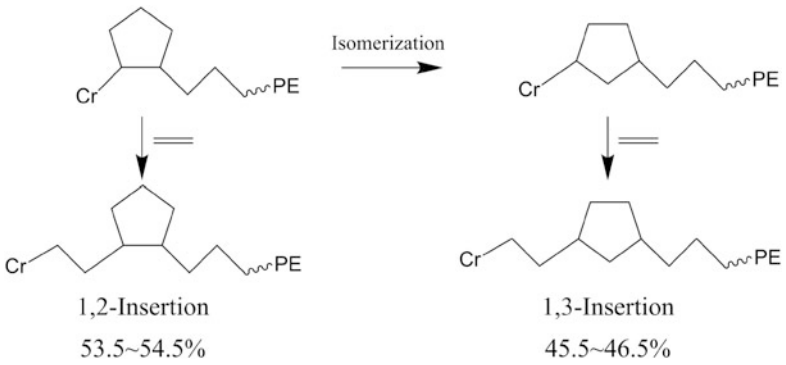

Fig. 7 Mechanisms of 1,2-insertion and 1,3-insertion of cyclopentene into the polyethylene main chain during ethylene and cyclopentene copolymerization over Phillips catalyst

Cr=C species (metathesis active sites) should be transformed into Cr–C species (polymerization active sites) in a mysterious way, as illustrated in Scheme 7. Such mysterious phenomenon of interconversion between catalysis of olefin metathesis and olefin polymerization with other types of catalysts has been previously reported [97, 98] and needs further investigation in the future.

2.4 Titanium Modification of the Phillips Catalyst

The Ti-modified Phillips catalyst is a very important industrial catalyst that is widely used in ethylene polymerization for promotion of polymerization activity and regulation of the microstructure of the polymer chains, but the mechanism of its action still remains mysterious. We characterized several industrial Ti-modified Phillips catalysts calcined at 650°C and 820°C using ^{1}H MAS solid state NMR and XPS. As shown in Fig. 8, the ^{1}H MAS solid-state NMR spectra provided the first direct evidence of surface residual Ti–OH groups on the Ti-modified Phillips catalysts. In Fig. 9, the high-resolution XPS studies on these industrial catalysts clearly demonstrated that the BE value of surface chromate species slightly increased with increased Ti loading of the catalysts, indicating the increased electron-deficiency of surface chromate species due to modification by Ti [71]. The slight increase in the FWHM values also indicated the broadening of the distribution of surface chromate species. Calcination temperatures of 650–820°C showed a similar effect to that of Ti loading in terms of the increased electron-deficiency of surface chromate species, which could be rationalized by the removal of more electron-donating surface hydroxyl groups and the increase in surface tension due to dehydroxylation of surface residual hydroxyl groups at higher calcination temperatures.

In summary, it has been demonstrated that much deeper understanding of the thermal activation during catalyst preparation, activation by CO or Al-alkyl

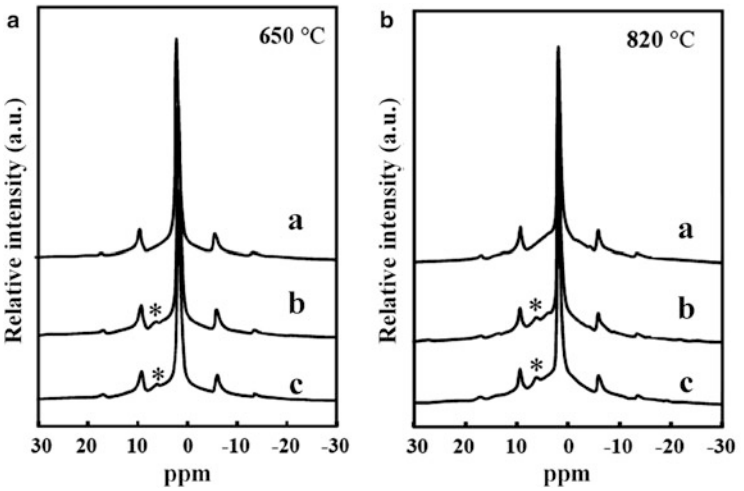

Fig. 8 ^{1}H MAS solid state NMR spectra for various Phillips catalysts calcined at (**a**) 650°C and (**b**) 820°C: Ti-free (*curve a*), modified by 2.38 wt% Ti (*curve b*), and modified by 3.45 wt% Ti (*curve c*). *Asterisks* indicate peak corresponding to surface Ti-OH groups

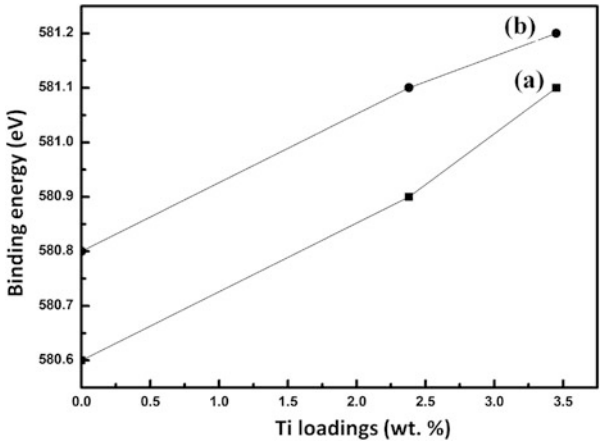

Fig. 9 Dependence of binding energy [Cr 2p (3/2)] of surface Cr^{6+} species of various Phillips catalysts on Ti content of the Phillips catalyst calcined at (*a*) 650°C and (*b*) 820°C

cocatalysts, activation by ethylene monomer during the induction period, and the effect of Ti-modification of Phillips catalysts has been achieved through various spectroscopic methods, in particular through combined multiple methodologies. Further development can be expected with the development of the spectroscopic techniques and the emergence of new techniques such as time- and temperature-resolved FTIR spectroscopy [62], pressure- and temperature-resolved FTIR spectroscopy under in-situ or operando conditions [63, 77], in-situ XAS

spectroscopy [99], LA-MS, and LDI-MS [75], which were frequently involved in recent studies of the Phillips catalyst. The characterization under close to actual commercial conditions is also a challenge as well as an opportunity to cast some light on the related mechanisms. At the same time, the combination of modern spectroscopic methods with other methodologies such as polymerization kinetic, model catalyst, and molecular modeling techniques as well as with analysis of the microstructures of polymer chains will play more and more important roles in the future and will be partially outlined in the following sections.

3 Approaches Using Polymerization Kinetics

Kinetic investigation through either polymerization experiments or mathematic modeling both for slurry and gas phase polymerization is one of the most important ways to investigate catalytic mechanisms and to provide basic data for polymerization reactor and process design. Mathematic modeling of ethylene polymerization kinetics over Phillips catalysts has been demonstrated as a powerful tool for the precise evaluation of the basic kinetic parameters and to establish equations for structure–property regulation through control of process parameters [100–103]. The polymerization kinetics of Phillips catalysts could be significantly affected by the reductive activation process for ethylene polymerization using different activators such as ethylene, CO, Al-alkyl cocatalysts (e.g., TEA), or even other reducing agents. The polymerization kinetics of Phillips catalysts using ethylene monomer itself as activator for ethylene polymerization has been systematically investigated [2]. Typically, a linearly built-up type of kinetic curve would be presented, with an induction period dependent on the polymerization temperature and ethylene pressure. Reductive activation by CO only diminishes the induction period without changing the character of the built-up type of kinetic curve. In recent years, activation of the Phillips catalyst by Al-alkyl cocatalysts is becoming one of the most important ways to improve the catalyst performance and the microstructure and properties of the polyethylene (PE) products. As is well known, Al-alkyl cocatalyst is an indispensable component for most of the olefin polymerization catalysts such as Ziegler–Natta and metallocene catalysts. The Al-alkyl cocatalyst could act as reducing agent, alkylation agent, poison scavenger, and have a marked impact on the polymer microstructure by control of the chain transfer and stereospecificity. Also, excess amount of Al-alkyl cocatalyst could deactivate the catalyst through over-reduction of the active Cr species. Ethylene polymerization with Phillips catalyst without using any organometal cocatalyst is taken as the most important evidence to support the monometallic active site mechanism. Therefore, Al-alkyl cocatalyst could be excluded as the active site former for Phillips catalysts.

During the last few decades, experimental reports about the combination of Al-alkyl cocatalyst with the Phillips catalyst have been very limited. Spitz et al. [104] reported the significant effect of TEA on Phillips catalyst for the activity,

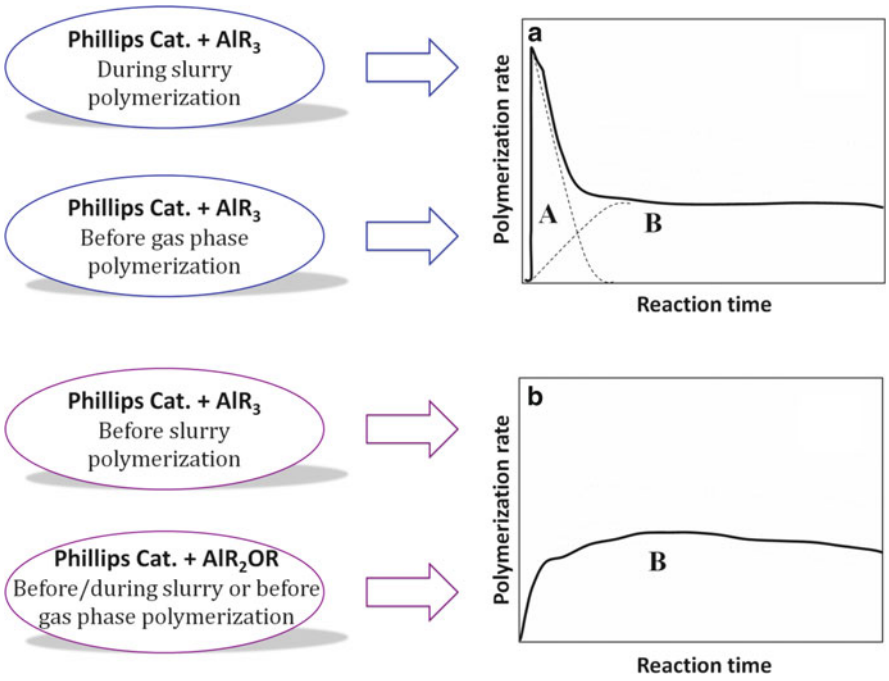

Fig. 10 Two types of kinetic curve for ethylene polymerization over Phillips-type catalysts. (**a**) Hybrid of two typical types of kinetic curve: fast activation followed by fast decay (*A*) and slow activation followed by slow decay (*B*). (**b**) Single-type curve with slow activation followed by slow decay (*B*)

kinetics and 1-hexene incorporation for ethylene/1-hexene copolymerization in liquid 1-hexene. McDaniel and Johnson [105, 106] studied the effects of TEB on the polymerization kinetics of the Phillips catalyst with different supports ($AlPO_4$, SiO_2, Al_2O_3). Tait and coauthors [107] studied the effects of TiBA on kinetics and polymer morphology with Phillips catalyst. Our series of studies on the Phillips catalyst combined with Al-alkyl cocatalyst revealed that the polymerization kinetics could be significantly affected by the type of Al-alkyl cocatalyst as well as by the timing of its introduction for both slurry and gas phase ethylene polymerization (see Fig. 10) [69, 80, 84, 95, 108–110]. For the same Al-alkyl cocatalyst, catalyst activation by the cocatalyst before polymerization (in catalyst preparation) or during polymerization with simultaneous interaction of catalyst with Al–alkyl cocatalyst and monomer would make a significant difference in the polymerization kinetics. As shown in Fig. 10a, the kinetic curve (type a) follows hybrid-type kinetics and can be deconvoluted into two basic types of typical kinetic curves: one type with fast activation followed by fast decay and the other type with slow activation followed by slow decay. They should be derived from two different types of active sites. The kinetic curve of type b (shown in Fig. 10b) follows only one single type of kinetics, with slow activation followed by slow decay. Sections 3.1

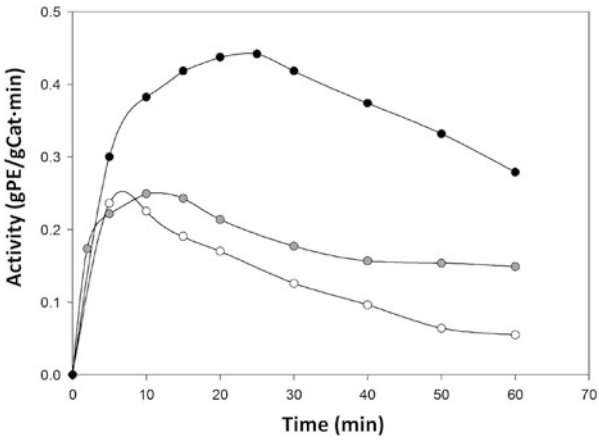

Fig. 11 Kinetic curves of the TEA-modified Phillips catalyst (PC600/TEA) at Al/Cr molar ratios of 2.08 (*white symbols*), 3.12 (*grey symbols*), and 4.16 (*black symbols*), before ethylene slurry polymerization. Polymerization conditions: catalyst amount, 100 mg; polymerization temperature, 60°C; ethylene pressure, 0.15 MPa; solvent heptane, 20 mL

and 3.2 will discuss how the type of cocatalyst (AlR_3 or AlR_2OR), the timing of introduction of cocatalyst (before or during polymerization), and the type of polymerization (slurry or gas phase), can dramatically affect the polymerization kinetics as shown in Fig. 10.

3.1 Activation by Al-alkyl Cocatalyst Before Polymerization

In the previous sections, a combined XPS and solid state NMR spectroscopic investigation of Phillips catalysts (PC400/TEA, PC600/TEA, and PC800/TEA) calcined at 400°C, 600°C, and 800°C, respectively, followed by activation with TEA cocatalyst before slurry polymerization showed that 4-coordinated Al species, rather than the 5- or 6-coordinated Al species, were directly related with the polymerization-active Cr species. Figure 11 shows the polymerization kinetics for the PC600/TEA catalyst at different Al/Cr molar ratios of 2.08, 3.12, and 4.16 [69]. Kinetic curves of type b (Fig. 10b) show a gradual built-up of polymerization rate from zero to a maximum followed by gradual decrease to a stationary rate, which was found to be the same typical form of kinetics as for $TiCl_3$/TEA and metallocene/MAO catalysts. This type of kinetics for TEA-modified Phillips catalysts was consistent with those reported by Spitz et al. [104] and McDaniel and Johnson [105, 106] using Cr/silica/TEA and Cr/$AlPO_4$/TEB catalysts, respectively.

The Phillips catalyst is mostly applied in ethylene slurry polymerization using loop reactors. It is also now being commercially used in gas phase ethylene polymerization processes. However, it is very difficult to find reports about ethylene gas phase polymerization using Phillips catalysts in the literature because it is a great challenge to perform gas phase polymerization on a laboratory scale. Recently, we carried out gas phase ethylene polymerization over silica-supported

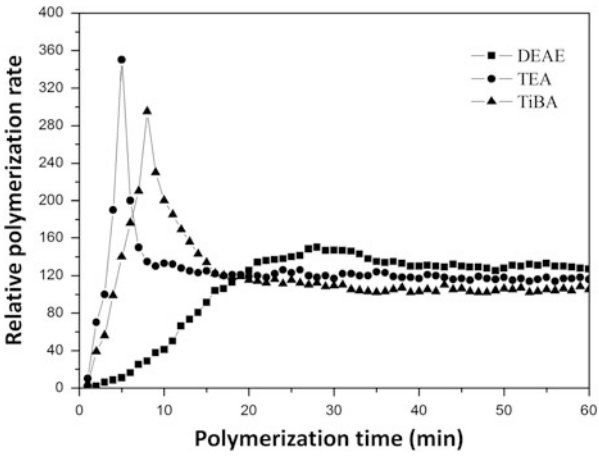

Fig. 12 Kinetic curves of ethylene polymerization of S-2 catalysts modified with various cocatalysts before gas phase polymerization. Polymerization conditions: catalyst amount, 200 mg; polymerization temperature, 92°C; ethylene pressure, 1.2 MPa

silyl chromate S-2 catalysts pre-reduced by three Al-alkyl cocatalysts in a specially designed gas phase high-speed stirred-autoclave reactor [109]. The catalyst was pre-activated by TEA, TiBA, or DEAE before the gas phase ethylene polymerization during the catalyst preparation step. As shown in Fig. 12, the gas phase ethylene homopolymerization kinetic curves over the TEA- or TiBA-modified S-2 catalysts belonged to type a (Fig. 10a), which is a hybrid type of kinetics composed of two basic types of typical kinetic curve: one type with fast activation followed by fast decay and the other type with slow activation followed by slow decay. Such type of polymerization kinetics might not be suitable for application in large-scale gas phase olefin polymerization processes because reactor fouling and agglomeration can easily occur. In the case of the DEAE-modified S-2 catalyst, the gas phase ethylene homopolymerization kinetic curve is type b (Fig. 10b), which is a simple type of polymerization kinetics with slow activation followed by slow decay. Although the polymerization activity for the DEAE-modified S-2 catalyst is slightly lower than the TEA- or TiBA-modified catalysts, its polymerization kinetics would be of benefit for the heat transfer within the gas phase polymerization fluidized bed reactor [111]. The differences in the structure and in the reducing and alkylation capabilities of AlR_3 (TEA and TiBA) and AlR_2OR (DEAE) cocatalysts might be responsible for their totally different ethylene polymerization kinetics, but the mechanism is still not known and awaits further exploration.

3.2 Activation by Al-alkyl Cocatalyst During Polymerization

The Al-alkyl cocatalyst could also be introduced during the polymerization stage, with simultaneous interaction of catalyst with Al–alkyl cocatalyst and monomer within the polymerization reactor. Ethylene homopolymerization using Phillips catalyst PC600 calcined at 600°C followed by activation with TEA cocatalyst

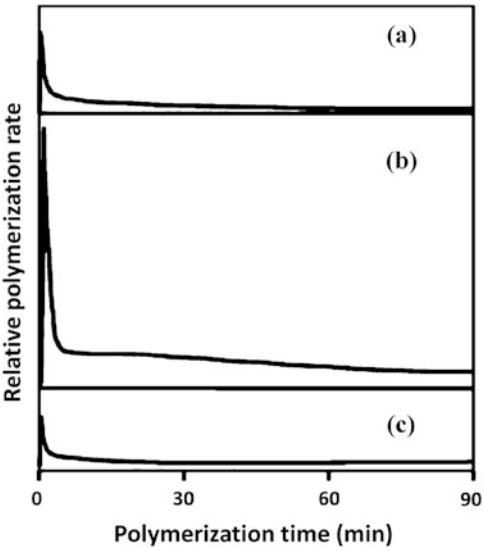

Fig. 13 Kinetic curves of ethylene polymerization using Phillips catalyst PC600 activated by TEA during slurry polymerization with Al/Cr molar ratio: (**a**) 7.5; (**b**) 15.0; (**c**) 22.5. Polymerization conditions: catalyst amount, 100 mg; polymerization temperature, 60°C; ethylene pressure, 0.13 MPa; solvent heptane, 20 mL; cocatalyst TEA in heptane, 1 M

during the slurry polymerization process was carried out with Al/Cr molar ratios of 7.5, 15.0, and 22.5 [84]. As shown in Fig. 13, the catalyst showed type a (Fig. 10a) ethylene polymerization kinetics, which is a hybrid type of kinetics composed of two basic types of typical kinetic curves. Such hybrid-type polymerization kinetics must originate from two different types of active sites (here named Site-**A** and Site-**B**). Our previous reports have described a mechanistic speculation of the origin of the two types of active sites for ethylene polymerization as well as their plausible transformation during activation of the Phillips catalyst either by Al-alkyl cocatalyst or by ethylene monomer and CO, which is illustrated in Scheme 8. Under the simultaneous interaction of TEA and ethylene monomer with PC600 catalyst, some chromate Cr(VI) species were reduced to Cr(II) species by ethylene monomer with formaldehyde as byproduct. The coordination of formaldehyde with Cr(II) species (named as Site-**C1** in Scheme 8) could occur, which could lead to the formation of Site-**A** through the desorption of formaldehyde by TEA or ethylene monomor. Due to the very exposed feature, Site-**A** could easily coordinate with ethylene monomer and could also easily be over-reduced by TEA cocatalyst. Therefore, Site-**A** showed high activity but fast decay. On the other hand, some chromate Cr(VI) species were reduced by TEA and then coordinated with Al-alkoxy resulting in Site-**B**, with slow activation and slow decay. Within Site-**B**, the Cr(II) center was strongly coordinated with Al-alkoxy byproduct, which may hinder the coordination of ethylene monomer but avoid further over-reduction by TEA. Therefore, Site-**B** had lower activity and higher stability compared with Site-**A**. The ^{13}C NMR spectra of the homopolymers obtained from this catalyst system showed the signal of the branching carbons of methyl, ethyl, propyl, and *n*-butyl. Site-**C1** was a metathesis site and could produce propylene, 1-butene, and 1-pentene, which was consistent with the ^{13}C NMR spectroscopic evidence of the ethylene

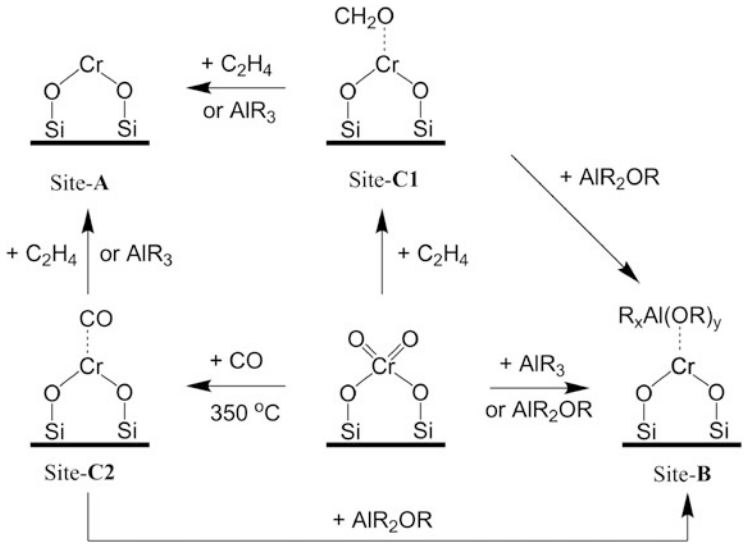

Scheme 8 Plausible mechanism for the formation of two kinds of ethylene polymerization active sites (Site-**A** and Site-**B**) and metathesis active sites (Site-**C1** and Site-**C2**) on Phillips-type catalysts under various conditions; $x = 1$ or 2; $y = 1$ or 2

homopolymers obtained from this catalyst system showing the signals of the branching carbons of methyl, ethyl, and propyl. With increase in the Al/Cr molar ratios in the polymerization, the relative amount of SCBs of polymers from the catalyst system also decreased, because the competition between ethylene monomer and TEA reduced the chromate Cr(VI) species into Cr(II) sites and accelerated the conversion of metathesis active site-**C1** to polymerization active Site-**B** with more TEA.

Ethylene homopolymerization using Phillips catalyst PC600 calcined at 600°C followed by activation with DEAE cocatalyst during the slurry polymerization process was carried out with Al/Cr molar ratios of 7.5, 15.0, and 22.5 [84]. As shown in Fig. 14, a typical single-type polymerization kinetics corresponding to type b in Fig. 10b was observed, which was completely different from the kinetics with the same catalyst activated by TEA at the same conditions (as shown in Fig. 13). This type of polymerization kinetics could be ascribed to one type of active site (Site-**B**) formed in two ways. One was similar with the PC600 activated by TEA: some chromate Cr(VI) species were reduced to Cr(II) species by ethylene monomer and coordinated with formaldehyde, then formaldehyde-coordinated Cr(II) sites were transformed to DEAE-coordinated Cr(II) sites by substitution, as shown in Scheme 8. On the other hand, some chromate Cr(VI) species were reduced by DEAE, and then the Al-alkoxy product coordinated with the Cr(II) sites. Site-**B** had relatively low activity and high stability. Based on the microstructure analysis, the relative amount of SCBs of polymers obtained from the DEAE systems was even more than that from TEA catalyst systems. This can be explained as follows. Firstly, the reduction ability of DEAE was weaker than that of TEA. More Cr(VI) species

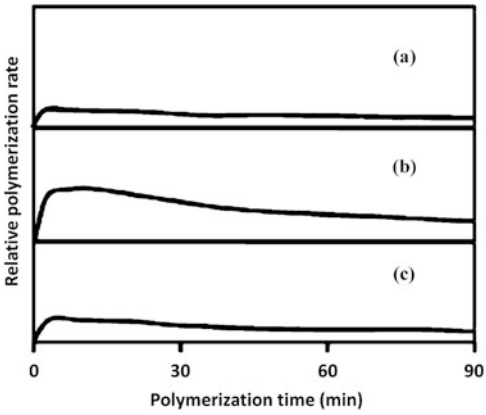

Fig. 14 Kinetic curves of ethylene polymerization using Phillips catalyst PC600 activated by DEAE during slurry polymerization with Al/Cr molar ratio: (*a*) 7.5; (*b*) 15.0; (*c*) 22.5. Polymerization conditions: catalyst amount, 100 mg; polymerization temperature, 60°C; ethylene pressure, 0.13 MPa; solvent heptane, 20 mL; cocatalyst DEAE in heptane, 1 M

could be reduced by ethylene and coordinated with formaldehyde to form Site-**C1**. Secondly, DEAE needed a longer time for the conversion of metathesis active sites into polymerization active sites. More α-olefin will be formed from metathesis active sites to insert into the polymer chains. Thirdly, different Al-alkoxyl byproducts of the reaction between TEA/DEAE and chromate species, subsequently coordinated with the chromium active site, will also affect the incorporation rate of α-olefin comonomers.

Ethylene homopolymerization or 1-hexene/ethylene copolymerization, using Phillips catalyst PC600/CO calcined at 600°C treated with activation by CO at 350°C followed by TEA cocatalyst activation during the slurry polymerization process, was carried out with Al/Cr molar ratios of 7.5, 15.0, and 22.5 [80, 110]. For this catalyst system, it was expected that N_2 could not remove all adsorbed CO from the Cr(II) due to the similar electron characteristics of CO and formaldehyde and due to the high coordinative unsaturation of the Cr(II) center. According to XPS results (Fig. 4), it was found that almost one-third of the chromate(VI) species still existed after the normal CO pre-reduction procedure. Under these complex conditions, a hybrid-type polymerization kinetics (corresponding to type a in Fig. 10a) was still found for both homo- and copolymerization, as shown in Fig. 15. One of the types with instant activation and fast decay originated from the active site (Site-**A** in Scheme 8), formed through desorption of formaldehyde (Site-**C1**) or CO (Site-**C2**) from the Cr(II) site by TEA or ethylene monomer. The other type with slow activation and slow decay was from the Site-**B**, formed from the reduction of residual chromate(VI) species by TEA. The formed Al-alkoxyl can strongly coordinate with the Cr(II) site and thus protect the Cr(II) center from further over-reduction by TEA. The first peaks of the copolymerization kinetic curves from Site-**A** became broader in comparison with those of homopolymerization, suggesting either that the decay of Site-**A** became slower in the presence of comonomer or that the transformation of metathesis

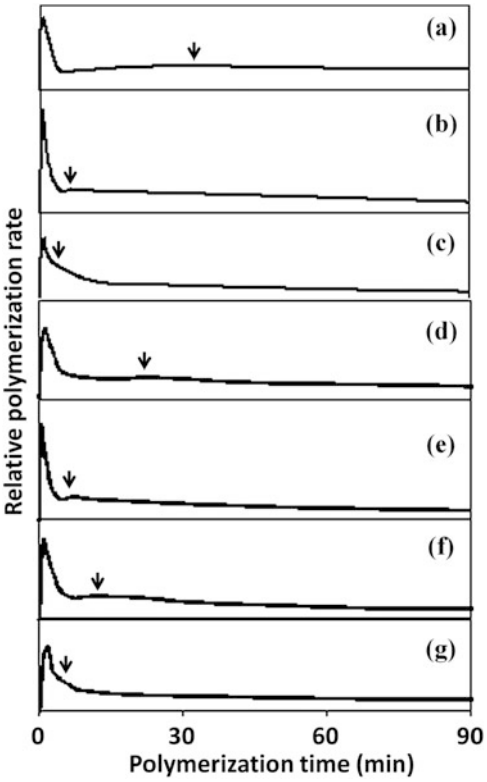

Fig. 15 (*a–c*) Kinetic curves of ethylene homopolymerization using Phillips catalyst PC600/CO activated by TEA during slurry polymerization with Al/Cr mole ratio of (*a*) 7.5, (*b*) 15.0,and (**c**) 22.5. (*d–g*) Kinetic curves of ethylene/1-hexene copolymerization under (*d*) Al/Cr ratio of 7.5 with 10 vol% of 1-hexene, (*e*) Al/Cr ratio of 15.0 with 5 vol% of 1-hexene, (*f*) Al/Cr ratio of 15.0 with 10 vol% of 1-hexene, and (*g*) Al/Cr ratio of 22.5 with 10 vol% of 1-hexene. The *arrow* indicates the maximum activity on Site-**B**. Polymerization conditions: catalyst amount, 100 mg; polymerization temperature, 60°C; ethylene pressure, 0.13 MPa; solvent, heptane, 20 mL; cocatalyst TEA in heptane, 1 M

Site-**C1** and/or Site-**C2** into polymerization Site-**A** was slowed down due to the stronger reduction of 1-hexene than of ethylene. With increasing Al/Cr mole ratio from 7.5 to 22.5, the time to reach maximum activity from Site-**B** in copolymerization became shortened from 25 to 5 min (Fig. 15, arrows). All the obtained homo- and copolymers were characterized by ^{13}C NMR. The peaks assigned to the branching carbons of methyl and butyl branches in the copolymers and methyl branches in the homopolymers were found, which could rationalize well the existence of Site-**C1** and/or Site-**C2** for ethylene metathesis to form propylene as a comonomer for the in-situ copolymerization. Similar polymerization kinetics were also observed in copolymerization of ethylene with cyclopentene using Phillips catalyst PC600 calcined at 600°C followed by TEA cocatalyst activation during the slurry polymerization process [95]. The only difference was that cyclopentene played the role of 1-hexene during the active site formation and transformation process. Besides the 1,2- and 1,3-insertion of cyclopentene into the polyethylene main chain (Fig. 7), the in-situ copolymerization of propylene, 1-butene, and 1-pentene in the same system was also confirmed by ^{13}C NMR, indicating the existence of ethylene metathesis active site (Site-**C1** and/or Site-**C2**) during the formation of the polymerization sites [95].

In summary, investigation of the polymerization kinetics over Phillips-type catalysts could provide deep mechanistic understanding and valuable information to guide the design and optimization of the polymerization processes. It has been demonstrated that the polymerization kinetics could be drastically affected by the types of cocatalysts, the timing of introduction of the cocatalyst, and the types of polymerization. From the industrial point of view, the direct activation of Phillips-type catalysts by AlR_3-type cocatalysts during the polymerization process within the polymerization reactor should be avoided in ethylene slurry polymerization. As for gas phase ethylene polymerization, activation of Phillips-type catalysts by AlR_3 during catalyst preparation before polymerization should also be forbidden. We could expect that more efforts should be devoted to the investigation of gas phase polymerization kinetics, combination of experiments with kinetic modeling and microkinetic modeling based on first principle calculations in the near future.

4 Approaches Using Heterogeneous Model Catalysts

The surface complexity of the traditional Phillips Cr/silica catalyst derives from the following aspects: the coexistence of mono-, di-, and polychromate species, the inevitable formation of Cr_2O_3 microcrystals [8, 11], the formation of surface chromium species in lower oxidation states due to thermally induced reduction of surface chromate species at high temperature, the low fraction of active Cr species in the total Cr loading [4, 11], the ambiguous and complicated reactions for the formation of the first chromium–carbon bond between ethylene monomer and surface chromate species. These factors greatly contribute to the surface complexity of the industrial Phillips catalyst and thus hinder academic progress in basic understanding of the nature of active sites and polymerization mechanisms for this important commercial polyolefin catalyst. During the last decades, various heterogeneous models with more uniform and well-defined structure of surface chromium species have been designed to facilitate the fundamental investigations in this field. Typical reported heterogeneous models for Phillips catalysts are listed in Scheme 9. These models can be generally divided into two groups: surface hexavalent chromate species (models **1c**, **2c**, **6c**, **9c**, and **10c**) and surface chromium species with lower oxidation states (models **3c**, **4c**, **5c**, **7c**, and **8c**).

S-2 catalyst prepared by wet impregnation of BC into thermally pretreated silica gel could be considered as a commercial heterogeneous model (**1c**) for Phillips catalysts [26, 112]. The S-2 catalyst shows an increased activity after supporting on silica gel compared with BC and produces HDPEs with even broader molecular weight distribution than that produced by the Phillips catalyst. Model **2c** was firstly prepared by McDaniel [113] via mild grafting (at 200°C) of CrO_2Cl_2 onto thermally pretreated silica. The CrO_2Cl_2 grafted onto silica pretreated at 400°C showed similar surface chromate structure and polymerization activity to the Phillips catalyst. Recently, Scott and colleagues [54, 114] prepared similar catalysts via ambient anhydrous grafting of CrO_2Cl_2 onto silica pretreated at 200°C, 450°C and

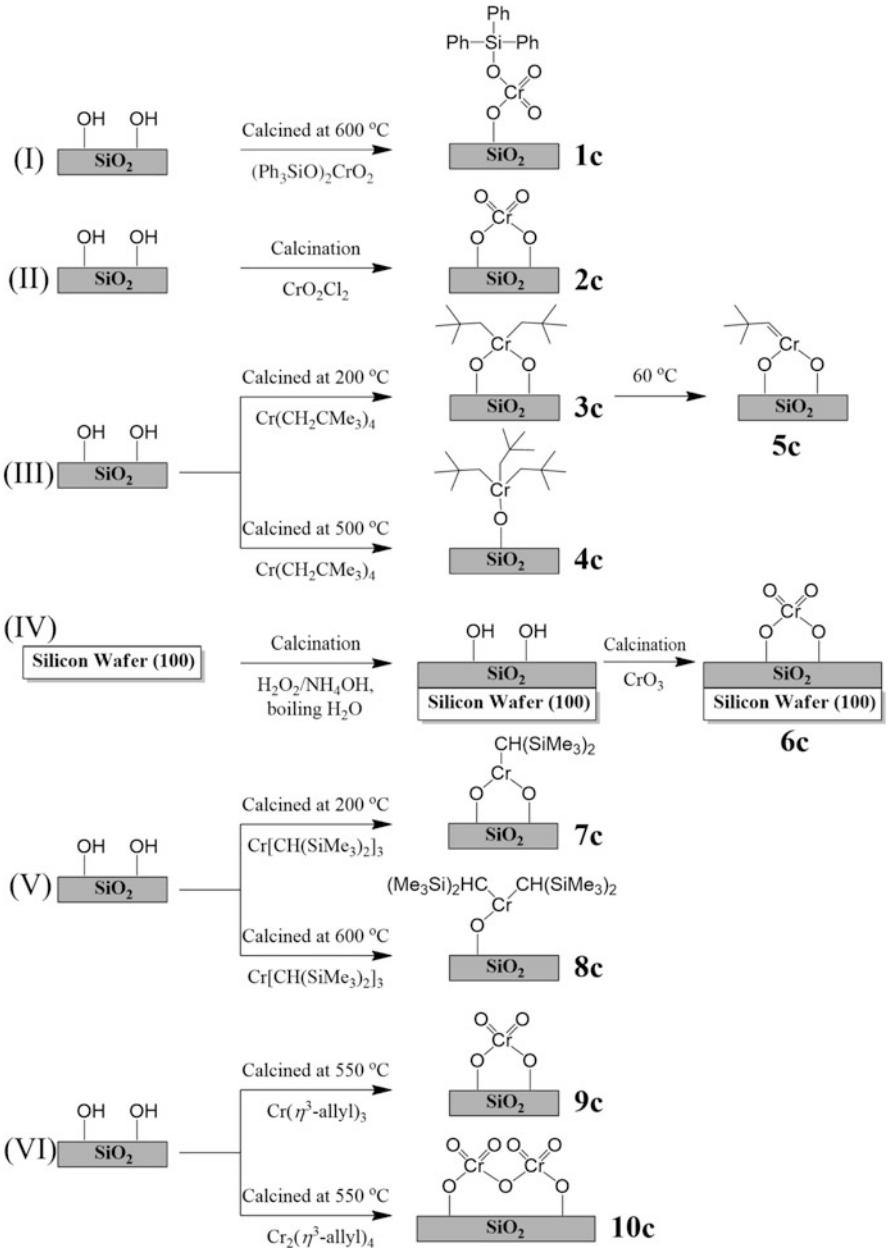

Scheme 9 Heterogeneous models reported in the literature for the Phillips Cr/silica catalyst

800°C. By combination of IR, XANES, and EXAFS, they explained that the higher polymerization activity over CrO_2Cl_2 grafted onto silica pretreated at 800°C was related to the more strained six-membered chromasiloxane rings. Thüne et al. [115]

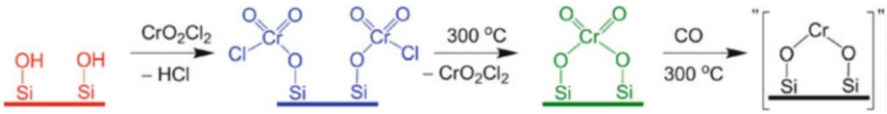

Scheme 10 Preparation procedure for the heterogeneous divalent model Phillips catalysts

reported a flat surface model catalyst by impregnating aqueous CrO_3 on a flat Si (100) substrate covered by an amorphous silica layer, shown as model **6c**. This flat catalyst covered with monochromate showed ethylene polymerization activity at 160°C, whereas the pre-reduced surface Cr(II) species failed to polymerize ethylene due to its extreme sensitivity to air and moisture [53]. Recently, Terano and colleagues [116] chose different starting materials [Cr(η^3-allyl)$_3$ and Cr_2(η^3-allyl)$_4$] to vary the surface structures of the catalysts (monochromate and dichromate, shown as models **9c** and **10c**, respectively). It was found that the surface dichromate model catalyst **10c** produced more methyl branching in its PE products. Models **3c**, **4c**, and **5c** were reported by Scott and coworkers [90–94, 117] via grafting of tetravalent Cr[$CH_2C(CH_3)_3]_4$ onto silica pretreated at 200°C (**3c**) or 500°C (**4c**). Upon mild heating at 60°C, a supported Cr-alkylidene complex **5c** was formed on silica pretreated at 200°C, which showed instant ethylene polymerization activity without using any cocatalyst. Monoi and coworkers [118, 119] reported a trivalent model catalyst by the supporting of Cr[$CH(SiMe_3)_2]_3$ on silica pretreated at 200 or 600°C. When the pretreating temperature was 200°C, Cr species were supported on silica through two Si–O–Cr bonds, shown as model **7c**, whereas for the case of 600°C, the grafting took place via only one Si–O–Cr bond to silica to form model **8c**. Compared to the Phillips catalyst, these catalysts showed high ethylene polymerization activity without using any cocatalyst and displayed very similar performance except for increased sensitivity of the hydrogen response. In addition, further reaction over **8c** with excess Cr[$CH(SiMe_3)_2]_3$ was likely to lead to the formation of new active sites for ethylene trimerization [119]. Although the above-mentioned heterogeneous model catalysts displayed representative polymerization activity at certain temperatures with or without the cocatalyst and offered the opportunity for further understanding of Phillips catalysts, no direct evidence on the real active sites and polymerization mechanisms has yet been achieved.

Very recently, we performed further studies over extremely air-sensitive divalent model Phillips catalysts via CO reduction (at 300°C) of model **2c** [55]. Two heterogeneous divalent model Phillips catalysts were prepared via ambient anhydrous grafting of CrO_2Cl_2 onto silica pretreated at 500 and 800°C, followed by heating and CO reduction at 300°C, as shown in Scheme 10. As shown in Fig. 16, the obtained Cr(II)/S948-800 [Cr(II) supported on silica pretreated at 800°C] catalyst showed higher ethylene polymerization activity than that of Cr(II)/S948-500 [Cr(II) supported on silica pretreated at 500°C] catalyst without any induction period at RT. Further characterizations were performed to explore the origin of the different activities of the two catalysts. From the CO stretching region in the IR spectra, two obvious peaks (ca. 2,190 and 2,180 cm^{-1}) were shown for Cr(II)/S948-500 catalyst,

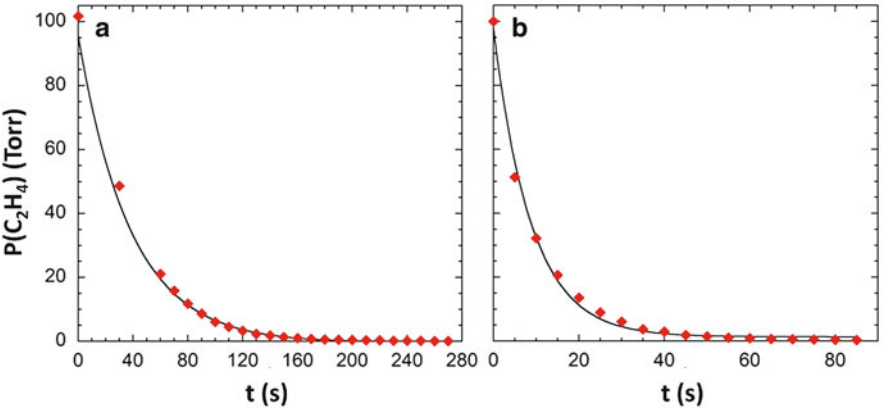

Fig. 16 Ethylene uptake profiles (*symbols*) in a batch reactor at 23°C, over (**a**) Cr(II) grafted on S948-500 (102.7 mg, 1.71 wt% Cr, 34.5 μmol Cr); and (**b**) Cr(II) grafted on S948-800 (314.3 mg, 0.62 wt% Cr, 38.1 μmol Cr). The *lines* are three-parameter fits to the first-order integrated kinetic rate equation

and three for Cr(II)/S948-800 (ca. 2,190, 2,187, and 2,180 cm^{-1}), shown in Fig. 17. After deconvolution of the IR spectrum of Cr(II)/S948-500 catalyst, a third peak at 2,187 cm^{-1} was also observed. Furthermore, the results of the IR deconvolution showed that the area ratio of the peaks at ca. 2,190 and 2,180 cm^{-1} was constant at 2.0 for both catalysts, which was not related to the variations in the pretreating temperature for silica or the evacuation time of adsorbed CO. We assumed that these two peaks (ca. 2,190 and 2,180 cm^{-1}) can be attributed to the symmetric and asymmetric stretching of the dicarbonyl species $(\equiv SiO)_2Cr(CO)_2$ while the other peak at ca. 2,187 cm^{-1} was assigned to the monocarbonyl species $(\equiv SiO)_2Cr(CO)$.

The speculated presence of dicarbonyl and monocarbonyl species on the silica surface was further confirmed by ONIOM calculations. The model cut from the (100) face of β-cristobalite was applied to mimic the local structures of the silica surface. Two different molecular models with replaceable and irreplaceable siloxane ligand were built for the dicarbonyl and monocarbonyl species, respectively, as shown in Fig. 18. The calculated relative shifting for the symmetric and asymmetric CO stretching was 11 cm^{-1}, very close to the experimental value of 12 cm^{-1}, which revealed information on the local coordination environment of the Cr(II) site (see structures **5e** and **6e** in Scheme 11).

For more direct evidence, an EXAFS analysis was performed for the model catalysts. Figure 19 shows that the fitting in *k* and *R* space was quite good, and the detailed structural parameters of the model for this fitting are presented in Scheme 11. The main difference between the catalysts was that the coordination numbers for the first shell of Cr(II) were four for Cr(II)/S948-500 and three for Cr (II)/S948-800, varying in the coordination number of siloxane ligand from the silica surface. A smaller average number of coordinated siloxane ligands, resulting in a great difference in the bonding of the two silanolate ligands, might be the key to the

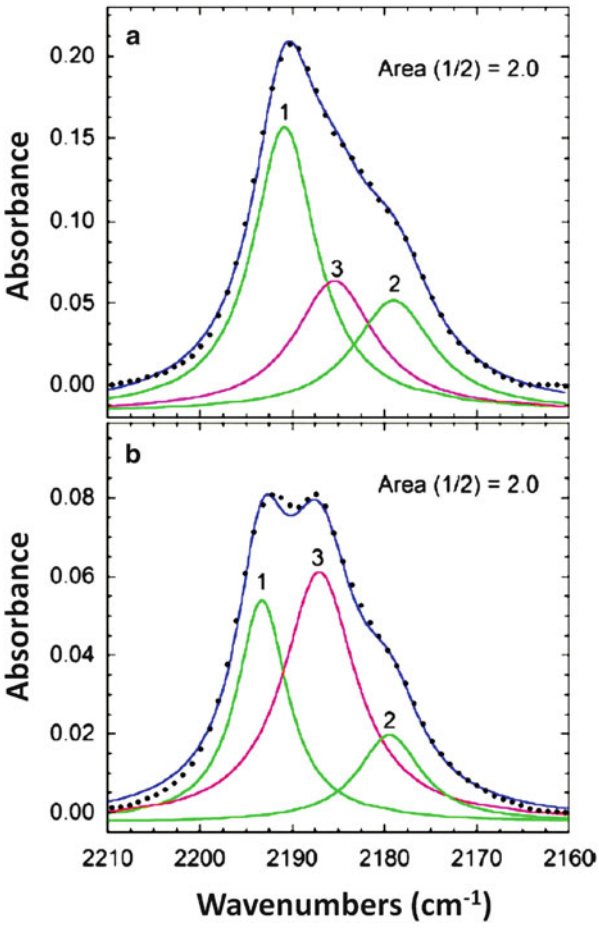

Fig. 17 Deconvolution of experimental IR spectra in the CO stretching region (*symbols*) into three Lorentzian components (*lines 1*, *2*, and *3*) for (**a**) Cr(II)/S948-500 and (**b**) Cr(II)/S948-800. The spectra predicted by the deconvoluted components is also shown

much higher ethylene polymerization activity of the model catalyst Cr(II)/S948-800 since its silica bears an irreplaceable siloxane ligand to keep the coordination number of Cr(II) at three when contacting with ethylene (as shown in Scheme 12). For model catalyst Cr(II)/S948-500, the more abundant species was the Cr(II) with coordination number of four, binding to two replaceable siloxane ligands.

In summary, it was made clear that the coordination of the divalent active site precursor with the siloxane ligands present on the silica support surface in terms of the catalyst calcination temperature was crucial for determination of the precise microstructures and coordination environment of the active Cr species and thus the performance of the Phillips catalyst. Multiple spectroscopic methods including FTIR and XAS (EXAFS/XANS) combined with molecular modeling and polymerization experiments probing into the heterogeneous Phillips model catalysts proved to be very effective. Spectroscopic investigation of the contact of ethylene with these two divalent heterogeneous model catalysts at low temperature is still in

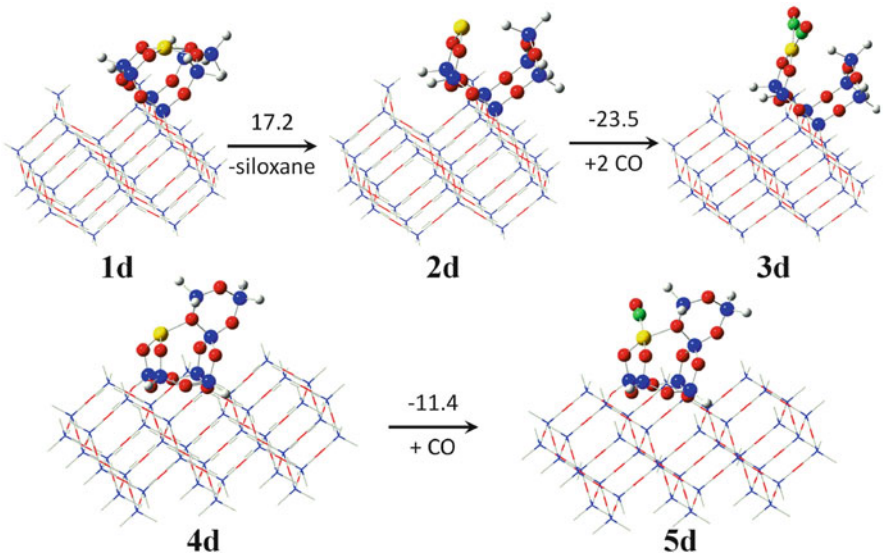

Fig. 18 Computational models for grafted "$(\equiv SiO)_2Cr$" sites, differing in total Cr coordination number, are shown without (**1d** and **4d**) and with (**3d** and **5d**) coordinated CO. The *numbers over* the *arrows* denote binding energies in kcal mol^{-1}, relative to the CO-free Cr(II) clusters (**2d** and **4d**) and free ligands (CO or siloxane). Color key: Cr (*yellow*), O (*red*), Si (*blue*), C (*green*), H (*white*). Inner layer: *ball-stick*; outer layer: *wireframe*

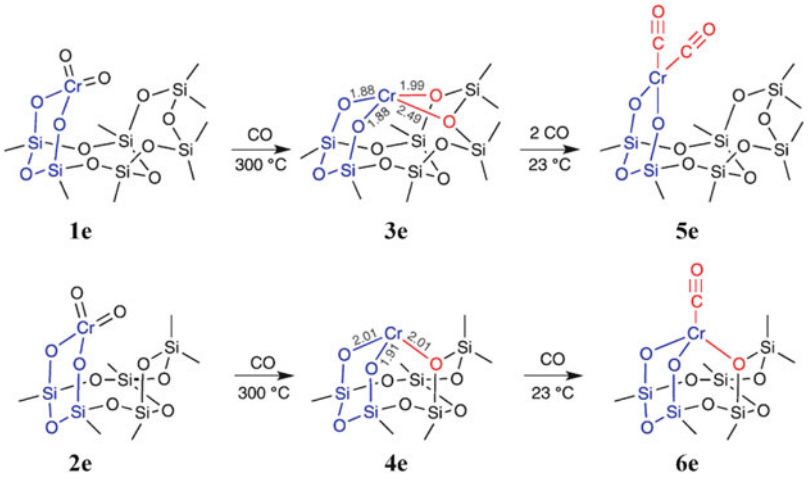

Scheme 11 Proposed structures for chromate sites (**1e**, **2e**) embedded in six-membered chromasiloxane rings (*blue*) on highly dehydroxylated amorphous silica; the corresponding Cr (II) sites, Cr(II)/S948-500 (**3e**) and Cr(II)/S948-800 (**4e**) formed upon reduction, (showing the distances obtained by EXAFS curve fitting); and their corresponding carbonyl complexes (**5e**, **6e**). Additional siloxane and carbonyl ligands are shown in *red*. Bond length is in Å

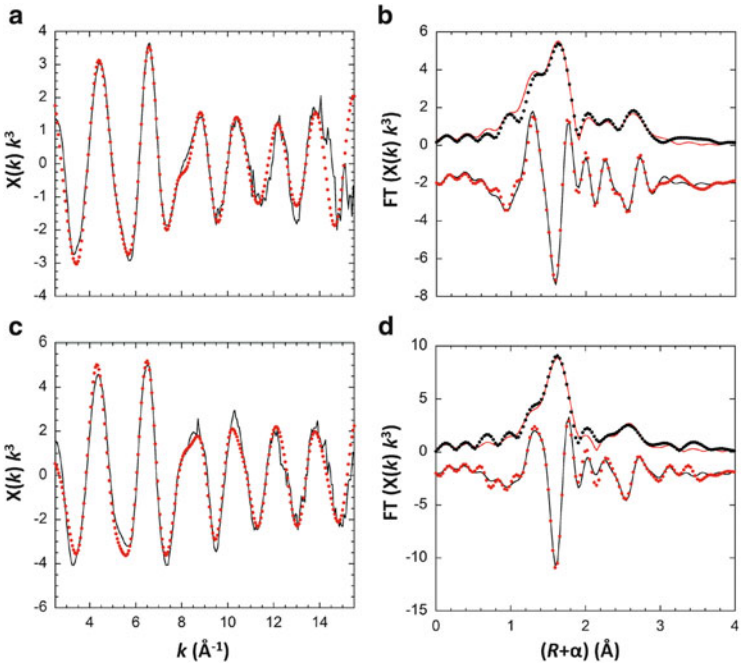

Fig. 19 Single-scattering refinements of the EXAFS for Cr(II) supported on S948-500 (**a**, **b**) and S948-800 (**c**, **d**). Frames (**a**) and (**c**) show the data (*dotted lines*) and curve fits (*solid lines*) in k^3-weighted *k*-space. Frames (**b**) and (**d**) show the FT magnitudes (*upper dotted lines*), imaginary components (*lower dotted lines*) and curve fits (*solid lines*) in *R* space

progress by our group via in-situ techniques in order to figure out the formation of the first Cr–C bond and the initiation mechanism of ethylene polymerization. A step forward in the interpretation of the nature of the active sites and polymerization mechanisms (especially the initiation mechanism of the first polyethylene chain) requires the combination of heterogeneous model catalyst systems with more advanced and multiple characterization techniques, especially in-situ/operando techniques as well as molecular modeling. The rational design and utilization of new heterogeneous model Phillips catalysts is expected to allow further progress in better understanding of the real and complex catalyst system.

5 Approaches Using Homogeneous Model Catalysts

In the previous section, investigations on heterogeneous model catalysts with more uniform and well-defined structure of surface chromium species supported on silica gel had been demonstrated as a powerful strategy for the basic study of Phillips catalysts. However, the complexity is still derived from the heterogeneity of the

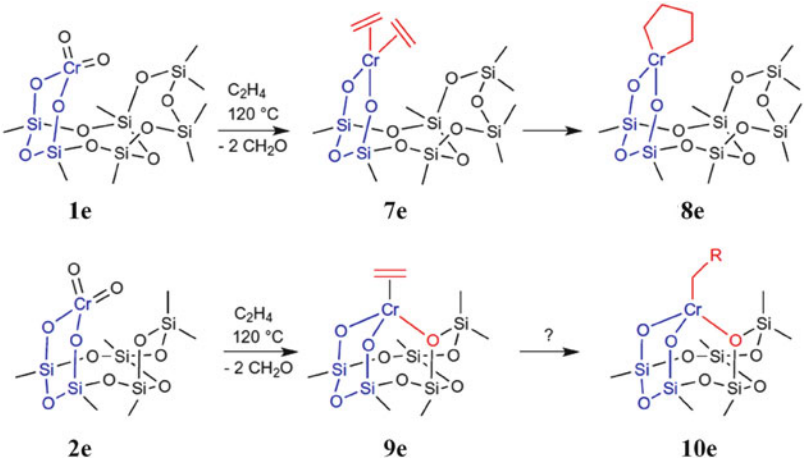

Scheme 12 Two different possible routes for ethylene reduction/activation of silica-supported chromates (**1e**, **2e**) embedded in six-membered chromasiloxane rings (*blue*). In the absence of coordinated siloxane ligands, the bis(ethylene) complex **7e** is transformed readily to the polymerization-inactive chromacyclopentane **8e** [120], while a non-displaceable siloxane ligand in the mono(ethylene) complex **9e** prevents metallacycle formation and therefore opens an alternate, as-yet unknown, path to a monoalkylchromium(III) site capable of polymerizing ethylene. Additional siloxane, ethylene monomer and subsequent formed bonds are shown in red

amorphous silica support as well as the fact that more than 99% of the active sites exist within the micro- and mesopores in the inner surface of the silica support. During the last few decades, various homogeneous model catalysts have been developed in order to simplify such complexity of the traditional Phillips catalyst originating from the silica support [121]. Some typical homogeneous model catalysts are listed in Scheme 13, including the $Cr(II)OH^+$ and $Cr(III)O^+$ cations (models **1f** and **2f**) [122, 123], bistriphenylsilyl chromate (BC) (model **3f**) [111], a POSS-supported Cr catalyst (model **4f**) [124, 125], siloxane chromate ester (model **5f**) [126], spirocyclic chromium(II) siloxane (model **6f**) [127], 1,3,5-triazacyclohexane complexes of chromium(III) (model **7f**) [128], cationic alkyl complexes of chromium (III) (model **8f**) [121, 129–131], and $[(Ph_3SiO)Cr \cdot (THF)]_2(\mu\text{-}OSiPh_3)_2$ (model **9f**) [40, 41]. Some recently reported novel homogeneous Cr-based complexes based on low-valence chromium species for ethylene polymerization or oligomerization, such as imido, β-diketiminates and reduced Schiff base [N, O] chelate derivatives, which are far from the character of the Phillips catalyst, will not be considered here [132–137].

Hanmura et al. [122, 123] found two simple chromium cations $Cr(II)OH^+$ and $Cr(III)O^+$ (models **1f** and **2f**) that could dimerize ethylene into 1-butene without using any organometallic cocatalyst, and proposed that they could be treated as simple homogenous cluster models for the Phillips catalyst. Baker and Carrick [111] reported ethylene polymerization over BC (model **3f**), a hexavalent chromate compound bearing two triphenylsilyl ligands, at elevated temperatures ($\geq$130°C)

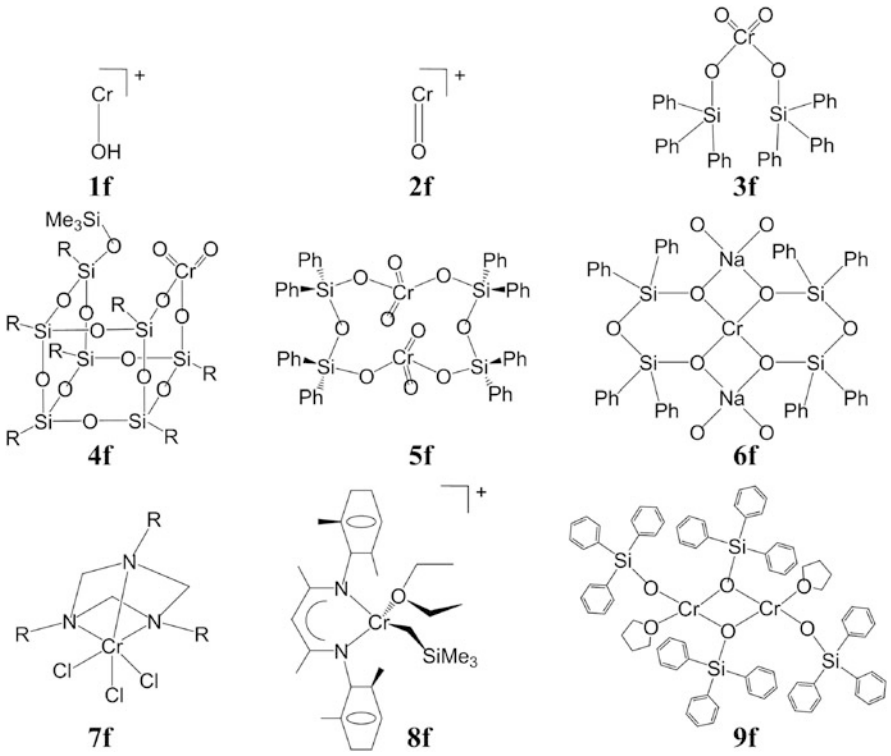

Scheme 13 Homogeneous models reported in the literature for the Phillips Cr/silica catalyst

and ethylene pressures (≥350 atm) in cyclohexane solution without adding any cocatalyst. In our opinion, BC could be taken as a homogeneous model for the Phillips catalyst and should be more extensively studied. A POSS-supported Cr complex $[(c\text{-}C_6H_{11})_7Si_7O_{11}(OSiMe_3)]CrO_2$ (model **4f**) developed by Feher and Blanski seemed to be a more realistic homogeneous model of the Phillips catalyst [124, 125]. Abbenhuis reported a homogeneous 12-membered inorganic heterocycle Cr(VI) model catalyst (model **5f**) that was active for ethylene polymerization [126]. Sullivan and coworkers reported a homogeneous spirocyclic Cr(II) siloxane model catalyst (model **6f**) for ethylene polymerization [127]. This catalyst showed no activity without Al-alkyl cocatalyst and poor activity in the presence of $AlMe_3$ cocatalyst, which was rationalized by the authors as being due to the partial deactivation of this homogeneous divalent model catalyst because of its ultrahigh sensitivity to air and moisture. The homogeneous triazacyclohexane Cr(III) complex (model **7f**) reported by Köhn et al. showed a high ethylene polymerization activity and resembled the Phillips catalyst in many important properties, such as the high dependence of MW on the polymerization temperature and the presence of methyl and vinyl end groups in each PE chain. However, a considerable amount of MAO was needed to activate the catalyst, presenting single-site catalyst characters

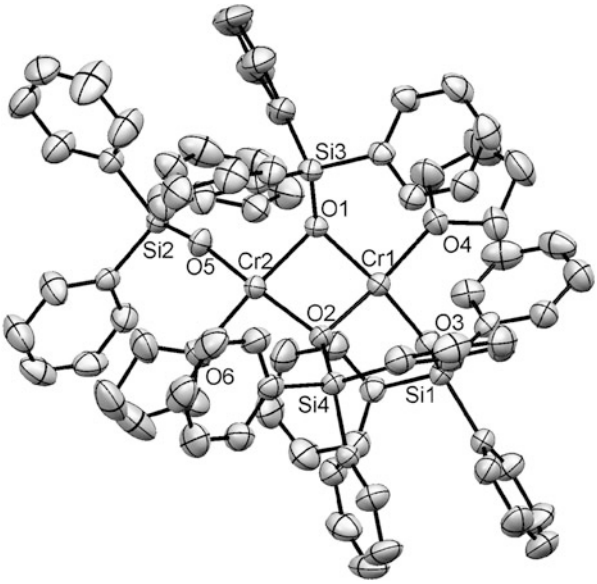

Fig. 20 Crystal structure of $[(Ph_3SiO)Cr \cdot (THF)]_2(\mu\text{-}OSiPh_3)_2$ (**9f**) with ellipsoids at the 50% probability level and hydrogen atoms omitted for clarity. Selected bond distances (Å) and angles (°): Cr(1)–O(3), 1.928(2); Cr(1)–O(2), 2.014(2); Cr(1)–O(1), 2.023(2); Cr(1)–O(4), 2.066(2); Cr(1)–Cr-(2), 2.880(1); O(3)–Cr(1)-O(2), 97.70(8); O(3)–Cr(1)–O(1), 167.00(8); O(2)–Cr(1)–O(1), 81.03(8); O(3)–Cr(1)–O(4), 90.51(8); O(2)–Cr(1)–O(4), 169.47(8); O(1)–Cr(1)–O(4), 92.43(8)

with a MWD of 2–4 for its PE products [128]. Theopold and coworkers [121, 129–131] reported a series of cationic alkyl Cr(III) catalysts for ethylene polymerization and claimed that these catalysts bearing β-diiminates ligand could mimic the hard coordination environment of the silica surface and thus could be taken as models of the Phillips catalyst (model **8f** shows one example). However, these catalysts showed ethylene living polymerization behavior, which was far from the character of the Phillips catalyst. It is still a great challenge to find ideal homogeneous model catalyst systems to mimic the polymerization behaviors of the industrial Phillips catalyst.

Recently, a novel homogeneous triphenylsiloxy complex of chromium(II) model catalyst $[(Ph_3SiO)Cr \cdot (THF)]_2(\mu\text{-}OSiPh_3)_2$ (model **9f**) was successfully synthesized and structurally characterized. Its ethylene polymerization performance was systematically investigated in a comparison with that of BC (model **3f**) [40, 41]. Model **9f** catalyst was prepared by a simple reaction of $CrCl_2$ with TPS and NaH (1:2:2) in THF. Figure 20 shows its crystal structure as a dinuclear Cr(II) complex bearing two bridging siloxy ligands in a tetrahedrally distorted square planar coordination geometry. Another example of such dinuclear Cr(II) complex bearing two bridging siloxo ligands in a similar tetrahedrally distorted square planar coordination geometry is $\{Cr[^{Me_3Ph}NSi(Me_2)N'Si(Me_2)O](THF)\}_2$ [138], which was not considered as a catalyst for ethylene polymerization. Model **9f** was found to be inactive for ethylene polymerization in the absence of Al-alkyl cocatalysts under 20 atm. and RT, even after increasing the temperature to 100°C for 16 h, which might be due to the existence of two strongly coordinated THF molecules within model **9f**. Therefore, an Al-alkyl cocatalyst such as MAO or TiBA was used for the ethylene slurry polymerization over the two model catalysts (**3f** and **9f**).

Table 2 Results of ethylene polymerization/oligomerization runs using BC (**3f**) and [$(Ph_3SiO)Cr \cdot (THF)]_2$ (μ-$OSiPh_3)_2$ (**9f**) with Al-alkyl cocatalysts[a]

Entry[b]	Cocatalyst	Al/Cr	PE (g)	M_w (g mol^{-1})	PDI	T_m (°C)	Activity[c]	Oligomer[d] (g)	Vinyl[e] (mol%)
1	MAO	100	1.20	191,000	2.6	134.7	152	0	–
2[f]	MAO	200	0.81	240,000; 5,400	2.1; 1.1	131.7	103	0	–
3[f]	MAO	500	0.64	254,000; 3,000	2.1; 1.6	129.8	386	2.4	90.3
4[f]	MAO	1,000	0.43	295,000; 1,900	2.8; 1.2	129.2	690	5.0	81.6
5[f]	MAO	1,500	0.55	313,000; 1,500	2.8; 1.4	127.4	413	2.7	84.6
6	TiBA	4	1.58	69,000	3.0	132.8	201	0	–
7	TiBA	10	0.71	158,000	2.4	132.9	90	0	–
8	TiBA	500	Traces[g]	–	–	–	–	–	–
9	MAO	50	1.67	185,000	5.2	134.5	226	0	–
10	MAO	100	1.44	223,000	4.1	122.1	195	0	–
11	MAO	200	0.43	141,000	2.9	120.4	709	4.8	92.6
12	MAO	500	0.31	64,000	2.2	N/A	743	5.2	84.2
13	MAO	1,000	0.34	49,000	2.3	N/A	827	5.8	89.1
14	TiBA	4	0.21	196,000	5.2	135.1	28	0	–
15	TiBA	10	0.16	136,000	4.6	134.4	22	0	–
16	TiBA	500	Traces[g]	–	–	–	–	0	–

[a]Standard conditions: $T = 22°C$, $V = 10$ mL, $P = 20$ atm., catalyst = 10 mg, time = 30 min
[b]Entries 1–8 for BC catalyst, entries 9–16 for $[(Ph_3SiO)Cr \cdot (THF)]_2$ (μ-$OSiPh_3)_2$ catalyst
[c]Activity in g $(mmol_{Cr})^{-1}$ h^{-1} by adding polymerization activity to oligomerization activity
[d]By integration of the NMR olefinic resonances with respect to the Me of the toluene solvent
[e]By integration of the NMR olefinic resonances
[f]Bimodal distribution from GPC analyses
[g]Less than 0.05 g

The ethylene polymerization results are summarized in Tables 2 and 3. Solid PE was obtained by using model **9f** with MAO at low Al/Cr molar ratios (Al/Cr $\leq$ 100) (Table 2, entries 9, 10). With a further increase in Al/Cr molar ratios (Al/Cr $\geq$ 200) (Tables 2 and 3, entries 11–13), liquid oligomers were surprisingly obtained together with a small amount of PE. ^{1}H NMR results revealed liquid oligomers with high contents of terminal vinyl groups (>84%), mostly linear α-olefins, thereby the predominant chain transfer mechanism could be β-H elimination in this model catalyst system. It is shown in Table 2 that the activities of entries 11–13 (average 760 g $mmol_{Cr}^{-1}$ h^{-1}) were much higher than the activities of entries 9 and 10 (average 210.5 g $mmol_{Cr}^{-1}$ h^{-1}). It was very interesting to find that a transformation of ethylene polymerization into ethylene nonselective oligomerization occurred over model **9f** catalyst using MAO as cocatalyst when the Al/Cr ratio was increased from 50 to 1,000. A similar transformation phenomenon was also discovered over BC (model **3f**) combined with MAO as cocatalyst (see entries 1–5 in Tables 2 and 3). The only difference was that the critical point of Al/Cr molar

Table 3 Distributions of ethylene oligomerization products over BC (**3f**) and $[(Ph_3SiO)Cr \cdot (THF)]_2$ (μ-$OSiPh_3)_2$ (**9f**) with Al-alkyl cocatalysts[a]

				Oligomer distribution[d] (%)						
Entry[b]	Cocatalyst	Al/Cr	Oligomer[c] (g)	C_6	C_8	C_{10}	C_{12}	C_{14}	C_{16}	Vinyl[e] (mol%)
3[f]	MAO	500	2.4	12.5	25.7	26.8	18.3	9.5	4.3	90.3
4[f]	MAO	1,000	5.0	9.5	19.2	18.4	25.3	14.6	7.3	81.6
5[f]	MAO	1,500	2.7	10.5	23.5	11.4	26.2	15.1	8.0	84.6
11	MAO	200	4.8	13.5	16.1	21.8	21.5	14.9	7.2	92.6
12	MAO	500	5.2	10.1	35.6	11.5	18.9	11.1	6.2	84.2
13	MAO	1,000	5.8	12.3	31.6	16.1	11.0	9.1	9.0	89.1

[a]Standard conditions: $T = 22°C$, $V = 10$ mL, $P = 20$ atm., catalyst = 10 mg, time = 30 min
[b]Entries 1–8 for BC catalyst, entries 9–16 for $[(Ph_3SiO)Cr \cdot (THF)]_2$ (μ-$OSiPh_3)_2$ catalyst
[c]By integration of the NMR olefinic resonances with respect to the Me of the toluene solvent
[d]By GC-MS, values of C_4 are not given due to volatility, remainder is C_4 and C_{18+}
[e]By integration of the NMR olefinic resonances
[f]Bimodal distribution from GPC analyses

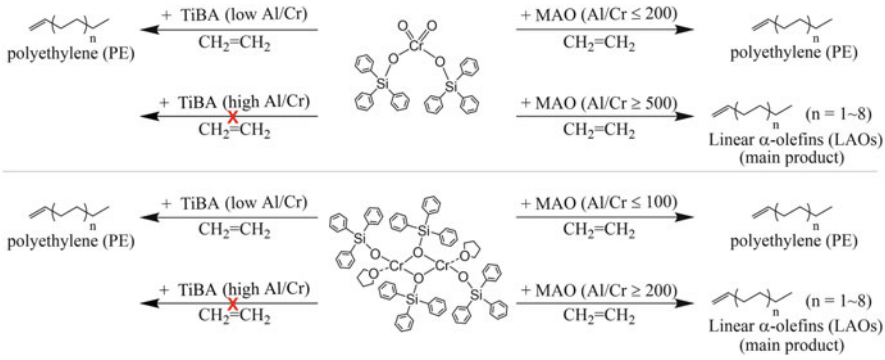

Scheme 14 Transformation of ethylene polymerization to ethylene nonselective oligomerization over BC (**3f**, *upper*) and $[(Ph_3SiO)Cr \cdot (THF)]_2$($\mu$-$OSiPh_3)_2$ (**9f**, *lower*) complexes

ratio for the transformation of model **3f** was much higher than that of model **9f**, which can be rationalized by assuming that reduction of the hexavalent chromate model **3f** into a lower valence state should consume more MAO. It was noteworthy that only a small amount of PE but no liquid oligomer was produced in the case of TiBA as cocatalyst for both model catalysts. Larger amounts of TiBA only completely deactivated the two model catalysts, probably due to its much stronger reducing power than MAO.

The transformation from ethylene polymerization to ethylene nonselective oligomerization over the two model catalysts (**3f** and **9f**) in the presence of Al-alkyl cocatalyst MAO with the increase in Al/Cr molar ratio is shown in Scheme 14. Such interesting transformation phenomenon could not be found using the same catalysts combined with TiBA. Similar polymerization/oligomerization transformation behavior has also been reported recently on Cr-based ethylene trimerization

catalysts by changing the cocatalyst from $[(^{i}Bu)_2Al]_2O$ to MAO [139]. Comprehensive theoretical molecular modeling focusing on such interesting polymerization/oligomerization transformation mechanisms is still in progress.

In order to shed some light on the nature of active sites relating to the transformation between ethylene polymerization and nonselective oligomerization over the two model catalyst systems, several spectroscopic methods including NMR, ESR, and MALDI-TOF MS were applied. For the case of the model **3f**/MAO system, a very characteristic isotropic, hyperfine structure multiplet assigned to a cationic $[Cr(\eta^6\text{-arene})_2]^+$ sandwich complex was observed from the ESR spectrum, indicating that part of the complex was reduced to a $Cr(I)^+$ species, which was coordinated by two molecules of toluene (or arenes from the dissociated Ph_3SiO groups) to yield the cationic $(\eta^6\text{-arene})_2$ complex. Similar ESR results for the same cationic $[Cr(\eta^6\text{-arene})_2]^+$ sandwich species were also obtained in the model **9f**/MAO catalyst system at different Al/Cr molar ratios.

In the ^{29}Si NMR spectrum of the model **9f** catalyst activated by MAO, aluminum species containing the Ph_3SiO group were observed. Thus, the Cr–C bond was likely to be produced by transferring the methyl group from MAO to the chromium center during the activation. Correspondingly, the Ph_3SiO group was transferred from the Cr center to the aluminum of MAO to produce the aluminum species containing a Ph_3SiO group, accompanied by the formation of a cationic $[Cr(\eta^6\text{-arene})_2]^+$ sandwich complex.

The alkyl radical is known to be an important intermediate during the activation reaction between transition metal-based polyolefin catalysts and metal alkyl cocatalysts. However, it is difficult to characterize by spectroscopic methods due to its high reactivity and short lifetime. An investigation to confirm the generation of alkyl radicals during the activation of model **3f** with TiBA by fullerene radical trapping combined with ESR as well as MALDI-TOF MS was performed. A new ESR signal (Fig. 21b) of the multiple addition paramagnetic adducts of butyl radicals to fullerene was successfully observed compared with the ESR signal without fullerene, and the addition of butyl radicals to fullerene was confirmed by MALDI-TOF MS analysis (Fig. 21a). The butyl radical intermediate could be considered to be generated during the reduction and alkylation of BC with TiBA. Similar ethyl and methyl radical formation has been previously reported during the activation reaction in other olefin polymerization catalyst systems [140, 141].

In order to understand the identity (active or inactive) of the cationic $[Cr(\eta^6\text{-arene})_2]^+$ species in model **3f**/TiBA catalyst system, a temperature-dependent ESR experiment (220–350 K) was performed to monitor ethylene polymerization (in the NMR tube). In Fig. 22, it can be seen that the multiplet ($g = 1.995$) of the cationic $[Cr(\eta^6\text{-arene})_2]^+$ species remained unchanged, indicating that this kind of species was not active at these reaction conditions. No other ESR signals were observed during the temperature raising process (220–350 K), although the solid PE had been observed at 290 K. This result indicated that the active species for ethylene polymerization cannot be observed by ESR spectroscopy. Therefore, the valence state of the active species in model **3f**/TiBA catalyst system might be Cr(II), which was always ESR silent. However, Cr(III) cannot be excluded on the basis of the

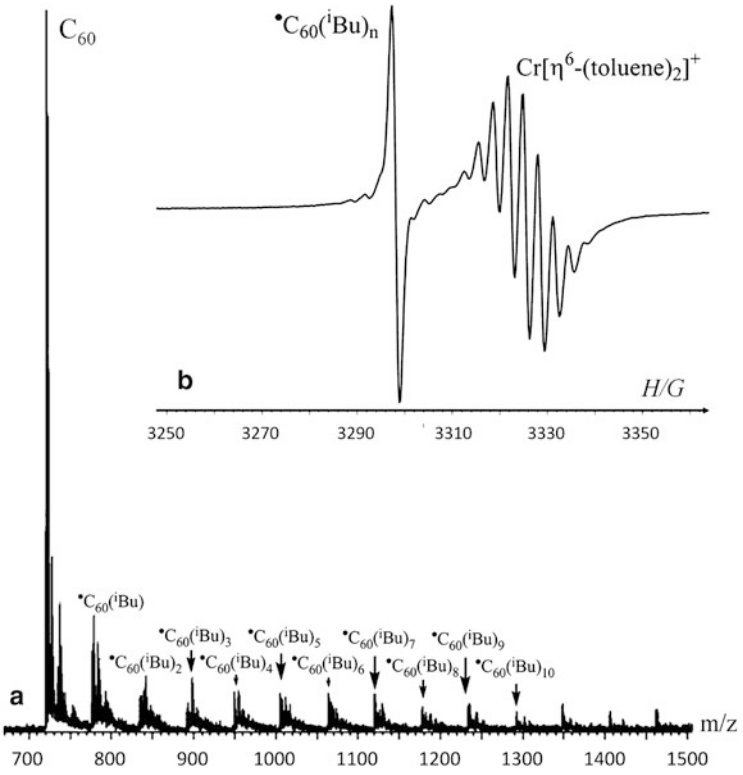

Fig. 21 ESR and MALDI-TOF monitoring of the mixture of BC (**3f**) with fullerene C60 activated by TiBA (Al/Cr = 4): (**a**) MALDI-TOF MS spectrum; (**b**) ESR spectrum at 290 K in toluene

limited experimental results, because it was generally observed by ESR spectroscopy at very low temperatures up to 77 K. Further mechanistic study through combined experimental and theoretical modeling is now still in progress in order to clarify the nature of the active sites and their transformation behavior.

In summary, two homogeneous model catalysts with triphenylsiloxy ligands of chromium(II) and chromium(VI) (models **3f** and **9f**) were systematically studied for ethylene polymerization in the presence of Al-alkyl cocatalyst. Similar transformation phenomenon from ethylene polymerization to nonselective oligomerization was discovered over both model catalysts using MAO as a cocatalyst depending on the Al/Cr molar ratios. A cationic $[Cr(I)(\eta^6\text{-arene})_2]^+$ sandwich complex was observed for both catalyst systems combined with MAO or TiBA and was excluded as being the active site for ethylene polymerization. Further mechanistic investigations on these model catalyst systems as well as their relevance to the Phillips catalyst are still in progress in order to elucidate the mechanisms of such interesting phenomena. The well-defined molecular structure of homogeneous catalysts provide good basis for their investigation with molecular modeling as well as other spectroscopic methods, especially in-situ or operando techniques. The

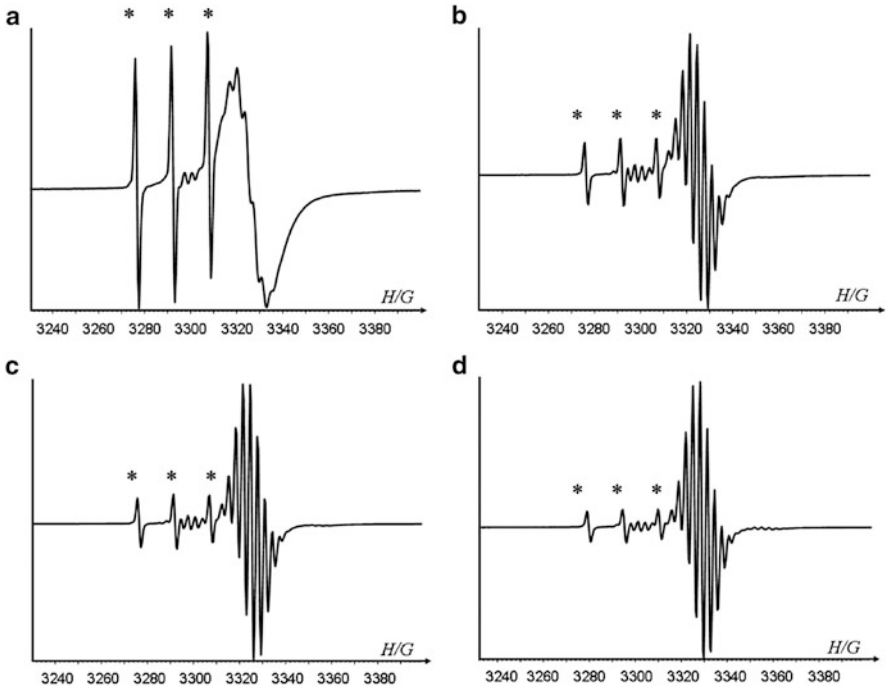

Fig. 22 Monitoring of ethylene polymerization over **3f**/TiBA (Al/Cr = 4) by in-situ ESR spectroscopy (from 220 to 350 K): (**a**) 220 K, (**b**) 270 K, (**c**) 290 K, and (**d**) 350 K. For determination of the *g* factor spectrum recorded with TEMPO ($g = 2.0058$), the three lines of TEMPO are marked with *asterisks*

development and utilization of novel and more realistic homogeneous Phillips catalysts are still great challenges and are expected for further progress in this important field in the near future.

6 Approaches Using Molecular Modeling

Although numerous experiments and spectroscopic characterizations have been conducted on the Phillips catalyst, the precise structure of the active site on the silica surface, reduction of the surface chromate species during the induction period, the formation of the first chromium–carbon bond, and the mechanism for ethylene polymerization still need to be further clarified [11]. In order to achieve more specific information, molecular modeling approaches could provide a useful complement to the experiments and enable us to study these obscure mechanistic problems directly at the atomic and molecular level. In the last decade, very precise mechanistic pictures of the Cr-based polymerization catalysts have been obtained using different theoretical methods, especially through a combination of the experimental findings with theoretical calculations.

6.1 Molecular Models

To understand the behavior of the heterogeneous catalyst, a molecular model must be first built to mimic the active sites anchored on the support. Regarding the Phillips catalyst, the hexavalent chromate species on a silica surface is believed to be reduced to lower valence states, usually Cr(II), resulting in a mononuclear or dinuclear Cr(II) site, which is bound to the silica surface through two oxygen linkages. During the last decade, various molecular models have been built for the active sites of the Phillips catalyst, as graphically shown in Fig. 23.

As early as 2004, we employed hexavalent chromic acid (**1g**) as a simple molecular model for simulating the coordination of ethylene on the pre-reduced monochromate site of the Phillips catalyst [142]. Soon after that, a more realistic silsesquioxane-supported cluster model **2g** was built for theoretical investigation in order to elucidate the effects of silica gel and its surface fluorination on the properties of the Phillips catalyst [143, 144]. Meanwhile, Hanmura et al. [122, 123] found that two simple chromium cations [$Cr(II)OH^+$ and $Cr(III)O^+$, as shown in **1f** and **2f**] could possibly dimerize ethylene into 1-butene without using any organometallic cocatalyst. Because the chromium centers in these two kinds of cations were directly bonded to an oxygen atom, and the Phillips catalyst was composed of chromium supported on silica gel through oxygen linkages, the authors claimed that **1f** and **2f** could be treated as homogenous cluster models for the Phillips catalyst.

A group of cluster models **3g**–**10g** created by Espelid and Børve in a series of systematic DFT investigations on the active sites of the Phillips catalyst are shown in Fig. 23 [120, 145–149]. Clusters **3g**–**6g** were four kinds of mononuclear Cr(II) sites varying in –O–Cr–O– angles. **4g** was a pseudo-tetrahedral cluster. **6g** was a pseudo-octahedral cluster, and the other two clusters were built with different bond angles to represent the heterogeneity of the silica surface. Cluster **3g** was a four-membered chromasiloxane ring with a much higher ring strain and thermodynamically unfavorable formation requiring a heat of 24.6 kcal mol^{-1}. For clusters **4g** and **5g**, the heats of Cr anchoring reaction decreased with the increasing ring size. Compared to the experimental frequencies of 986 ± 46 cm^{-1} for a dehydrated silica-supported chromium oxide catalyst [83], the two computed harmonic Cr=O stretching frequencies were 1,016 and 1,054 cm^{-1} for the cluster **4g**. Furthermore, the computed *d*–*d* transition of $^5A'$-$^5A''$ at a vertical transition energy of 10,400 cm^{-1} also agreed with the experimental observation of *d*–*d* transition in Cr^{2+} ions conducted by Weckhuysen and Wachs [150]. Therefore, the six-membered chromasiloxane ring **4g** was chosen by Espelid and Børve as a key model for a series of DFT studies on the Phillips catalyst. The cluster **6g** with geometry constraint to reserve D_{3h} symmetry was only used in chromium *d*–*d* transition study for comparison with clusters **4g** and **5g** [145]. The hydrogen transfer was also evaluated by means of DFT studies using a large cluster **7g** [147]. Two dinuclear clusters, **8g** and **9g**, represented the silica-supported dichromate species sited on narrow and wide sites [146]. The cluster **10g** was a trivalent

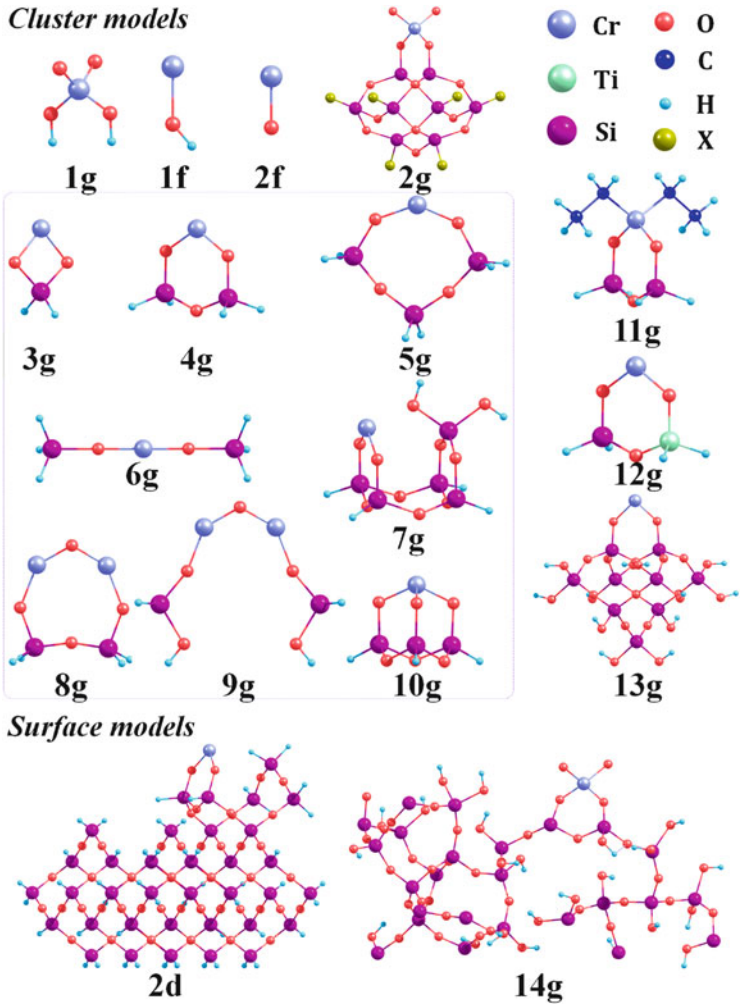

Fig. 23 Various molecular models for the Phillips Cr/silica catalyst that have been reported in the literatures

cluster model for modeling the properties of Cr(III) species on the silica surface of the Phillips catalyst [145].

The six-membered chromasiloxane(II) ring was also adopted and confirmed as a model of active Cr species in many theoretical investigations [54, 71, 146, 151, 152]. In a parallel study, Schmid and Ziegler [153] reported a theoretical calculation on the surface-supported Cr(IV) species (**11g**) for ethylene polymerization. A low barrier for chain propagation was found through a transformation from neutral chromium-alkylidene (Cr-carbene) complex to cationic chromium-alkyl complex in the early stage of ethylene polymerization. Demmelmaier et al. further confirmed the validity of the six-membered chromasiloxane ring **4g** as an ideal model rather

than the larger ring **5g** for the Phillips catalyst through a combination of experiments and theoretical calculations [54, 114]. Recently, Zecchina et al. reported the adsorption of probe molecules (CO, N_2) on the six-membered chromasiloxane(II) ring **4g** and found a good agreement between the calculated vibrational frequencies and the experimental observations by increasing the percentage of Hartree−Fock exchange in the hybrid density functional B3LYP [151]. Alternatively, we [71] studied the effects of Ti-modification of the Phillips catalyst using the modified six-membered chromasiloxane ring **12g**. Combined with the experimental findings, a reasonable mechanistic understanding has been made for the effects of Ti-modification of Phillips catalysts, such as promotion of the polymerization activity, extension of MWD to the low molecular weight region, and improvement of the distribution of inserted comonomers. Moreover, we [154] studied the reduction of the hexavalent chromate species by ethylene during the induction period and unraveled the behavior of Cr(II) active sites (**4g**) with or without coordination of formaldehyde, which was generated through the reduction of chromate species by ethylene. Recently, Tonosaki et al. [152] found that the calculated activation energies for both ethylene insertion and chain transfer were in good agreement using the six-membered chromasiloxane ring **4g** and a slightly larger cluster **13g**. It was pointed out that the intrinsic origin of the broad MWD of the polyethylene produced by Phillips catalysts might be derived from the multiple coordination environments around the active Cr site on the silica surface.

It has long been recognized that the silica support is not an inert component of the catalyst that simply directs polymer particle morphology. The neglect of the real silica surface could introduce some artificial effects and provide an unrealistic environment for the adsorption of monomer on active chromium centers [155]. Nowadays, with the improvement in computing resources and the development of quantum methodologies, full quantum calculations using a large surface-supported model or a periodic model of silica gel surface can be performed. Very recently, we developed a surface model **2d** containing 37 Si atoms through supporting of a six-membered chromasiloxane ring onto a silica surface cutting from the β-cristobalite crystal structure, whose surface was proposed to resemble that of amorphous silica [55]. The results were in good agreement with the experimental spectra as discussed in Sect. 4. Guesmi and Tielens [156] reported an amorphous silica surface slab containing 120 atoms ($Si_{27}O_{54}{\cdot}13H_2O$) that represented the amorphous character of the hydroxylated silica surface involving different silanol types. Through a periodic DFT calculation, a higher stability of mono-oxo and di-oxo chromium species was confirmed in comparison with chromium-hydroxyl species. The main conclusion of their study was a strong support of the six-membered chromasiloxane ring on the amorphous silica surface as a valuable molecular model for the Phillips catalyst. Thus far, all the related theoretical calculations mentioned above agree that the six-membered chromasiloxane ring **4g** could serve as a reasonable cluster model for the Phillips catalyst, but that the effects of the silica support should be considered as well.

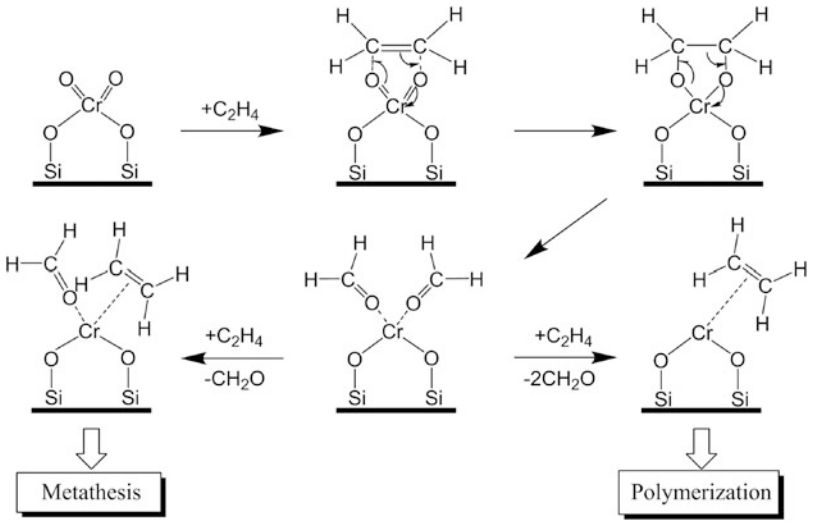

Scheme 15 Plausible monomer reaction mechanism between ethylene and monochromate site on the Phillips Cr/silica catalyst during the induction period of ethylene polymerization

6.2 Reaction Mechanism During the Induction Period

In the absence of organometallic cocatalyst, the hexavalent chromate species on the Phillips catalyst is first reduced to a lower valence state by ethylene monomers. Experimentally, we found that the exposure of ethylene to Phillips catalyst during the induction period at RT led to the reduction of $Cr(VI)O_{x,surf}$ precursors to $Cr(II)O_{x,surf}$ species with the simultaneous formation of formaldehyde and unsaturated hydrocarbon species, such as propylene and butene. The proposed reaction mechanisms during the induction period are shown in Scheme 15 [79].

In order to elucidate the proposed reaction mechanism for the Phillips catalyst during the induction period, we recently performed a theoretical investigation to study the role of formaldehyde [154]. Through extensive calculations on all the possible configurations, three kinds of stationary complexes were located and are referred to as **4g** for a complex without any formaldehyde, **4g-1** for a complex with one adsorbed formaldehyde, and **4g-2** with two adsorbed formaldehydes. The optimized geometries are graphically shown in Fig. 24.

There were three kinds of Cr(II) sites generated after the reduction of hexavalent chromate species by ethylene monomers. **4g** represented the naked cluster model for the Cr(II) site of the Phillips catalyst, providing more room for ethylene coordination to the Cr center. The calculations showed that the initiation reactions between the $Cr(II)O_{x,surf}$ species and ethylene molecules may occur after the desorption of one or two formaldehyde molecules (on **4g-1** or **4g-2**). For **4g-2**, two formaldehyde molecules were adsorbed on the Cr(II) center from the opposite side above the chromasiloxane ring, with formation of two Cr–O bonds of 2.131 Å.

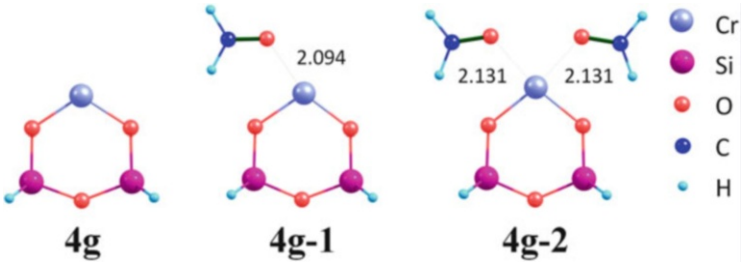

Fig. 24 Stable geometries of Cr(II) catalyst models adsorbed with different numbers of formaldehyde molecules after the reduction of chromate species by ethylene

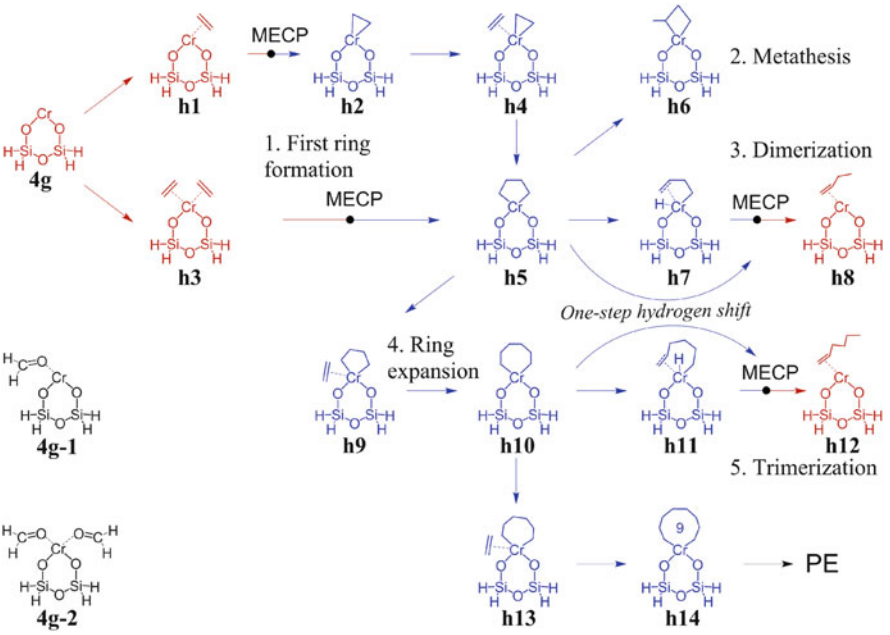

Scheme 16 Reaction pathways over the cluster model **4g** during the induction period

Scheme 16 describes all the possible reaction networks during the induction period, and the naked cluster model **4g** is taken as an example.

The electronic spin state of a transition metal species may have a dramatic effect on the catalytic reactivity. Cr-catalyzed reactions often show a two-state manner, in which the spin crossing plays a vital role in determining the behavior of the catalyst [157–159]. For the reaction initiated on **4g**, a spin crossover from quintet to triplet state occurred during the formation of chromacyclopentane from the Cr(II) complex, which dramatically lowered the activation energy barrier from 42.4 kcal mol^{-1} on a single quintet surface to 23.7 kcal mol^{-1} on a triplet surface through a spin-flipping reaction via a minimum energy crossing point

(MECP), as shown in Scheme 17, reaction 1. The following reaction may occur from the chromacyclopentane species **h5** on the triplet surface to generate a methyl-chromacyclobutane species **h6** through an intramolecular 2,1-hydrogen shift, which would lead to a metathesis reaction to produce propylene and butene molecules, as observed experimentally [79]. However, the hydrogen transfer was prohibited by a much higher energy barrier of 57.2 kcal mol^{-1} without formaldehyde adsorption, as shown in Scheme 17, reaction 2. Alternatively, the reaction from **h5** to a dimerization product 1-butene was found to be finished in a two-step manner via a Cr-hydride intermediate **h7** with an energy barrier of 39.4 kcal mol^{-1}. The reaction crossover to the quintet surface before the second triplet barrier through another MECP and 1-butene was finally released on the quintet surface, as shown in Scheme 17, reaction 3. For the ring expansion step, ethylene molecule may be directly inserted into the Cr–C bond of **h5**, generating a chromacycloheptane structure **h10** on the triplet surface with an insertion barrier of 26.9 kcal mol^{-1}, as shown in Scheme 17, reaction 4. In contrast to **h5**, the ring opening of **h10** took place in a one-step manner assisted by a direct β-H agnostic interaction. The trimerization product 1-hexene was also released on the quintet surface with a barrier of 28.0 kcal mol^{-1} and the corresponding spin crossing took place in the product channel, as shown in Scheme 17, reaction 5. The further ring expansion from chromacycloheptane **h10** was prohibited because ethylene coordination complex could not be located for **h10** due to steric hindrance.

The calculated activation barriers over models **4g**, **4g-1**, and **4g-2** for all the typical reactions (similar to reactions 1–5 in Scheme 17) during the induction period are summarized in Table 4. After a complete desorption of the formaldehyde molecules, the first initiation reaction occurred on **4g** via a MECP to generate a chromacyclopentane species on the triplet surface. The following ring expansion gave a chromacycloheptane species and a subsequent one-step reductive elimination yielded 1-hexene on the quintet surface through another MECP. On the site **4g-1**, the ring expansion step was forbidden because a third ethylene molecule could not be adsorbed on the chromacyclopentane species with one formaldehyde coordinated on the Cr center. Therefore, the reaction of ethylene trimerization on model **4g-1** was absent. Although the dimerization on model **4g-1** was likely to take place with an energy barrier of 35.5 kcal mol^{-1}, a metathesis reaction was still possible on site **4g-1** to produce short olefins. There was no reaction initiated by **4g-2** because the chromium site was completely shielded by the two coordinated formaldehyde molecules.

Table 4 also summarizes the calculated activation barriers of all the typical reactions (in Scheme 17) during the induction period over catalyst models similar to **4g**, **4g-1**, and **4g-2** except that both Si atoms within each model were fully fluorinated. Fluorination of the silica support for the F-modified Phillips catalyst showed negligible influence on ethylene dimerization to 1-butene and metathesis to propylene [160]. However, the energy barrier was increased significantly in reaction 5 of Scheme 17, in which 1-hexene was formed from the chromacycloheptane species through a one-step intramolecular hydrogen shift. Fluorination showed a positive effect on ring expansion in reaction 4 of Scheme 17.

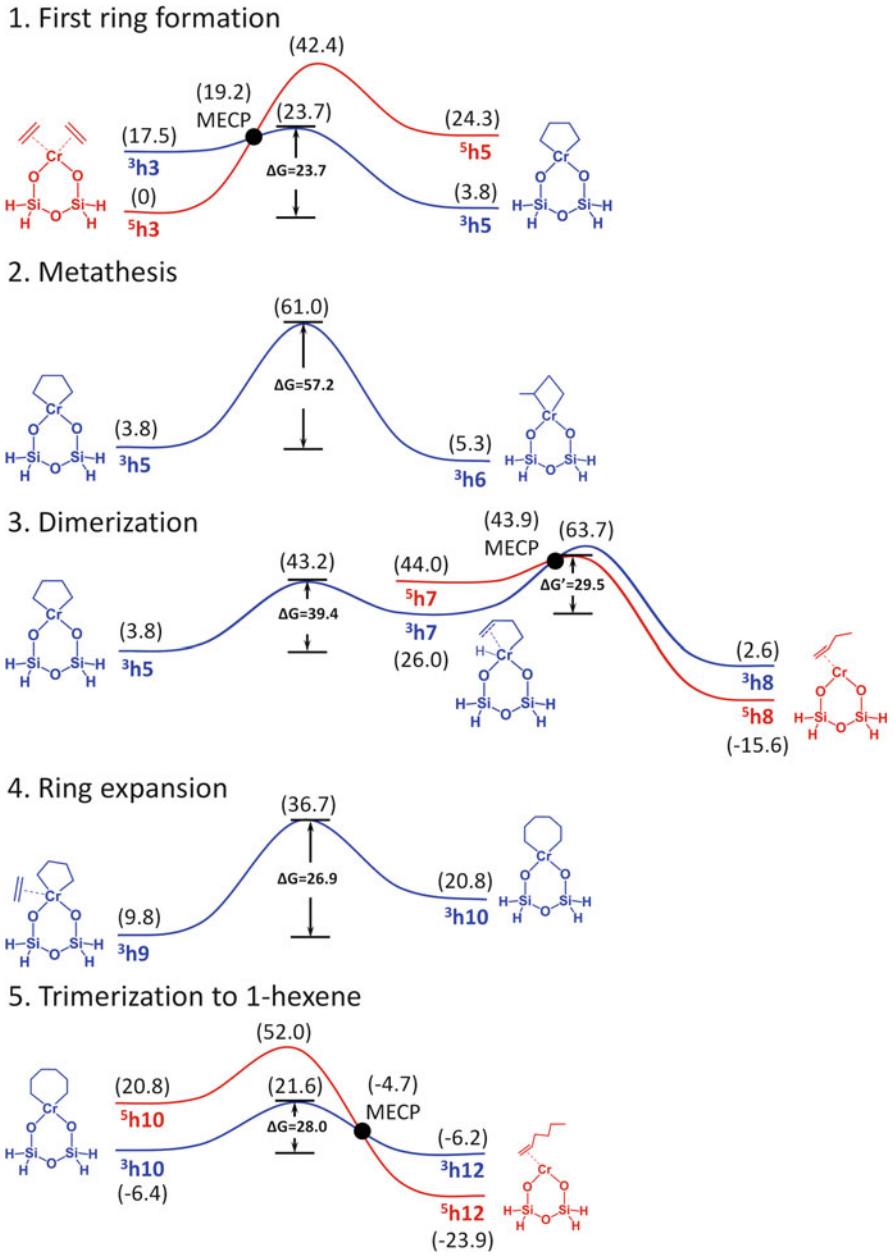

Scheme 17 Gibbs free energy profiles of reactions *1–5* over the cluster model **4g** without adsorbing formaldehyde. The triplet (^3h) and quintet (^5h) energy profiles are depicted. Energies are in kcal mol^{-1}

Table 4 Energy barriers on the proposed reaction pathways over catalyst models coordinated with different numbers of formaldehyde molecules considering spin crossing

	Energy barrier (kcal mol^{-1})					
	Without fluorination[a]			With fluorination[b]		
Reaction	$n_{HCHO} = 0$	$n_{HCHO} = 1$	$n_{HCHO} = 2$	$n_{HCHO} = 0$	$n_{HCHO} = 1$	$n_{HCHO} = 2$
First ring formation	23.7	27.4	–	27.5	29.3	–
Metathesis	57.2	46.7	–	58.4	43.0	–
Dimerization	39.4	35.5	–	46.6	34.5	–
Ring expansion	26.9	–	–	21.5	–	–
Trimerization to 1-hexene	28.0	–	–	38.2	–	–

[a]Over catalyst models **4g**, **4g-1**, and **4g-2**
[b]Over catalyst models similar to **4g**, **4g-1**, and **4g-2** except that both Si atoms within each model were fully fluorinated

6.3 *Polymerization Mechanisms and the First Cr–C Bond Formation*

Phillips catalysts initiating ethylene polymerization without using any organometallic cocatalyst brings us a long standing question: how is the first polyethylene chain initiated on the naked chromium site? That is to say, the initiation mechanism of ethylene polymerization in terms of the formation of the first polymer chain over the active site on a Phillips catalyst is the key problem awaiting elucidation. In the literature, three typical mechanisms, as previously shown in Scheme 2, have been proposed for ethylene polymerization over a Phillips catalyst: (1) the formation of an acyclic Cr–C or Cr–H bond followed by chain propagation through the classic Cossee–Arlman mechanism; (2) the formation of Cr=C (Cr-carbene) bond followed by chain propagation through the Green–Rooney mechanism; and (3) the formation of metallacycle in which both ends of the alkyl group are attached to the chromium site, followed by chain propagation through the metallacycle mechanism.

Espelid and Børve [120] first studied different routes of initiation and chain propagation mechanisms for ethylene polymerization over the Phillips catalyst using the cluster models **3g–10g**, and the six-membered chromasiloxane ring **4g** was regarded as one of the most plausible active Cr species. The potential catalytic activities of monomeric and dimeric chromium species on the silica surface were also evaluated [146, 147]. Starting from a Cr-cyclopropane, Espelid and Børve compared three different initiation mechanisms including the formation of the acyclic ethenylhydridochromium species, the ethylidenechromium species, and the cyclic chromacyclopentane species [120]. The calculations showed that initiation through a direct Cr–carbene formation could be safely excluded, while a metallacycle pathway exhibited a much lower energy barrier. Meanwhile, Schmid and Ziegler [153] found that a cationic Cr–C species could be generated by protonation of the Cr=C (Cr-carbene), which showed a lower energy barrier for chain propagation compared with that through Cr-carbene propagation. The absence of

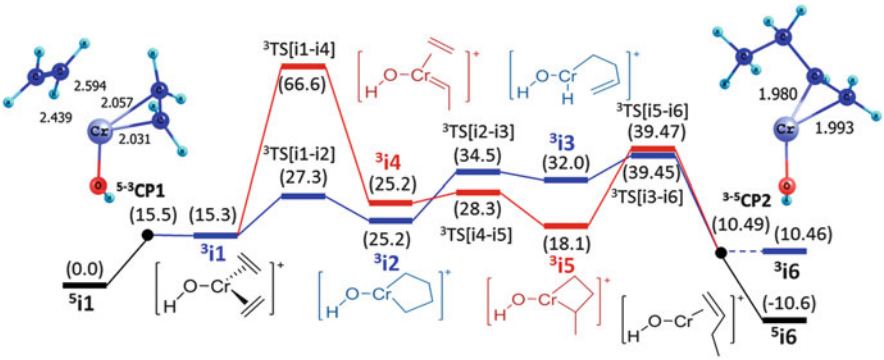

Fig. 25 Potential energy surfaces for the most feasible two-state reaction pathways for ethylene dimerization catalyzed by $Cr(II)OH^+$ (**1f**), via either a Cr-carbene mechanism or a metallacycle mechanism determined at the M06 level of theory. Also shown are the crossing points optimized at CASSCF level. The triplet metallacycle reaction pathway is depicted in *blue*, and the triplet Cr-carbene reaction pathway is shown in *dark red*. The quintet parts are in *black*. Energies are in kcal mol^{-1} and relative to ^{5}i1. Bond lengths are in angstroms. Angles are in degrees

internal C=C bonds in the copolymer produced by copolymerization of ethylene and cyclopentene over the Phillips catalyst also suggested the transformation of Cr=C into Cr–C species as polymerization active sites during the polymerization stage, as confirmed experimentally [95]. Espelid and Børve suggested that the adjacent hydroxyl group might be responsible for the formation of a Cossee-type active site. However, this proposal is questioned due to the fact that Phillips catalyst calcined at higher temperature with much less surface residual hydroxyl groups usually shows higher activity than that calcined at lower temperature. The metallacyclic mechanism through a chromacyclopentane species was supported by strong experimental evidence concerning the intermediacy of large metallacycles in polyethylene chain growth, resulting in the selective trimerization of ethylene to 1-hexene [161]. It could be concluded that the metallacycle mechanism is most probably responsible for the initiation of ethylene polymerization, especially for the formation of the first polymer chain on each active site on the Phillips catalyst.

In the above-mentioned theoretical studies of the initiation mechanism for Phillips catalysts, the spin state of the chromium center, which might play a very important role in the formation of the first chromium–carbon chain, was not considered. As discussed in Sect. 6.2, although formation of the chromacyclopentane species as the key intermediate of the metallacyclic mechanism is prohibited by the much higher energy barrier on a single quintet surface, a transition of the reaction to the adjacent triplet surface through an MECP could lower the energy barrier dramatically. Our recent work [162] proved that ethylene dimerization over **1f** model showed a two-state metallacyclic reaction pathway with the formation of chromacyclopentane as the rate-determining step. Figure 25 shows the energy surfaces for the ethylene dimerization together with two optimized geometries of the spin crossing points. In the first crossing point $^{5\text{-}3}$CP1, the Cr–C bonds are already formed between the chromium center and one of the coordinated

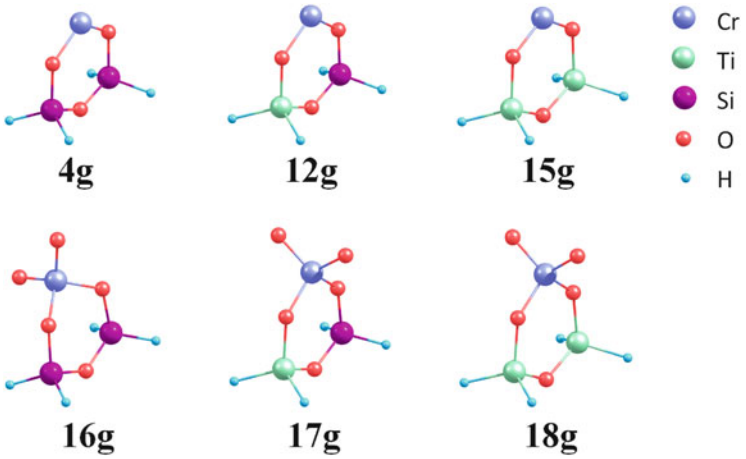

Fig. 26 Models for Cr(VI) sites (**16g**, **17g**, **18g** for Ti:Cr = 0:1, 1:1, 2:1, respectively) and Cr(II) sites (**4g**, **12g**, **15g** for Ti:Cr = 0:1, 1:1, 2:1, respectively) for the Phillips catalyst

ethylene molecules, with two Cr–C bonds of 2.057 and 2.031 Å. After the first spin-flipping to the triplet surface, the metallacycle reaction pathway was found to be more favorable than the Cr-carbene reaction pathway. 1-Butene was formed from the chromacyclopentane by a two-step reductive elimination pathway through a chromium(IV) hydride intermediate. Therefore, the initiation reaction of the ethylene polymerization could not proceed on a single quintet surface, but a spin-flipping to an adjacent triplet surface facilitated the formation of the first Cr–C bond at the crossing point of the two adjacent potential energy surfaces.

6.4 Polymerization Mechanisms for the Ti-Modified Phillips Catalyst

As an important industrial catalyst, the Ti-modified Phillips catalyst is widely used in ethylene polymerization. Recently, the mechanism of ethylene polymerization by the Ti-modified Phillips catalyst has been studied theoretically and experimentally [71]. In the DFT calculations, six mononuclear chromium cluster models including three hexavalent chromate sites (**16g**, **17g**, and **18g**) and the corresponding divalent chromium sites (**4g**, **12g**, and **15g**) were employed to mimic various Ti-modification environments on the surface of the Phillips catalyst, as shown in Fig. 26. Among these cluster models, **16g/4g** represented Cr(VI)/Cr(II) sites without Ti-modification. In **17g/12g** and **18g/15g**, the Ti/Cr atomic ratio was set to 1:1 and 2:1, respectively.

For the Ti-modified Phillips catalyst, the inclusion of small amounts of titanium on the catalyst has a promotional effect both on polymerization activity and the

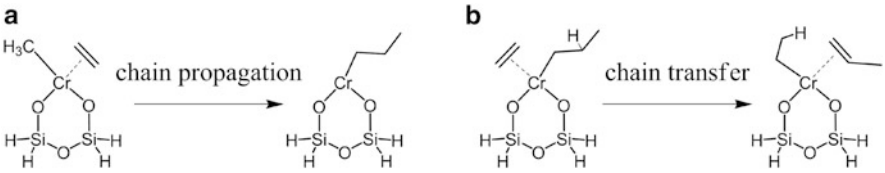

Scheme 18 (**a**) Chain propagation through classical Cossee–Arlman mechanism, (**b**) Chain transfer by β-H elimination to monomer

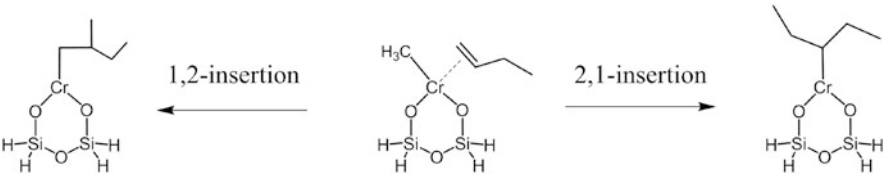

Scheme 19 Regiospecific insertion of 1-butene as comonomer in 1,2-orientation and 2,1-orientation for the Phillips catalyst

Table 5 Energy barriers[a] for chain initiation, chain propagation, and chain transfer reactions on various models of the Phillips catalyst

	Chain propagation[b]			Chain transfer[c]			Δ[d]		
Model	C_2H_4	1-C_4H_8	1-C_6H_{12}	C_2H_4	1-C_4H_8	1-C_6H_{12}	C_2H_4	1-C_4H_8	1-C_6H_{12}
Ti:Cr = 0:1	19.2	21.7	21.8	25.9	26.1	24.3	6.7	4.4	2.5
Ti:Cr = 1:1	18.4	20.2	21.2	24.7	23.5	23.3	6.3	3.3	2.1
Ti:Cr = 2:1	17.7	19.6	20.3	24.1	21.7	22.1	6.4	2.1	1.8

[a]Energy barrier is given in kcal mol^{-1}
[b]Based on primary 1,2-insertion
[c]Based on β-H elimination to monomer after 1,2-insertion of the corresponding monomer or comonomer
[d]Energy barrier differences between ethylene insertion of chain propagation and chain transfer steps, in kcal mol^{-1}

chain transfer rate. The polymerization activity is primarily determined by the feasibility of the chain propagation reaction. We considered chain propagation through the classical Cossee–Arlman mechanism through alkylated trivalent Cr(III)-alkyl active sites, as depicted in Schemes 18 and 19. The energy barriers for the chain propagation and chain transfer are listed in Table 5. The calculations showed that the Cr active sites in Ti-modified models exhibited an increased electron deficiency, and the corresponding energy barriers of the first ethylene insertion were 19.2, 18.4, and 17.7 kcal mol^{-1} for cluster models **4g**, **12g**, and **15g**, respectively. This indicated that Ti-promotional effects could enhance the polymerization activity of the Phillips catalyst. The MW and MWD of the polyethylene are known to be determined by the relative rate between chain propagation and chain transfer. β-H elimination to monomer was believed to be the predominating chain transfer mode for Phillips catalysts (reaction b in Scheme 18).

Table 6 Energy barriers[a] through different regiospecific insertion modes with comonomers in terms of regioselectivity on various models of the Phillips catalyst

Models	Insertion modes	1-Hexene	Δ^b	1-Butene	Δ^b
Ti:Cr = 0:1	1,2-insertion	21.8	1.9	21.7	2.2
	2,1-insertion	23.7		23.9	
Ti:Cr = 1:1	1,2-insertion	21.2	1.2	20.2	1.2
	2,1-insertion	22.4		21.4	
Ti:Cr = 2:1	1,2-insertion	20.3	1.8	19.6	1.8
	2,1-insertion	22.1		21.4	

[a]Energy barriers are given in kcal mol^{-1}
[b]Energy barrier difference between 2,1-insertion and 1,2-insertion, in kcal mol^{-1}

As can be seen from Table 5, the chain transfer rate was enhanced more than the chain propagation rate after Ti-modification. Consequently, Ti-modification could result in an increased in the low MW fraction of polyethylene, and thus the MWD was broadened to the lower MW region.

Copolymerization with α-olefins over a Phillips catalyst is a key method for controlling the density and microstructures of the polyethylene products in industrial processes. Table 5 also listed the energy barriers for the primary 1,2-insertion of 1-butene and 1-hexene, and the subsequent chain transfer by β-H elimination for all the three kinds of Ti-modified models. The calculated energy barriers showed that Ti-modification could also promote the activity for ethylene copolymerization with α-olefins. The energy differences between comonomer insertion and chain transfer can lead to a conclusion on the effect of Ti-modification on the distribution of the inserted comonomers in polyethylene chains. As listed in Table 5, the difference between energy barriers for chain propagation and for chain transfer decreased for model sites **4g**, **12g**, and **15g**. Therefore, it was reasonable to conclude that Ti-modified catalyst was likely to make low MW polyethylene with much less comonomer insertion because the inserted comonomer mainly led to a chain transfer reaction and left the inserted comonomer at the chain end. As a result, the increased chain termination by comonomer resulted in less SCBs in the low MW fraction and higher density of the polyethylene product for the Ti-modified Phillips catalyst.

For traditional heterogeneous olefin polymerization catalysts such as Ziegler–Natta and Phillips catalysts, the regioselectivity usually prefers 1,2-insertion (primary insertion) of α-olefins compared with 2,1-insertion (secondary insertion) due to obvious steric hindrance in the second insertion mode. The effect of Ti-modification of the Phillips catalyst on the energy barriers of 1,2-insertion and 2,1-insertion of α-olefins was calculated by a DFT method based on the three catalyst models. The regiospecific insertion of 1-butene is shown in Scheme 19. All the energy barriers of the two insertion modes for both 1-butene and 1-hexene on the three catalyst models are listed in Table 6. The calculated energy barriers for 1,2-insertion were lower than for the corresponding 2,1-insertion, indicating the dominant nature of 1,2-insertion in the copolymerization by Phillips catalyst. Ti-modification lowered the energy barriers for both

1,2-insertion and 2,1-insertion of comonomer, which was consistent with the Ti-promotional effect on activity. Moreover, the energy barriers for 2,1-insertion of comonomer decreased more than those for 1,2-insertion. The calculated results indicated that 2,1-insertion of comonomer might be enhanced by Ti-modification of the Phillips catalyst, which was consistent with McDaniel's suggestion of the plausible enhancement of the 2,1-insertion versus 1,2-insertion during ethylene copolymerization with α-olefin on Ti-modified Phillips catalyst [4].

Up to now, most of the theoretical studies on the Phillips catalyst have been conducted using cluster models built for modeling the active species on the silica surface. Through a combination of molecular modeling and experimental spectroscopy, a general agreement has been achieved on the cluster model. The reactions during the induction period, the initiation mechanisms for ethylene polymerization, and the effects of Ti-modification and fluorination of the silica surface were elucidated through DFT calculations together with comparison with the experimental results. Because the real Phillips catalyst contains an amorphous silica support with much higher heterogeneity, the cluster model may neglect the effect of the silica surface, which is believed to be very important for understanding the active sites of the Phillips catalyst. Thankfully, with the fast growth in computing power and the in-depth development of quantum packages, one can perform theoretical calculations on the Phillips catalyst using a more realistic silica-supported model, which opens a new era in modeling of the Phillips catalyst. Although the theoretical calculations using a silica-supported surface model are very limited at present, there are bright prospects for the realistic molecular modeling of the Phillips catalyst. It is always crucial to do molecular modeling with a comparison to experiments. The combination of experiments and theoretical calculations results in more interesting findings, which probably could not be obtained by means of a single technique. For the theoretical work in the study of Phillips catalysts, a more realistic mechanistic description could probably be achieved through a full ab initio quantum molecular dynamics simulation using a surface-supported model [163]. Believe it or not, molecular modeling will be playing a more and more important role in the catalytic field. Theoretical calculation is a powerful tool for interpretation of experimental results and in guidance of catalyst development through state-of-the-art catalyst design.

7 Catalyst Innovations Through Modification of the Phillips Catalyst

Parallel to the progress in the basic understanding on the nature of active sites and polymerization mechanisms, several modified Phillips catalysts with better performance and improvements in the structures and properties of PE products through surface modification of the silica support and catalyst with Ti, F, Al, or B compounds have been successfully developed and commercially applied during

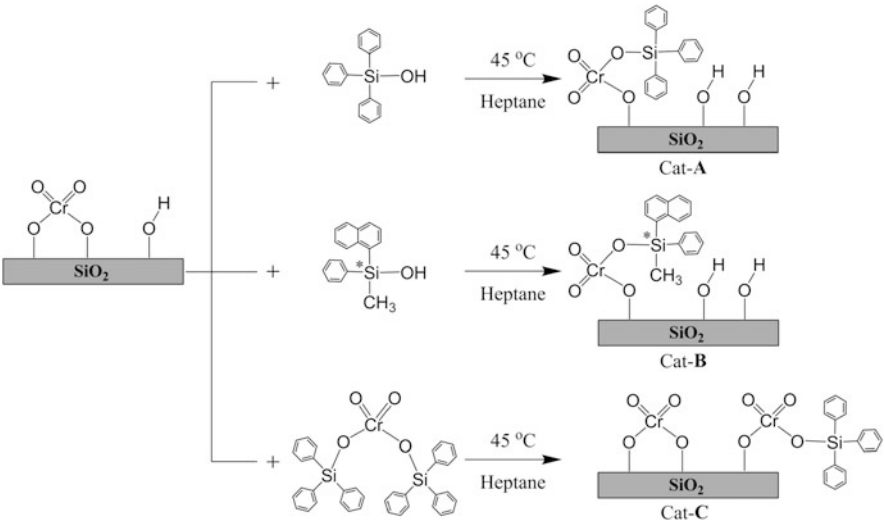

Scheme 20 Procedures for preparation of novel catalysts (Cat-**A**, Cat-**B** and Cat-**C**) by modification of the Phillips catalyst

the past 60 years [2–4, 11]. It is obvious that the catalyst innovations are very limited. During the past few years, we have successfully developed several novel Cr-based Phillips-type catalysts through simple surface modifications of the traditional Phillips catalyst, as shown in Scheme 20. Two basic procedures were taken into consideration for the innovations. One procedure was modification of surface chromate species using various types of organic silanols (to give Cat-**A** and Cat-**B**). The other procedure was modification of surface residual hydroxyl groups using various types of organometallic compounds, which could be chemically anchored on the catalyst surface and provide extra active sites for ethylene polymerization (giving Cat-**C**).

7.1 Modification of Surface Chromate Species on the Phillips Catalyst

Modification of surface chromate species on the Phillips catalyst using various types of organic silanols could be a general procedure for synthesis of various novel Cr-based polymerization catalysts. The reactions are shown in Scheme 20 for Cat-**A** and Cat-**B**. The first example of Cat-**A** was reported by Cann and coworkers through the reaction between TPS and a Phillips catalyst with the original purpose of transformation of the Phillips catalyst into UCC S-2 catalyst in order to avoid the use of toxic and expensive BC [27]. In our opinion, the Cat-**A** was similar to the UCC S-2 catalyst but differed with respect to the simultaneously formed surface

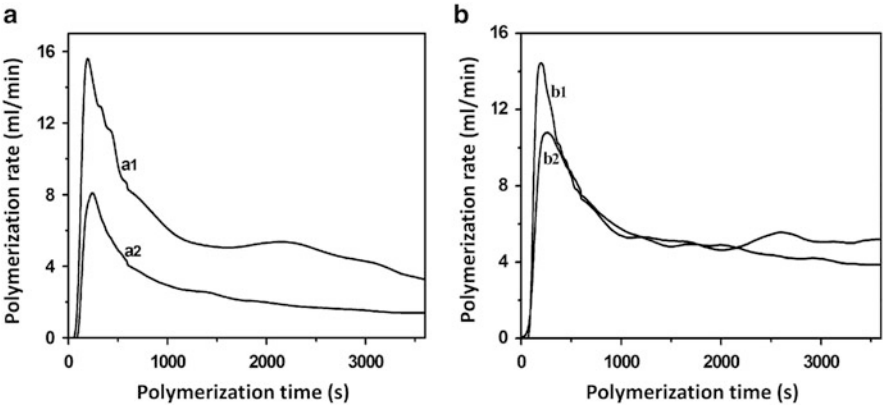

Fig. 27 Ethylene polymerization kinetic curves of catalysts activated by TEA cocatalyst during slurry polymerization: (**a**) Phillips catalyst (*a1*) and Cat-**A**/1.5 catalyst (*a2*) (Al/Cr molar ratio = 20.0); (**b**) Cat-**A**/1.5 catalyst (*b1*) and S-2 catalyst (*b2*) (Al/Cr molar ratio = 15.0). Polymerization conditions: catalyst amount, 160 mg; polymerization temperature, 90°C; ethylene pressure, 0.15 MPa; solvent, heptane, 70 mL

hydroxyl group very close to the active Cr site. Therefore, a detailed study on the synthesis of Cat-**A** was further carried out by a combination of experimental and theoretical methods [28]. The results showed that the molar ratio of TPS to Cr was important for the catalyst structure and the polymerization performance as well as the structure and properties of the PE products. An increase in TPS amount seemed to accelerate the loss of surface hexavalent chromium species from the support, suggesting that the conversion from Phillips catalyst to S-2 catalyst by the addition of TPS could not occur completely. The optimal molar ratio of TPS to Cr was 1.5 for the preparation of Cat-**A** (named Cat-**A**/1.5). Ethylene slurry polymerization kinetics activated by Al-alkyl cocatalyst during polymerization over the Phillips, Cat-**A**/1.5 and S-2 catalysts are shown in Fig. 27. All three catalysts showed hybrid-type polymerization kinetics (as shown in Fig. 10a). The polymerization activity of Cat-**A**/1.5 catalyst was much lower than that of the Phillips catalyst. For Cat-**A**/1.5 and S-2 catalysts, the kinetic curves for the two catalysts with the same cocatalyst were similar, and only a slightly higher activity of Cat-**A**/1.5 catalyst than that of S-2 catalyst was obtained, as shown in Fig. 27b. The significant decline in polymerization activity from Phillips catalyst to Cat-**A**/1.5 catalyst might be due to the different coordination environment of the Cr active site, the release of surface strain by opening of the Si–O–Cr–O–Si–O ring, and the appearance of a simultaneously formed hydroxyl group next to the Cr center after TPS modification. The theoretical studies by DFT showed that coordination of the hydroxyl to the reduced Cr site were favorable for ethylene polymerization and might be the reason for its higher polymerization activity than the S-2 catalyst. But, further modification of the hydroxyl group on the Cat-**A**/1.5 catalyst by a series of alkyl chlorosilane compounds showed that the effect of an electron-withdrawing group was limited at a certain distance away from the Cr active site.

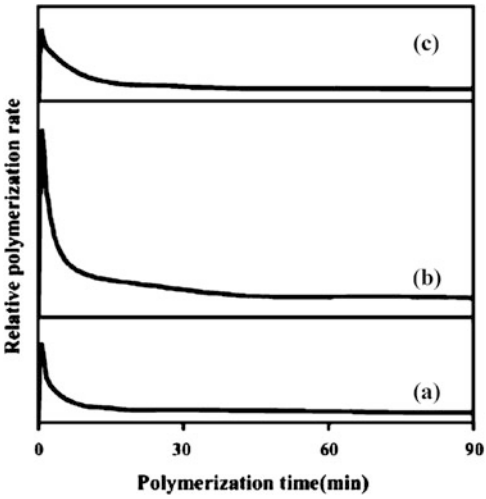

Fig. 28 Polymerization kinetic curves of catalysts activated by TEA cocatalyst during the slurry polymerization process: (**a**) Cat-**B**/600-S catalyst with 15.0 Al/Cr molar ratio; (**b**) Cat-**B**/600-S and (**c**) Cat-**B**/600-4S catalysts with 22.5 Al/Cr molar ratio. Polymerization conditions: catalyst amount, 100 mg; polymerization temperature, 60°C; ethylene pressure, 0.13 MPa; solvent, heptane, 20 mL; cocatalyst TEA in heptane, 1 M

By similar method, a new chiral organo-silanol species, methyl (1-naphthyl) phenylsilanol has been successfully introduced onto Phillips catalyst PC600 calcined at 600°C in order to synthesize a novel Phillips-type catalyst (Cat-**B**) [164]. There was a decrease in BE values of the Cr 2p core level in the XPS spectra for the catalyst samples with increasing molar ratios of chiral ligand to Cr from chiral ligand-free 1:0 (PC600), 1:1 (Cat-**B**/600-S) to 1:4 (Cat-**B**/600-4S). This could be explained by the electron donation effect of chiral organo-siloxane ligand and the formation of hydroxyl groups after anchoring of the ligand, which can release the strong surface tension on the silica support formed during high temperature calcination. The ethylene polymerization kinetic curves of Cat-**B**/600-S and Cat-**B**/600-4S activated by Al-alkyl cocatalyst with different Al/Cr molar ratios are shown in Fig. 28 and illustrate the hybrid-type kinetic behavior (as shown in Fig. 10a). At the same time, it was very interesting to find relative amounts of methyl and *n*-butyl branches in these ethylene homopolymers, which were considered to be generated from the metathesis site (as shown in Scheme 8). Therefore, this catalyst was similar to a Phillips catalyst in the transformation of ethylene metathesis sites into polymerization sites during the early stage of ethylene polymerization.

7.2 Modification of Surface Residual Hydroxyl Groups on the Phillips Catalyst

Another general procedure for synthesis of novel Cr-based ethylene polymerization catalysts could be through modification of surface residual hydroxyl groups on a Phillips catalyst using various types of organometallic compounds, which could be chemically anchored on the catalyst surface and provide extra active sites for

ethylene polymerization. Recently, a novel hybrid catalyst presented the merits of two important chromium-based catalysts, namely inorganic Phillips and organic S-2 catalysts. It was successfully prepared, and named Cat-**C**, as shown in Scheme 20 [165]. This method utilized the surface residual hydroxyl groups on a Phillips catalyst and anchored the BC complex under mild conditions. Thus, the surface residual hydroxyl group population could greatly influence the degree of supported BC, as well as the polymerization activity and the structure of the polymers. For a series of catalysts with total 0.5 wt% Cr loading prepared with increasing Cr_{BC} loading of 20% (Cat-**C1**), 50% (Cat-**C2**), and 80% (Cat-**C3**), the thermogravimetric peaks from the catalysts after the reaction of HMDS and the residual hydroxyl groups became more and more apparent, suggesting that the residual surface hydroxyl group population increases with the increasing relative addition amount of Cr_{BC}. The ethylene polymerization kinetic curves over the Cat-**C** catalysts activated by Al-alkyl cocatalyst during polymerization were insensitive to the type of cocatalyst (TEA, TiBA, and MAO) and similar to the kinetic type shown in Fig. 10a, implying the existence of two kinds of active sites. As can be seen from Table 7, Cat-**C2** catalyst with 50 wt% Cr_{BC} relative loading showed well-balanced properties of ethylene homopolymerization and ethylene/1-hexene copolymerization in terms of activities and MW of the polymers. Its copolymers had a higher average MW and broader MWD than those obtained from the Phillips catalyst, as well as higher 1-hexene incorporation than those obtained from Phillips and S-2 catalysts.

In order to investigate the SCB distribution of the ethylene/1-hexene copolymers made by Cat-**C**, TREF combined with SSA was applied according to a method established by us previously [166, 167]. The SCBs contents for each PE fraction from TREF were qualitatively obtained from the lamella thickness measured by SSA. The lamella thickness distribution of the fractions obtained by TREF for each copolymer is shown in Fig. 29. Comparison of the lamella thickness distribution of the copolymers in the highest temperature fraction (124°C fraction, corresponding to the highest MW part of the copolymer) suggested that the lamella thickness of copolymers obtained from Phillips and Cat-**C2** catalysts were similar and slightly thinner than those obtained from S-2 catalyst. This result indicated that the corresponding relative SCB content of copolymers in the highest MW part obtained from Phillips and Cat-**C2** catalysts were slightly higher than that obtained from S-2 catalyst. In the lowest temperature fraction (40°C fraction, corresponding to the lowest MW part), the copolymers obtained from the Phillips catalyst showed much thinner lamella thickness (corresponding to much higher relative SCB content) than those obtained from S-2 and Cat-**C2** catalysts. The copolymer obtained from Cat-**C2** catalyst showed thinner lamella than that obtained from S-2 catalyst. Hence, it should have the thickest lamella thickness (corresponding to the least relative SCB content) in the copolymers in the lowest MW part. Simultaneously, considering the relative SCB contents in both the lowest and highest temperature fractions of the copolymers, it was suggested that the SCB distribution of copolymers obtained from Cat-**C2** catalyst was the best: the copolymer had similar relative SCB contents in the highest MW part to those obtained from the Phillips

Table 7 Polymerization activities of different Cr-based catalysts and characterization of the polymers

Sample	1-Hexene (vol%)	Activity (kg mol^{-1} h^{-1})[a]	T_m (°C)[b]	ΔH_f (J g^{-1})[c]	M_w ($\times 10^5$)[d]	MWD	1-Hexene (mol%)[e]
Cat-**C2**	0	336	134	194.6	3.5	18.1	nd
Cat-**C2**	1	201	134	189.5	nd	nd	nd
Cat-**C2**	3	160	133	188.8	3.4	17.9	1.2
Cat-**C2**	5	110	131	179.1	4.8	25.4	nd
Cat-**C2**	7	139	131	175.6	4.0	22.1	2.7
Phillips	0	1,635	135	nd	2.5	14.5	nd
Phillips	3	405	131	175.3	2.1	11.3	0.8
Cat-**C1**	0	1,360	134	nd	3.1	21.2	nd
Cat-**C1**	3	162	131	183.4	2.2	14.2	nd
Cat-**C3**	0	242	134	nd	4.1	17.9	nd
Cat-**C3**	3	127	132	190.4	5.0	18.1	nd
S-2	0	221	134	nd	4.7	19.6	nd
S-2	3	76	133	194.2	5.0	20.8	0.7

Polymerization conditions: catalyst amount, 100 mg; polymerization temperature, 90°C; ethylene pressure, 0.3 MPa; solvent, heptane, 200 mL; cocatalyst TEA in heptane, Al/Cr molar ratio = 15
nd not detected
[a]Activities in kg_{PE} $(mol_{Cr})^{-1}$ h^{-1}
[b]By DSC thermograms
[c]Enthalpy of fusion by DSC thermograms
[d]By GPC in TCB versus polystyrene standards
[e]1-Hexene incorporation estimated by ^{13}C NMR in DCB-d_4 at 130°C and 75 MHz with delay index of 3 s for at least 4,000 times (sample concentration: ca. 100 mg mL^{-1})

catalyst, and slightly higher SCBs in the highest MW part than those of the S-2 catalyst. In contrast, it had the least relative SCB content in the lowest MW part. Therefore, the SCB distribution for the copolymers from Cat-**C2** should be much more beneficial for improvement of the long-term mechanical properties and gives these copolymers great potential for application as high grade HDPE pipe materials.

In summary, it has been demonstrated that various novel Cr-based polyethylene catalysts with better performance and with improved structures and properties of the PE products can be expected through successive surface modifications of either the chromate species or the silica support through the reaction with the surface residual hydroxyl groups on the traditional Phillips catalyst. Furthermore, by combination of the performance of two metal active sites in the ethylene polymerization, silica-supported bimetallic catalysts are expected to be able to yield PE products with bimodal MWD, which would attract more and more attention from the polyolefin field. One kind of catalyst utilized group 4 metals supporting Cp_2ZrCl_2 or $(n\text{-BuCp})_2HfCl_2$ metallocene catalysts on Cr-montmorillonite and was studied as a binuclear catalyst system to produce HDPEs with bimodal molecular weight distribution [168]. Chromium oxide and $(n\text{-BuCp})_2ZrCl_2$/MAO species supported onto several inorganic supports could produce PE with bimodal MWD [169]. Another group of catalysts based on chromium and vanadium would be more promising catalysts for commercial application in the near future. Examples are the

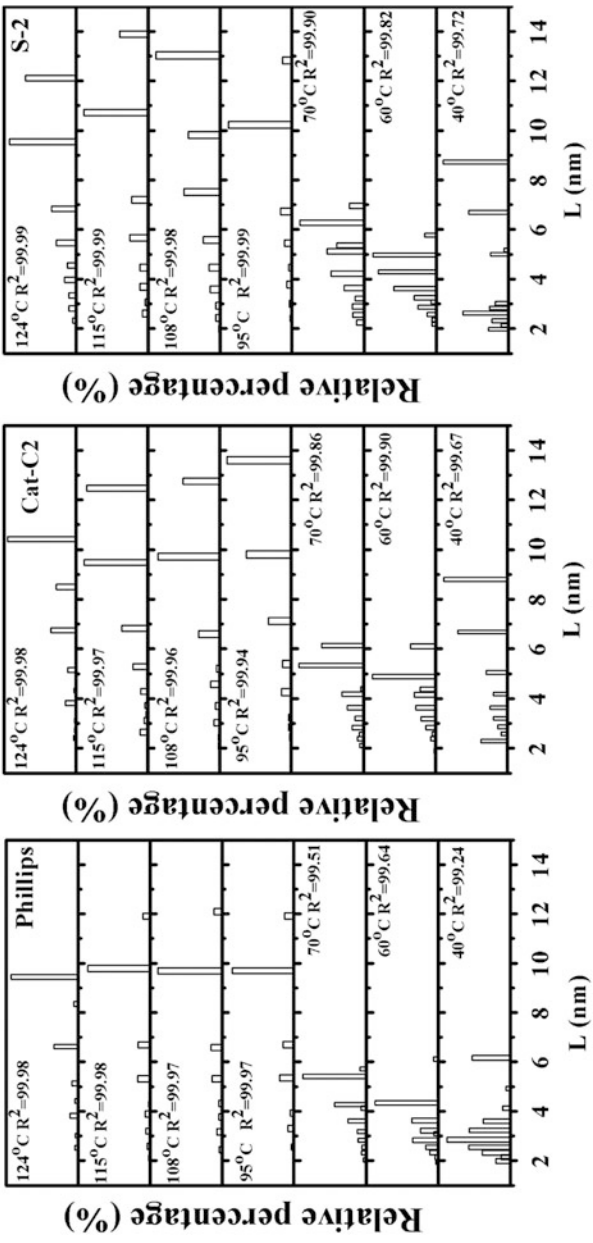

Fig. 29 Lamella thickness distribution of different TREF fractions of copolymers obtained from different catalysts (Phillips, Cat-**C2**, and S-2 catalysts)

recently reported silica-supported inorganic Cr-V bimetallic catalysts [30, 170] and silica-supported organic Cr-V bimetallic catalysts [171] have been successfully synthesized. Much improved SCB distribution of the PE products with better properties and performance made from such bimetallic catalysts within single polymerization reactor could be expected commercially in the near future.

8 Conclusions and Outlook

Since the discovery of the Phillips Cr/silica catalyst by Hogan and Banks in the early 1950s, it has achieved great success as one of the most important industrial catalysts for production of more than ten million tons of HDPE per year. However, academic progress regarding basic understanding of the nature of active sites and polymerization mechanisms is lagging far behind due to the complexity of this heterogeneous catalyst system and the limitation of current technologies. The complexity of Phillips-type catalysts mainly originates from the low percentage of active Cr species in the total Cr loading, the multiple valence states of Cr including +1, +2, +3, +4, +5, and +6, the high surface heterogeneity of the amorphous silica support, the concealment of over 99% of the active sites on the inner surface within the micro- and mesopores of the silica support, the instant encapsulation of active sites by produced polymer and the very short lifetime of the growing polymer chains due to the ultrafast polymerization rate, as well as the coexistence of many side reactions in the polymerization system during the whole process, such as catalyst deactivation and various chain transfer reactions.

During the last decade, increasing research efforts have focused on Phillips-type catalysts through various approaches, including spectroscopic methods, polymerization kinetics, heterogeneous model catalysts, homogeneous model catalysts, and molecular modeling, accompanied by successive catalyst innovations through modification of the traditional Phillips catalyst. Much deeper and better understanding of the nature of active sites and polymerization mechanisms has been achieved by various explorations concerning the activation by high temperature calcination, CO, or Al-alkyl cocatalysts during catalyst preparation; activation by ethylene monomer and Al-alkyl cocatalysts during polymerization; promotional effects of modification of the catalyst by Ti; spin-crossover phenomenon and its effects on the reactivity; and analysis of the microstructures of the produced PE chains, etc. Combined experimental and computational methodologies have been used. Investigations of polymerization kinetics over Phillips-type catalysts combined with different Al-alkyl cocatalysts have provided deeper understanding on formation and transformation of plausible active sites as well as strategies of cocatalyst introduction for design and optimization of commercial polymerization processes. It was also made clear that coordination of divalent active site precursor with siloxane ligands on the silica surface in terms of catalyst calcination temperature was crucial for determination of the precise microstructure and coordination environment of the active Cr species and thus for the performance of the catalyst.

The strategies for catalyst innovations are also shown to be greatly dependent on the progress in surface science of Phillips-type catalysts. More and more novel Cr-based polyethylene catalysts with better performance and products of improved structure and properties can be expected through successive surface modifications of either the chromate species or the silica support on the traditional Phillips catalyst.

In spite of the progress achieved so far, the long-standing key question concerning the precise structure of the active sites and the initiation mechanism in terms of the formation of the Cr–C bond and the first polyethylene chain on the Phillips catalyst have not yet been completely elucidated. A step forward in interpretation of these basic questions requires the combination of heterogeneous and homogeneous model catalyst systems with more advanced and multiple characterization techniques, especially in-situ or operando techniques as well as theoretical molecular modeling. The rational design and utilization of novel heterogeneous and homogeneous model catalysts resembling the traditional Phillips catalyst will greatly facilitate research on the real and complex catalyst system. The ever-growing computational power will enable us to handle more and more complex catalyst systems. A state-of-the-art catalyst design with greatly improved efficiency based on computational high-throughput screening techniques is expected in the polyolefin field in the near future. All in all, further progress in this important field still greatly depends on a combination of multiple techniques for basic research on both catalyst and polymer, as well as on persistent efforts and collaboration of scientists with different expertise from all over the world.

Acknowledgements We are gratefully thankful for the financial support by the National Natural Science Foundation of China (No. 21104019 and 21274040), the National High Technology Research and Development Program 863 (2012AA040306), and the Shanghai Science and Technology Commission (Key Project for Basic Research 10JC1403700). This work is also financially supported by the Fundamental Research Funds for the Central Universities, Research Program of Introducing Talents of Discipline of University (B08021).

References

1. Hogan JP, Banks RL (1954) Patent US 2825721
2. McDaniel MP (1985) Adv Catal 33:47
3. McDaniel MP (2008) Polymerization reactions. In: Ertl G, Knozinger H, Schüth F, Weitkamp J (eds) Handbook of heterogeneous catalysis. Wiley-VCH, Weinheim
4. McDaniel MP (2010) Adv Catal 53:123
5. McDaniel MP (1981) J Catal 67:71
6. Merryfield R, McDaniel MP, Parks G (1982) J Catal 77:348
7. McDaniel MP (1982) J Catal 76:37
8. Liu B, Terano M (2001) J Mol Catal A Chem 172:227
9. Qiu P, Li X, Zhang S, Cheng R, Dong Q, Liu B, Li L, Yu Y, Tang Y, Xie J, Wang W (2009) Asia Pac J Chem Eng 4:660
10. Clark A (1970) Catal Rev 3:145
11. Groppo E, Lamberti C, Bordiga S, Spoto G, Zecchina A (2005) Chem Rev 105:115

12. Kantcheva M, Lana IGD, Szymura JA (1995) J Catal 154:329
13. Nishimura M, Thomas JM (1993) Catal Lett 19:33
14. Ghiotti G, Garrone E, Coluccia S, Morterra C, Zecchina A (1979) J Chem Soc Chem Comm 1032
15. Al-Mashta F, Davanzo CU, Sheppard N (1983) J Chem Soc Chem Comm 1258
16. Ghiotti G, Garrone E, Zecchina A (1988) J Mol Catal 46:61
17. Zielinski P, Lana IGD (1992) J Catal 137:368
18. Ruddick VJ, Badyal JPS (1998) J Phys Chem B 102:2991
19. Vikulov K, Spoto G, Coluccia S, Zecchina A (1992) Catal Lett 16:117
20. Krauss HL (1988) J Mol Catal 46:97
21. Scarano D, Spoto G, Bordiga S, Carnelli L, Ricchiardi G, Zecchina A (1994) Langmuir 10:3094
22. Rebenstorf B, Larsson R (1981) J Mol Catal 11:247
23. Groppo E, Lamberti C, Bordiga S, Spoto G, Zecchina A (2006) J Catal 240:172
24. Hogan JP (1970) J Polym Sci Part A Polym Chem 8:2637
25. Cossee P (1964) J Catal 3:80
26. Cann K (2010) Silica-supported silyl chromate-based ethylene polymerization catalysts. In: Hoff R, Mathers RT (eds) Handbook of transition metal polymerization catalysts. Wiley, Blackwell
27. Cann K, Apecetche M, Zhang MH (2004) Macromol Symp 213:29
28. Li X, Cheng R, Luo J, Dong Q, He X, Li L, Yu Y, Da J, Liu B (2010) J Mol Catal A Chem 330:56
29. Karol FJ, Karapinka GL, Wu C, Dow AW, Johnson RN, Carrick WL (1972) J Polym Sci Part A Polym Chem 10:2621
30. Matta A, Zeng Y, Taniike T, Terano M (2012) Macromol React Eng 6:346
31. Weckhuysen BM, Wachs IE, Schoonheydt RA (1996) Chem Rev 96:3327
32. Vuillaume G, Spitz R, Revillon A, Charcosset H, Turlier P, Guyot A (1971) J Catal 21:159
33. Groeneveld C, Wittgen PPMM, van Kersbergen AM, Mestrom PLM, Nuijten CE, Schuit GCA (1979) J Catal 59:153
34. Wang SB, Murata K, Hayakawa T, Hamakawa S, Suzuki K (2000) Appl Catal A Gen 196:1
35. Vuurman MA, Hardcastle FD, Wachs IE (1993) J Mol Catal 84:193
36. Jozwiak WK, Lana IGD (1997) J Chem Soc Faraday Trans 93:2583
37. Cimino A, Cordischi D, De Rossi S, Ferraris G, Gazzoli D, Indovina V, Occhiuzzi M, Valigi M (1991) J Catal 127:761
38. Ellison A, Overton TL, Bencze L (1993) J Chem Soc Faraday Trans 89:843
39. Bensalem A, Weckhuysen BM, Schoonheydt RA (1997) J Chem Soc Faraday Trans 93:4065
40. Qiu P, Cheng R, Liu B, Tumanskii B, Batrice RJ, Botoshansky M, Eisen MS (2011) Organometallics 30:2144
41. Qiu P, Cheng R, Liu Z, Liu B, Tumanskii B, Eisen MS (2012) J Organomet Chem 699:48
42. Ellison A, Overton TL (1993) J Chem Soc Faraday Trans 89:4393
43. Zaki MI, Fouad NE, Leyrer J, Knoezinger H (1986) Appl Catal 21:359
44. Hardcastle FD, Wachs IE (1988) J Mol Catal 46:173
45. Richter M, Reich P, Oehlmann G (1988) J Mol Catal 46:79
46. Dines TJ, Inglis S (2003) Phys Chem Chem Phys 5:1320
47. Groppo E, Damin A, Bonino F, Zecchina A, Bordiga S, Lamberti C (2005) Chem Mater 17:2019
48. Moisii C, Deguns EW, Lita A, Callahan SD, van de Burgt LJ, Magana D, Stiegman AE (2006) Chem Mater 18:3965
49. Damin A, Bonino F, Bordiga S, Groppo E, Lamberti C, Zecchina A (2006) Chemphyschem 7:342
50. Groppo E, Damin A, Arean CO, Zecchina A (2011) Chem Eur J 17:11110
51. Ellison A, Diakun G, Worthington P (1988) J Mol Catal 46:131

52. Groppo E, Prestipino C, Cesano F, Bonino F, Bordiga S, Lamberti C, Thüne PC, Niemantsverdriet JW, Zecchina A (2005) J Catal 230:98
53. Agostini G, Groppo E, Bordiga S, Zecchina A, Prestipino C, D'Acapito F, van Kimmenade E, Thüne PC, Niemantsverdriet JW, Lamberti C (2007) J Phys Chem C 111:16437
54. Demmelmaier CA, White RE, van Bokhoven JA, Scott SL (2009) J Catal 262:44
55. Zhong L, Lee MY, Liu Z, Wanglee YJ, Liu B, Scott SL (2012) J Catal 293:1
56. Rahman A, Mohamed MH, Ahmed M, Aitani AM (1995) Appl Catal A Gen 121:203
57. Schmidt H, Riederer W, Krauss HL (1996) J Prakt Chem 338:627
58. Nishimura M, Thomas JM (1993) Catal Lett 21:149
59. Groppo E, Lamberti C, Bordiga S, Spoto G, Damin A, Zecchina A (2005) J Phys Chem B 109:15024
60. Groppo E, Lamberti C, Spoto G, Bordiga S, Magnacca G, Zecchina A (2005) J Catal 236:233
61. Groppo E, Lamberti C, Cesano F, Zecchina A (2006) Phys Chem Chem Phys 8:2453
62. Groppo E, Estephane J, Lamberti C, Spoto G, Zecchina A (2007) Catal Today 126:228
63. Barzan C, Groppo E, Quadrelli EA, Monteil V, Bordiga S (2012) Phys Chem Chem Phys 14:2239
64. Cimino A, De Angelis BA, Luchetti A, Minelli G (1976) J Catal 45:316
65. Okamoto Y, Fujii M, Imanaka T, Teranishi S (1976) Bull Chem Soc Jpn 49:859
66. Best SA, Squires RG, Walton RA (1977) J Catal 47:292
67. Liu B, Nakatani H, Terano M (2002) J Mol Catal A Chem 184:387
68. Liu B, Fang Y, Terano M (2004) J Mol Catal A Chem 219:165
69. Liu B, Sindelar P, Fang Y, Hasebe K, Terano M (2005) J Mol Catal A Chem 238:142
70. Fang Y, Liu B, Terano M (2005) Appl Catal A Gen 279:131
71. Cheng R, Xu C, Liu Z, Dong Q, He X, Fang Y, Terano M, Hu Y, Pullukat TJ, Liu B (2010) J Catal 273:103
72. Xia W, Liu B, Fang Y, Fujitani T, Taniike T, Terano M (2010) Appl Catal A Gen 389:186
73. Thüne PC, Loos J, Chen X, van Kimmenade EME, Kong B, Niemantsverdriet JW (2007) Top Catal 46:239
74. van Kimmenade EME, Kuiper AET, Tamminga K, Thüne PC, Niemantsverdriet JW (2004) J Catal 223:134
75. Aubriet F, Muller JF, Poleunis C, Bertrand P, Di Croce PG, Grange P (2006) J Am Soc Mass Spectrom 17:406
76. Groppo E, Seenivasan K, Barzan C (2013) Catal Sci Technol 3:858
77. Lamberti C, Zecchina A, Groppo E, Bordiga S (2010) Chem Soc Rev 39:4951
78. Panchenko VN, Zakharov VA, Paukshtis EA (2006) Appl Catal A Gen 313:130
79. Liu B, Nakatani H, Terano M (2003) J Mol Catal A Chem 201:189
80. Liu B, Fang Y, Nakatani H, Terano M (2004) Macromol Symp 213:37
81. Weckhuysen BM, Wachs IE (1997) J Phys Chem B 101:2793
82. Cimino A, Cordischi D, De Rossi S, Ferraris G, Gazzoli D, Indovina V, Minelli G, Occhiuzzi M, Valigi M (1991) J Catal 127:744
83. Weckhuysen BM, De Ridder LM, Schoonheydt RA (1993) J Phys Chem 97:4756
84. Xia W, Liu B, Fang Y, Hasebe K, Terano M (2006) J Mol Catal A Chem 256:301
85. Terano M, Fang Y, Liu B (2003) Polymer Preprints 44:22
86. O'Neill PP, Rooney JJ (1972) J Am Chem Soc 94:4383
87. Ivin KJ, Mol JC (1997) Olefin metathesis and metathesis polymerization. Academic Press, San Diego
88. Krauss HL, Hums E (1979) Naturforsch 34B:1628
89. Hugues F, Besson B, Basset JM (1980) J Chem Soc Chem Comm 719
90. Ajjou JAN, Scott SL (1997) Organometallics 16:86
91. Ajjou JAN, Scott SL, Paquet V (1998) J Am Chem Soc 120:415
92. Ajjou JAN, Rice GL, Scott SL (1998) J Am Chem Soc 120:13436
93. Ajjou JAN, Scott SL (2000) J Am Chem Soc 122:8968
94. Scott SL, Ajjou JAN (2001) Chem Eng Sci 56:4155

95. Xia W, Tonosaki K, Taniike T, Terano M, Fujitani T, Liu B (2009) J Appl Polym Sci 111:1869
96. McGuinness DS, Davies NW, Horne J, Ivanov I (2010) Organometallics 29:6111
97. Grubbs RH, Tumas WS (1989) Science 243:907
98. Natta G, Dall'Asta G, Mazzanti G (1964) Angew Chem Int Ed 3:723
99. Bordiga S, Groppo E, Agostini G, van Bokhoven JA, Lamberti C (2013) Chem Rev 113:1736
100. Choi KY, Tang S, Yoon WJ (2004) Macromol Theory Simul 13:169
101. Choi KY, Tang S (2004) J Appl Polym Sci 91:2923
102. Matos I, Zhang Y, Lemos M, Freire F, Fonseca IF, Marques MM, Lemos F (2004) J Polym Sci Part A Polym Chem 42:3464
103. Kissin YV, Brandolini AJ, Garlick JL (2008) J Polym Sci A Polym Chem 46:5315
104. Spitz R, Florin B, Guyot A (1979) Eur Polym J 15:441
105. McDaniel MP, Johnson MM (1986) J Catal 101:446
106. McDaniel MP, Johnson MM (1987) Macromolecules 20:773
107. Wang S, Tait PJT, Marsden CE (1991) J Mol Catal 65:237
108. Fang Y, Liu B, Terano M (2006) Kinet Catal 47:295
109. Li L, Wu Y, Dong Q, Hao A, Cheng R, Zhong L, Liu B (2012) Asia Pac J Chem Eng. doi:10.1002/apj.1692
110. Fang Y, Liu B, Hasebe K, Terano M (2005) J Poly Sci A Poly Chem 43:4632
111. Baker LM, Carrick WL (1970) J Org Chem 35:774
112. Carrick WL, Turbett RJ, Karol FJ, Karapinka GL, Fox AS, Johnson RN (1972) J Polym Sci A Polym Chem 10:2609
113. McDaniel MP (1982) J Catal 76:17
114. Demmelmaier CA, White RE, van Bokhoven JA, Scott SL (2008) J Phys Chem C 112:6439
115. Thüne PC, Verhagen CPJ, van den Boer MJG, Niemantsverdriet JW (1997) J Phys Chem B 101:8559
116. Tonosaki K, Taniike T, Terano M (2011) Macromol React Eng 5:332
117. Scott SL, Fu A, MacAdams LA (2008) Inorg Chim Acta 361:3315
118. Ikeda H, Monoi T, Sasaki Y (2003) J Polym Sci A Polym Chem 41:413
119. Monoi T, Ikeda H, Sasaki Y, Matsumoto Y (2003) Polym J 35:608
120. Espelid Ø, Børve KJ (2000) J Catal 195:125
121. Theopold KH (1998) Eur J Inorg Chem 1998(1):15
122. Hanmura T, Ichihashi M, Monoi T, Matsuura K, Kondow T (2004) J Polym Sci A Polym Chem 108:10434
123. Hanmura T, Ichihashi M, Monoi T, Matsuura K, Kondow T (2005) J Polym Sci A Polym Chem 109:6465
124. Feher FJ, Blanski RL (1990) J Chem Soc Chem Comm 1614
125. Feher FJ, Blanski RL (1993) Macromol Sym 66:95
126. Abbenhuis HCL, Vorstenbosch MLW, van Santen RA, Smeets WJJ, Spek AL (1997) Inorg Chem 36:6431
127. Motevalli M, Sanganee M, Savage PD, Shah S, Sullivan AC (1993) J Chem Soc Chem Comm 1132
128. Köhn RD, Haufe M, Mihan S, Lilge D (2000) Chem Comm 1927
129. MacAdams LA, Kim WK, Liable-Sands LM, Guzei IA, Rheingold AL, Theopold KH (2002) Organometallics 21:952
130. Thomas BJ, Noh SK, Schulte GK, Sendlinger SC, Theopold KH (1991) J Am Chem Soc 113:893
131. Bhandari G, Kersten JL, Kucharczyk RR, White PA, Liang Y, Theopold KH (1996) Stud Surf Sci Catal 101:153
132. Britovsek GJP, Gibson VC, Wass DF (1999) Angew Chem Int Ed 38:428
133. Budagumpi S, Kim KH, Kim I (2011) Coord Chem Rev 255:2785
134. Coles MP, Gibson VC (1994) Polym Bull 33:529

135. Coles MP, Dalby CI, Gibson VC, Little IR, Marshall EL, da Costa MHR, Mastroianni S (1999) J Org Chem 591:78
136. Al Thagfi J, Lavoie GG (2012) Organometallics 31:2463
137. Chen F, Lu X, Chen X, Li H, Hu Y (2012) Inorg Chim Acta 387:407
138. Haftbaradaran F, Mund G., Batchelor RJ, Britten JF, Leznoff DB (2005) Dalton Trans 2343
139. Albahily K, Al-Baldawi D, Gambarotta S, Duchateau R, Koc E, Burchell TJ (2008) Organometallics 27:5708
140. Boor J (1979) Ziegler–Natta catalysts and polymerizations. Academic Press, New York
141. Jabri A, Crewdson P, Gambarotta S, Korobkov I, Duchateau R (2006) Organometallics 25:715
142. Liu B, Fang Y, Terano M (2004) Mol Simulat 30:963
143. Liu B, Fang Y, Xia W, Terano M (2006) Kinet Catal 47:234
144. Cheng R, Liu Z, Qiu P, Zhang S, Liu B (2008) Chin J Polym Sci 26:579
145. Espelid Ø, Børve KJ (2001) Catal Lett 75:49
146. Espelid Ø, Børve KJ (2002) J Catal 206:331
147. Espelid Ø, Børve KJ (2002) J Catal 205:366
148. Espelid Ø, Børve KJ (2002) J Catal 205:177
149. Børve KJ, Espelid Ø (2003) Theoretical models of active sites: general considerations and application to the study of Phillips-type Cr/silica catalysts for ethylene polymerization. In: Scott SL, Crudden CM, Jones CW (eds) Nanostructured Catalysts. Springer, Berlin
150. Weckhuysen BM, Wachs IE (1996) J Chem Soc Faraday Trans 92:1969
151. Damin A, Vitillo JG, Ricchiardi G, Bordiga S, Lamberti C, Groppo E, Zecchina A (2009) J Phys Chem A 113:14261
152. Tonosaki K, Taniike T, Terano M (2011) J Mol Catal A Chem 340:33
153. Schmid R, Ziegler T (2000) Can J Chem 78:265
154. Zhong L, Liu Z, Cheng R, Tang S, Qiu P, He X, Terano M, Liu B (2012) ChemCatChem 4:872
155. Sautet P, Delbecq F (2010) Chem Rev 110:1788
156. Guesmi H, Tielens F (2012) J Phys Chem C 116:994
157. Liu Z, Cheng R, He X, Wu X, Liu B (2012) J Phys Chem A 116:7538
158. Hess JS, Leelasubcharoen S, Rheingold AL, Doren DJ, Theopold KH (2002) J Am Chem Soc 124:2454
159. Estephane J, Groppo E, Vitillo JG, Damin A, Gianolio D, Lamberti C, Bordiga S, Quadrelli EA, Basset JM, Kervern G, Emsley L, Pintacuda G, Zecchina A (2010) J Phys Chem C 114:4451
160. Zhong L, Liu Z, Cheng R, He X, Liu B (2013) Chin J Chem Eng 64:539
161. Tomov AK, Chirinos JJ, Jones DJ, Long RJ, Gibson VC (2005) J Am Chem Soc 127:10166
162. Liu Z, Zhong L, Yang Y, Cheng R, Liu B (2011) J Phys Chem A 115:8131
163. Xu R, Klatt G, Enders M, Koppel H (2012) J Phys Chem A 116:1077
164. Fang Y, Xia W, He M, Liu B, Hasebe K, Terano M (2006) J Mol Catal A Chem 247:240
165. Zhang S, Dong Q, Cheng R, He X, Wang Q, Tang Y, Yu Y, Xie K, Da J, Liu B (2012) J Mol Catal A Chem 358:10
166. Zhang S, Zhao N, Wu Y, Dong Q, Wang Q, Tang Y, Yu Y, Da J, He X, Cheng R, Liu B (2012) Macromol Symp 312:63
167. Zhang S, Cheng R, Dong Q, He X, Wang Q, Tang Y, Yu Y, Xie K, Da J, Terano M, Liu B (2013) Macromol React Eng 7:254
168. Yamamoto K, Ishihama Y, Sakata K (2010) J Polym Sci Polym Chem 48:3722
169. Moreno J, van Grieken R, Carrero A, Paredes B (2011) Polymer 52:1891
170. Xue X (2010) Study on novel and highly efficient hybrid CrO_x-VO_x/SiO_2 catalyst for ethylene polymerization. Master Dissertation. East China University of Science and Technology, Shanghai, China
171. Zhao N, Cheng R, He X, Liu Z, Liu B (2012) Patent CN 102627710A

Adv Polym Sci (2013) 257: 203–252
DOI: 10.1007/12_2013_216

Published online: 16 May 2013

Polyolefin Characterization: Recent Advances in Separation Techniques

Benjamín Monrabal

Abstract New polyolefin resins, in spite of their simple chemistry, just carbon and hydrogen atoms, have become by design complex polymers with improved performance for the desired application. Besides the fundamental molar mass distribution, there are many other features that can be controlled when dealing with copolymers and new multireactor/multicatalyst resins. The average properties measured by spectroscopic techniques are not enough to define the microstructure of the new resins; it is necessary to fractionate the polymer according to certain parameters such as molar mass, branching, or stereoregularity. Separation techniques have become essential for the control and characterization of these polymers; nevertheless, full characterization is not a simple task and has demanded the development of new separation methodologies in recent years, and in many cases multiple separation techniques are required to define the microstructure. A review of the most important separation techniques with emphasis on the new technologies is given and the applications of these new polyolefin resins discussed.

Keywords Cross-fractionation chromatography · Crystallization analysis fractionation · Crystallization elution fractionation · Field flow fractionation · Gel permeation chromatography · High temperature liquid chromatography · Size-exclusion chromatography · Solvent gradient interaction chromatography · Temperature rising elution fractionation · Thermal gradient interaction chromatography

Contents

B. Monrabal (✉)
Polymer Char, Valencia, Spain
e-mail: benjamin.monrabal@polymerchar.com

Abbreviations

AF4	Asymmetric flow field flow fractionation
aPP	Atactic polypropylene
CCD	Chemical composition distribution
CEF	Crystallization elution fractionation
CR	Crystallization rate
CRYSTAF	Crystallization analysis fractionation
DC	Dynamic crystallization
DSC	Differential scanning calorimetry
EGMBE	Ethylene glycol monobutyl ether
ELSD	Evaporative light scattering detector
EMA	Ethylene-methyl acrylate
EP	Ethylene propylene copolymer
EPDM	Ethylene-propylene diene
ESL	Ethylene sequence length
EVA	Ethylene-vinyl acetate
FC	Crystallization flow
FDSC	Fractional DSC
FE	Elution flow
FFF	Field flow fractionation
FTIR	Fourier transform infrared
HDPE	High-density polyethylene
HPLC	High-performance liquid chromatography
HR	Heating rate
HT	High temperature
IC	Interaction chromatography
ICPC	International Conference on Polyolefin Characterization
iPP	Isotactic polypropylene
IR	Infrared
LCB	Long chain branching
LDPE	Low-density polyethylene
LLDPE	Linear low-density polyethylene
LS	Light scattering
M	Molar mass

MALS	Multi-angle light scattering
MCT	Mercury cadmium telluride
MMD	Molar mass distribution
NMR	Nuclear magnetic resonance
ODCB	1,2-Dichlorobenzene
PE	Polyethylene
PP	Polypropylene
RI	Refractive index
SCB	Short chain branching
SCBD	Short-chain branching distribution
SEC	Size-exclusion chromatography
SGIC	Solvent gradient interaction chromatography
SGIC2D	Two-dimensional solvent gradient interaction chromatography
SIST	Stepwise isothermal segregation
sPP	Syndiotactic polypropylene
SSA	Successive self-nucleation annealing
STAF	Solvated thermal analysis fractionation
TCB	1,2,4-Trichlorobenzene
TGIC	Temperature gradient interactive chromatography
TREF	Temperature rising elution fractionation

1 Introduction

Polymer characterization at the time Ziegler and Natta synthesized the first linear polyolefins in the 1950s was not yet a mature science. Staudinger [1] was among the first to recognize the importance of molar mass for product properties. Molar mass was being measured by dilute solution viscosity, osmometry, ultracentrifugation or light scattering and different types of averages were obtained depending on the technique being used. It was also understood in the 1930s that synthetic polymers are polydisperse, but in the case of polyolefins it was not possible to measure the molar mass distribution until the late 1960s.

In the early stages of polyolefin development, most characterization work was focused on the catalyst itself and the understanding of polymerization mechanisms. The new polyethylenes being synthesized were being characterized by the bulk polymer properties and most effort was given to understanding the crystal structure and physical properties for a given molar mass average.

The synthesis of polypropylene brought a new scenario and major efforts at that time concentrated on controlling the stereoregularity, synthesizing the most regular isotactic polypropylene, and understanding its polymorphism; these efforts have continued for many years.

Polymer microstructure became more complex when short chain branches were inserted into the linear chains, with the addition of α-olefin comonomers with the

intention of modifying the polyethylene density. In the case of polypropylene, the addition of ethylene extended the product range to copolymers.

Characterization techniques being used in the 1950s and 1960s, such as NMR, infrared spectroscopy, X-ray diffraction, microscopy etc., could only measure the average values; this was also the case for the molar mass measurement. In some cases, there was a need to separate the amorphous and crystalline fractions by solvent extraction methods because no other means to measure the distributions were available.

We had to wait for quite some years for the development of new separation principles like gel permeation chromatography (GPC) in the late 1960s and temperature rising elution fractionation (TREF) in the late 1970s to better define the polyolefins microstructure by its distributions (molar mass and composition distributions). It took a significant time and effort to fully develop these separation techniques. Separation first means dissolution, which with the good chemical resistance of polyolefins demands a high temperature with special solvents; the second challenge is good detection, which with the lack of chemical functionality could only be done by refractive index and later on with more sensitive infrared detectors.

The development of single-site catalysts in the 1980s together with new multi-reactor processes and new comonomers opened the route for the design of new resins with improved performance for different applications. New polyolefin copolymers may have a complex microstructure and, besides molar mass and composition distribution, it is necessary to characterize the bivariate distribution (interdependence of molar mass and composition) and, on occasions, the level of long chain branching and stereoregularity.

Spectroscopic techniques have improved significantly in the last 50 years, especially in sensitivity, and they are of great value for investigating new structures or understanding the intramolecular inhomogeneity of polyolefins. However, more effort has been demanded in separation science, and the new developments to deal with the analysis of these complex structures will be the subject of this chapter.

2 Polyolefin Microstructure

Polyolefins have the simplest chemistry of all synthetic polymers, just carbon and hydrogen atoms, but can have complex microstructures. Besides the molar mass distribution, there exists a wide range of significant features in the polyolefin molecular architecture such as:

- The presence of short chain branches, by the addition of one or various comonomers, which could result in intermolecular homogeneous (single-site catalyst) or heterogeneous (multiple-site catalysts) incorporation
- The presence of long chain branches, which even in small quantities have a significant influence on rheological properties

- Stereoregularity differences in the case of polypropylene
- The recent appearance of block copolymers

Very often, with the goal of optimizing final product performance, the industrial polyolefin products are a complex combination of resins with some of the features listed above. It is not surprising that various separation techniques may be required to cover a full characterization task.

In the following sections, the microstructure features of the most important polyolefins are described.

2.1 Polyethylene Microstructure

The chemical structure of a linear polyethylene homopolymer is solely defined by the molar mass distribution (MMD) of the resin. This important distribution, together with the additives incorporated and the final morphology achieved in the processing, defines the polymer performance in a given application.

In the resin manufacturing process, and due to the difficulties in obtaining fast MMD data, homopolymer resins are controlled by a parameter related to the average molar mass (M), the melt index, and on occasions by additional rheology measurements that reflect the broadness of the distribution; however, when full characterization of a linear high-density polyethylene (HDPE) homopolymer product is required, the whole MMD must be measured.

To expand the application range of polyethylene produced with Ziegler-type [2, 3] or chromium oxide catalyst processes [4, 5], comonomers such as propylene, butene, hexene, or octene are incorporated into the linear chain and become short chain branches that reduce the crystallizability of the polymer, extending the density range from 0.96 g/mL of the HDPE homopolymer through medium density resins (0.94 g/mL) down to the linear low-density polyethylene (LLDPE) resin types (0.91 g/mL) and below to the elastomers region. The density value of a given polyethylene resin correlates to the average comonomer mole percentage incorporated; however, when dealing with multiple-site catalyst systems (Ziegler-type), the intermolecular incorporation of comonomer is not uniform and, in those cases, there is further need to know the chemical composition distribution (CCD) and the molar mass–composition interdependence.

A scheme of the extended chain molecular population and branching in an LLDPE resin is shown in Fig. 1a, where it is seen that the larger the molecule the lower chances of comonomer incorporation (lower branch content). Most interesting in LLDPE is the bimodality of the CCD, sometimes referred to as the short-chain branching distribution (SCBD), as shown in Fig. 1b, due to the population discontinuity observed between (1) the fraction of linear molecules, practically excluding the comonomer incorporation in certain catalyst sites, and (2) the remaining fractions with increasing amounts of comonomer incorporated. Catalyst sites, where the bulkier and less reactive comonomer can be incorporated,

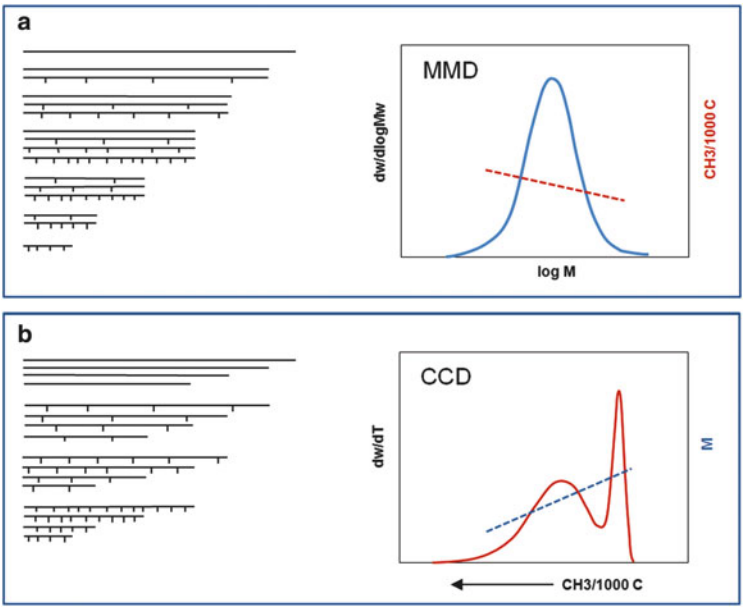

Fig. 1 (**a**) LLDPE molecular population organized by size and the corresponding MMD curve. (**b**) Molecular population organized by composition (branching) and the corresponding CCD curve. *M* molar mass

result in higher chances of thermal termination and thus lower molar mass, as shown by the crossing lines in the MMD and CCD plots of Fig. 1 which provide a two-dimensional (2D) view of the molar mass–composition interdependence.

The development in 1980 of single-site metallocene catalysts by Kaminsky [6, 7] resulted in a better-defined polyethylene microstructure, with uniform intermolecular comonomer incorporation and narrow MMD; this development opened new applications by copolymerizing new comonomers, extending the polyethylene range to the elastomers region, and providing a means to resin design through multiple reactor-catalyst technologies. A good example is shown schematically in Fig. 2, where a high molar mass polymer of low density produced with a single-site catalyst is combined with a Ziegler-type resin of lower molar mass. The design possibilities for optimizing the polymer performance with this particular combination by changing the comonomer incorporation and thermal termination in each reactor are also illustrated in Fig. 2.

The development of improved performance HDPE pipe resins by the so-called inverse process, incorporating the comonomer in the high molar mass (not possible with Ziegler-type catalysts in a single reactor) is also an excellent example of design through dual reactor and multiple catalyst technologies.

Another family of low density polyethylenes (LDPE) can be obtained by high-pressure free radical polymerization, resulting in complex microstructures where side chain branches (mainly ethyl and butyl) are obtained through chain transfer reactions without the need of comonomer incorporation. The presence of long

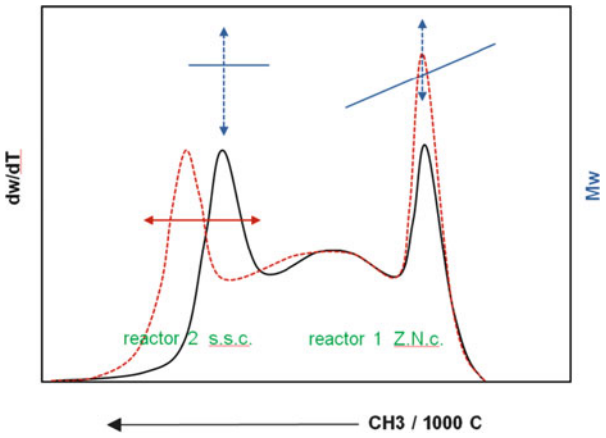

Fig. 2 CCD of a multireactor resin. Combination of a Ziegler-type resin (*reactor 1*) with a single-site resin (*reactor 2*) and possible combinations of comonomer incorporation and molar mass changes

chain branches (LCB) and the possibility of incorporating polar comonomers like vinyl acetate are features of the free radical polymerization process. The measurement of the MMD and the LCB distribution are the most important characterization tasks in these complex LDPE resins.

2.2 Polypropylene Microstructure

Polypropylene homopolymers besides the measurement of the MMD need further characterization to fully describe their microstructure due to the existence of the tertiary carbon in the propylene molecule.

When the insertion of propylene molecules in the growing chain is such that all methyl branches are on the same hand, the regularity of the chain allows it to crystallize; this is the isotactic polypropylene (iPP), synthesized by Natta [8, 9] and the most commercial type obtained by the Ziegler–Natta stereoregular polymerization process. When the monomer insertion is consistently in the opposite hand to previous monomer insertion, the polymer obtained is syndiotactic polypropylene (sPP), which achieves lower crystallinity and today has less commercial interest. The random stereo incorporation of monomer units results in an amorphous resin, atactic polypropylene (aPP).

Besides the three types discussed above and represented schematically in Fig. 3a, there may happen undesired stereo errors in the growing chain which will reduce the tacticity or, regio errors when instead of inserting the new monomer head to tail, it does head to head or tail to tail, disrupting the methyl sequence. These features have been extensively investigated by NMR and in all cases result in modification of the stereoregularity and crystallinity.

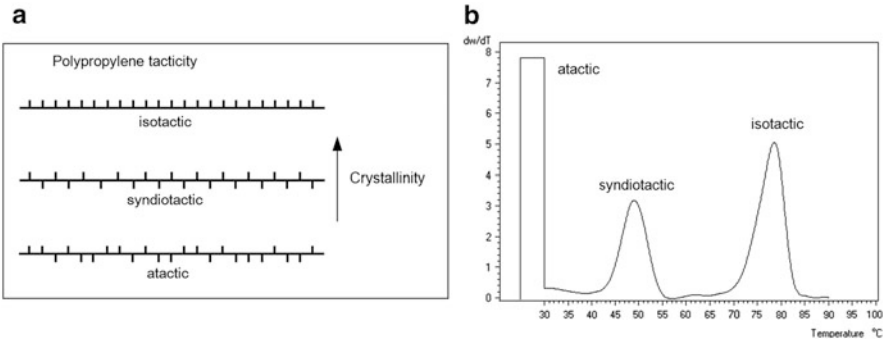

Fig. 3 (**a**) Various tacticity configurations in PP. (**b**) Crystallization temperatures in solution (CRYSTAF) of the three tacticity forms of PP

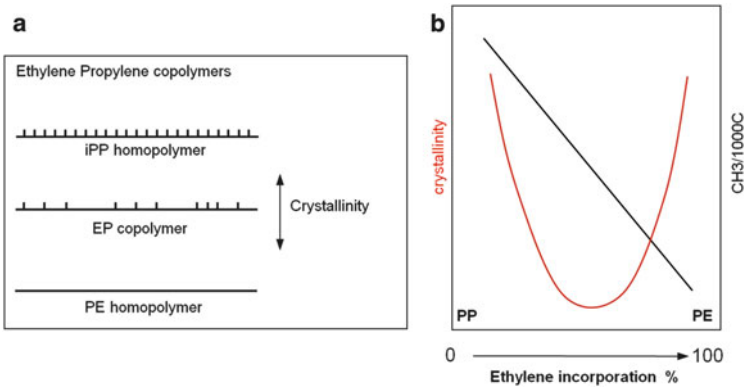

Fig. 4 (**a**) Disruption of the methylene sequence in iPP by randomly incorporating ethylene to produce an EP copolymer. (**b**) Crystallinity and branching of PE, PP, and the range of EP copolymers

The analysis of the distribution of intermolecular tacticity in a blend of the three PP types discussed above is shown in the crystallization analysis of Fig. 3b. Any additional disruption of the stereoregularity of iPP or sPP will result in lower crystallinity and peaks will be shifted towards lower crystallization temperatures.

In the case of polypropylene copolymers, typically ethylene propylene (EP) copolymers, the insertion of ethylene into the growing PP chain will result (for the same reasons as discussed above) in disruption of the methyl sequence and thus reduce the crystallizability, as shown in Fig. 4a. In terms of crystallinity, the addition of ethylene in EP copolymers result in a u-shape curve, as shown in Fig. 4b where both homopolymers have a higher crystallinity than the intermediate EP copolymers.

When analyzing the microstructure of polypropylene homo- and copolymer resins by crystallization techniques, all those aspects need to be considered in the interpretation of the crystallization/dissolution curves (often referred to as CCD, as in the case of PE resins). The analysis of polypropylene and polyethylene

blends is further complicated by the large differences in undercooling of both resins, as will be discussed in sect. 4.1.3.

3 Molar Mass Distribution Characterization Techniques

The molar mass distribution (MMD) is the most fundamental structural parameter for all homopolymers and, together with the CCD and their interdependence (bivariate distribution), defines the microstructure of most polyolefin copolymers. Until the late 1960s, only molar mass averages could be obtained by light scattering, osmometry or viscosity measurements. It requires a separation process to measure the full MMD, and this only became available with the development of gel permeation chromatography (GPC) by Moore in 1964 [10], which represented a significant contribution in the polymer chemistry field. Today most MMD data for synthetic polymers are obtained by this chromatographic technique.

In recent years, field flow fractionation (FFF) [11], which has been used with success in biological macromolecule separation, has become available for the measurement of the MMD of very high molar mass resins.

3.1 GPC/SEC

Gel permeation chromatography (GPC) is also known as size-exclusion chromatography (SEC) and both names are used today in the literature. The GPC technique has been extensively used in the last 50 years and has contributed to the development of polyolefin catalysts, processes, and the improvement of resin performance. There exist good references that deal with the fundamentals of the technique [12, 13], calibration procedures [14–16], and the analysis of LCB [17–23], which still demands significant attention.

In this review, we will focus on the new and most recent technological developments in automation, infrared detection, and its applications in polyolefin analysis.

GPC instrumentation for high temperature analysis, being a niche market, has remained unchanged for a long time. In recent years, new instrumentation has been introduced with significant engineering advances [24] like modular design to facilitate maintenance tasks, larger volume vials to reduce sample non-homogeneity, automated sample preparation (filtration included), and having a separate column oven compartment to prevent column damage during maintenance tasks.

A large amount of attention has been put into minimizing polymer degradation during the sample preparation because of the high temperature and large time required for polyolefins dissolution (including the waiting time for injection in autosamplers) and to reduce the potential shear degradation during stirring and filtration. The dual temperature zone autosamplers developed in the 1990s and the incorporation of antioxidant in the dissolution process provided an improvement, but not enough for the very labile polypropylene resins that may suffer chain

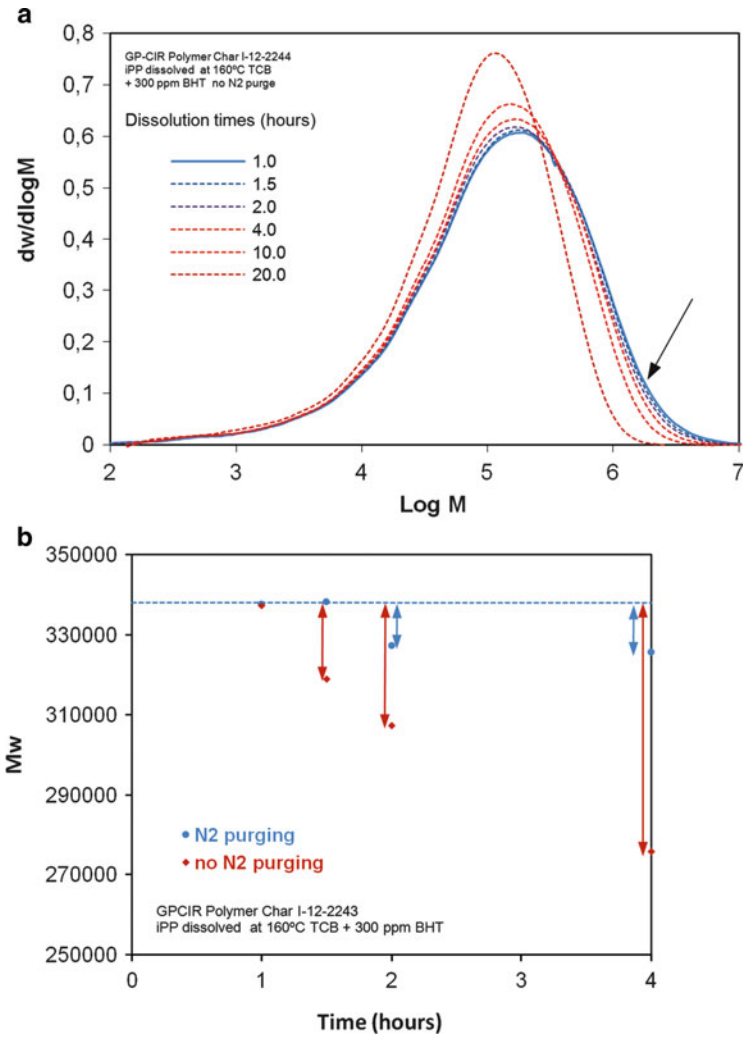

Fig. 5 Polypropylene degradation during dissolution at high temperature. (**a**) Shift of MMD and (**b**) weight-average molecular mass (M_w) versus dissolution time in TCB with 300 ppm BHT, with and without nitrogen purge

scission during dissolution even at shorter times than expected [25]. New approaches have been presented recently to prevent polymer degradation, like using a better solvent (decaline) for the sample dissolution step at lower temperatures [26] or by new autosamplers that allow for nitrogen purging of the vial and precise dissolution time of each sample [27], eliminating the waiting time for injection of the current systems. The importance of nitrogen purging and the influence of dissolution time in degradation of the various polyolefins have been presented recently [28] and can be seen in Fig. 5 for polypropylene.

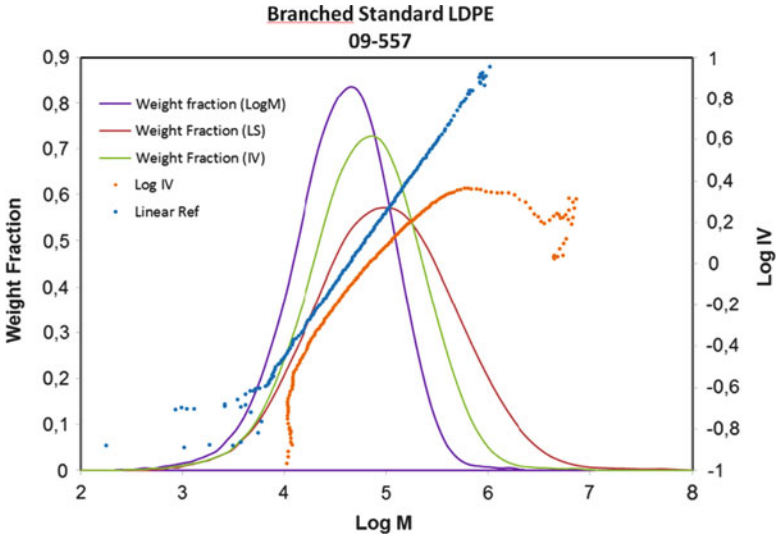

Fig. 6 Triple detector GPC analysis of a LDPE resin; only one light scattering (*LS*) angle is shown, *IV* intrinsic viscosity

For detection, modern multiangle light scattering (LS) detectors have appeared on the market for comprehensive molar mass and size measurements, e.g., from Wyatt Technology (Santa Barbara, CA) [29] as well as single small-angle compact LS system integrated into the detection block (e.g., from Malvern Instruments, Worcestershire, UK) [30]. The use of triple detector GPC (GPC-3D) remains a very active field. An example of GPC-3D analysis is shown in Fig. 6, using concentration, viscosity, and light scattering signals to measure the LCB in a LDPE resin [17–23].

Refractive index detectors remained for many years the most popular concentration detectors in GPC. In the case of polyolefin analysis, however, infrared (IR) detection was shown quite early to be more appropriate [31, 32]. These detectors are filter-based pyroelectric sensing elements (at specific wavelengths) with a heated flow-through cell attached at the exit of the GPC columns; they were used by some polyolefin laboratories in the 1970s although IR detector technology was not yet fully developed, and it did not become popular until the early 2000s [33]. The chlorinated solvents used in the GPC analysis of polyolefins [1,2-dichlorobenzene (DCB), 1,2,4-trichlorobenzene (TCB), and perchloroethylene] do not contain aliphatic C–H bonds and, thus, allow for the analysis of polymer concentration by measuring absorption at around 3.5 μm (aliphatic C–H stretching band).

With the development of FTIR, infrared detection attached to GPC with a flow-through cell became interesting in the 1990s for obtaining the comonomer incorporation (short chain branches) in polyolefin copolymers by measuring, besides concentration, the number of methyl groups per 1,000 carbon atoms (CH_3/1000C) along the molar mass [34–36]. The measurement of very low levels

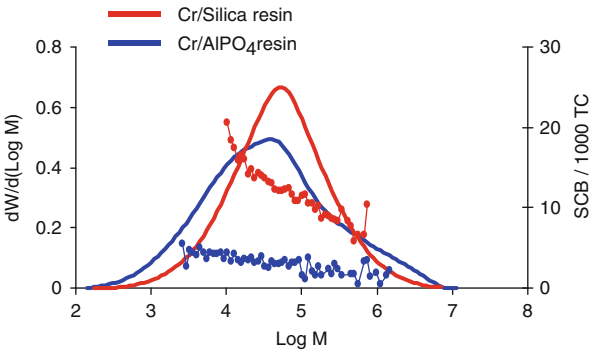

Fig. 7 Analysis of a HDPE pipe resin by GPC FTIR. *SCB* short chain branches, *TC* total number of carbon atoms [37]

of branches was shown to be possible by DesLauriers et al. [37, 38] using nitrogen-cooled MCT detectors (mercury cadmium telluride sensing element) in combination with a chemometric approach, as shown in Fig. 7. This technique has been further optimized by Piel [39] and Albrecht [40].

In the late 1990s, new and compact optoelectronic IR detectors [33] were developed using interference filters at selective wavelengths. They soon became popular for polyolefin GPC analysis because of their sensitivity, short stabilization time, and low temperature dependence. The IR detector results in a cleaner detection of sample components in the low molar mass tail of the GPC elution curve as compared to the refractive index, which often shows solvent impurities and negative peaks in the very low molar mass region. IR detectors used with a flow-through cell are, however, restricted to applications where the solvent is transparent enough in the spectrum region of interest. Typically, two interference filters are used, one measuring the overall absorption of the C–H region and a second centered at the absorption of the C–H from the methyl groups. The analysis of a polypropylene and polyethylene blend is shown in Fig. 8a, with the two signals obtained simultaneously. The ratio of the two signals is directly proportional to the presence of methyl groups, and it can be easily calibrated as the percentage of ethylene incorporated in EP copolymers. The analysis of three EP resins having similar MMD but completely different ethylene incorporation is shown in Fig. 8b.

The simultaneous analysis of concentration and composition in GPC measurements is of significant interest for today's complex polyolefin copolymers. The same IR detector can be used to analyze ethylene-vinyl acetate (EVA) or other functional polyolefin copolymers (with a carbonyl group) as a function of molar mass. All that is needed is to replace the "methyl" interference filter by a "carbonyl" region filter. An example of a maleic anhydride-modified PE is shown in Fig. 9, with an IR interference filter measuring at 1,740 cm^{-1}.

More recently a new filter-type IR detector has been developed [41] with a highly sensitive MCT thermoelectrically cooled sensing element. It has similar response in the C–H region to that of FTIR detectors but it does not require nitrogen cooling. The integration of this detector, in a thermostated compartment, into a GPC system has resulted in an improvement of sensitivity of around ten times

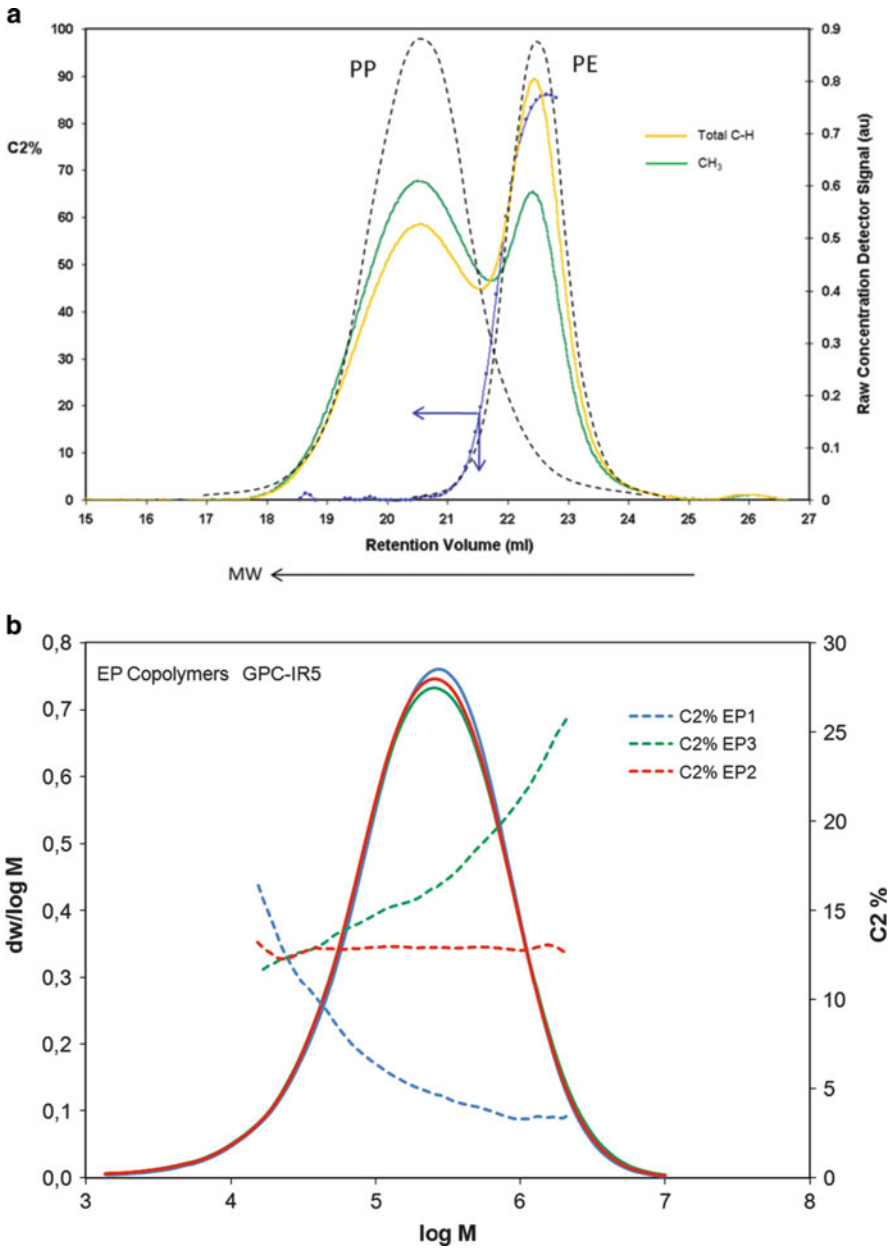

Fig. 8 (**a**) Analysis of a PE resin of low molar mass and a PP resin of high molar mass in a GPC-IR instrument (*dashed lines*) and a 50/50 blend of both resins, showing the total C–H concentration (*gray solid line*) and the C–H centered at CH3 absorption (*solid line*). The *dotted solid line* corresponds to the ratio of methyls to total concentration, calibrated in percentage ethylene incorporation (*C2%*). (**b**) Analysis by GPC-IR of three different EP copolymers (*EP1*, *EP2*, and *EP3*) having similar MMD but completely different ethylene incorporation along the molar mass (*M*)

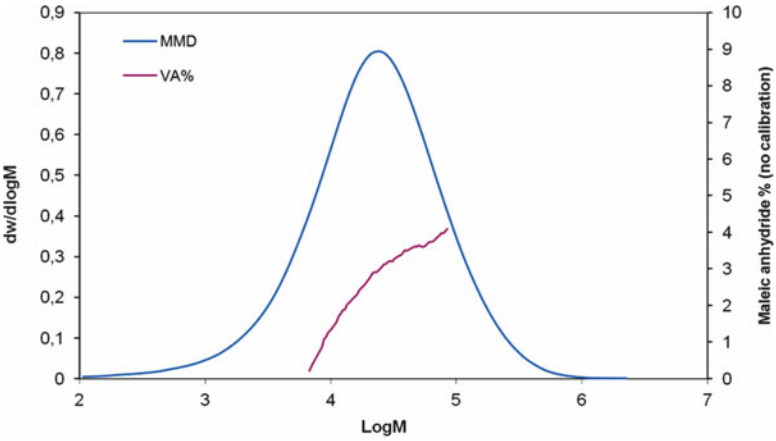

Fig. 9 Analysis of a maleic anhydride-modified PE by GPC-IR to characterize the interdependence of composition and molar mass. Calibration was with vinyl acetate (*VA*) standards

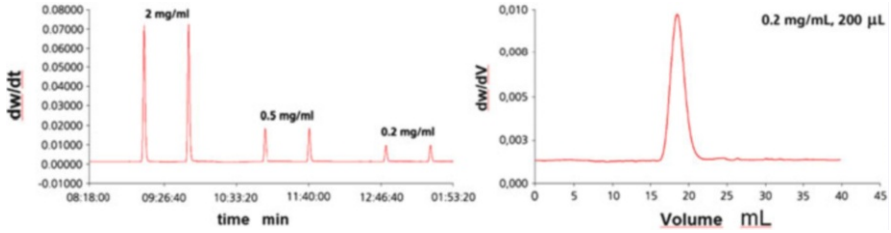

Fig. 10 (**a**) Duplicate analysis of an ethylene octene copolymer at different concentrations by GPC-IR using an integrated thermoelectrically cooled MCT detector. (**b**) Expanded view of the GPC-IR analysis at a very low concentration of 0.2 mg/L

over existing IR detectors [42], as shown in Fig. 10 by the good signal-to-noise ratio and baseline stability obtained after injecting a PE sample that was ten times more dilute than the concentration used under standard GPC conditions.

The sensitivity improvement with this new detector is obtained for both concentration and composition signals, and thus it is being used with success for the difficult analysis of HDPE pipe resins that have low comonomer incorporation [43]. The calibration and error analysis in this difficult application have been studied recently by Ortín et al. [44] and an example of a pipe resin analysis is shown in Fig. 11.

In previous sections we have referred to the combination of IR and GPC, with online detection using a flow-through cell, and the IR system being an integrated filter-type detector or an external FTIR spectrometer. There exists the option to deposit the fractions coming from the GPC column onto a germanium disk while evaporating the solvent, and later measuring the full FTIR spectrum of the various polymer spots in the disk to obtain similar information on composition and molar mass interdependence [45–47] as in previous sections. This approach has been

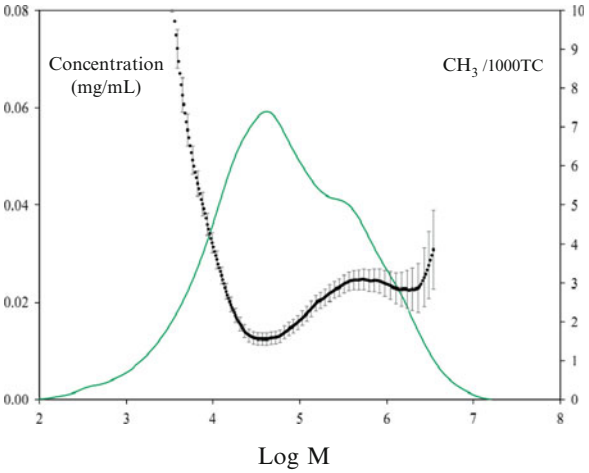

Fig. 11 GPC-IR of a pipe resin. Branching and error analysis

recently improved by using microscopic technology on the IR beam [48, 49]. In those cases, the information obtained from the IR spectra (without the presence of solvent) is superior and very powerful for the qualitative identification of unknown copolymers and additives, although it demands more time for analysis and method optimization. On the other hand, GPC-IR with a flow-through cell is being used for analysis of copolymers of known chemistry and provides better quantitation in a shorter time and with less manpower requirements.

The combination of proton NMR and GPC was shown to be possible by Hiller et al. [50], who built a setup to analyze a blend of PE and poly(methyl methacrylate) (PMMA).

3.2 Asymmetric Flow Field Flow Fractionation

Field flow fractionation (FFF) developed by Giddings [11] in 1966 is a non-column separation technique that has been shown to be of great value for the separation of biological macromolecules. The separation takes place by flowing the solution in a flat channel with no stationary phase, and when being used in the asymmetric flow field flow fractionation (AF4) mode [51], a cross-flow perpendicular to the solvent flow is added, as shown in Fig. 12, which leaves through a semipermeable membrane. A field force against the membrane is formed, with polymer molecules being driven to different heights in the channel over the membrane depending on their diffusion coefficients. The smaller molecules, diffusing faster, are positioned far from the membrane and are flushed at a higher flow velocity than the larger molecules that stay closer to the membrane, where the flow is lower due to the channel parabolic flow profile.

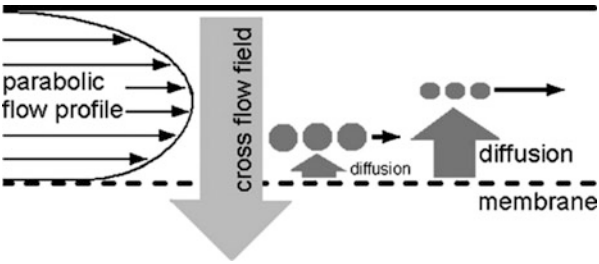

Fig. 12 Separation mechanism of asymmetric flow field flow fractionation (AF4). Small molecules diffuse faster and away from the wall, eluting at higher flow velocity than larger molecules [53]

The limitations of GPC for separation of large macromolecules, i.e., the unavailability of proper columns and the potential shear degradation of high macromolecules in a frit or column packing, are avoided in AF4 by the separation at the empty channel.

The application of high-temperature AF4 to polyolefins was first investigated by Mes et al. [52], who showed better separation with AF4 in very high molar mass LDPE and HDPE than with GPC. This work was continued by Otte et al. [53, 54], who optimized the operation conditions. The major drawback of the technique at this time was the limit for low molar mass materials (50,000 g/mol) because of the difficulties in producing membranes of low-enough pore size.

4 Chemical Composition Distribution: Characterization Techniques

In the previous section, we have seen that the combination of GPC with IR detection provides a measurement of the comonomer incorporation (composition) versus molar mass; however, this does not tell us about the intermolecular distribution of branches (or any other polar comonomer incorporated) into the linear chains, which we refer as the CCD. This also needs to be measured independently in most polyethylene copolymers.

In the case of polypropylene homo and copolymer resins, besides the CCD, which is related to the ethylene incorporation, there is an additional feature, the tacticity, which very often is measured combined with the CCD. In all cases, low tacticity or the incorporation of comonomers result in reduced crystallinity; therefore, it is understandable that most popular techniques for the measurement of the CCD are based on the crystallizability of the polymer.

Calorimetric methods have been used to obtain qualitative data or parameters that could correlate with the CCD [55–57]. It should be clear, however, that differential scanning calorimetry (DSC), although very powerful in other areas, does not provide the ideal environment for crystallization, does not result in

quantitative mass measurements (measuring the heat flow instead of concentration), and has less sensitivity for less crystalline materials; nevertheless, DSC methods have been available and used with certain success before solution crystallization techniques were developed. A short review of the calorimetric techniques used in this application will be presented in Sect. 4.1.1.

The most comprehensive analytical methods being used today to measure the CCD are based on a separation process according to crystallizability. They are performed in solution (higher chain mobility), which result in improved resolution and less co-crystallization effects. In following sections, three separation techniques to measure the CCD based on crystallizability will be described (see Sects. 4.1.2, 4.1.3, and 4.1.4):

Temperature rising elution fractionation (TREF)
Crystallization analysis fractionation (CRYSTAF)
Crystallization elution fractionation (CEF)

In the last 5 years, a new chromatographic approach has been developed to separate polyethylene copolymers by adsorption on a carbon-based column according to composition, with a significant interest in the characterization of less crystalline materials (elastomers). This high temperature liquid chromatography separation process can be performed by solvent gradient or through thermal gradient and has evolved into the following two techniques:

Solvent gradient interaction chromatography (SGIC)
Thermal gradient interaction chromatography (TGIC)

which will also be described in coming sections (Sects. 4.2.1 and 4.2.2).

4.1 Crystallization-Based Techniques

The principles of polymer fractionation by solubility or crystallization in solution have been extensively reviewed on the basis of Flory–Huggins statistical thermodynamic treatment [58, 59], which accounts for melting point depression by the presence of solvents. For random copolymers the classical Flory equation [60] applies:

$$\frac{1}{T_m} - \frac{1}{T_m^0} = -\frac{R}{\Delta H_u} \cdot \ln(p), \tag{1}$$

where p is the molar fraction of the crystallizing unit. Equation (1) can be reduced to:

$$T_m \cong T_m^0 - \frac{R\left(T_m^0\right)^2}{\Delta H_u} \cdot N_2, \tag{2}$$

where N_2 is the molar fraction of the comonomer incorporated. The presence of non-crystallizing comonomer units, diluents, and polymer end-groups all have an equivalent effect on melting point depression when the concentration of each is low and they do not enter into the crystal lattice. From (2), a linear dependence of melting or crystallization temperature T_m with the amount of comonomer incorporated N_2 should be obtained.

In experimental practice, a straight-line correlation between temperature and comonomer composition has been obtained by various authors with TREF [61, 62], DSC [63], and CRYSTAF [64]. These correlations are practically independent of molar mass.

The importance of co-crystallization in polyethylene has been widely investigated by Alamo et al. [65]. Co-crystallization will always be present to a certain degree when crystallizing a heterogenous resin, and especially when carrying it in the melt [66] or in concentrated solutions. At the low concentrations used in modern separation techniques like TREF, CRYSTAF, or CEF, the co-crystallization effects [64, 67, 68], although present, can be in most cases neglected if low-enough crystallization rates are being used, and the separation considered to occur on the basis of comonomer incorporated (assuming intramolecular uniformity). Crystallization will happen according to the ethylene sequence length (ESL) and, if broad distributions of ESL are present, separation by crystallizability will take place according to the largest ESL, complicating the microstructure characterization. Preparative fractionation and subsequent analysis by NMR will provide more light on the analysis of branching clusters in resins with non-uniform intramolecular incorporation of branching.

4.1.1 Calorimetric Methods

Differential scanning calorimetry (DSC) has been used to obtain semi-quantitative data of the CCD. The most significant methods, or parameters, using DSC are: stepwise isothermal segregation, SIST [55]; solvated thermal analysis fractionation, STAF [69]; DSC index [57]; step crystallization [56]; successive self-nucleation/annealing, SSA [70, 71]; and fractional DSC, FDSC [72]. The advantage of calorimetric methods is the technique simplicity, not requiring the polymer dissolution. Calorimetric methods, however, suffer from low resolution and high co-crystallization due to the low mobility of polymer chains in the melt. Calorimetric methods provide a response in heat flow (not mass) and therefore overemphasize the CCD curve as moving towards the more crystalline fractions. In spite of possible correction for the nonlinear detector response, the signal-to-noise ratio will decrease with lower crystallinity of the material.

A review on thermal fractionation methods has been presented by Müller and Arnal [73], who recall that DSC methods are sensitive to both intra- and intermolecular defects whereas solution crystallization methods, where separation takes place according to crystallizability, are more sensitive to inter- than intramolecular heterogeneity.

When dealing with block copolymers, the calorimetric methods may provide some additional information not accessible by TREF, where the dominating separation mechanism is according to the most crystalline part of the block copolymer.

4.1.2 Temperature Rising Elution Fractionation

The most comprehensive analytical approach to characterizing the CCD in recent years has been TREF, implemented in the polyolefin characterization world by Wild et al. in the late 1970s [74, 75], which led to an understanding of the LLDPE structure in relation to the multiple sites in Ziegler-type catalyst.

The initial dissolution fractionation of polyethylene according to composition by increasing temperature was first described by Desreux and Spiegels [76] in 1950 using an extraction technique with a single solvent at increasing temperatures. This was used with success by Hawkins and Smith [77] and Shirayama et al. [78], who first named the technique temperature rising elution fractionation, but it was the work of Wild et al. [74, 75] in the late 1970s with the development of analytical TREF that established the technique as a standard in the polyolefin industry. Various reviews on TREF have been published by Wild [79], Glöckner [68], Monrabal [80], Fonseca and Harrison [81], Soares and Hamielec [82, 83], and recently by Monrabal in a comprehensive review chapter in the *Encyclopedia of Analytical Chemistry* [84].

The TREF analytical process resembles a liquid chromatography separation with a column, an eluent, and a detector or collecting device depending on whether an analytical or preparative approach is intended. TREF needs to be performed at the high temperatures (up to 160°C) demanded by the polyolefin dissolution step. In TREF, the separation requires two temperature cycles (crystallization and dissolution) as shown schematically in Fig. 13. Once the polymer sample is dissolved in a proper solvent at high temperature, the solution is introduced into a column containing a non-active support; this is followed by a crystallization step at a slow cooling rate during which polymer fractionation will occur, as the temperature drops, by deposition (crystallization) of layers of decreasing crystallinity or increasing branch content on the column support particles; fractionation takes place within this cycle that is usually carried out at a low crystallization rate.

At this stage, the polymer is already segregated into crystal aggregates of different composition on the inert support particles inside the column although all of them are still mixed together (there is not yet a physical separation of fractions). The TREF technique still requires a second temperature cycle to quantify or collect those fractions of different crystallinity. This is achieved by washing the column with new solvent while the temperature is being increased. The eluent dissolves fractions of increasing crystallinity, or decreasing branch content, as temperature rises. These fractions are monitored with an IR detector (analytical TREF) to generate the CCD curve, or collected (preparative TREF) to perform further analysis. The name temperature rising elution fractionation comes from this second temperature cycle.

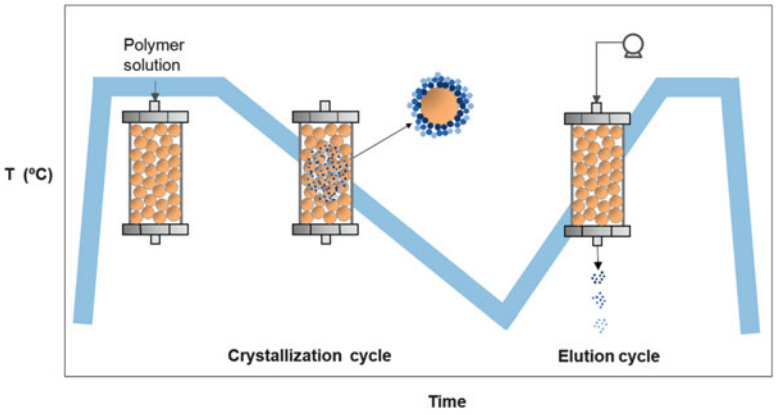

Fig. 13 The TREF process

A TREF apparatus is essentially an HPLC system with a high temperature oven to perform the crystallization and elution steps. TREF did not become commercially available until the early 1990s and most TREF users developed their own instrumentation, in most cases using an IR detector measuring the absorbance at around 3.5 μm (C–H stretching band).

As with GPC, automation of a TREF apparatus is important to minimize solvent handling and to reduce manpower involvement and there have been various approaches in the past. Hazlitt et al. [85] reported an automated TREF apparatus with four columns in independent ovens. More recently, a fully automated TREF apparatus was introduced commercially [86] in which a significant effort was made on the sample preparation step. Up to five samples can be loaded at a time and the whole process is automated from sample dissolution to column loading and temperature rising elution; once the analysis of the first sample has been completed, the equipment continues with the dissolution and analysis of the other samples. A schematic diagram is shown in Fig. 14.

The demand for faster TREF analysis prompted the use of autosamplers, which can replace the dissolution vessels shown in Fig. 14 and avoid keeping samples at high temperature for longer times than required [87]. Yau and Gillespie [88] built a combined GPC and TREF apparatus on an existing GPC instrument that could share autosampler, pump, and detectors for both techniques.

TREF columns are typically 10–15 cm long and with an internal diameter of 3–9 mm. The columns are filled with an inert support such as glass beads, diatomaceous earth (Chromosorb), or stainless steel shots of 100–200 μm particle size.

The solvents used in analytical TREF are limited to chlorinated solvents, mainly *ortho*-dichlorobenzene and 1,2,4 tri-chlorobenzene (perchloroethylene and α-chloronaphtalene have also been used), which can dissolve the polyolefins at high temperature and are transparent enough in the IR region of measurement. These solvents are the same as used in GPC/SEC analysis of polyolefins and are also appropriate for detection by refractive index, although this detector has not

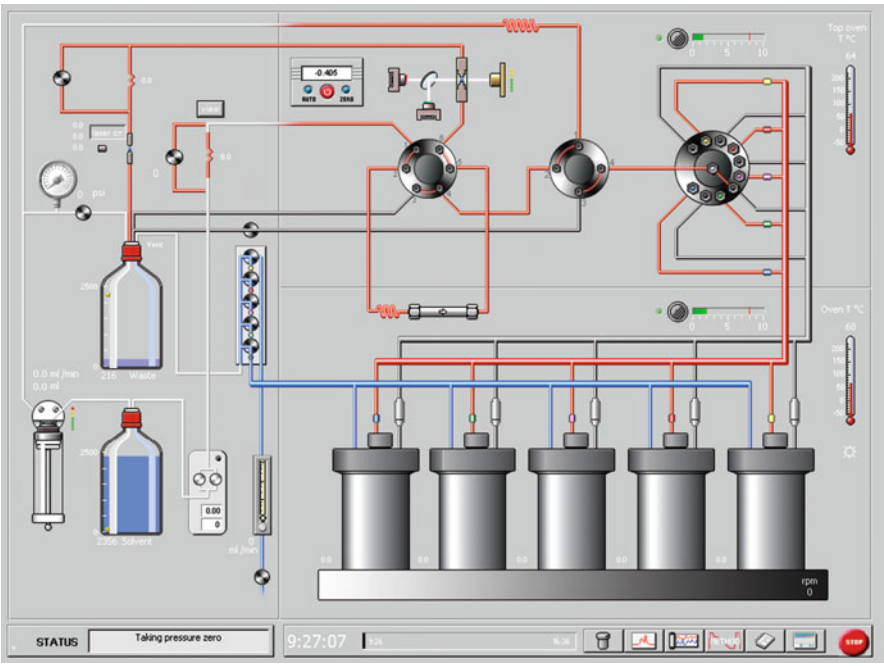

Fig. 14 TREF instrument operation diagram. In-line viscometer and light scattering detectors

been very popular in TREF due to its strong sensitivity to temperature changes in this non-isothermal process. Today, the solvent most used is *ortho*-dichlorobenzene because of its low freezing point (−17°C), which allows crystallization to sub-ambient conditions, thus extending the crystallization range for the analysis of less crystalline resins. The solvent does not influence the separation mechanism in TREF analysis but elution temperatures will be shifted depending on the solvent power, as discussed by Glöckner [68]. Monrabal et al. [89] have shown the possibility to extend the TREF analysis to less crystalline polymers by the use of more polar solvents.

Solution concentrations of 0.5% are usually prepared in vials or dissolution vessels and injection of 1–5 mg of polymer are loaded onto the column in analytical TREF. The more sensitive detectors should be used to allow for the lowest concentration possible in order to reduce co-crystallization and entrapment effects. Polyolefin homopolymers, which elute in a narrow temperature range, may often result in column plugging, especially if they have large molar mass; in those cases, a lower concentration of sample should be used for injections.

In TREF analysis, besides the mass of polymer injected into the column, the dissolution and flow rates will contribute to the detector signal response. The mass of polymer being dissolved per unit time is proportional to the heating rate, thus the concentration reaching the detector can be expressed by (3), where HR is the heating rate, F the flow rate and k is a function of the polymer microstructure and mass injected:

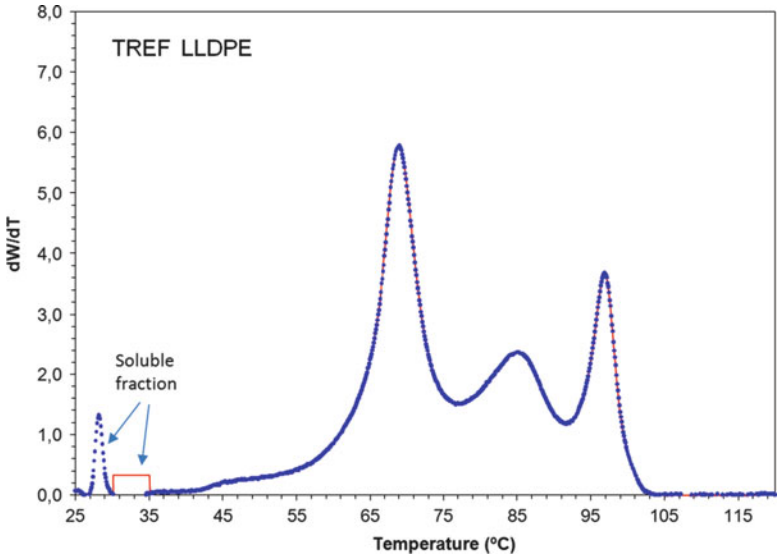

Fig. 15 TREF analysis of a LLDPE resin. Soluble fraction as eluted (*peak*) or after calculation (*rectangle*)

$$c = k \cdot \mathrm{HR}/F. \tag{3}$$

For the same amount of sample injection, keeping the HR/F ratio constant will maintain the same detector response.

The crystallization process is the most important step in the TREF analysis; it is in this process where fractions are segregated according to their crystallizability and it is preferably used at the lowest cooling rate to minimize co-crystallization effects. The lowest crystallization rate (CR) will also result in most stable crystal aggregates and will prevent unwanted re-organization during the following melting process. Typically CR of 0.1–0.5°C/min are used.

The temperature rising elution step, which gives the name to the technique, can be performed at higher rates than the crystallization step and, typically, heating rates (HR) of 0.5–5°C/min are used. Most important is to relate the heating to the flow rate used, as discussed above with (3). A slow HR with a high flow rate would elute polymer fractions in a large solvent volume and therefore with a reduced signal-to-noise ratio whereas a low flow rate and fast HR would result in a too-concentrated solution going through the column, which may result in plugging (besides loss in resolution, as discussed later in this section). Typically, flow rates of 0.5–2 mL/min are used depending on the HR being used, and are optimized for column dimensions and sample size.

The TREF elution curve resembles a chromatogram with a small peak at the beginning (typically obtained at isothermal elution), which corresponds to the fraction that has not crystallized at the lowest crystallization temperature chosen in the analysis method; this is followed by the continuous elution of the fractions of increasing crystallinity as temperature rises (as shown in Fig. 15). Cooling down

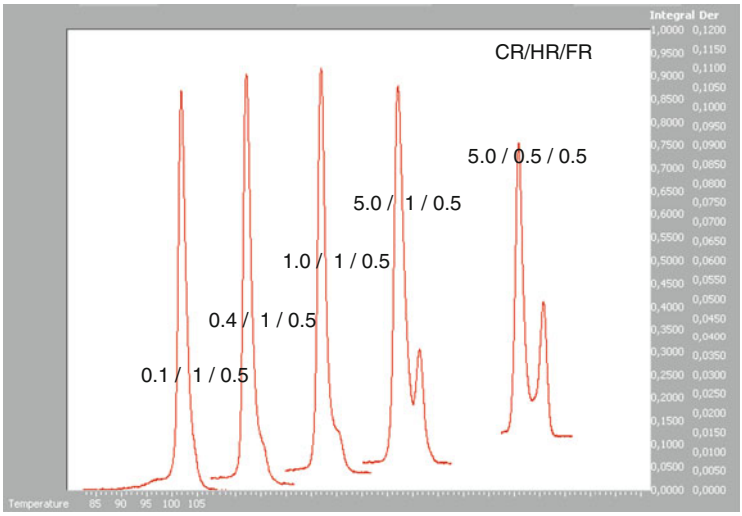

Fig. 16 TREF analysis of HDPE resin. Appearance of a double peak artifact by melt and re-crystallization phenomena

the solution to very low temperatures to achieve the overall crystallization of the sample is not always practical and, quite often, with low crystallinity samples it is not possible to reach it before the solvent itself crystallizes. In those cases, a more precise representation of the CCD is shown in Fig. 15, where the continuity of the CCD is represented down to the lowest temperature analyzed and the remaining soluble fraction is represented by a rectangle with the corresponding surface area at the lowest analysis temperature.

In TREF analysis, with a finite and usually large sample solution volume (V) injected into the column, there is a physical limit to the maximum resolution achievable, which we have defined as geometric dispersion (gd) [90], given by (4):

$$gd = \mathrm{HR} \cdot V/F, \tag{4}$$

which corresponds to the temperature range in which the same type of polymer molecules are going to be eluted at a given heating rate HR and flow rate F. For a sample volume of 0.5 mL injection (assuming that it will be diluted into the column to double that volume) and using a HR of 1°C/min, a flow rate of 1 mL/min or higher is required to achieve a gd of 1°C or lower, which is acceptable given the intrinsic low resolution of the TREF technique. The low HR/F ratios required to achieve the lowest gd in (4) compete with the high HR/F ratios demanded by (3) to have good detector response.

The use of faster crystallization rate in TREF may result in formation of metastable crystals that re-crystallize during the heating cycle and result in anomalous double peaks, as shown in Fig. 16 for the analysis of an HDPE resin at different crystallization and heating rates. Increasing the heating rate can also overcome this effect by not giving time for re-crystallization.

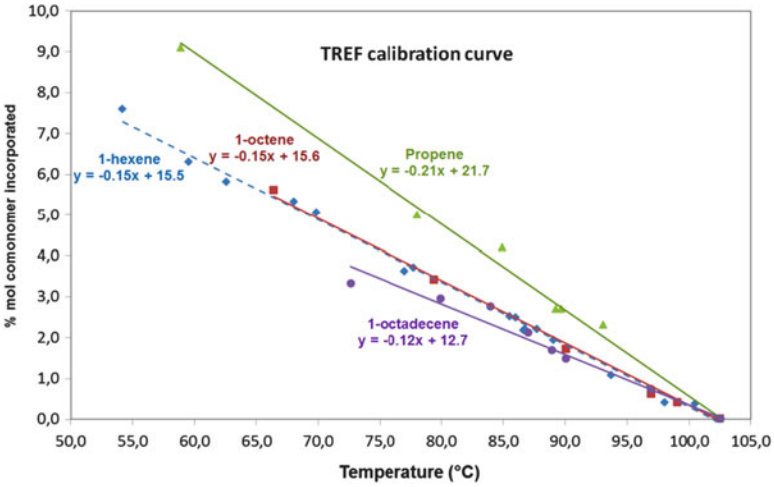

Fig. 17 TREF calibration with copolymers of different type of branches [92]

To reduce co-crystallization in polypropylene, Iiba et al. [91] proposed a temperature cycling scheme during crystallization, which they implemented in a home-made TREF using a narrow bore TREF column.

TREF analysis is still reported quite often on the basis of dissolution temperature scale, but as discussed in the introduction of Sect. 4.1 there is a linear relation between dissolution temperature and comonomer incorporation, which has been confirmed experimentally [62]. The calibration of temperature to comonomer content can be performed by using narrow composition standards (metallocene-type resins) of the same comonomer type. Boisson et al. [92] recently presented TREF calibration curves for different types of PE copolymers, as shown in Fig. 17. At the same mole percentage of comonomer incorporated, the dissolution temperature (TREF) decreases with increasing branch length. Propylene incorporation in PE with the lowest short chain branch (methyl), results in the highest dissolution temperature indicating that the methyl branch, besides being able to enter into the crystal lattice, has the lowest crystallizability perturbance. Octene and hexene copolymers can use the same calibration curve as shown in Fig. 17.

The elution order in TREF has been shown to be independent of molar mass above 10,000 g/mol [61, 62]. On the other hand, it has been shown that in the case of single-site catalyst resins the lowest molar mass results in broader composition distributions [93], as expected for purely statistical reasons [94].

The CCD curve shown in Fig. 15 contains all the information on composition distribution and it is a common practice to compare the CCD curves of the different resins to be evaluated: In addition to the CCD curve, it is convenient to work with some easy-to-use average parameters. In the case of multiple peaks (like those shown in Fig. 15), integration of the peaks is most appropriate. In bimodal LLDPE, the most important parameters to measure are the homopolymer (linear) and soluble fraction percentages. Calculation of moments similar to

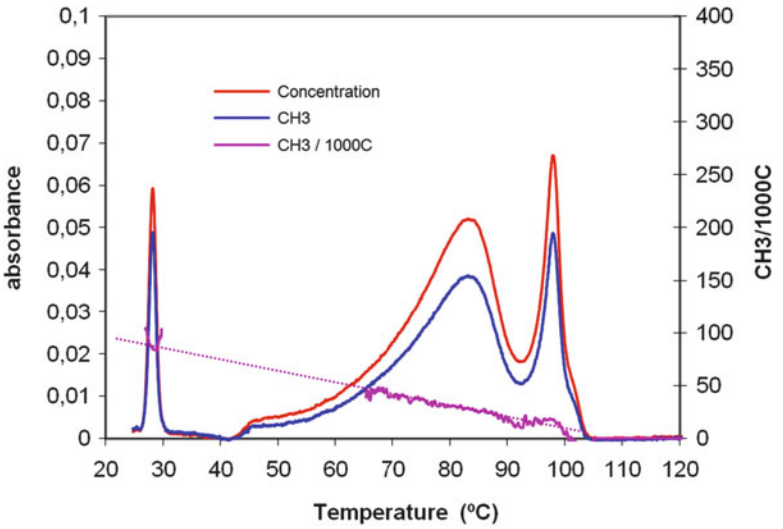

Fig. 18 TREF analysis of a LLDPE with IR detection and composition sensor. The *straight line* corresponds to the calibration curve for CH_3/1000C versus elution temperature obtained with the integrated composition sensor

average M_n and M_w values can also be practical [84], in terms of temperature or comonomer mole percentage (when calibration is performed) as shown with (5–7):

$$T_n = \frac{\sum c_i}{\sum c_i / T_i}, \tag{5}$$

$$T_W = \frac{\sum c_i \cdot T_i}{\sum c_i}, \tag{6}$$

$$r = \frac{T_w}{T_n}. \tag{7}$$

Other parameters have been proposed in the patent literature to describe the CCD, such as the composition distribution breadth index (CDBI), defined as the weight percentage of the copolymer molecules having a comonomer content within 50% of the median total molar comonomer content [95], or the solubility distribution breadth index (SDBI), which is analogous to the standard deviation of the CCD [96].

The possibility to incorporate a composition sensor in the TREF IR detector has been shown by Monrabal [97]. Two simultaneous signals are obtained, one for total concentration and a second signal emphasizing the methyl absorption in a similar way as discussed for GPC in Fig. 8. The ratio of the two signals measures the CH_3/1000C value, as shown in Fig. 18, which in the case of a PE resin analysis corresponds in fact to the TREF calibration curve and shows a linear dependence on temperature.

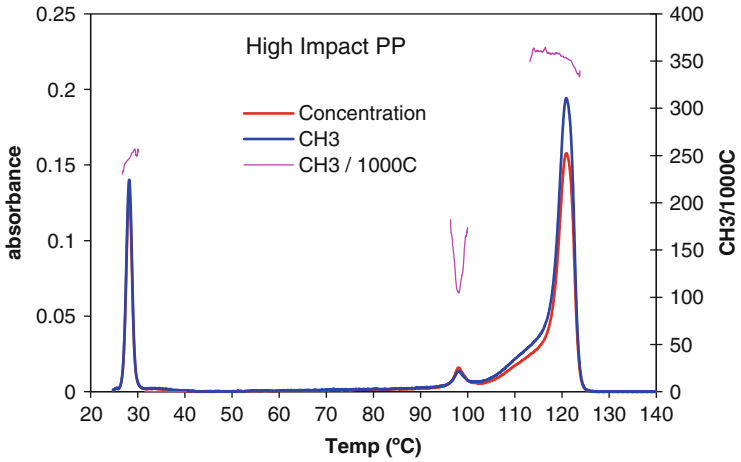

Fig. 19 TREF analysis of a high impact polypropylene. The small peak at 98°C corresponds to PE homopolymer, as deducted from the CH_3/1000C signal

The incorporation of a composition sensor is important when analyzing PP copolymers because both tacticity and branching play a role in the separation by crystallizability, as discussed in Sect. 2.2. The analysis of a high impact PP copolymer is shown in Fig. 19, where a small peak of linear PE on the tail of the PP curve is easily identified by the sudden change in methyl content.

Besides concentration and composition sensors, viscometer and/or light scattering detectors can be added to a TREF apparatus, as shown in Fig. 14, thus obtaining information on composition–molar mass interdependence, which is of important value when analyzing complex multireactor resins. An example of a TREF analysis of a complex resin with both detectors is shown in Fig. 20, where it can be seen that the less crystalline fraction is of higher molar mass than the more crystalline fraction.

TREF has also been used in the mathematical modeling of PE copolymers, as shown by Soares et al. [98].

4.1.3 Crystallization Analysis Fractionation

Crystallization analysis fractionation (CRYSTAF) was developed by Monrabal [99] in 1991 as a process to speed up the analysis of the CCD, which at that time lasted around 1 week per sample with the TREF technique. CRYSTAF shares with TREF the same principle of separation according to crystallizability. In CRYSTAF, the samples are not crystallized in a column but in a stirred vessel with no support, and only a temperature cycle (crystallization) is required [64], thus speeding up the analysis process and simplifying the hardware requirements.

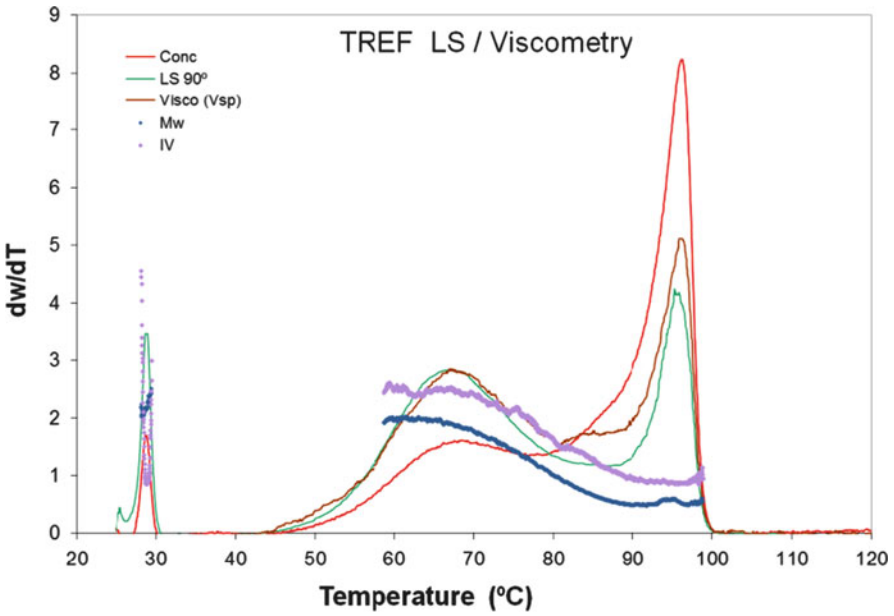

Fig. 20 TREF analysis of a complex resin with light scattering (*LS*) and viscometer (*visco*) detectors; *IV* intrinsic viscosity

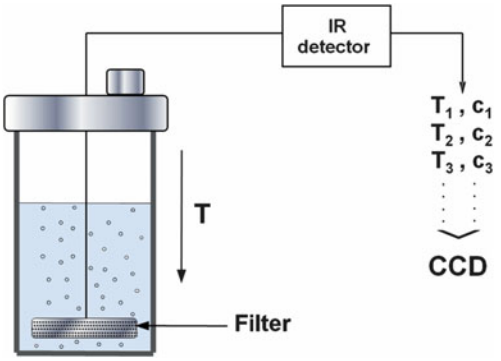

Fig. 21 CRYSTAF sampling process in a vessel with an internal filter; *T* temperature, *c* concentration

In CRYSTAF, the analytical process is followed by monitoring the polymer solution concentration during crystallization by temperature reduction. Aliquots of the solution are filtered (through an internal filter inside the vessel) and analyzed by a concentration detector at different temperatures, as shown in Fig. 21. The whole process is similar to a classical stepwise fractionation by precipitation with the exception that, in this new approach, no attention is paid to the polymer being precipitated but to the one that remains in solution.

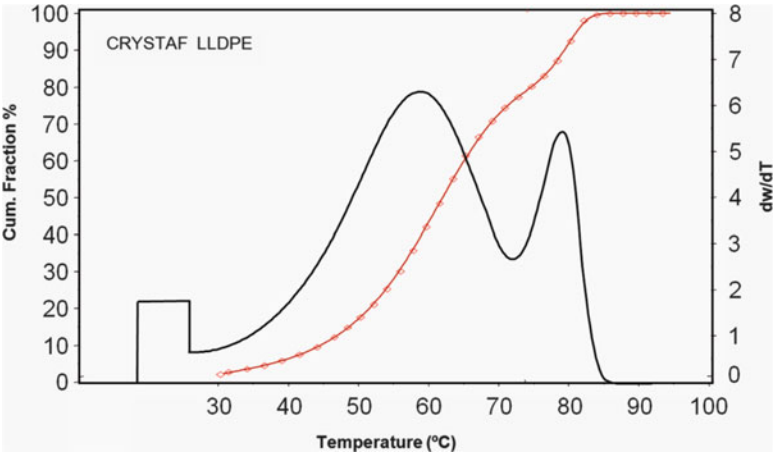

Fig. 22 CRYSTAF cumulative data points (*circles*) and the first derivative CCD curve

The first sampling points, taken at high temperatures where all polymer remains in solution, provide a constant concentration equal to the initial polymer solution concentration, as shown by the flat part of the cumulative curve in Fig. 22. As the temperature drops the most crystalline fractions, composed of molecules with less irregularities (high crystallinity), will precipitate first, resulting in a steep decrease in the solution concentration on the cumulative plot. This is followed by precipitation of fractions of increasing irregularities or branch content (lower crystallinity) as the temperature continues to drop; the last data point, which corresponds to the lowest temperature of the crystallization cycle, represents the polymer fraction that has not crystallized (mainly highly branched or amorphous material) and remains in solution at that temperature. The first derivative of this curve, shown in Fig. 22 (in this example being a LLDPE resin), corresponds to the CCD when the temperature scale is calibrated in number of branches per 1,000 carbon atoms. With this approach, the CCD can be analyzed in a single crystallization cycle without physical separation of the fractions. The term "crystallization analysis fractionation" (CRYSTAF) stands for this process.

The way the analysis is performed, by using a discontinuous sampling process while the crystallization proceeds, provides the possibility to easily automate the technique, as shown in Fig. 23 where five different samples introduced in separate crystallization vessels can be analyzed simultaneously.

During the crystallization cycle, all the vessels are "sampled" many times in a sequential manner and at the end of the analysis there are enough temperature–concentration data points for each resin to properly draw the cumulative curves, as shown in Fig. 24, with the simultaneous analysis of five LLDPE resins of different density. The complete dissolution and crystallization analysis of five samples can be carried out simultaneously in around 7 h in a fully automated way.

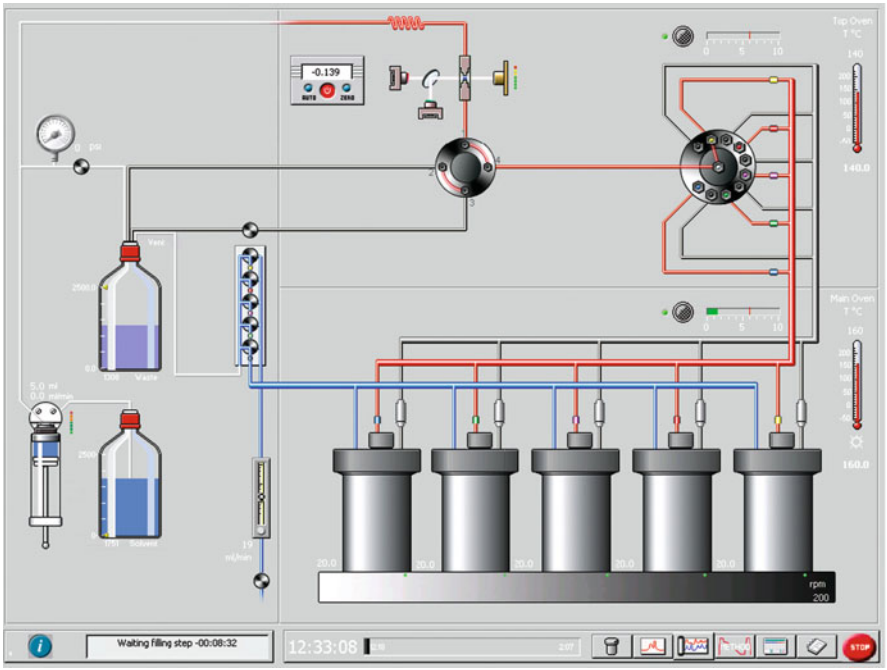

Fig. 23 CRYSTAF instrument

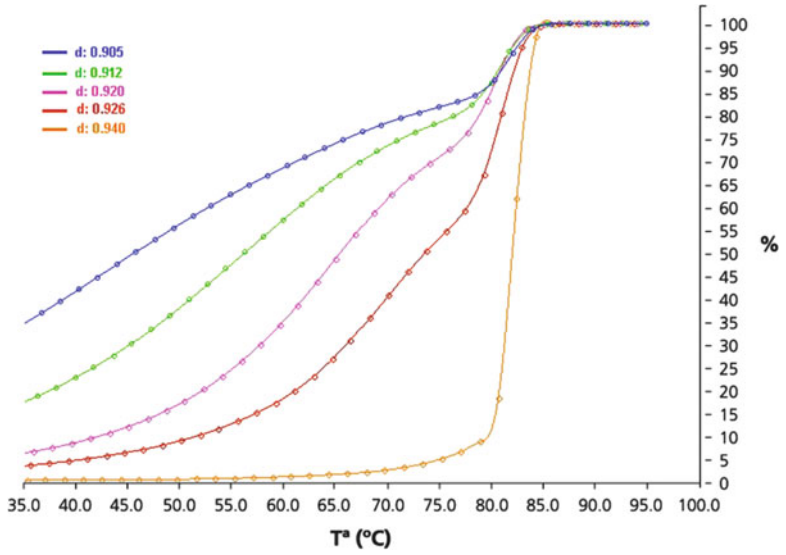

Fig. 24 Simultaneous CRYSTAF analysis of five LLDPE resins of different density (cumulative curves). 40 mg/40 mL in TCB; crystallization rate 0.2°C/min

The same solvents, same IR detector and similar calculation parameters to those presented in Sect. 4.1.2 for TREF are applicable for CRYSTAF analysis. The calibration of temperature to comonomer content can be performed by using narrow composition standards (metallocene-type resins) of the same comonomer type, with similar results to TREF as discussed in Sect. 4.1.2. Octene and hexene copolymers follow the same calibration curve [92].

Reviews of the CRYSTAF technique and applications have been presented [80, 83, 84]. Mathematical modeling of CRYSTAF crystallization kinetics has also been investigated [100].

Comparison of TREF and CRYSTAF

Both techniques share the same principles of fractionation on the basis of crystallizability. TREF is carried out in a packed column and demands two full temperature cycles, crystallization and elution (dissolution), to obtain the analysis of the composition distribution. In CRYSTAF, the analysis is performed in a single step, the crystallization cycle, which results in faster analysis time and simple hardware requirements.

TREF has the advantage that a continuous elution signal is obtained and molar mass detectors can be easily added to obtain composition molar mass interdependence; an autosampler can also be added for multiple sample analysis. CRYSTAF takes advantage of discontinuous sampling to analyze a set of samples simultaneously.

Both techniques provide similar results; the comparison of TREF and CRYSTAF has already been discussed [84] and the most significant difference is the temperature shift due to the undercooling, as analytical conditions are far from equilibrium; CRYSTAF data are obtained during the crystallization whereas TREF data are obtained in the melting-dissolution cycle. Both techniques, however, can be calibrated and the results expressed in branches/1000C will be similar for PE copolymers.

The large difference in undercooling between polypropylene and polyethylene makes the analysis of complex resins containing both PE and PP an interesting case, whereby both TREF and CRYSTAF must be used to obtain unequivocal results, as discussed in a recent publication [101]. TREF, which analyzes samples in the dissolution (melting), provides best resolution for the analysis of blends containing isotactic polypropylene and polyethylene; on the other hand, CRYSTAF, which obtains the data during the crystallization, is the preferred technique when analyzing combinations of polyethylene with ethylene-propylene copolymers resins, as seen in Fig. 25.

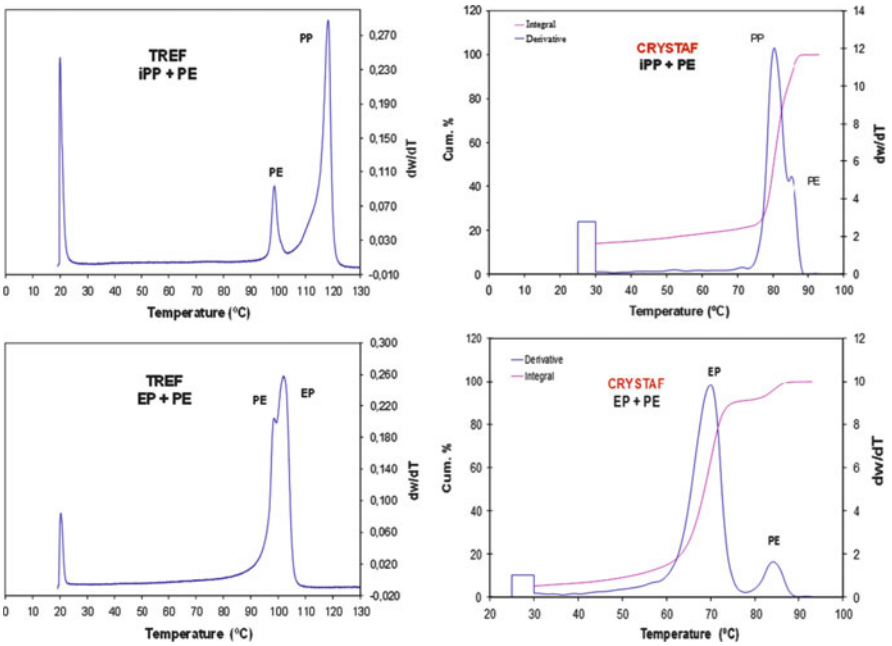

Fig. 25 TREF and CRYSTAF analysis of PE–PP combinations. TREF separates iPP + PE better and CRYSTAF separates EP + PE better

4.1.4 Crystallization Elution Fractionation

Crystallization elution fractionation (CEF) is a new separation technique developed by Monrabal [102] for the analysis of the CCD that combines the separation power of CRYSTAF and TREF. The CEF technique is based on a new and patented separation principle, referred to as dynamic crystallization (DC) [87], that separates fractions inside a column according to crystallizability while a small flow of solvent passes through the column. The separation by DC occurs during the crystallization step. CEF combines the separation power of DC in the crystallization step with the separation during dissolution of the TREF technique.

The principles of DC and CEF are presented in Fig. 26 and compared with classical TREF analysis. In TREF, the crystal aggregates formed during crystallization from the various composition families in the resin are all mixed together at the column spot where the sample was loaded. In Fig. 26a, the three different composition families crystallized in this example are deposited at the head of the column with no physical separation of the corresponding molecules. The physical separation in TREF takes place in the elution cycle.

CEF analysis follows similar steps as in TREF, but during the crystallization cycle a small solvent flow, FC, is passed through the column in such a way that when molecules of a given composition reach their crystallization temperature, they are segregated from solution and anchored on the support. Meanwhile, the

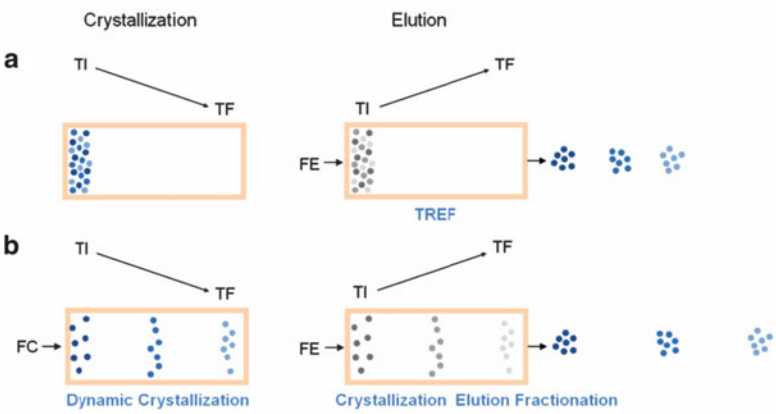

Fig. 26 Separation by crystallizability: (**a**) TREF separation process, (**b**) dynamic crystallization and crystallization elution fractionation. TI initial crystallization and elution temperatures, TF final crystallization and elution temperatures, FE elution flow, FC crystallization flow

other components of lower crystallinity, still in solution, move along the column until they reach their own crystallization temperature. At the end of the crystallization cycle, the three composition families shown in Fig. 26b are physically separated inside the column according to crystallizability; this process is referred to as dynamic crystallization and can separate components in a similar fashion as CRYSTAF although all polymer molecules still remain inside the column in three different locations.

Once the DC separation step has been completed, it is easy to realize the possibility to combine it with a final elution cycle as in TREF to obtain a new *extended* separation as shown in Fig. 26b by the improved separation of the three components at the exit of the column in CEF analysis as compared to the TREF approach. It is quite interesting that the separation power of CRYSTAF and TREF are combined in CEF when both systems are based on the same crystallizability principles. To obtain the maximum benefit of the DC process, the column volume must be large enough and the flow rate in the crystallization (FC) has to be adapted to the crystallization rate (CR), crystallization temperature range (ΔT_c) of the components to be separated, and column volume (V) as described by (8):

$$\mathrm{FC} = \frac{V}{\Delta T_c} \times \mathrm{CR}. \tag{8}$$

The calculated flow FC implies that all the components will be separated along the whole length of the column.

The CEF instrument is similar to an HPLC or TREF apparatus, as shown in the schematic diagram of Fig. 27; the main CEF characteristic is the ability to provide a small controlled flow during the crystallization process.

CEF has been shown to provide reproducible and very fast analysis of the composition distribution of polyolefins for high-throughput applications [87], as

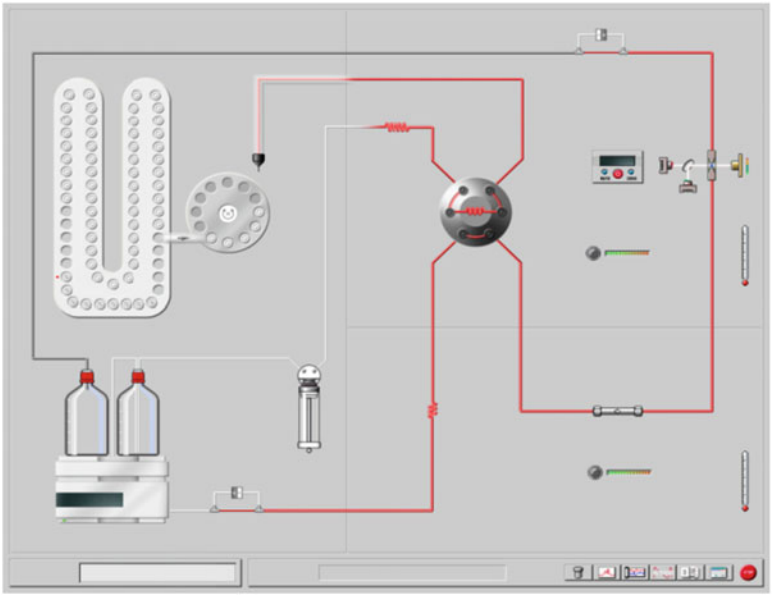

Fig. 27 CEF/TREF apparatus with autosampler

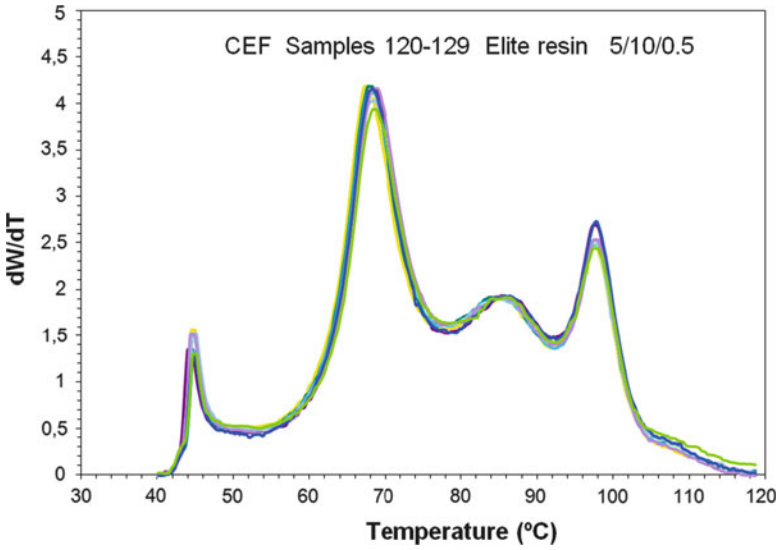

Fig. 28 Multiple CEF analysis (×10) of an Elite resin obtained at crystallization rate of 5°C/min and heating rate of 10°C/min; injection volume, 20 μL of 0.5%w/v; elution flow, 0.5 mL/min; analysis time per sample, 25 min

shown in Fig. 28. The analysis of a complex multireactor LLDPE resin is completed in less than 30 min with reasonable resolution and good reproducibility, as shown by the repeated analysis (ten times) of the same sample.

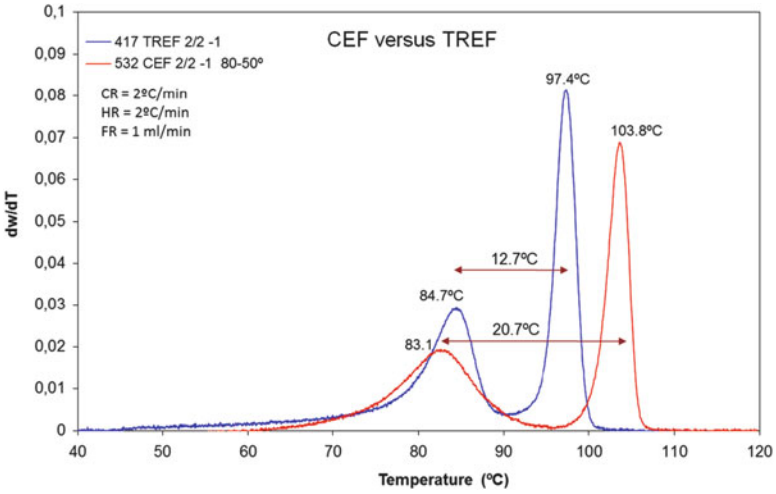

Fig. 29 CEF and TREF analysis of a 50/50 blend of two metallocene-type resins of very close density at 2°C/min cooling rate. Crystallization flow in CEF was 0.4 mL/min; elution flow in both CEF and TREF was 1 mL/min [90]

A comparison of techniques has shown a significant improvement in separation with CEF over TREF [90] when analyzing blends of very close comonomer content, as presented in Fig. 29. The importance of optimizing the DC step, responsible for the extended CEF separation, has been shown in this example. The better separation obtained in CEF as well as a lower co-crystallization can be interpreted by the combination of the two separation processes.

4.2 Chromatography-Based Techniques

The use of HPLC in the analysis of copolymers was already quite established in the 1990s [103, 104]. A significant effort was demanded to apply this technique to the analysis of polyolefins because of the high temperatures required for the dissolution of the polymer and the new solvents and detectors needed for work under gradient conditions. It was the work of Professor Pasch's group at DKI (German Institute for Polymers, Darmstadt) during the last decade that established the basis of this new tool, which is sometimes referred to as "interaction chromatography."

Most extensive work has been done by Macko et al. using a solvent gradient on silica- or carbon-based columns and using an evaporative light scattering detector (ELSD), as reviewed recently [105] and discussed in Sect. 4.2.1.

In recent years, a new approach by Cong et al. using a thermal gradient instead of a solvent gradient system on the same carbon-based column has demanded

significant attention because of the simplicity of the isocratic system and easy detection, as will be discussed in Sect. 4.2.2.

Both solvent gradient and thermal gradient systems have become new tools for characterizing copolymers in short analysis times and for extending the range of polymers to be analyzed towards the elastomers region that could not be characterized by crystallization techniques.

4.2.1 Solvent Gradient Interaction Chromatography

The use of a solvent/non-solvent approach to separating PE and PP in a preparative mode was shown by Lehtinen et al. [106] using ethylene glycol monobutyl ether (EGMBE) as a non-solvent. Macko et al. [107] were the first to implement this approach in analytical HPLC, using EGMBE as a mobile phase in an isocratic mode but depositing the polymer in the column with TCB; a separation of PE and PP was obtained but without full recovery of the PE resin. Heinz et al. [108], from the same group at DKI, used a solvent gradient approach (EGMBE-TCB) to achieve a separation of PE and PP (for PE of molecular weight higher than 50,000 g/mol) with full recovery of PE. A similar approach was used by Albrecht et al. [109] to separate EP copolymers and ethylene-vinyl acetate (EVA) resins [110], and by Dolle et al. [111] to characterize an LLDPE resin.

In all cases, an ELSD was the only possible detection system because of the solvent gradient. Pasch et al. [112] reported the separation of EVA and ethylene-methyl acrylate (EMA), and also combined the solvent gradient separation with collection of germanium disks for FTIR measurement.

A significant breakthrough came with the separation of polyolefins by adsorption on a carbon-based column (Hypercarb); Macko and Pasch [113] obtained a separation of isotactic, syndiotactic, and atactic polypropylene together with linear polyethylene using a gradient of decanol-TCB in a very short analysis time, as shown in Fig. 30.

Using the same Hypercarb column and eluents, Macko et al. have shown a separation of ethylene copolymers by the level of comonomer incorporation [114, 115]. Similar results were obtained by Miller et al. [116] on the same Hypercarb column. The presence of branches in the ethylene copolymers reduces the adsorption potential on the atomic level flat surface of graphite and a linear correlation is obtained between the comonomer mole percentage incorporated and the elution volume, as shown in Fig. 31 for various types of copolymers.

Solvent gradient interaction chromatography (SGIC) can be used to analyze copolymers in the whole range of 0–100% of comonomer incorporation, which was not possible with crystallization techniques.

The combination of SGIC with SEC in a second dimension (SGIC2D) was shown by Roy et al. [117] using a gradient of decanol or EGMBE and TCB on a Hypercarb column; a second dimension with the standard GPC columns and isocratic TCB solvent was used with IR detection. Besides the convenience and linearity of the IR detector, the molar mass–composition interdependence could be

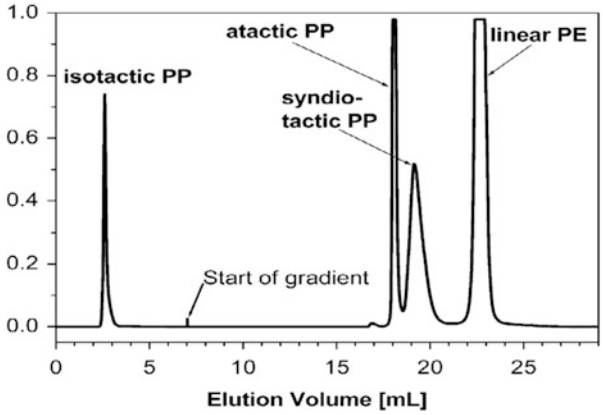

Fig. 30 SGIC analysis of polyethylene and polypropylenes of different tacticity on a Hypercarb column [113]

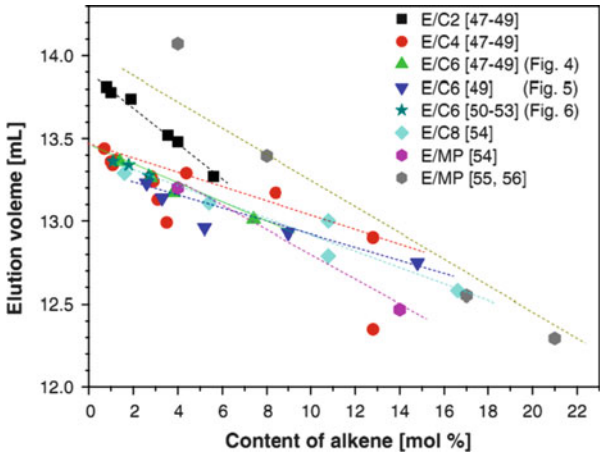

Fig. 31 Analysis of different ethylene copolymers by interaction chromatography on a Hypercarb column [115]

analyzed as shown in the analysis of ethylene octene copolymers in Fig. 32. Another advantage of SGIC2D is that a light scattering or viscometer detector could be added in the second isocratic dimension.

Ginsburg et al. [118] have used SGIC2D for the characterization of ethylene propylene and ethylene propylene diene (EPDM) rubbers; the technique provides a new approach to full characterization of resins in terms of composition–molar mass interdependence that cannot be fully analyzed by TREF-GPC because of the low crystallinity of the resins. Cheruthazhekatt et al. [119] have used SGIC2D together with other techniques to fully characterize high impact polypropylene. The SGIC technique attracted interest at the recent International Conference on Polyolefin Characterization (ICPC, Houston, October 2012), with general

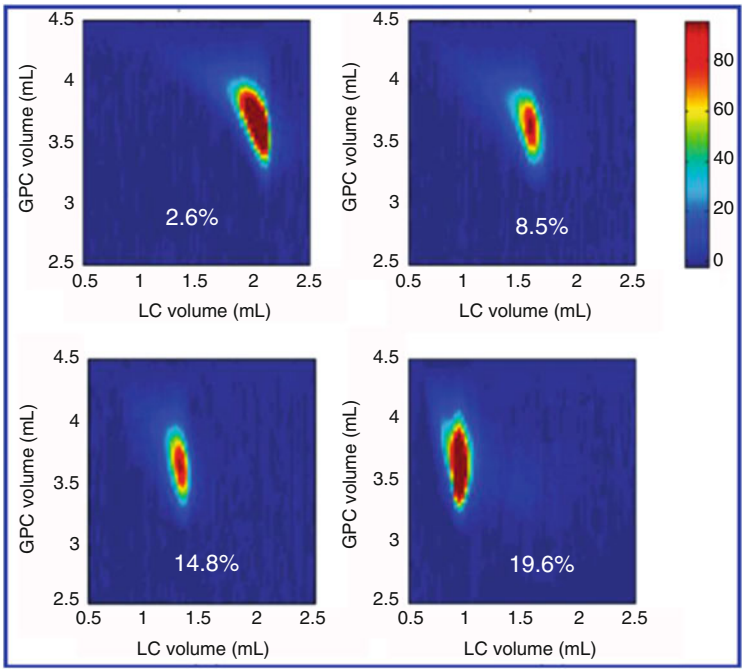

Fig. 32 SGIC2D analysis of ethylene octene copolymers [117]

papers from Pasch and Brüll, investigations on the graphite porosity influence on the separation mechanisms by Mekap, and combinations of SGIC with DSC and FTIR by Cheruthazhekatt.

4.2.2 Thermal Gradient Interaction Chromatography

Solvent gradient HPLC can be successfully replaced by thermal gradient using reverse phase columns to analyze copolymers, as shown by Chang et al. [120]. At the 3rd International Conference on Polyolefin Characterization in 2010, Cong et al. [121] showed the possibility of using the Hypercarb column with a thermal gradient for the analysis of ethylene copolymers [122]. The separation obtained was similar to the results previously discussed in SGIC but in this case at isocratic conditions, which allowed the use of a linear IR detector as well as an in-line viscometer or LS molar mass detection. The separation of a series of ethylene octene copolymers covering a broad range of comonomer incorporation is shown in Fig. 33. A linear relation is obtained between elution time and mole percentage of comonomer incorporation, and elution is independent of molar mass for molecular weights higher than 20,000 g/mol.

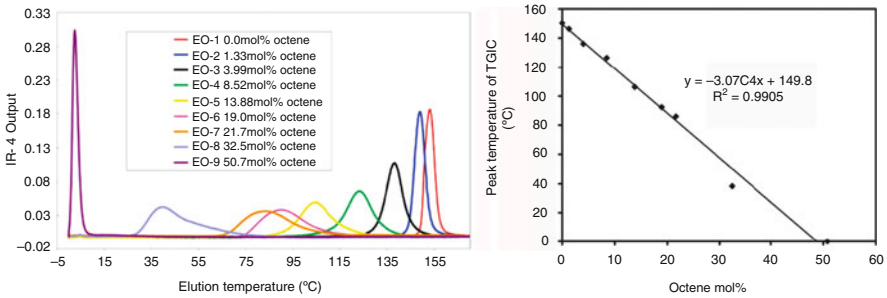

Fig. 33 TGIC analysis of a series of octene copolymers on a Hypercarb column (*left*) and calibration curve (*right*) [122]

The comparison of TGIC and TREF for a series of ethylene octene copolymers has been reported by Monrabal et al. [123], showing that resolution on TREF is slightly better than TGIC. TGIC, however, does not suffer from co-crystallization effects and covers a broader copolymer range down to the elastomer region, which crystallization techniques cannot reach.

Cong et al. [124, 125] have shown that other graphitized carbon packings provide similar results to those of Hypercarb. Monrabal [126] explained the separation mechanism on graphite by weak van der Waals forces and steric hindrance on an atomic-level flat surface like graphene, where the chemical structure of graphene should not be as important for interaction with the non-polar polyolefins; this was confirmed by using other types of layered packing materials like molybdenum sulfide, which provided the same separation order as the Hypercarb column [126, 127] in spite of totally different surface chemistry and polarity, as shown in Fig. 34 for a series of ethylene octene copolymers. The peaks were broader in the molybdenum sulfide column due to the broad particle size used as compared to the Hypercarb narrow particle size packing.

Other layered packings like boron nitride and tungsten sulfide showed adsorption and similar selectivity for ethylene copolymers and polypropylenes as the Hypercarb packing [126, 127] shown in Fig. 35, whereas the TREF column with metal shots or glass beads (but non-layered packings) separated by crystallization at significantly lower temperatures.

The speed and simplicity of the TGIC technique together with the possibility of using multiple detectors are of great significance for the characterization of polyolefins, especially in the elastomers region, and has attracted attention, with various papers being presented at the recent International Conference on Polyolefins Characterization (ICPC, Houston October 2012), which will be published in a forthcoming Macromolecular Symposia book. Cong [125] reported the application of TGIC in the analysis of block copolymers and emphasized the use of triple detector in the analysis by TGIC. Monrabal [127] presented the separation on non-carbon packings like molybdenum sulfide and boron nitride, proposed a new separation mechanism on atomic-level flat surfaces packings, and showed that addition of polar solvents did not change the selectivity of adsorption on those layered packings by TGIC. An explanation for the unusual elution of iPP in TGIC

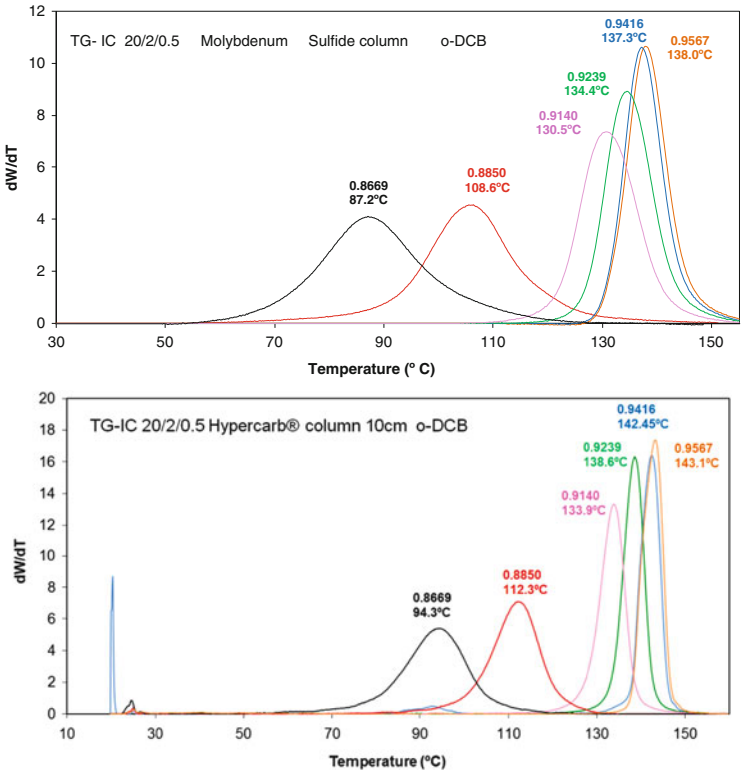

Fig. 34 TGIC analysis of a series of octene copolymers on Hypercarb and molybdenum sulfide [126]

was provided, i.e., that the adsorption of iPP on Hypercarb or other layered packings is so weak that polymer crystallizes at a higher temperature than that at which adsorption occurs, and thus iPP is eluted in TREF mode.

5 Bivariate Distribution: Characterization Techniques

The CCD and the MWD are the most relevant microstructure parameters of a polyolefin resin with a given comonomer type. There are other features, however, that need to be characterized such as LCB and its distribution or the intramolecular homogeneity, but most important for full characterization of a classic polyolefin resin is analysis of the dependence of molecular mass on composition, also known as the bivariate distribution.

For many years the only possibility to measure the bivariate distribution was by preparative fractionation followed by analysis of the fractions by the second

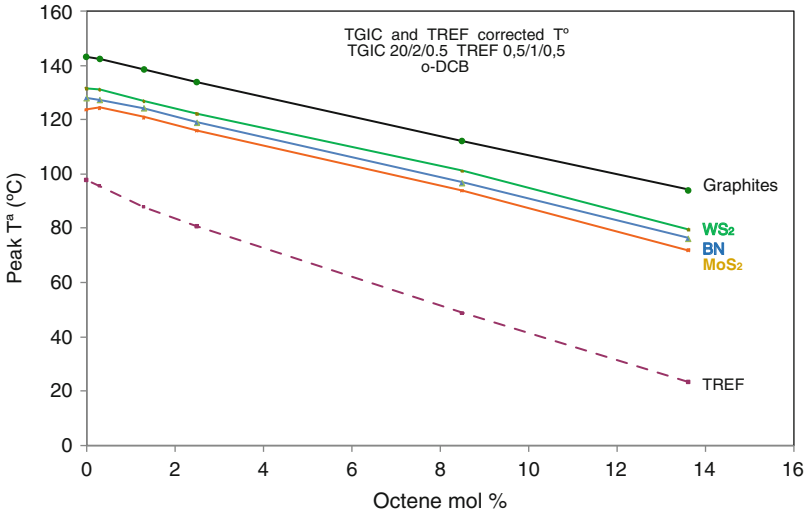

Fig. 35 TGIC analysis of a series of octene copolymers on different adsorbents and comparison with a TREF column [127]

dimension technique. In that case there are two possible analytical routes to perform the cross-fractionation:

1. To first fractionate the polymer on the basis of molecular mass followed by composition analysis (TREF)
2. To first fractionate the polymer on the basis of composition (TREF) followed by molar mass analysis (GPC)

Aust et al. [128] have used the molar mass fractionation first on a medium density polyethylene, and Faldi and Soares [129] the composition fractionation first on an LLDPE resin. One should choose the fractionation technique that results in the most discriminated fractions [80] in the first step. The most general approach is to use preparative TREF fractionation because the CCD is usually more discriminating than the MMD in complex polyolefins.

A major achievement in automation was done by Nakano and Goto [130], who combined a TREF with a GPC as early as 1981 and presented the full information of the bivariate distribution in three dimensional (3D) plots (contour maps or bird's-eye views) as shown in Fig. 36.

More recently, Li Pi Shan et al. [131] built a home-made TREF-GPC cross-fractionation apparatus, which was later modified by Gillespie et al. [132] to perform GPC-TREF as well. However, in subsequent years the TREF-GPC combination has been the preferred mode of operation.

A commercial TREF-GPC bench-top apparatus was developed by Polymer Char in collaboration with Mitsubishi Petrochemical in 2005. A description of the technique is given by Ortín et al. [133] and a schematic diagram is shown in Fig. 37.

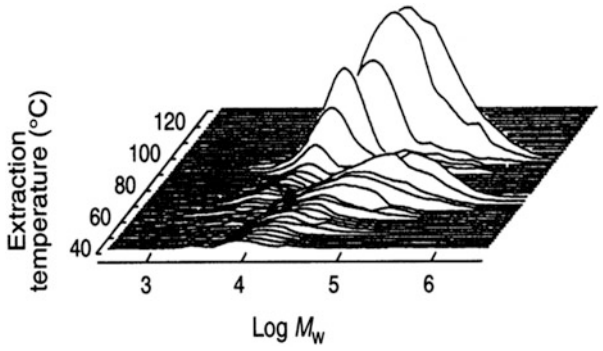

Fig. 36 TREF-GPC [130]

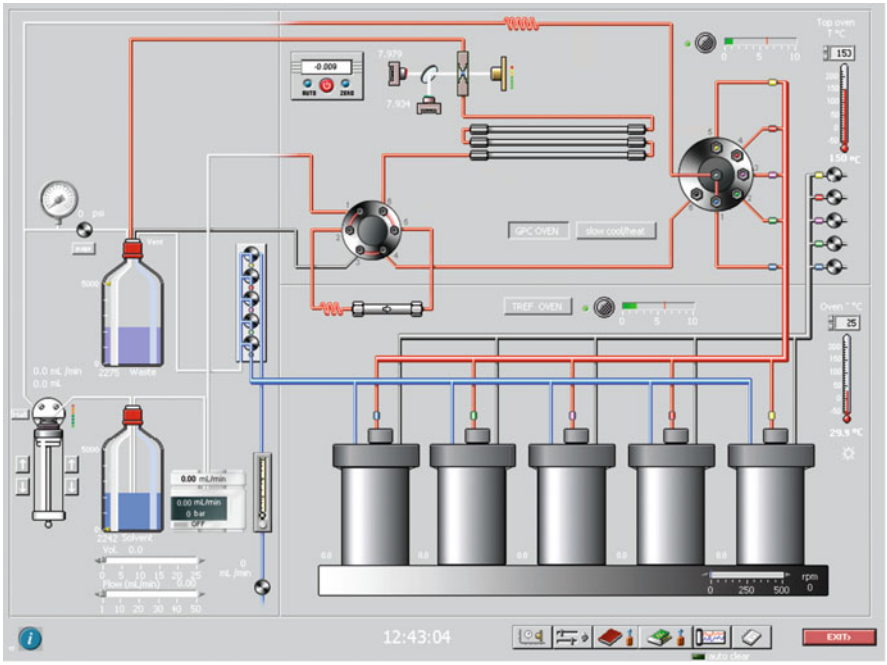

Fig. 37 Cross-fractionation instrument TREF-GPC

The sample is dissolved automatically and loaded into the TREF column to undergo crystallization. The temperature rising elution is performed in isothermal steps, as shown in Fig. 38, and at each temperature step the column is washed and the solution injected into the GPC columns, in this particular example being an LLDPE resin.

Cross-fractionation analysis performed with a sufficient number of isothermal steps (high resolution) takes a longer time but provides unexpected views of the

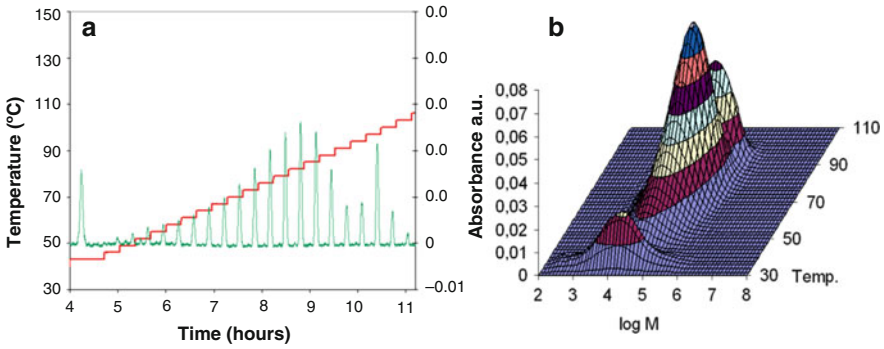

Fig. 38 (**a**) TREF isothermal steps with GPC obtained at each temperature. (**b**) 3D plot of the reconstructed bivariate distribution of an LLDPE resin

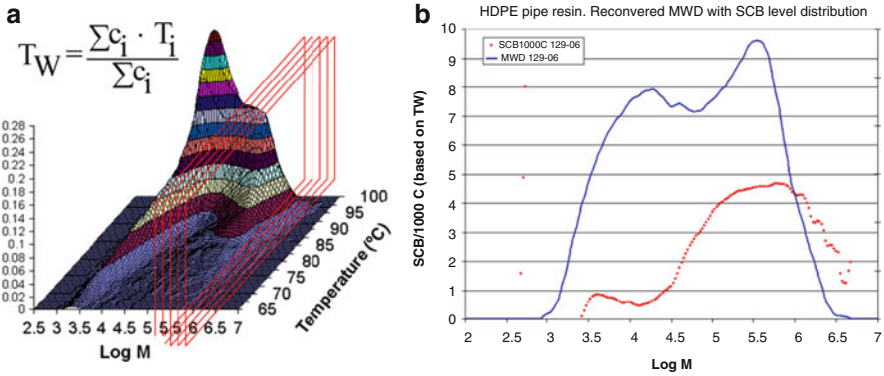

Fig. 39 (**a**) High resolution cross-fractionation (TREF-GPC) of a pipe resin and (**b**) reconstructed MMD with comonomer content plotted against the molar mass (*M*)

polymer structure [133], as shown by the analysis of a bimodal pipe resin in Fig. 39. By calculating the average temperature of each slice in the temperature axis and transfering the value to methyls per thousand carbons, the 2D view could be reconstructed with similar results to those obtained by GPC-IR, as shown in Fig. 39b.

The TREF-GPC analysis can be performed with an additional composition sensor (CH_3 sensor), as discussed in previous sections. This is especially important for ethylene propylene copolymers or blends since crystallizability is influenced in the case of PP by both tacticity and ethylene incorporation, as discussed for Fig. 4. The composition sensor provides a means to assign the crystallization temperature to one or the other polymer. The analysis of a high impact PP containing a significant amount of PE homopolymer is shown in Fig. 40. A small peak eluted before the iPP is clearly associated with PE by having a significantly lower methyl content than the overall concentration response. The PE peak is eluted on the tail of the iPP where other EP species are also eluted (as discussed with Fig. 19) and the molar mass of the PE peak could be differentiated from the polypropylene part.

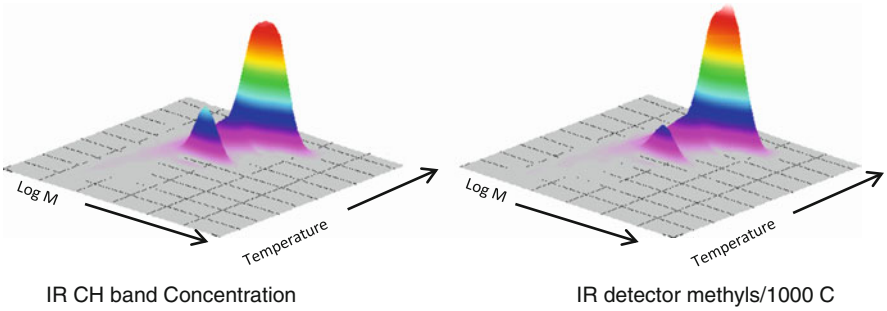

Fig. 40 TREF-GPC of a high impact PP with a significant amount of PE homopolymer. The analysis was performed with an additional CH_3 sensor. The amorphous fraction was not analyzed

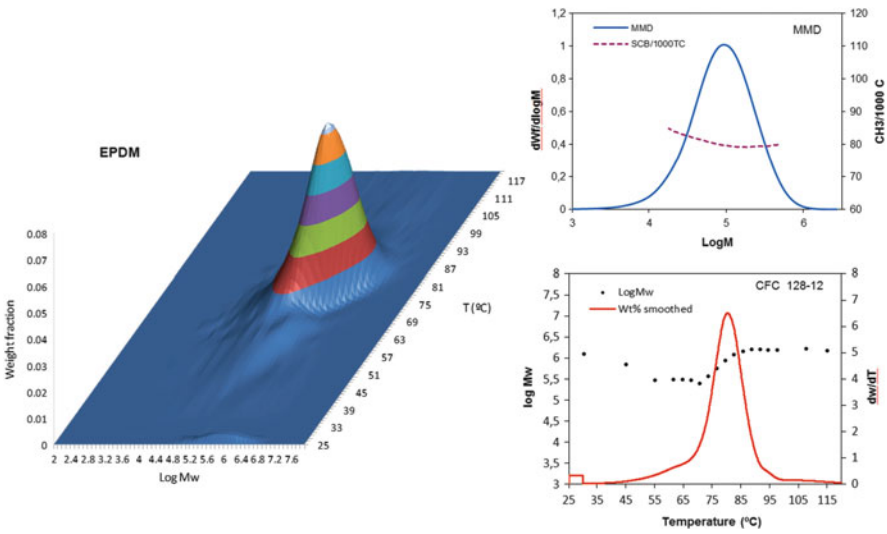

Fig. 41 *Left*: TGIC-GPC of an EPDM sample. *Right*: Reconstructed CCD and MMD with second dimensions

Besides TREF-GPC, we discussed in Sect. 4.2.1 that SGIC with a carbon-based column combined with GPC (SGIC2D) could also provide composition–molar mass interdependence [117, 118]. When dealing with more amorphous polymers, the interaction chromatography modes SGIC or TGIC are the most appropriate.

Quite interestingly, the combination of TGIC and GPC can be performed in the same instrument as the TREF-GPC; it only requires to replace the TREF column with the TGIC one. This is especially interesting given the method simplicity of the TGIC and TREF modes, with no requirement for a solvent gradient and easier availability of detectors than for the SGIC approach.

The analysis of an EPDM sample by TGIC-GPC is shown in Fig. 41 [134]. The amorphous EPDM polymer would not crystallize in TREF but it is adsorbed

on a atomic-level flat surface like carbon or molybdenum sulfide. The desorption volumes at increasing isothermal steps are injected into the GPC column, to obtain the composition–molar mass interdependence in a 3D plot or the 2D projections on the molar mass or composition curves of Fig. 41.

6 Summary, Conclusions, and Outlook

Polyolefins account for more than 50% of all synthetic polymers being produced today. The volume and applications of polyolefins have been substantially growing since the time of the Ziegler and Natta discoveries. With the introduction of metallocene and other single-site catalysts, polyolefins, with the simple chemistry of carbon and hydrogen, have evolved into complex microstructures that can be designed through multiple reactor–catalyst processes to achieve a desired performance for specific applications.

The characterization of the new polyolefins necessarily demands a separation step of the polymer by certain parameters and, in most cases, a cross-fractionation is required to obtain the full bivariate distribution. Other features like long chain branching and stereoregularity need to be characterized as well and eventually as a function of molar mass.

Molar mass distribution is a dominant microstructure parameter that, in copolymers, needs to be measured with additional information to account for long chain branching, comonomer incorporation, or ethylene propylene combinations (in the case of EP copolymers). The combination of GPC and IR spectroscopy has been shown to be of great value in the characterization of copolymers. The importance of automation and sample care, especially in the case of polypropylene, has been discussed as well as the significant improvement in sensitivity by the use of IR MCT detectors. There are big expectations for the analysis of ultrahigh molar mass polyolefins by the new AF4 technology.

Chemical composition distribution has become the most significant microstructure parameter in the new complex polyolefins, where different polymer families are often part of the same resin. Crystallization techniques are the most used for measurement of the CCD and a new technique, CEF, has been shown to be of value for high-throughput applications, with CCD measurements in less than 1 h. Crystallization techniques can be combined with viscosity and light scattering detectors to obtain the composition–molar mass interdependence.

The most recent development in separation is the development of high temperature interaction chromatography, which extends the composition distribution analysis to polyolefin copolymers of very low crystallinity, which is not possible to analyze by crystallization techniques. The analysis of complex polymers with different composition can be analyzed in a short time by solvent gradient interaction chromatography, SGIC, on an atomically flat surface like carbon or molybdenum sulfide packing. The addition of a second separation step by GPC (SGIC2D) provides the capability to obtain full composition–molar mass dependence.

Thermal gradient interaction chromatography (TGIC), with same type of columns as with SGIC, has been shown to be a very attractive variation because of easier detection by IR and the possible use of integrated in-line molar mass detectors.

Cross-fractionation chromatography, separating in a first step by composition followed by molar mass, is a very powerful approach to obtaining the full bivariate distribution of classical polyolefins and the most complete characterization of complex resins. TREF-GPC, TGIC-GPC, and SGIC2D are the various modes that can be used to obtain the three-dimensional analyses. Although not covered in this review, one should not forget the value of preparative fractionation combined with other separation techniques to obtain the three-dimensional plots as well as intramolecular characterization by spectroscopic techniques.

References

1. Staudinger H, Heuer W (1930) Highly polymerized compounds XXXIII. A relation between the viscosity and the molecular weight of polystyrenes. Ber dtsch Chem Ges B 63:222–234
2. Ziegler K, Holzkamp E, Breil H, Martin H (1955) Angew Chem 67:426–541
3. Haenel M (2008) Historical sites of chemistry. Karl Ziegler. Max Planck Institute for Coal Research, Mülheim an der Ruhr
4. Hogan JP, Banks RL (1958) US patent 2,825,721
5. Hogan JP, Banks RL (1986) History of crystalline polypropylene. In: Seymour RB, Cheng T (eds) History of polyolefins. D Reidel, Dordrecht, pp 103–115
6. Sinn H, Kaminsky W (1980) Adv Organomet Chem 18:99
7. Kaminski W (2004) J Polym Sci A Polym Chem 42:3911–3921
8. Natta G (1955) Makromol Chem 16:213
9. Natta G, Danusso F (eds) (1967) Stereoregular polymers and stereospecific polymerizations. Pergamon, Oxford
10. Moore JC (1964) J Polym Sci A2:835–843
11. Giddings JC (1966) Sep Sci 1:123–125
12. Yau WW, Kirkland JJ, Bly DD (1979) Modern size exclusion liquid chromatography. Wiley, New York (2nd edn. with Striegel AM in 2009)
13. Provder T (ed) (1999) Chromatography of polymers. ACS symposium series, vol 731. ACS, Washington
14. Grubistic Z, Rempp R, Benoit H (1967) J Polym Sci B 5:753
15. Cheung P, Lew R, Balke S, Mourey T (1993) J Appl Polym Sci 47:1701–1706
16. Scholte T, Meijerink N, Schoffeleers H, Brands A (1984) J Appl Polym Sci 29:3763–3782
17. Drott EE, Mendelson RA (1970) J Polym Sci A 2(8):1361–1371
18. Cote JA, Shida M (1971) J Polym Sci A 2(9):421–430
19. Servotte A, De Bruille R (1975) Die Makromolekulare Chemie 116:203–212
20. Usami T, Gotoh Y, Takayama S (1991) J Appl Polym Sci 43:1859–1863
21. De Groot W, Wayne J, Hamre J (1993) Chromatography 648:33–39
22. Wang W, Kharchenko S, Migler K, Zhu S (2004) Triple-detector GPC characterization and processing behavior of long-chain-branched polyethylene prepared by solution po-lymerization with constrained geometry catalyst. Polymer 45:6495–6505
23. Yu Y, DesLauriers P, Rohlfing DC (2005) Polymer 46:5165–5182
24. Monrabal B, Yau W (2011) Engineering advances in high temperature GPC instrumentation. The Column 7(7):8–15

25. Cong et al (2007) In: Proceedings international symposium on polymer analysis and characterization (ISPAC), Crete, June 2007
26. Wong WS (2012) Application of high temperature chromatographic and viscometric techniques for the characterization of highly isotactic polypropylene samples. In: Proceedings 4th international conference on polyolefin characterization, Houston, October 2012
27. Monrabal B, Sancho-Tello J (2009) High temperature GPC analysis of polyolefins with infrared detection. In: The applications book, July 2009. LCGC Europe, Chester
28. Monrabal B, del Hierro P, Roig A (2012) Improvements in the sample preparation of polyolefins to prevent polymer degradation prior to GPC/SEC and CEF analysis. In: Proceedings 4th international conference on polyolefin characterization, Houston, October 2012
29. Wyatt Technology Corporation, Santa Barbara www.wyatt.com
30. Malvern Instruments Ltd, Worcestershire www.malvern.com/viscotek
31. Ross JH, Casto ME (1968) J Polym Sci C 21:143–152
32. Dawkins JV, Hemming M (1975) J Appl Polym Sci 19:3107–3118
33. Bosch JV, Ortín A, Monrabal B (1998) Development of a highly stable multiple wavelength IR detector fon on-line GPC, CRYSTAF and TREF analysis. In: Proceedings International GPC Symposium, Arizona, October 1998, 633–640
34. Housaki T, Satoh K, Nishikida K, Morimoto M (1988) Makromol Chem Rapid Commun 9:525–528
35. Nishikida K, Housaki T, Morimoto M, Kinoshita T (1990) J Chromatogr A 517:209–217
36. Markovich RP, Hazlitt LG, Smith-Courtney L (1993) Chromatography of polymers. In: Provder T (ed) Characterization by SEC and FFF. ACS symposium series, vol 521. American Chemical Society, Washington
37. DesLauriers PJ, Rohlfing DC, Hsieh ET (2002) Polymer 43:159–170
38. DesLauriers PJ (2005) Measuring compositional heterogeneity in polyolefins using SEC/FTIR spectroscopy. In: Striegel A (ed) Multiple detection in size exclusion chromatography. ACS symposium series, vol 893. American Chemical Society, Washington
39. Piel C, Albrecht A, Neubauer C, Klampfl CW, Reussner J (2011) Anal Bioanal Chem 400:2607–2613
40. Albrecht A (2012) Multidimensional fractionation techniques for the characterisation of HDPE pipe grades. In: Proceedings 4th international conference on polyolefin characterization, Houston, October 2012
41. Montesinos J, Tarín R, Ortín A, Monrabal B (2006) In: Proceedings 1st ICPC conference, Houston, October 2006
42. Monrabal B, Sancho-Tello J, Montesinos J, Tarín R, Ortín A, del Hierro P, Bas M (2012) High temperature gel permeation chromatograph (GPC/SEC) with integrated IR5 MCT detector for polyolefin analysis: a breakthrough in sensitivity and automation. In: The applications book, July 2012. LCGC Europe, Chester
43. Ortín A, Montesinos J, López E, del Hierro P, Monrabal B, Torres-Lapasió J, García-Álvarez-Coque MC (2013) Characterization of chemical composition across molar mass distribution in polyolefin copolymers by GPC-IR using a filter-based IR detector. In: Proceedings of the 4th international conference on polyolefin characterization, Houston, October 2012 Macromolecular Symposia (in press)
44. Ortín A, López E, Monrabal B, Torres-Lapasió JR, García-Álvarez-Coque MC (2012) J Chromatogr A 1257:66–73
45. Wheeler LM, Willis JN (1993) Appl Spectrosc 47:1128–1130
46. Willis JN, Dwyer JL, Wheeler LM (1993) Polym Mater Sci 69:120–121
47. Verdurmen-Noel L, Baldo L, Bremmers S (2001) Polymer 42:5523–5529
48. Kearney T, Dwyer JL (2008) Am Lab 40:8–9
49. Carson WW, Dwyer JL, Boumajny B (2008) Copolymer compositional drift across molecular weight measured by LC-FTIR. Int J Polym Anal 13:463–470

50. Hiller W, Pasch H, Macko T, Hoffmann M, Ganz J, Spraul M, Braumann U, Streck R, Mason J, Van Damme F (2006) J Magn Reson 183:290–302
51. Miller ME, Giddings JC (1998) J Micro Sep 10:75–78
52. Mes EPC, de Jonge H, Klein T, Welz R, Gillespie DT (2007) J Chromatogr A 1154:319
53. Otte T, Brull R, Macko T, Klein T, Pasch H (2010) J Chromatogr A 1217:722–730
54. Otte T, Pasch H, Macko T, Br ull R, Stadler FJ, Kaschta J, Becker F, Buback M (2011) J Chromatogr A 1218:4257–4267
55. Kamiya T, Ishikawa N, Kambe S, Ikegami N, Nishibu H, Hattori T (1990) ANTEC Proc. 1990 48:871–873
56. Starck P (1996) Polym Int 40:111
57. Hosoda S (1988) Polym J 20:383
58. Flory PJ (1953) Principles of polymer chemistry, Chaps XII and XIII. Cornell University Press, Ithaca
59. Huggins ML, Okamoto H (1967) Chapter A: theoretical considerations. In: Cantow MJ (ed) Polymer fractionation. Academic, New York, pp 1–66
60. Flory PJ (1948) Trans Farad Soc 51:848
61. Wild L, Ryle T, Knobeloch D, Peat IR (1982) J Polym Sci Polym Phys Ed 20:441
62. Wild L, Blatz C (1993) In: Chung T (ed) New advances in polyolefins. Plenum, New York, pp 147–157
63. Alamo R, Mandelkern L (1989) Macromolecules 22:1273
64. Monrabal B (1994) J Appl Polym Sci 52:491
65. Alamo RG, Glaser RH, Mandelkern L (1988) J Polym Sci Polym Phys Ed 26:2169
66. Neves CJ, Monteiro E, Habert AC (1993) J Appl Polym Sci 50:817
67. Soares JBP, Hamielec AE (1995) Macromol Theory Simul 4:305
68. Glöckner G (1990) J Appl Polym Sci Appl Polym Symp 45:1–24
69. Parikh D, Childress BS, Knight GW (1991) Structural Characterization of LLDPE by STAF ANTEC Conf Proc 1543
70. Addison A, Ribeiro M, Deffieux A, Fontanille M (1992) Polymer 33(20):4337
71. Müller AJ, Hernández ZH, Arnal ML, Sánchez JJ (1997) Successive self-nucleation/annealing (SSA): a novel technique to study molecular segregation during crystallization. Polym Bull 39:465–472
72. Keating MY, McCord EF (1994) Thermochim Acta 243:129
73. Müller A, Arnal L (2005) Prog Polym Sci 30:559–603
74. Wild L, Ryle T (1977) Polym Prepr 18:182
75. Wild L, Ryle T, Knobeloch D (1982) Polym Prepr 3:133
76. Desreux V, Spiegels ML (1950) Bull Soc Chim Belg 59:476
77. Hawkins SW, Smith H (1958) J Polym Sci 23:341
78. Shirayama K, Okada T, Kita SI (1965) J Polym Sci A 3:907
79. Wild L (1991) Adv Polym Sci 98:1–47
80. Monrabal B (1996) In: Hosoda S (ed) New trends in polyolefin science and technology. Research Signpost, Trivandrum, p 126
81. Fonseca CA, Harrison IR (1999) In: Pethrick RA (ed) Modern techniques for polymer characterisation. Wiley, New York, pp 1–13
82. Soares JBP, Hamielec AE (1995) Polymer 36(8):1639
83. Soares JBP, Hamielec AE (1999) In: Pethrick RA (ed) Modern techniques for polymer characterisation. Wiley, New York, pp 15–55
84. Monrabal B (2000) Temperature rising elution fractionation and crystallization analysis fractionation. In: Meyers RA (ed) Encyclopedia of analytical chemistry. Wiley, Chichester, pp 8074–8094
85. Hazlitt LG (1990) J Appl Polym Sci Appl Polym Symp 45:25
86. Monrabal B, Ortin A, Romero L (1999) In: Proceedings of the 12th International symposium on polymer analysis and characterization (ISPAC), La Rochelle, 28 June 1999
87. Monrabal B, Sancho-Tello J, Mayo N, Romero L (2007) Macromol Symp 257:71–79

88. Yau W, Gillespies D (2001) Polymer 42:8947
89. Monrabal B (2004) Microstructure Characterization of Polyolefins. TREF and CRYSTAF. In: Proceedings of the 17th International symposium on polymer analysis and characterization (ISPAC), Heidelbergh, 6–9 June 2004
90. Monrabal B, Romero L, Mayo N, Sancho-Tello J (2009) Macromol Symp 282:14–24
91. Iiba K, Kusano Y, Sakata K (2010) Novel approach for determination of precise crystallinity distribution by TREF. In: Proceedings 3rd international conference on polyolefin characterization (ICPC), Shanghai, November 2010
92. Boisson C, Boyron O, Macko T, Cossoul E, Baverel Laetitia, Martigny E (2013) Homogeneous copolymers of ethylene with α-olefins synthesized with metallocene catalysts and their use as standards for TREF calibration. In: Proceedings 4th international conference on polyolefin characterization, Houston, October 2012. Macromolecular Symposia (in press)
93. Monrabal B, Blanco J, Nieto J, Soares J (1999) J Polym Sci 37:89–93
94. Soares J, Monrabal B, Nieto J, Blanco J (1998) Macromol Chem 199:1917–1926
95. Stehling CF (1990) International Patent WO 90/03414
96. Davey CR et al (1994) US Patent 5,322,728
97. Monrabal B (2007) Microstructure characterization of polyolefins. In: Abstracts advances in polyolefins, 23–26 September 2007, Santa Rosa. ACS, Division of Polymer Chemistry, Blacksburg
98. Siriwongsarn E, Anantawaraskul S, Chokputtanawuttilerd N, Alghyamah A, Soares J (2012) Macromol Chem Phys 213:1892–1906
99. Monrabal B (1991) Crystallization analysis fractionation. US Patent 5,222,390
100. Anantawaraskul S, Soares J, Jirachaithorn P (2007) Macromol Symp 257:94–102
101. Monrabal B, del Hierro P (2011) Analytical and bioanalytical chemistry. Sep Sci Macromol 399(4):1557–1561
102. Monrabal B (2007) CEF. Patent WO 2007/104804 A2
103. Glöckner G (1992) Gradient HPLC of copolymers and chromatographic cross-fractionation. Springer, Berlin
104. Pasch H, Trathnigg B (1998) HPLC of polymers. Springer, Berlin
105. Macko T, Brull R, Zhu Y, Wang Y (2010) J Sep Sci 33:3446–3454
106. Lehtinen A, Paukkeri R (1994) Macromol Chem Phys 195:1539–1556
107. Macko T, Pasch H, Kazakevich YV, Fadeev AY (2003) J Chromatogr A 988:69
108. Heinz LC, Pasch H (2005) Polymer 46:12040
109. Albrecht A, Heinz LC, Lilge D, Pasch H (2007) Macromol Symp 257:46–55
110. Albrecht A, Brüll R, Macko T, Pasch H (2007) Macromolecules 40:5545–5551
111. Dolle V, Albrecht A, Brull R, Macko T (2011) Macromol Chem Phys 212:959–970
112. Pasch H, Albrecht A, Brüll R, Macko T, Hiller W (2009) Macromol Symp 282:71–80
113. Macko T, Pasch H (2009) Macromolecules 42:6063–6067
114. Macko T, Brüll R, Wang Y, Coto B, Suarez I (2011) J Appl Polym Sci 122:3211–3217
115. Macko T, Brüll R, Alamo RG, Stadler FJ, Losi S (2011) Anal Bioanal Chem 399:1547–1556
116. Miller MD, de Groot W, Lyons JW, Van Damme FA, Winniford BL (2012) J Appl Polym Sci 123:1238–1244
117. Roy A, Miller MD, Meunier DM, de Groot AW, Winniford WL, Van Damme FA, Pell RJ, Lyons JW (2010) Macromolecules 43:3710–3720
118. Ginsburg A, Macko T, Dolle V, Bruell R (2011) Eur Polym J 47:319–329
119. Cheruthazhekatt S, Pijpers TFJ, Harding GW, Mathot VBF, Pasch H (2012) Macromolecules 45:2025–2034
120. Chang T, Lee HC, Lee W, Park S, Ko C (1999) Macromol Chem Phys 200(10):2188
121. Cong R, de Groot AW, Parrott A, Yau W, Hazlitt L, Brown R, Cheatham M, Miller MD, Zhou Z (2012) Macromol Symp 312:108–114
122. Cong R, de Groot W, Parrott A, Yau W, Hazlitt L, Brown R, Miller M, Zhou Z (2011) Macromolecules 44:3062–3072
123. Monrabal B, Mayo N, Cong R (2012) Macromol Symp 312:115–129
124. Cong et al (2011) Patent WO 084786 A1

125. Cong et al (2012) Determination of the microstructure of polyolefins using thermal gradient interaction chromatography and its hyphenated techniques. In: Proceedings 4th international conference on polyolefin characterization, Houston, October 2012
126. Monrabal B (2011) New tools in the characterization of polyolefin microstructure. In: Abstracts advances in polyolefins, 25–28 September 2011, Santa Rosa. ACS, Polymer Chemistry Division, Blacksburg
127. Monrabal B, Lopez E (2013) Advances in thermal gradient interaction chromatography and crystallization techniques for composition analysis in polyolefins. In: Proceedings of the 4th international conference on polyolefin characterization, Houston, October 2012. Macromolecular symposia 2013 (in press)
128. Aust N, Beytollahi-amtmann I, Lederer K (1995) Int J Polym Anal Character 1:245
129. Faldi A, Soares JBP (2001) Polymer 42:3057–3066
130. Nakano, Goto Y (1981) Mitsubishi Petrochemical Co, Ltd. J Appl Polym Sci 26:4217–4231
131. Li Pi Shan C, Gillespie D, Hazlitt L (2005) The Dow Chemical Company. Ecorep, Lyon
132. Gillespie D, Hazlitt L, Li Pi Shan C (2006) In: Proceedings 1st international conference on polyolefin characterization (ICPC), Houston, October 2006
133. Ortín A, Monrabal B, Sancho-Tello J (2007) Macromol Symp 257:13–28
134. Monrabal B (2012) Advances in microstructure characterization of polyolefins. In: Proceedings Chemelot International Polyolefins Symposium (CIPS), Maastricht, 7–10 October 2012

Adv Polym Sci (2013) 257: 253–254
DOI: 10.1007/12_2013_259

Published online: 6 October 2013

Erratum to: Phillips Cr/Silica Catalyst for Ethylene Polymerization

Ruihua Cheng, Zhen Liu, Lei Zhong, Xuelian He, Pengyuan Qiu, Minoru Terano, Moris S. Eisen, Susannah L. Scott, and Boping Liu

Erratum to: Adv Polym Sci
DOI: 10.1007/12_2013_222

In Page 50, Scheme 17 was revised as (In original Scheme 17, the energy of ^{3}h10 in step 4 was wrong.)

R. Cheng, Z. Liu, L. Zhong, X. He, P. Qiu, and B. Liu (✉)
State Key Laboratory of Chemical Engineering, East China University of Science and Technology, Meilong Road 130, Shanghai 200237, PR China
e-mail: boping@ecust.edu.cn

M. Terano
School of Materials Science, Japan Advanced Institute of Science and Technology, 1-1 Asahidai, Nomi, Ishikawa 923-1292, Japan

M.S. Eisen
Schulich Faculty of Chemistry, Technion-Israel Institute of Technology, Technion City, Haifa 32000, Israel

S.L. Scott
Department of Chemical Engineering, University of California, Santa Barbara, CA 93106-5080, USA

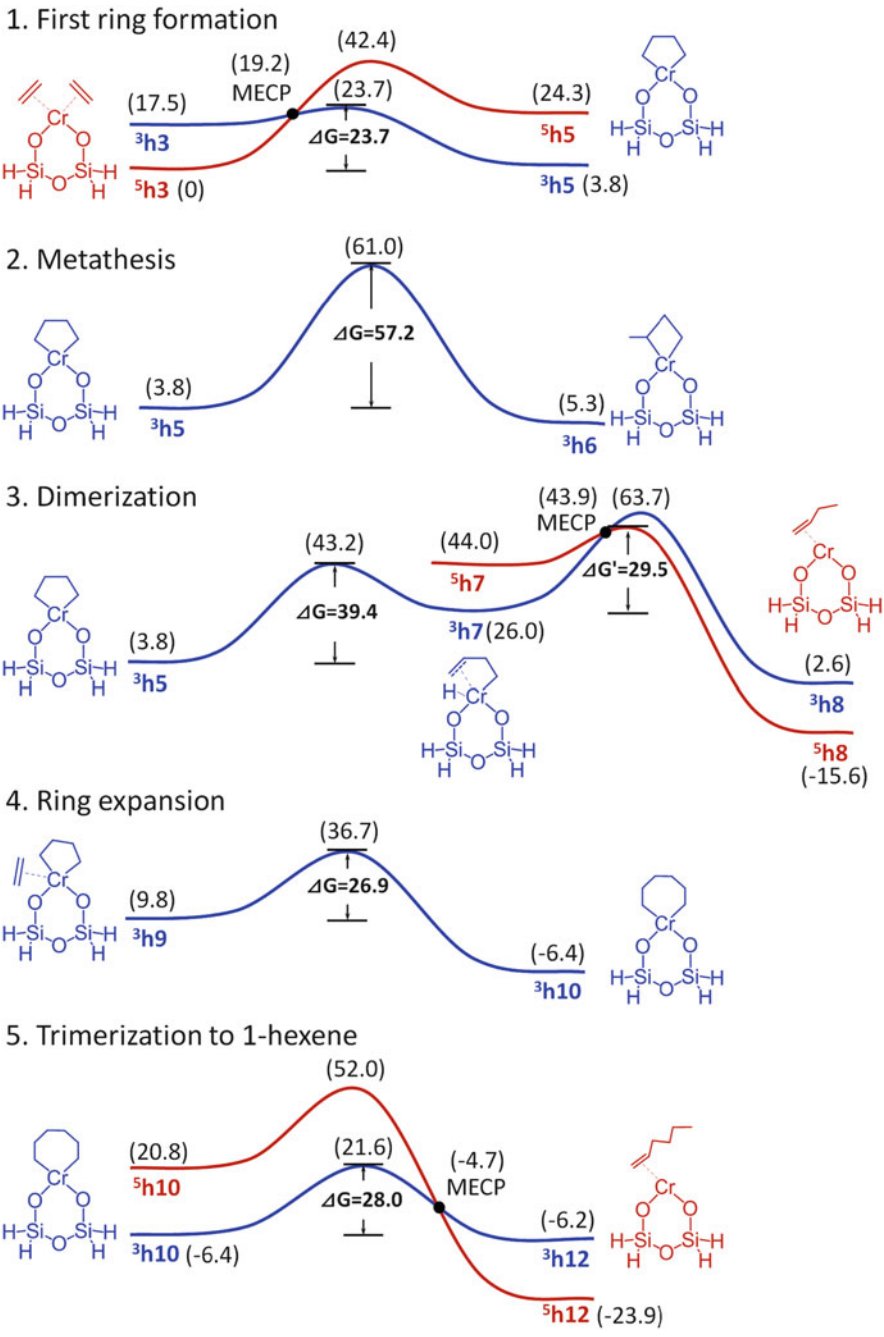
1. First ring formation
(42.4)
(19.2)
MECP
(23.7)
(17.5)
(24.3)
3h3
5h5
ΔG=23.7
5h3 (0)
3h5 (3.8)
2. Metathesis
(61.0)
ΔG=57.2
(3.8)
(5.3)
3h5
3h6
3. Dimerization
(43.9) (63.7)
MECP
(43.2)
(44.0)
5h7
ΔG'=29.5
ΔG=39.4
(3.8)
3h7 (26.0)
(2.6)
3h5
3h8
5h8
(-15.6)
4. Ring expansion
(36.7)
ΔG=26.9
(9.8)
(-6.4)
3h9
3h10
5. Trimerization to 1-hexene
(52.0)
(20.8)
(21.6)
(-4.7)
MECP
5h10
ΔG=28.0
(-6.2)
3h10 (-6.4)
3h12
5h12 (-23.9)

Index